Université de Montréal

Identification of copper metabolism as a KRAS-specific vulnerability in colorectal cancer

par

Neethi Nandagopal

Programmes de biologie moléculaire
Institut de Recherche en Immunologie et en Cancérologie (IRIC)
Faculté de médecine

Thèse présentée à la Faculté de médecine en vue de l'obtention du grade de
Ph.D. en biologie moléculaire, option biologie des systèmes

Octobre 2020

Résumé

KRAS est parmi les gènes les plus fréquemment mutés dans les cancers humains, tel que ~ 45% des cancers colorectaux (CCR). Malgré les efforts déployés pour réduire son potentiel oncogénique, KRAS muté est fréquemment associé à la résistance aux médicaments et est extrêmement difficile à cibler sur le plan thérapeutique. Les protéines à la surface cellulaire sont souvent dérégulées dans les cancers et sont des cibles thérapeutiques attrayantes en raison de leur accessibilité aux anticorps. Nous avons séquençé les ARNm de cellules épithéliales intestinales exprimant KRAS muté et observé que ces dernières présentaient des changements importants dans les gènes codant pour des protéines de surface cellulaire. Par conséquent, notre objectif était d'identifier de nouvelles cibles thérapeutiques exprimées à la surface de cellules transformées par l'oncogène KRAS. En utilisant une approche de pointe en protéomique de surface cellulaire, nous avons identifié plusieurs protéines différentiellement exprimées dans les cellules avec KRAS muté par rapport à leurs homologues de type sauvage. Nous avons ensuite effectué un crible CRISPR/Cas9 basé sur les protéines de surface cellulaire, qui a révélé que la perte de la protéine Atp7a affectait de manière différentielle les cellules épithéliales intestinales, en fonction de leur statut KRAS. De façon intéressante, nous avons constaté que ATP7A était régulé à la hausse dans les cellules avec KRAS muté par rapport à leurs homologues de type sauvage. ATP7A a un double rôle dans les cellules; alors qu'il est essentiel pour la maturation des enzymes dépendantes du cuivre (Cu), ATP7A protège les cellules d'une toxicité excessive induite par le Cu (cuproptose). Chez l'homme, les mutations dans ATP7A entraînent des troubles caractérisés par des déficiences systémiques dans le transport et les niveaux de Cu. Chez les animaux et dans les modèles de culture cellulaire, tel que les cellules épithéliales intestinales, les niveaux intracellulaires de Cu sont directement corrélés avec l'abondance post-transcriptionnelle d'ATP7A. Dans le même ordre d'idées, nous avons observé que les cellules de CCR avec KRAS muté avaient relativement plus de Cu intracellulaire, et la surexpression d'ATP7A protégeait les cellules KRAS muté de la cuproptose, par rapport à leurs homologues de type sauvage. Nous avons également observé que la croissance *in vivo* des xénogreffes KRAS mutées était réduite lorsque les souris étaient nourries avec un régime pauvre en Cu. Le Cu est utilisé par plusieurs enzymes qui régulent des fonctions cellulaires critiques, notamment la respiration mitochondriale, la motilité cellulaire et la prolifération. Nous montrons que les cellules mutantes KRAS étaient plus sensibles au chélateur de Cu, ammonium tetrathiomolybdate (TTM), par rapport aux cellules de type sauvage. De plus,

les cellules avec KRAS muté traitées avec le TTM ont présenté des activités réduites de MEK1/2 dépendant du Cu et de l'enzyme de la chaîne de transport d'électrons mitochondriale, cytochrome c oxidase (CCO). Nous avons été surpris de constater que le transporteur de Cu de haute affinité, CTR1, est régulé à la baisse dans les cellules avec KRAS muté, et avons donc émis l'hypothèse que les cellules KRAS mutées doivent absorber le Cu par d'autres moyens. Ainsi, nous avons constaté que la macropinocytose agit comme une voie non canonique d'approvisionnement en Cu dans les cellules avec KRAS muté. Le traitement de cellules *in vivo* avec l'inhibiteur de la macropinocytose, EIPA, a inhibé l'expression d'ATP7A et diminué le Cu biodisponible dans les xénogreffes KRAS mutées. En conclusion, nos résultats montrent que les cellules avec KRAS muté augmentent les niveaux de Cu et d'ATP7A pour soutenir la tumorigenèse en augmentant l'activité cuproenzymatique et diminuant la cuproptose. Cette étude est pertinente pour le cancer, car les tissus tumoraux contiennent fréquemment des niveaux de Cu plus élevés que les tissus normaux. Des études récentes ont mis en évidence un potentiel de repositionnement du chélateur de Cu TTM, qui est disponible en clinique et utilisé pour traiter les troubles du Cu. Nos résultats démontrent que la biodisponibilité du Cu pourrait être exploitée pour traiter le CCR avec KRAS muté avec de tels inhibiteurs. Les travaux futurs comprennent l'identification de stratégies combinatoires qui peuvent être améliorer les effets anti-cancéreux de la chélation du Cu.

Mot clés: Cuivre, RAS, ATP7A, Cancers colorectaux, Surface cellulaire

Abstract

KRAS is amongst the most frequently mutated genes driving human cancers, including ~ 45% of colorectal cancers (CRC). Despite intense efforts to curb its oncogenic potential, mutant KRAS is frequently associated with drug resistance and is extremely challenging to target therapeutically. Cell-surface proteins are often spatially dysregulated in cancers and are attractive therapeutic targets due to their easy accessibility. We performed RNA sequencing of mutant KRAS-expressing intestinal epithelial cells and observed that cells undergoing transformation exhibited dramatic changes in cell surface-coding genes. Therefore, our goal was to identify novel druggable targets expressed at the cell surface of mutant KRAS-transformed cells. Using a cutting-edge cell surface proteomics approach, we identified several differentially expressed proteins at the surface of KRAS-mutant cells compared to wild-type counterparts. We then performed a cell surface based CRISPR/Cas9 screen, which revealed that loss of the copper exporter *Atp7a* differentially affected the fitness of intestinal epithelial cells, depending on their KRAS status. Interestingly, we found that ATP7A was upregulated in KRAS-mutant cells compared to wild-type counterparts. ATP7A has a dual role in cells; while it is essential for maturation of copper (Cu)-dependent enzymes, ATP7A protects cells from excess Cu-induced toxicity (cuproptosis). In humans, ATP7A mutations result in disorders characterized by systemic deficiencies in Cu transport and levels. In animals and in tissue culture models, including intestinal epithelial cells, intracellular Cu levels are directly correlated with the post-transcriptional abundance of ATP7A. In line with this, we observed that KRAS-mutant CRC cells and tissues had relatively more intracellular Cu, and ATP7A-overexpression protected KRAS-mutant cells from cuproptosis, compared to wild-type counterparts. We also observed that in vivo growth of KRAS-mutant xenografts was reduced when mice were fed a Cu-deficient diet. Cu is utilized by several enzymes that regulate critical cellular functions including mitochondrial respiration, cell motility and proliferation. We show that KRAS-mutant cells were more sensitive to the Cu chelating drug ammonium tetrathiomolybdate (TTM), compared to wild-type cells. Moreover, TTM-treated KRAS-mutant cells displayed reduced activities of Cu-dependent MEK1/2 and mitochondrial electron transport chain enzyme, cytochrome c oxidase (CCO). We were surprised to find that the high-affinity CTR1 importer is downregulated in KRAS-mutant cells, and so we hypothesized that KRAS cells must uptake Cu through alternate means. In accordance with this, we found that macropinocytosis acts as a non-canonical Cu-supply route in KRAS-mutant cells. In vivo, treating cells with the macropinocytosis

inhibitor EIPA, inhibited the expression of ATP7A and decreased bioavailable Cu in KRAS xenografts. In conclusion, our results show that KRAS-mutant cells increase Cu and ATP7A levels, likely to support tumorigenesis by elevating cuproenzymatic activity and parallelly dealing with cuproptosis. This study is relevant to cancer as tumor tissues and patients contain higher Cu levels than normal controls. Recent studies have highlighted a potential for repurposing the clinically available copper chelator TTM, which is used to treat Cu disorders. Our results demonstrate that copper bioavailability could be exploited to treat KRAS-mutated CRC with such inhibitors. Future work includes identification of combinatorial strategies that may be synthetic lethal to copper chelation.

Keywords: Copper, RAS, ATP7A, Colorectal cancer, Cell surface

Acknowledgements

I would like to begin by thanking my parents and sister. It was a difficult decision for them to let me come to Canada to pursue my long-term dream of doing a Ph.D. They have been patiently waiting for the day of my graduation and have been very supportive of my decision to finish my Ph.D., although the physical separation between us was hard to overcome. I thank my family for taking good care of me and for providing me a good education. On that note, I owe quite a bit to my uncle in Canada, who has provided me with emotional support and assistance whenever I needed it. He made sure that my transition to Canada was smooth and comfortable. Secondly, I would like to thank my master's thesis supervisor, Dr. Seung Hwan Lee, it was due to him that I had the opportunity to move to Canada. He spent a lot of time to teach me several techniques, and conduct experiments when I was a novice with very little lab experience. He also made sure I had my first paper. All the above helped me in my Ph.D. I am equally thankful to my Ph.D. supervisor, Dr. Philippe Roux. He believed in me and gave me the chance to work in his laboratory. Under his support and tutelage, I have learnt a lot about how-to do-good research, good work ethics, effective communication of scientific ideas, and scientific writing. I will forever cherish the years spent in his laboratory which was formative not only for my scientific career, but also to my personal growth. Thank you for your constructive criticism, being in your lab has made me a stronger and better person!

A special thanks to my mentor and friend, Léo Aubert, to whom I owe a lot. Over the years I have imbued so much from him that has significantly improved my presentation and communication skills, not to mention how to efficiently conduct experiments. It was hard in the beginning for both of us together, but I am impressed and grateful that we persevered and became good buddies. He provided me with strength and emotional support when I wanted to give up, constructive criticism when I needed to improve, and challenged me to push myself. I would also like to thank our ex-lab member and a dear friend, Beichen Gao, he gave me a shoulder to lean on when the going got tough, was a patient listener and provided me with useful suggestions. His enthusiasm was infectious, and I miss our time together talking about everything under the sun, exploring Montreal, and indulging in great food. A big thanks to our very skilled lab manager and a strong woman, Geneviève Lavoie, who taught me how to do basic techniques in the lab. I appreciate that she gave me the time for troubleshooting and discussing experiment ideas and details. I will also cherish the

countless conversations we had over the years ranging from serious to funny topics. I am grateful to my lab members Sami Nourreddine, Thibault Houles, Louis Théret for the many fun times and conversations we had together. Gabriel and I are going to miss the weekend getaways, we appreciate that we got to hang out with you guys. I am also grateful for the many scientific discussions, which helped us improve our data. Through you guys, I was able to see the importance of discussing my ideas to get a different perspective on our research. I hope to never forget the amazing time at the Christmas parties!!! I'm glad that I got to know Alizée Gouronnec, a sweet colleague and an excellent baker. Her surprise treats improved many drudging workdays. She is considerate and always checked on me to make sure I was doing well, thank you for doing that. A shout out to Dhanaraman Seetharaman Thillai Villalan for his friendship, advice and help with the many administrative and non-administrative processes that often confused and overwhelmed me. I miss the countless hours spent with Shubadhra and Sundar from the Kathy Borden laboratory, they were extremely supportive and always lent their time for me when I was feeling down and wanted to talk. Thank you for the advice and friendship.

A big thank you to the kindest person I know at IRIC, Christian Charbonneau, from the Microscopy platform. I will always remember him for his patience, his immense knowledge on cameras, microscopes, lenses and softwares. He was always available and a great teacher, showed me a lot of cool tricks with softwares, and helped me design good microscopy experiments. I also appreciate the kind help and service of Pierre Melançon and Julie Hinsinger, also from IRIC platforms. I am thankful for my thesis committee members, Dr. Sylvain Meloche and Dr. Gerardo Ferbeyre, for their time, advice, constructive criticism and support. I am glad that I had financial support from FRQNT, FRQS, and UdeM throughout my Ph.D., which let me carry out my research stress free.

Last but not the least, I am happy that I had Gabriel Parent by my side during my Ph.D. It was a tough journey and his emotional support and unconditional love made the difficult times bearable. I always turned to him for advice on the many decisions I had to take during my Ph.D. He was also a big help to me for big data analysis and automatization of analysis. I will be forever grateful that my decision to come to Montreal and pursue my Ph.D. led to the meeting of my life partner. Another major pillar of support for me is my strong mom-in-law, Micheline Cusson. I am grateful

for her advice and help through the years. I am glad for the immense emotional support and encouragement from Michel Parent, Félix Parent, Andréane Nepveu, and Barbara Bédard. It was a huge help for me to have a second family away from my own in India. My two friends Jacinthe Pilon and Juliette Dubois deserve a special mention. They continually inspire me to be a better person. I thank you both for being there for me, for inviting me into their lives, for looking out for me. I would also like to extend my thanks to Amandeep Kaur Komal and Raja, Rachel Philip, Prahatha Venkatraman, and Menakshi Priya for their being a part of my life, and for the continual emotional support through their years.

This work was possible because of all of you!

Table of Contents

List of Figures

List of Tables

List of Abbreviations

0-9	2-NBDG	2-deoxy-2-((7-nitro-2,1,3-benzoxadiazol-4-yl)amino)-D-glucose
A		
	ATP7A	Copper-transporting ATPase 1
	AJCC	American Joint Committee on Cancer
	APC	Adenomatous polyposis coli
	ACVR2	Activin type 2 receptor
	AXIN2	Axis Inhibition protein 2
	ABCG	ATP-binding cassette subfamily G
	ATP	Adenosine triphosphate
	APC	Antigen Presenting Cells
	ALK	Anaplastic Lymphoma Kinase
	Atg	Autophagy-related
	AMPK	AMP-activated protein Kinase
	APC/C	Anaphase-promoting complex/cyclosome
	ATOX1	Antioxidant Protein 1
	Ag	Silver
	AOC3	Amino-Oxidase Copper-containing 3
	ATN-224	Choline Tetrathiomolybdate
	ATSM	Diacetylbis-[N4-methylthiosemicarbazonato
	ANOVA	Analysis Of Variance
	ACN	Acetonitrile
	ATR	Ataxia Telangiectasia and Rad3-related
	ACC	Acetyl-CoA Carboxylase
B		
	BubR1	Budding uninhibited by benzimidazole-related 1
	Bub3	Budding uninhibited by benzimidazole 3
	BAX	Bcl-2-associated X protein
	BMP	Bone Morphogenetic Protein
	BMPR1A	Bone Morphogenetic Protein Receptor 1A
	BAD	Bcl-2 Associated Death promoter
	BIRC5	Baculoviral IAP repeat containing 5
	BST2	Bone marrow stromal antigen 2
	BCS	Bathocuproine disulfonate
	BF	Bayes Factor
	BAGEL	Bayesian Analysis of Gene EssentiaLity
	BSA	Bovine Serum Albumin
	BCL2	B-cell lymphoma 2
	BAK1	BCL2 Antagonist/Killer 1
	BRCA1/2	Breast Cancer gene
C		
	CRC	Colorectal Cancer
	CRISPR	Clustered Regularly Interspaced Short Palindromic Repeat
	Cu	Copper
	CCO	Cytochrome C Oxidase

CTR1	Copper Transport protein 1
CIMP	CpG island methylator phenotype
CENPE	Centromere-associated Protein E
CDKN2A	Cyclin-Dependent Kinase Inhibitor 2A
CDK8	Cyclin-Dependent Kinase 8
CTNNB1	Catenin Beta 1
CCNE1	Cyclin E1
CBC	Crypt-Base Columnar cells
CTLA-4	Cytotoxic T-Lymphocyte-Associated protein-4
CD28	Cluster of Differentiation 28
CEA	CarcinoEmbryonic Antigen
COX	CycloOXygenase
COX17	C OXidase 17 copper chaperone
CTKD	C-Terminal Kinase Domain
CDC42	Cell Division Cycle 42
CDCP1	CUB domain-containing protein 1
CSB	Cell Surface Biotinylation
CHO	Bathocuproine disulfonate
CSC	Cell Surface Capture
CP	Ceruloplasmin
CCO	Cytochrome C Oxidase
CCS	Copper Chaperone for SOD1
CHGs	Cu homeostasis genes
COMMD1	Copper Metabolism Domain Containing 1
CID	Collision-Induced Dissociation
CIN	Chromosomal Instability
CAM	Cell Adhesion Molecule
CRCHUM	Center Hospitalier de l'Université de Montréal
CuD	Copper Deficiency
CDEA	Comité de Déontologie en Expérimentation Animale
CCAC	Canadian Council on Animal Care
CQ	Chloroquine
COQ2	Coenzyme Q2
CRANKS	Condition-specific Robust Analytics and Normalization for Knockout Screens
CIHR	Canadian Institutes for Health Research
CRS	Cancer Research Society

D

DNA	Deoxyribonucleic Acid
DCC	Deleted in Colorectal Cancer
DPD	Dihydropyrimidine Dehydrogenase
DDR	Discoidin Domain Receptor
DUSPs	Dual-Specificity Phosphatases
DOCK1	Dedicator of Cytokinesis 1
DMT1	Divalent Metal Transporter 1
DDP	Cisplatin

DSF	Disulfram
DTDP	2,2′-dithiodipyridine
DMEM	Dulbecco's modified Eagle's medium
DTT	Dithiothreitol
DMSO	Dimethyl Sulfoxide
DIC	Differential Interference Contrast

E

EIPA	5-N-Ethyl-N-Isopropyl Amiloride
EGFR	Epidermal Growth Factor Receptor
EGF	Epidermal Growth Factor
ERK	Extracellular signal-Regulated Kinase
ELK1	Erythroblast Transformation Specific-like protein 1
EMT	Epithelial-Mesenchymal Transition
ECM	Extracellular Matrix
ENO	Enolase
Evc2	Ellis van Creveld syndrome 2
EphA2	Ephrin A2
EDTA	Ethylenediaminetetraacetic Acid
ER1	Epitope Retrieval
ECAR	Extracellular Acidification Rate
ETC	Electron Transport Chain
eEF2K	Eukaryotic elongation factor 2 kinase
ENT1	Equilibrative Nucleoside Transporter 1

F

FAP	Familial Adenomatous Polyposis
FBXW7	F-box and WD repeat domain-containing 7
FDA	Food and Drug Administration
FGF	Fibroblast Growth Factor
FLT3	Fms Like Tyrosine kinase 3
FTase	Farnesyltransferase
FTI	Farnesyltransferase inhibitors
FOXO	Forkhead box O
Fe	Iron
FC	Fold Changes
FCCP	Carbonyl Cyanide 4-(Trifluoromethoxy) Phenylhydrazone
FBS	Fetal Bovine Serum
FDR	False Discovery Rate
FACS	Fluorescence-activated cell sorting
FRQS	Fonds de la recherche du Québec-Santé
FRQNT	Fonds de la recherche du Québec-Nature and Technologies

G

GSK3β	Glycogen Synthase Kinase-3β
GTP	Guanosine Triphosphate
GAPs	GTPase activating proteins
GEF	Guanine nucleotide Exchange Factors

	GGTase	Geranylgeranyltransferase
	GRB2	Growth-factor-Receptor-Bound protein 2
	GADD45A	Growth arrest and DNA-damage-inducible protein 45 Alpha
	GLUT1	Glucose Transporter 1
	GOT1	Glutamate Oxaloacetate Transaminase 1
	GATA2	guanine-adenine-thymine-adenine binding protein 2
	GSH	Glutathione
	GTSM	Glyoxalbis N4-methylthiosemicarbazonato
	GSEA	Gene Set Enrichment Analysis
	gRNA	guide Ribonucleic Acid
	GO	Gene Ontology
	GO.CC	Gene Ontology Cellular Component
	GAPDH	Glyceraldehyde-3-Phosphate Dehydrogenase
	GYS1	Glycogen Synthase 1
	GPCR	G-protein coupled receptors
	GRB10	Growth factor Receptor Bound protein 10
H		
	HNPCC	Hereditary Nonpolyposis Colorectal Cancer
	HER2	Human Epidermal growth factor Receptor 2
	HIC1	Hypermethylated in Cancer 1
	HGF	Hepatocyte Growth Factor
	HVR	Hypervariable Regions
	HEPHL1	Hephaestin like 1
	HIF-1α	Hypoxia Inducing Factor
	HRP	Horseradish Peroxidase
	HNO3	Nitric Acid
	HMGCR	HMG-CoA reductase
	HTS	High throughput Screening
I		
	ICP-MS	Inductively coupled plasma mass spectrometry
	IB	Immunoblotting
	IRS	Insulin Receptor Substrate
	IGF	Insulin-like Growth Factor
	IGF-1R	Insulin-like growth factor receptor-type 1
	IEC-6	Intestinal Epithelial Cells-6
	IFN	Interferon
	IgG	Immunoglobulin G
	ICMT	Isoprenylcysteine Carboxyl Methyltransferase
	ITGB5	Integrin Beta 5
	IHC	Immunohistochemistry
J		
	JNK	c-Jun N-terminal Kinase
K		
	KRAS	Kirsten Rat Sarcoma
	kDa	Kilodaltons
	KEGG	Kyoto Encyclopedia of Genes and Genomes

L

LINE-1	Long interspersed nuclear element-1
LAG-3	Lymphocyte Activation Gene 3
LKB1	Liver Linase B1
LC3	Microtubule-associated proteins 1A/1B light chain 3B
LC-MS/MS	Liquid Chromatography and tandem Mass Spectrometry
LDHA	Lactate Dehydrogenase A
LOXL	Lysyl Oxidase

M

MEK 1/2	Mitogen-activated protein Kinase 1/2
mCRC	Metastatic Colorectal Cancer
mm	millimeter
MAPK	Mitogen-activated protein Kinase
MSI	Microsatellite Instability
MSS	Microsatellite Stable
MYC	Myelocytomatosis oncogene
MAD2	Mitotic arrest deficient 2
NEUROG1	Neurogenin 1
MSH2	mutS homolog 2
MLH1	mutL homolog 1
MET	Mesenchymal-Epithelial Transition
MHC-I	Major Histocompatibility Complex I
MSKCC	Memorial Sloan-Kettering Cancer Center
MKP	Mitogen-activated protein Kinase Phosphatases
mTORC	Mechanistic Target Of Rapamycin Complex
MCL-1	Myeloid Leukemia Cell 1
MDM2	Murine Double Minute 2
MMP	Matrix Metalloproteases
MT	Metallothionein
µM	Micromolar
MBD	Metal Binding Domain
MTF1	Metal regulatory transcription factor 1
MEF	Mouse Embryonic Fibroblasts
MEM	Modified Eagle's Medium
MTT	Thiazolyl Blue Tetrazolium Bromide
MFI	Mean Fluorescence Intensity
MMR	Mismatch Repair genes
MWCO	Molecular Weight Cut-Off
MOI	Multiplicity Of Infection

N

NRAS	Neuroblastoma Rat Sarcoma
NK	Natural Killer
NSAID	Nonsteroidal Anti-Inflammatory Drugs
NF1	Neurofibromatosis 1
NTKD	N-Terminal Kinase Domain
NHS	N-hydroxysulfosuccinimide

	NIH	National Institute of Health
	NSG	NOD Scid Gamma mouse
	NT	Nontargeting
	NSAF	Normalized Spectral abundance factors
	NTPs	Nucleotide triphosphates
O		
	OS	Overall Survival
	OXPHOS	Oxidative Phosphorylation
	OCR	Oxygen Consumption Rate
P		
	PIK3CA	Phosphatidylinositol-4,5-Bisphosphate 3-Kinase Catalytic Subunit Alpha
	PI3K	Phosphatidylinositol-3-Kinase
	PTEN	Phosphatase and Tensin homolog
	PMS1	Post Meiotic Segregation increased 1
	PFS	Progression Free Survival
	PIGF	Placental Growth Factor
	PD-1	Programmed cell death protein-1
	PDGFR-β	Platelet derived growth factor receptor-β
	PM	Plasma Membrane
	$PtdIns(3,4,5)P_2$	Phosphatidylinositol 3-4,5-bisphosphate
	PH	Pleckstrin homology
	PKC	Protein Kinase C
	PDK1	Phosphoinositide Dependent Kinase 1
	PKC	Protein Kinase C
	PDAC	Pancreatic Ductal Adenocarcinoma
	PGK	Phosphoglycerate Kinase
	PKM2	Pyruvate Kinase M2
	PDEδ	Phosphodiesterase-δ
	PREX1	PtdIns(3,4,5)P3-dependent Rac exchanger 1
	PBS	Phosphate Buffered Saline
	PMSF	Phenylmethylsulfonyl Fluoride
	PVDF	Polyvinylidene Fluoride
	PE	Phycoerythrin
	PPR	Proton Production Rate
	PARP	Poly(ADP-ribose) Polymerase
	PDSS	Prenyldiphosphate Synthase, Subunit
	PI	Propidium Iodide
	PRKAG	Protein Kinase subunit Gamma-1
	PRKAA	Protein Kinase AMP-Activated Alpha catalytic subunit
	PRKAB	Protein Kinase, AMP-activated, Beta non-catalytic subunit
Q		
	qPCR	quantitative Polymerase Chain Reaction
R		
	RNA	Ribonucleic Acid
	RAF	Rapidly Accelerated Fibrosarcoma
	RUNX3	RUNX family transcription factor 3

	RTK	Receptor Tyrosine Kinase
	RON	Recepteur d'origine Nantais
	ROS	ROS proto-oncogene 1, receptor tyrosine kinase
	RBD	RAS Binding Domain
	RA	RAS association
	RSK	90 kDa ribosomal S6 kinase
	RALGDS	RAL guanine nucleotide dissociation stimulator
	RAL	RAS-like GTPases
	RALBP1	RAL binding protein 1
	RHOA	Ras Homolog family member A
	RB	Retinoblastoma
	RCE1	Ras-converting enzyme 1
	ROS	Reactive Oxygen Species
	RNAi	RNA-interference
	ROI	Region Of Interest
	RPKM	Reads Per Kilobase per Million
S		
	SMAD	Small Mothers Against Decapentaplegic
	SFRP	Secreted Frizzled-Related Protein
	SOCS1	Suppressor Of Cytokine Signaling 1
	SLC29A1	Solute Carrier family 29 member 1
	STAT-3	Signal Transducer and Activator of Transcription 3
	SV40	Simian Virus 40
	SOS	Son Of Sevenless
	S6K1	S6 Kinase 1
	SGK	Serum Glucocorticoid Kinase
	SOX	SRY-related HMG-box
	SOD1	Copper/zinc superoxide dismutase 1
	SSAO	Semicarbazide-Sensitive Amine Oxidase
	STEAP	Six-transmembrane Epithelial Antigen of the Prostate
	SCO 1/2	Synthesis of Cytochrome C Oxidase
	SRC	Spare Respiratory Capacity
	SEM	Standard Error of the Mean
	SiRNA	Small interference RNA
	ShRNA	Short hairpin RNA
	SDS	Sodium Dodecyl Sulfate
	SLB	Surfaceome Lysis Buffer
	SPRI	Solid-Phase Reversible Immobilization
T		
	TTM	Tetrathiomolybdate
	TSG	Tumor Suppressor Gene
	TNM	Tumor growth, lymph Nodes, metastases
	TGFβ	Tumor Growth Factor Beta
	TGFBR2	Tumor Growth Factor Beta Receptor 2
	TP53	Tumor protein 53
	TCF4	T-cell factor 4

	TCF7L2	Transcription factor 7-like 2
	TCF/LEF	T cell factor/lymphoid enhancer family
	TGN	Trans Golgi Network
	TEM	Transanal Endoscopic Microsurgery
	TNF	Tumor Necrosis Factor
	TIM-3	T cell immunoglobulin and mucin domain containing protein- 3
	TIE2	Tyrosine kinase with Immunoglobulin-like and EGF-like domains 2
	TSC	Tuberous Sclerosis Complex
	TIAM1	T lymphoma invasion and metastasis-inducing protein 1
	TWIST	Twist-related protein 1
	TCA	Tricarboxylic acid
	TFAM	Transcription factor A, Mitochondrial
	TSP	Thrombospodins
	TBK1	TANK-binding kinase 1
	TMS	Transmembrane Segments
	TCGA	The Cancer Genome Atlas
	Tln1	Talin-1
	TLR4	Toll Like Receptor 4
	TMR	Tetramethylrhodamine
U		
	UGT1A1	Uridine diphosphate GlucuronosylTransferase 1A1
	ULK1	Unc-51-like Kinase 1
	uPA	Urokinase Plasminogen Activator
	UQCC	Ubiquinol-cytochrome c reductase Complex Chaperone
	UQCRQ	Ubiquinol-Cytochrome C Reductase Complex III Subunit VII
	UBAP2L	Ubiquitin-Associated Protein 2-Like
V		
	VEGF	Vascular Endothelial Growth Factor
	VEGFR	Vascular Endothelial Growth Factor Receptor
	VAP-1	Vascular Adhesion Protein 1
	VS	VISiopharm score
W		
	WNT	Wingless-related integration site
	WT1	Wilms' tumor 1
X		
	XIAP	X-linked inhibitor of apoptosis protein
Z		
	ZEB1	Zinc finger E-box Binding homeobox 1
	Zn	Zinc

Chapter 1: Introduction

1.1 Cancer has a major impact on Canadian population

Cancer is the leading cause of mortality globally and ranked second highest in Canada, responsible for nearly 30% of all deaths (http://cancer.ca/Canadian-Cancer-Statistics-2019-EN, Canadian Cancer Society 2019). In 2018, nearly 181 million people were diagnosed with cancer, and a reported 9.6 million succumbed to the disease globally. The most frequently diagnosed cancers are the lung cancers, followed by breast and colorectal cancers. According to the 2020 projected estimates of Canadian Cancer statistics (Brenner et al., 2020), cancer-related mortality is expected to be the highest for lung cancers, followed by colorectal, pancreatic and breast cancers. Although the five-year survival rates and cancer incidence rates have reduced overall, largely due to better treatment options and early detection methods, people with lower economic status have comparatively worse outcomes. This is mainly attributed to a lack of access and affordability for advanced techniques (World Health, 2020). Given our increasing lifespans, economic progress in developing nations, amongst other contributing environmental and dietary factors, the number of cancer cases are expected to progressively rise in the upcoming years.

Several decades of research have shown that cancer is a complex and heterogeneous disease. Normal cell growth is tightly controlled by a network of signaling pathways that collectively ensure that cells proliferate only when needed. The myriad pathways and barriers that regulate cell homeostasis are disrupted in cancers. Hanahan and Weinberg in their seminal paper outlined the key disrupted processes or hallmarks in cancers: sustained proliferation, inactivation of tumor growth suppressors, increased cell survival, unchecked replicative potential, induction of metastasis and invasion, increased vasculature or angiogenesis, and increased energy metabolism (Hanahan & Weinberg, 2011). Ongoing research is continually uncovering new hallmarks that add to the complexities of cancer development such as evading the immune system, reprogramming energy metabolism and the influence of microenvironment in tumor growth. These features are acquired progressively by normal cells enabling them to progress to a neoplastic state. Acquisition of these hallmarks largely depend on myriad changes in the genomes of tumor cells. Multistep tumor progression can be visualized as several rounds of clonal expansions, each of which is marked by acquisition of a genetic event such as a mutation of a gene. Simply put, these genetic

phenotypes confer selective advantage and tumor-promoting properties to subclones of cells, causing them to outgrow and dominate over other cells in the tissue microenvironment. Majority of such genetic changes fall into two categories: gain-of-function mutations in proto-oncogenes that enable cancer cells to proliferate, survival and grow, whereas loss-of-function mutations in tumor suppressor genes (TSG) which normally prevent uncontrolled proliferation, and activate DNA repair and cell cycle checkpoint responses. Clonal expansions can also be triggered by non-mutational, epigenetic changes such as DNA methylation and histone modifications. In cancer cells, hypermethylation of promoters of many genes is frequently observed in the classical TSGs such as retinoblastoma (*RB*), breast cancer genes 1/2 (*BRCA1/2*) and phosphatase and tensin homology (*PTEN*), leading to transcriptional silencing and gene inactivation. Genetic and epigenetic events can also be inherited via the germinal cells, which underly development of familial cancers. While studying molecular mechanisms of inherited cancers, knudson first described the "second hit" hypothesis. Within cells that develop to tumors, there exists one functionally-inactive allele which could be inactivated due to a point mutation or any other mechanism, and the second wild-type allele will be subsequently inactivated by several mechanisms including but not restricted to mutations, loss of all or part of a chromosome, or homologous recombination events (Tischfield, 1997). This loss of heterozygosity (LOH) is widely accepted as the mechanism of completely turning off activity of TSGs. However, the presence of several LOH events at locations not known to contain TSGs suggests general chromosomal instability (CIN) in a tumor cell. Mis-segregation and chromosomal aneuploidy, marked by loss or rearrangements of chromosomes are considered to contribute to inactivation of TSG and acquisition of mutations, thereby contributing to cancer progression (Heng et al., 2013). In conclusion, several decades of cancer research have improved our understanding of the multiple cancer-promoting genomic events and hallmarks that contribute to the complexities of tumor progression. With the rise of new technologies such as clustered regularly interspaced short palindromic repeat (CRISPR)/Cas9 and single cell sequencing, the future of cancer research adds hope to our collective abilities to advance our understanding (with increased precision) of individual human cancers, and identify sophisticated therapeutic combinations to treat human cancers.

1.2 Colorectal cancers: a major cause of mortality in Canada

CRC is a class of solid tumors that accounts for ~12% of all newly diagnosed cancer cases in Canada and ~10% of global cancer cases. It is the second and third highest cause of cancer-related mortality in men and women, respectively, as of 2019 (http://cancer.ca/Canadian-Cancer-Statistics-2019-EN, Canadian Cancer Society 2019). The highest rates of CRC incidence are in developed countries. Both hereditary and environmental factors are attributed to the incidence of CRC. CRC is associated more with industrialized nations, suggesting a strong role for dietary and lifestyle factors including but not limited to alcohol, smoking, physical inactivity, obesity, and diets high in processed or red meats. In addition, individuals with chronic inflammatory bowel disease or ulcerative colitis have increased risk of CRC (Dekker, Tanis, Vleugels, Kasi, & Wallace, 2019). While the majority of tumors are sporadic, family history of CRC contributes to roughly 10-30% of all cases (Taylor, Burt, Williams, Haug, & Cannon–Albright, 2010). A portion of familial cases have common clinical features that indicate underlying Mendelian inheritance of cancer pre-disposing genes. A significant majority of highly penetrant CRC cases are hereditary nonpolyposis colorectal cancer (HNPCC), the familial adenomatous polyposis (FAP), juvenile polyposis syndrome and lynch syndromes (Fearon, 2011). The quest to identify the genetics of hereditary CRC has greatly contributed to the understanding of molecular events predisposing sporadic CRC such as the occurrence of genomic instability in majority of tumors. Prevalence of the disease is associated with age, the risk progressively increasing past 50 years of age for sporadic CRC, and around the third to fifth decade of life for hereditary CRC. Although better screening protocols and access to new therapeutic options have reduced incidence in developed countries, mortality is significantly higher for metastatic CRC (mCRC) cases. Nearly a quarter of newly diagnosed cases are metastatic, which are difficult to treat despite new advancements in surgery and chemotherapy. It is estimated that the incidence of CRC will increase to 2.5 million cases by 2035 in developing countries (Bray et al., 2018).

1.2.1 Progression of CRC is a multistep process

In the 1990s, Fearon and Vogelstein proposed a modified four step histopathological model for CRC progression, beginning with the transformation of epithelial crypt cells in the gastrointestinal tract to benign precursor lesions called adenomatous polyps. The cellular origin of the polyps are

debated and thought to be arising from stem cell-like precursors at the base of the crypt (Munro, Wickremesekera, Peng, Tan, & Itinteang, 2018). Crypts display an abnormal architecture with the polyps measuring ~5 mm and characterized by dysplastic morphology and dysregulated differentiation of epithelial cells (Fearon, 2011). Hereditary polyposis syndromes are easily identified by the presence of such polyps in large numbers. The polyps progress to form larger neoplastic lesions or adenomas and further to an *in-situ* carcinoma over a period of 10-15 years. This process is accelerated in hereditary lynch syndromes which display frequent alterations in mismatch repair genes (MMR). Ultimately, the tumor proceeds to become metastatic and invasive carcinomas.

Once diagnosis is made, the stage of CRC progression is determined according to the american joint committee on cancer (AJCC) TNM system, which takes into account the extent of tumor growth (T) through the wall of the colon or rectum, spread to the nearby lymph nodes (N), and spread to distant sites or metastases (M) (https://www.cancer.org/cancer/colon-rectal-cancer/detection-diagnosis-staging/staged.html). The stages are roughly described as follows: Stage 0 is the beginning stage where the "*in situ*" tumor has not grown beyond the inner mucosal layer of colon or rectum. Stage I has grown through the mucosal and submucosal layers or muscularis propria but not spread to the lymph nodes. Stage IIA has grown through the outermost layers of colon or rectum but not yet spread to the nearby tissues or lymph nodes. Stage IIB the tumor has grown to the lining of the abdomen, whereas in stage IIC the tumor has spread beyond the lining to nearby tissues and may or may not have spread to a few lymph node regions. In stage IIIA the tumor has spread to a few lymph nodes or to the area adjacent to the lymph nodes, but not yet grown into nearby organs or distant sites. Stage IIIB is characterized by tumor growth through the bowel wall, to nearby organs, and several lymph nodes. At stage IIIC, the tumor has spread to several lymph nodes, and nearby organs or tissues but not distant regions. The IV stage is characterized by metastases: Stage IVA has spread to a distant organ such as liver or lung (two most common sites), whereas stage IVB is spread to several distant organs, and further to distant parts of peritoneum (lining of abdominal cavity) in the stage IVC. The 5-year survival is directly

correlated with the stage of tumor, ranging from 90% survival rates early in the disease to reduced rates of 7% at later stages of metastasis (Weitz et al., 2005).

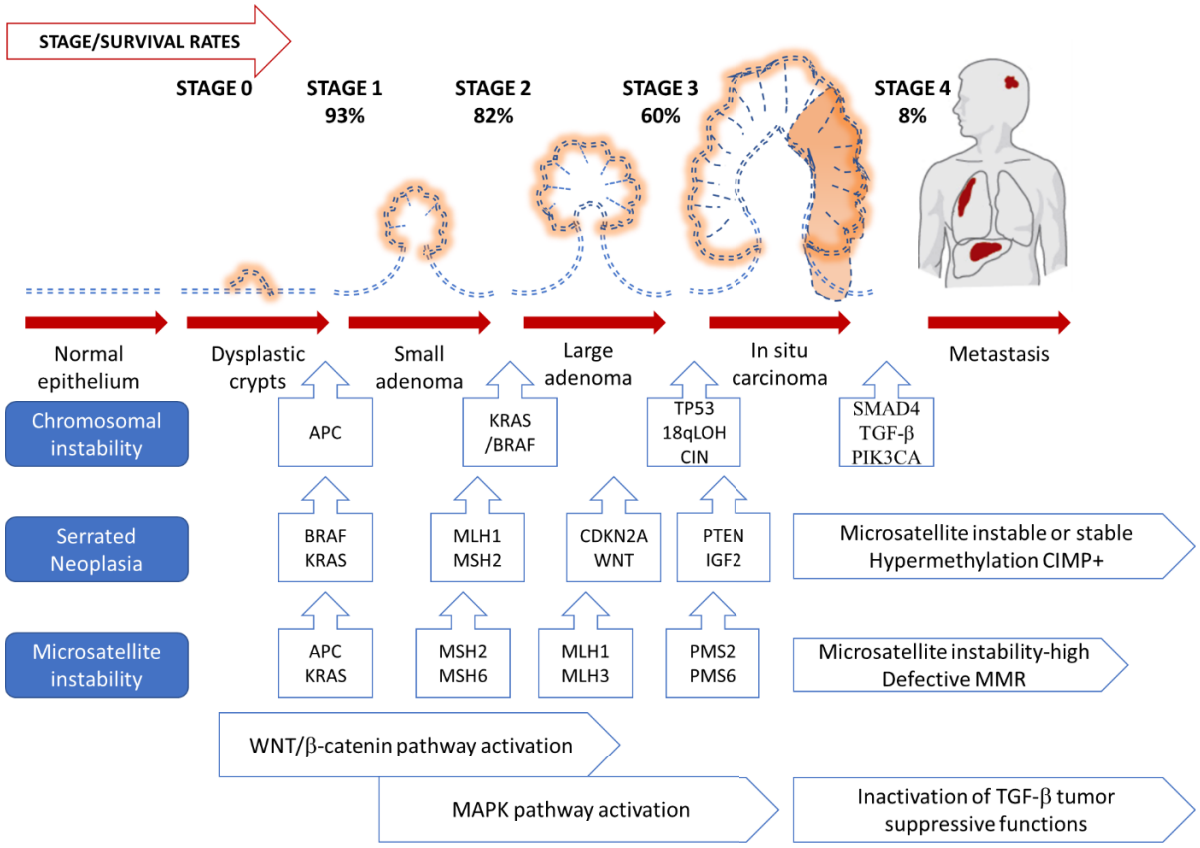

Figure 1.1. Models of CRC pathogenesis

Depiction of progressive degree of growth (red arrows) of adenomas and intestinal neoplasia to carcinoma and metastasis. Average 5-year survival rates of patients during diagnosis, according to the clinical stage is indicated at the top. The most common genetic and epigenetic alterations (squared box with arrows), and the three classical genomic instability pathways (blue rectangles) that underlie CRC tumor progression are indicated. The most common genetic/epigenetic alternations belong to the MAPK, WNT or TGF-β cell signaling pathways.

1.2.2 The three classical genetic classifications of CRC

CRC is a highly heterogeneous disease with many subtypes associated with somewhat distinct and sequential combinations of genetic and epigenetic aberrations in cancer-related genes that lead to overall genomic instability (Dekker et al., 2019; Fearon, 2011). The order of accumulation of these genomic aberrations in CRC progression is not random. Thus far, there is a general consensus on three different pathogenic models for CRC progression which are as follows: traditional or

chromosomal instability pathway accounting for the majority of CRC cases, a serrated neoplasia pathway accounting for ~10-20% cases, and ~7-15% of cases are classified under a microsatellite stability model (Dekker et al., 2019). Typically, one of the genomic instability pathways predominates in the tumor, however, CpG island methylator phenotype (CIMP) and microsatellite instability (MSI) phenotypes can overlap due to shared defects in MMR genes.

The traditional pathway includes progression of both hereditary and sporadic cases (Dekker et al., 2019; Fearon, 2011). Loss of activity of the tumor suppressor gene adenomatous polyposis coli (*APC)* that disrupts the wingless-related integration site (WNT)/*β*-catenin pathway is a major initial step and detected in early lesions. Approximately 70-80% of sporadic tumors harbor mutations in the APC pathway. Kirsten rat sarcoma (*KRAS*) or B rapidly accelerated fibrosarcoma (*BRAF*) oncogenic mutations occur frequently at early stages of adenoma formation and in a mutually exclusive manner. Loss of tumor suppressor p53 function and/or LOH of chromosome 18 occur at the later stages of carcinoma. In addition, mutations in phosphatidylinositol-4,5-bisphosphate 3-kinase catalytic subunit alpha (*PIK3CA*), small mothers against decapentaplegic 4 (*SMAD4*), and transforming growth factor beta receptor (*TGFBR*) genes, are also associated with the later stages of CRC progression. Although the order of gene defects can vary, the above-mentioned gene mutations are frequently associated with certain stages of CRC progression. Another characteristic trait of this CRC subtype is the CIN phenotype, occurring in ~60% of CRC. It is predominantly associated with *APC* mutations in early stages of progression. CIN positive tumors are associated with gene duplications, LOH at the loci of TSG, aneuploidy and chromosomal arrangements. Some recurring features include loss of chromosome 18q [which contains the tumor suppressor gene deleted in colorectal cancer (*DCC*)], loss of 17p, allelic deletions in chromosome 5q, as well as gains of chromosomes 8, 13 and 20. Additionally, CIN tumors have DNA copy number variations resulting in amplifications of myelocytomatosis viral oncogene homologue (*MYC*), epidermal growth factor receptor (*EGFR*), insulin receptor substrate 2 (*IRS2*) and homozygous deletions of tumor protein 53 (*TP53*), *PTEN*, *SMAD2* genes (Leary et al., 2008). While key factors that underlie CIN are poorly defined, genetic defects in genes involved in chromosomal segregation and mitotic spindle formation such as mitotic arrest deficient 2 (Mad2), budding uninhibited by benzimidazole-related 1 (BubR1), budding uninhibited by

benzimidazole 3 (Bub3), and centromere-associated protein E (CENPE) proteins have been suggested to contribute this phenotype.

The serrated neoplasia pathway is associated with a *RAS* or *BRAF* mutation in early lesions, and the latter is very common in CIMP tumors (Dekker et al., 2019; Ijspeert, Vermeulen, Meijer, & Dekker, 2015; Oikonomou, Koustas, Goulielmaki, & Pintzas, 2014). CIMP is a characteristic feature of this pathway, referring to the hypermethylation patterns at multiple loci enriched in CpG motifs. Promoters of ~50% of all genes have many cytosine-guanosine nucleosides called CpG motif-rich islands. At motifs containing the CpG dinucleotide sequence, a methyl group can be added to the 5' end of cytosine, serving as a recognition site for methyl-binding proteins. Analysis of methylation loci markers allows further classification of tumors to three epigenotypes as CIMP-high, CIMP-low and non-CIMP. In CRC, hypermethylation of CpG islands compared to normal tissues is common. CRC is also associated with unique, tumor-specific methylation patterns especially in several putative TSGs. This is likely associated with transcriptional repression and gene silencing (Esteller, 2002). Hypermethylation and loss of function of the MMR gene mutL homolog 1 (*MLH1*) is a frequent occurrence in sporadic and hereditary CRC. Some other methylation-prone gene loci include cyclin-dependent kinase inhibitor 2A (*CDKN2A*) (p16), *PTEN*, hypermethylated in cancer 1 (*HIC1*), secreted frizzled-related protein (*SFRP*), insulin-like growth factor 2 (*IGF2*), neurogenin 1 (*NEUROG1*), RUNX family transcription factor 3 (*RUNX3*), and suppressor of cytokine signaling 1 (*SOCS1*) (Tse, Jenkins, Chionh, & Mariadason, 2017). While methylation patterns are associated with loss of function of select TSGs in CRC, we still do not know if other "methylated in tumor" loci contribute functionally to CRC progression. Conversely, ~10-40% CRC cells have global reductions in methylation within the long interspersed nuclear element-1 (LINE-1) and ALU repeat sequences or chromosomal pericentric sequences. The functional contribution of hypomethylation *versus* hypermethylation in CRC progression is less clear. It is proposed that hypomethylation at these regions contributes to genomic stability by likely activating transposon activity, affecting chromosome segregation, or leading to loss of imprinting of key genes that regulate cellular processes.

Finally, MSI tumors have a significantly high mutational burden compared to other tumor subtypes. They have relatively distinct features including lymphocyte infiltration, mucinous or

signet ring appearance and are located at the proximal colon (De' Angelis et al., 2018). MSI is associated with both sporadic tumors (~12-17% of CRC) and the hereditary Lynch syndromes (~3% of CRC). It is characterized by deletions and, less commonly, amplifications in the microsatellite repeat tracks of DNA. If tumors display >30% variation in microsatellite lengths of a panel of mononucleotide and dinucleotide sequences they are termed high frequency MSI (MSI-H) and are otherwise classified as MSI-low (MSI-L) or microsatellite-stable (MSS). A well-defined phenotype of this pathway are mutations or large deletions in sequences that inactivate DNA-mismatch repair MMR genes such as mutS homolog 2 (*MSH2*), *MLH1,* post meiotic segregation increased 1 (*PMS1*), *PMS2*, and *MSH6*. Notably, the majority of sporadic CRC have lost expression of *MLH1* and *PMS2* genes. Defective MMR genes will be unable to correct mistakes in the error-prone genomic regions with microsatellite repeats further contributing to the MSI phenotype. Other TSGs such as *TGFBR2,* activin receptor type 2 (*ACVR2*), Bcl-2-associated X protein (*BAX*), T-cell factor 4 (*TCF4*), etc., have been reported to be transcriptionally silenced in CRC via this mechanism (Boland & Goel, 2010). MSI-H sporadic tumors are also often associated with oncogenic *BRAF* mutations and have better prognosis that CIN+ or MSS-CRCs for reasons that are not yet clear. Despite the progress in defining the common genetic and epigenetic alterations in CRC pathogenesis, we still lack understanding of clinically and molecular distinct subsets of CRC besides the three main types described above. With further research more oncogenes and TSG that drive other distinct CRC subsets remains to be identified.

1.2.3 Most common gene defects driving CRC pathogenies

Mutation is a stable, irreversible change in DNA sequence. They are of two types- gain-of-function mutations that lead to activation of oncogenes, and loss-of-function mutations that inactivate TSGs. A point mutation is a single-base change, which in the case of missense mutations can lead to coding of different amino acids, while a nonsense mutation inserts a premature termination codon. Silent mutations do not induce amino acid changes but rather affect gene transcription. Insertions or deletions of nucleotides (not divisible by three) can affect the reading frame causing a frameshift mutation and truncated protein products. **Table 1** below summarizes the major germline and somatic mutations that are associated with CRC progression (Fearon, 2011). Some of the major pathways that these genes belong to are also discussed below.

Table 1.1 Most common genetic alterations in oncogenes and tumor suppressor genes (TSG) that drive CRC pathogenesis. (adapted from (Fearon, 2011)**).**

GENE	TYPE OF MUTATION	FREQUENCY	TYPE OF CRC
ONCOGENES			
KRAS	Point mutation (codons 12, 13, 61)	>40%	Sporadic
NRAS (neuroblastoma rat viral oncogene homologue)	Point mutation (codons 12, 13, 61)	<5%	Sporadic
PIK3CA	Point mutation	15-25%	Sporadic
BRAF	Point mutation (*V600E)*	5-10%	Sporadic, MSI-H tumors
EGFR	Gene amplification	5-15%	Sporadic
MYC	Gene amplification	5-10%	Sporadic
CDK8 (cyclin-dependent kinase 8)	Gene amplification	10-15%	Sporadic
CTNNB1 (catenin beta 1)	Point mutation, deletions	<5%	Sporadic
CCNE1 (cyclin E1)	Gene amplification	5%	Sporadic
TUMOR SUPPRESSOR GENES			
APC	Frameshift, point mutation, deletion, LOH	>70%	Sporadic, FAP
MSH2, MLH1	Epigenetic modification, germline mutations	70%	HNPCC
TP53	Point mutation, LOH	70%	Sporadic

FBXW7 (F-box and WD repeat domain-containing 7)	Point mutations	20%	Sporadic
PTEN	Point mutations	10%	Sporadic, juvenile polyposis syndrome
SMAD4	Point mutations, LOH	10-15%	Sporadic, juvenile polyposis syndrome
SMAD2	Point mutations, LOH	5-10%	Sporadic
TGFBR2	Point mutation, frameshift	25%	Sporadic, >90% MSI-H CRC
ACVR2	Frameshift	-	Sporadic, >80% MSI-H CRC

1.2.3.1 WNT pathway in CRC

Constitutive ligand-independent activation of the WNT signaling pathway via *APC*, axis inhibition protein 2 (*AXIN2*), β-catenin (*CTNNB1*), and transcription factor 7-like 2 (*TCF7L2*) mutations is a frequent occurrence in sporadic and hereditary CRC. Notably, *APC* mutations occur in ~70-80% of sporadic CRC. The importance of APC in adenoma development is highlighted by a $Apc^{Min/+}$ mouse model that develops intestinal polyps due to a heterozygous mutation in *Apc* (Moser, Pitot, & Dove, 1990). APC is part of Axin protein complex consisting of AXIN, casein kinase 1 (CK1) and glycogen synthase kinase-3β (GSK3β) that lead to degradation of β-catenin levels, in the absence of WNT ligands. WNT/β-catenin pathway is activated when WNT ligands bind to frizzled (Fz) receptor and co-receptor low-density lipoprotein receptor related protein (LRP). AXIN complex is recruited to the activated receptors, stabilizing β-catenin levels. In CRC, mutations that lead to a loss of APC or AXIN function, or stabilizing mutations in the phosphorylation and ubiquitin-mediated degradation motifs of β-catenin, cause the accumulation of β-catenin levels which usually happens in response to WNT ligands. β-catenin then translocates to the nucleus and associates with DNA-binding proteins from the family of T cell factor/lymphoid enhancer family (TCF/LEF), driving transcription of genes involved in survival, proliferation and adhesion

(Kolligs, Bommer, & Göke, 2002). The WNT pathway is essential for maintenance of intestinal stem cells, regulating tissue organization, patterning, and regeneration of crypts. Intestinal stem cells called crypt-base columnar cells (CBCs) divide continuously to form rapidly proliferating crypt cells to regenerate the epithelium (Beumer & Clevers, 2016). Inactivating mutations in *TCF7L2* prevent the formation of proliferative crypts (Basu, Haase, & Ben-Ze'ev, 2016). However, the importance of β-catenin signaling in CRC is highlighted by two schools of thought that suggest that CRC either arises from differentiated epithelial cells that acquire stem cell-like features (Schwitalla et al., 2013), or by increased proliferation of crypt stem cells due to accumulation of nuclear β-catenin (Barker et al., 2009). Nearly, 70-80% CRC have defects in the WNT pathway, highlighting its importance in tumorigenesis and therapeutic targeting of CRC. Given the frequency of *APC* mutations in CRC, it is argued that APC plays a gatekeeper role in normal colorectal epithelial cells (Fearon, 2011; Kolligs et al., 2002).

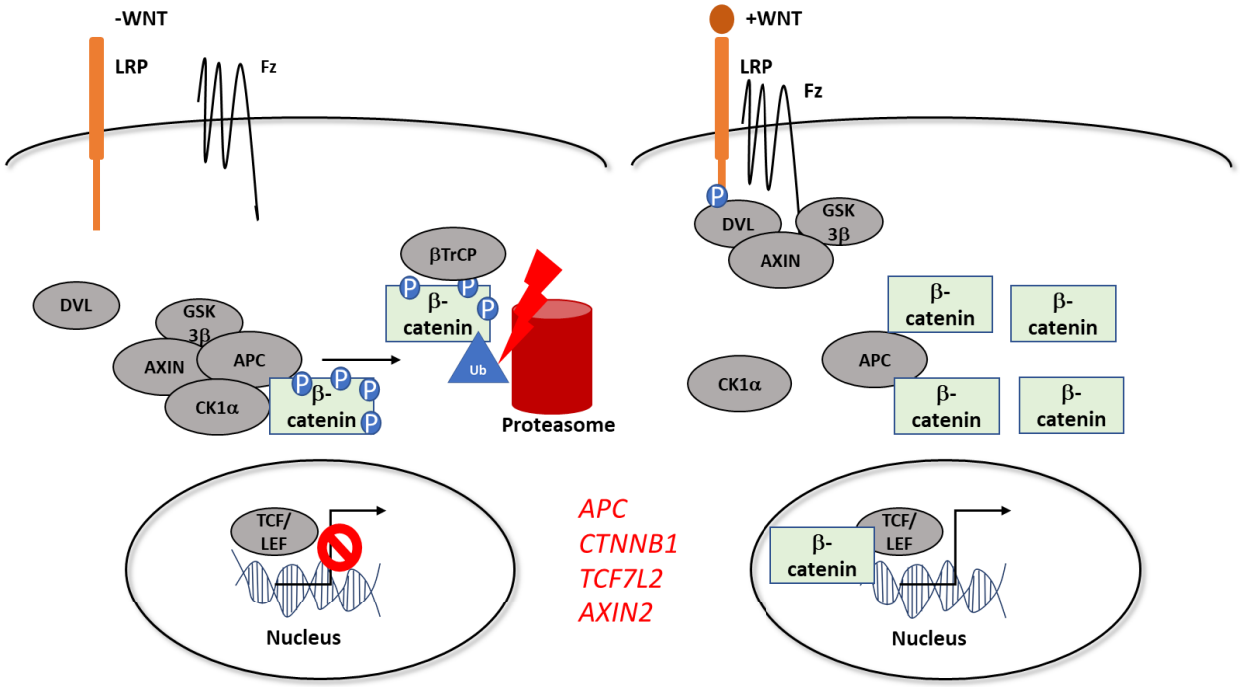

Figure 1.2. Model of WNT pathway activation

In cells not stimulated by WNT ligands (-WNT), APC is part of the β-catenin destruction complex along with AXIN, GSK3β, and CK1α. This complex phosphorylates (P) β-catenin at conserved serine and threonine residues at the N-terminus. This phosphorylation is recognized by the F-box protein β-transducin repeat–containing protein (βTrCP) as part of a ubiquitin ligase complex, which leads to polyubiquitination of β-catenin and its subsequent proteasomal degradation. Thus,

levels of β-catenin are tightly regulated in absence of WNT pathway activation, and transcription of TCF/LEF target genes is kept repressed. Binding of WNT ligands (+WNT) to cognate receptor complex consisting of LRP and Fz inhibits the destruction complex, partly due to the recruitment of AXIN to the receptor complex, and partly due to the action of dishevled (DVL) on GSK3β. Consequently, β-catenin protein levels accumulate and translocate to the nucleus, which activates transcription of TCF/LEF target genes. Genes depicted in red are components of the pathway that when mutated in CRC lead to constitutive ligand-independent activation of WNT pathway.

1.2.3.2 MAPK pathway in CRC

The mitogen activated protein kinase (MAPK) pathway is involved in several cellular functions such as proliferation, survival, invasion, differentiation, and adhesion (Fang & Richardson, 2005). Mutations in *KRAS*, *NRAS*, *BRAF*, and *EGFR* lead to the constitutive activation of the MAPK pathway in cancers. An upstream activator of MAPK signaling is the receptor tyrosine kinase (RTK) epidermal growth factor receptor (EGFR), which is activated by its ligand EGF. Activation of EGFR leads to activation of the small GTPase protein RAS, which in turn leads to the recruitment and activation of RAF kinase. This initiates the downstream MAPK signaling cascade via activation of multiple substrates including mitogen-activated protein kinases (MEK1 and MEK2), extracellular signal-regulated kinases (ERK1 and ERK2) and 90kDa ribosomal S6 kinases (RSK) (Roux & Blenis, 2004). EGFR is an important player in CRC progression, as EGF induces the proliferation and inhibits apoptosis of intestinal cells and is also required for the regeneration of intestinal stem cells after injury (Jiang, Grenley, Bravo, Blumhagen, & Edgar, 2011). Overexpression of EGFR or somatic mutations that activate EGFR signaling are associated with a small fraction of CRC. *EGFR* mutations most frequently occur in the kinase domain and lead to constitutive activation of downstream signaling in the absence of ligand (AF Gazdar, 2009). The majority of CRC tumors are associated with mutations in *RAS* isoforms- *KRAS* and *NRAS*, and the *RAF* isoform- *BRAF* (Costigan & Dong, 2020). *In vivo* $Apc^{Min/+}$ mice models expressing wild-type or the oncogenic variant $Kras^{G12V}$ resulted in a rapid increase in intestinal neoplasia formation (Sansom et al., 2006), highlighting the importance of KRAS in the adenoma-carcinoma sequence. Somatic mutations in codon 600 of *BRAF* turn on its kinase activity, which leads to constitutive phosphorylation and activation of its substrates MEK1 and MEK2. Interestingly, expression of constitutively active MEK1 and MEK2 in rat intestinal epithelial cells (IEC-6) results in increased proliferation, resistance to anoikis *in vitro* and tumor development *in vivo* (Voisin et al., 2008),

suggesting that MEK activation was sufficient to transform IEC. The MAPK pathway is a crucial driver of CRC tumorigenesis, biological implications of this pathway in CRC is discussed in detail a later chapter.

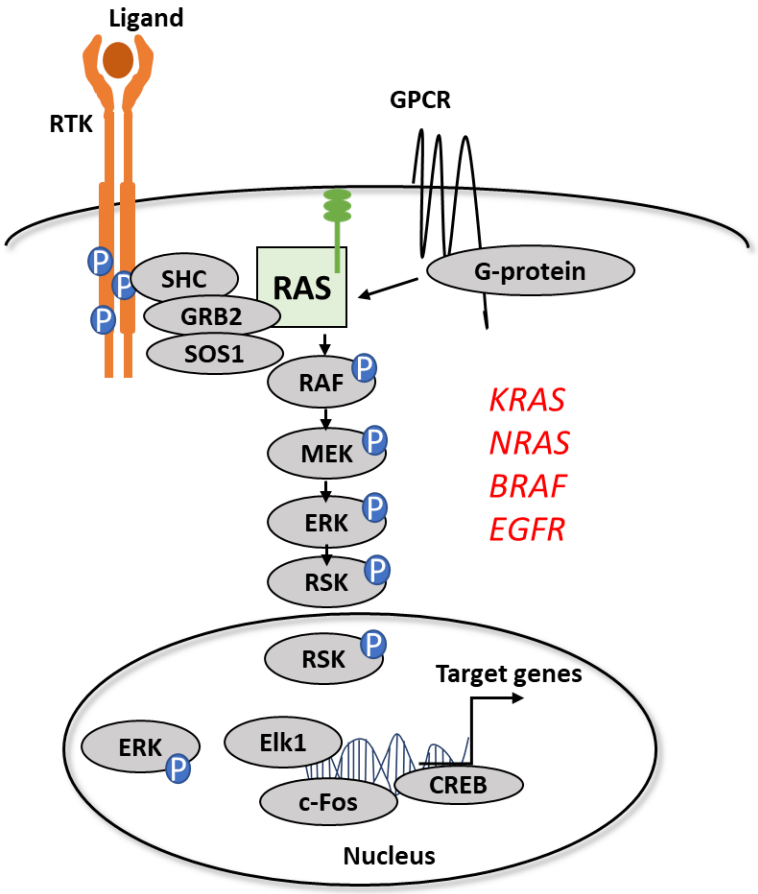

Figure 1.3. Model of MAPK pathway activation

Binding of RTK such as EGFR to ligands such as EGF results in autophosphorylation of the tyrosine residues on the intracellular side of receptor. Docking proteins such as GRB2 bind to the phosphorylated (P) tyrosine residues via its SH2 domain and recruits the RAS-guanine exchange factor SOS1 via its SH3 domain. SOS1 is now at proximity to membrane locates RAS and activates RAS by mediating the exchange of GDP to GTP. Active RAS then binds RAF via the RAS-binding and cysteine-rich domains, which results in recruitment of RAF to the plasma membrane. RAF is then activated by phosphorylation at multiple residues. MEK1 and MEK2 kinases are bonafide substrates of RAF, and ERK1 and ERK2 are substrates of MEK kinases. Activated ERK translocate to the nucleus where it phosphorylates and activates several transcription factors such as c-Fos and Elk1. ERK also phosphorylates several cytoplasmic substrates including the well-known RSK kinases. Like ERK, phosphorylated RSK can translocate to the nucleus and activate several transcription factors such as CREB. Genes depicted in red are components of the pathway that when mutated in CRC lead to constitutive ligand-independent activation of MAPK pathway.

1.2.3.3 TGF pathway in CRC

TGF-β along with activin and bone morphogenetic protein (BMP) ligands bind their cognate receptor families TGFβR1/2, ACVR1, BMPR1, etc., wherein downstream signaling is activated following phosphorylation of SMADs (Bellam & Pasche, 2010). The TGF superfamily has broad tumor-promoting roles including regulation of tissue homeostasis, embryogenesis, evasion of immune system, invasion, and angiogenesis. Microenvironments rich in TGF-β are associated with poor prognosis, increased tumor vascularization and metastasis. Paradoxically, TGF-β also inhibits cellular proliferation. *In vivo* loss of Tgfbr2 in a conditional knockout mice, increased the number and pathology of colorectal neoplasia suggesting a tumor-suppressive role in CRC progression (Biswas et al., 2004). Germline mutations in *SMAD4* and *BMPR1A* involved in the TGF-β pathway are commonly associated with juvenile polyposis syndrome while somatic mutations in *SMAD2*, *SMAD3*, *SMAD4*, *TGFβIIR*, and *ACVR2* are associated with sporadic CRC. Mutations in *TGFβIIR* is the most common way to turn off TGFβ signaling (~20-30% CRC), primarily through frameshift mutations in the microsatellite sequences. SMAD2 and SMAD4 (also known as DCC) are localized to chromosome 18q region that is frequently deleted in CRC. Similar to Tgfbr2 conditional knockout mice, loss of Smad4 or Smad3 enhances intestinal tumorigenesis when crossed with $Apc^{Min/+}$ mice (Sodir et al., 2006; Takaku et al., 1998). Notably, phosphorylated-SMAD1/5/8 expression was observed in ~70% of sporadic CRC cases (Kodach et al., 2008). In conclusion, several signaling pathways have been well studied in the context of CRC pathogenesis, and genes belonging to these pathways are frequently mutated in CRC tumors.

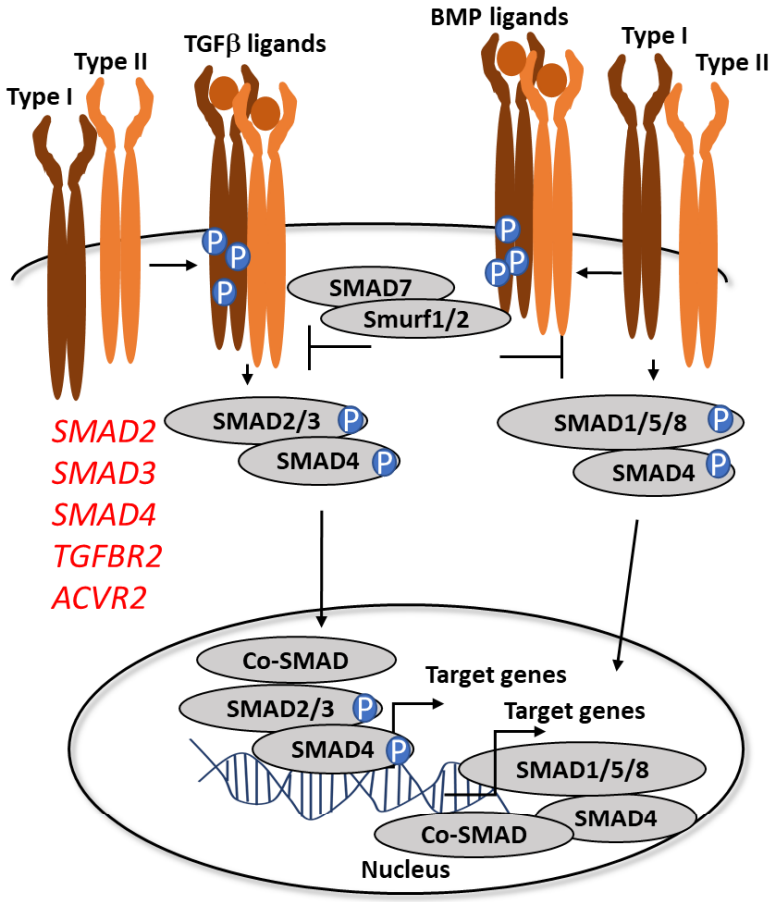

Figure 1.4. Model of TGFβ pathway activation

TGFβ superfamily ligands such as TGFβ, BMP, activin, exert their effects via heterotetrameric complexes comprising of type 1 and type 2 receptors. Upon ligand binding, type 2 phosphorylates (P) type 1, which initiates a phosphorylation cascade of downstream SMAD proteins. TGFBR1, ACVR1B, and ACVR1C receptors phosphorylate SMAD2 and SMAD3, whereas ACVRL1, ACVR1, BMPR1A, and BMPR1B receptors phosphorylate SMAD1, SMAD5, and SMAD8. Once phosphorylated these SMADs transduce the signal to the nucleus along with SMAD4. The SMAD4-SMAD complexes associate with other DNA-binding cofactors (co-SMAD) to transcriptionally activate or repress target genes. The inhibitory SMADs, SMAD6 and SMAD7, recruit E3 ubiquitin ligase SMURF1/2 to the receptor complexes to degrade them. Genes depicted in red are components of the pathway that when mutated in CRC lead to constitutive ligand-independent activation of TGFβ pathway.

1.2.4 Current standards of care and recent advancements in therapeutic targeting of CRC

Early diagnosis is required for full recovery, and this has largely improved by implementing early screening programs in Canada and worldwide. Advances in primary and advanced CRC treatment has significantly improved survival in developed countries. Treatment of CRC depends on the clinical stage and involves different therapeutic arms such as surgery, chemotherapy, radiotherapy, immunotherapy and targeted therapy, as outlined below. Identification of molecular subtypes helps to predict patient subgroups that do not respond to certain treatments and customize therapeutic combinations. Systemic approaches are no longer being considered as "one size fits all", and tumor-specific predictive markers are necessary to optimize therapy for each patient. The choice of palliative and adjuvant chemotherapeutic regimens should take into consideration the associated toxicity profiles, comorbidity, affordability and cost of treatment, risks to underlying diseases and quality of life.

1.2.4.1 Surgery is a central tenant of CRC therapy

In early stages, as the polyp is localized to inner layers, surgical removal can provide complete disease control. Incidence of this early low-risk CRC that can be treated with surgery has increased largely due to better screening programs (Dekker et al., 2019). Both small and large polyps can be resected (polypectomy) via transanal excision by endoscopic techniques limited to the mucosal, submucosal layers or full-section resection. Lesions with high grade invasion that have increased risk of lymph node metastasis must be operated via open surgical techniques such as total mesorectal excision, which has been the most successful approach for rectal cancer and has reduced recurrence rates significantly. The extent of resection depends on the location and stage of the tumor (Daaboul & El-Sibai, 2018). Techniques such as minimally invasive transanal endoscopic microsurgery (TEM) with robot-assisted laproscopy is used for small tumors in low-risk stage I CRC. In case of bigger and distant tumors for high-risk stage I, some stage II and III cancers, sections of rectum or entire rectum (protectomy), or colon (colectomy) are removed with adjacent lymph nodes and surrounding tissues. For stages II-IV, chemoradiation is often given to shrink the size of tumors before surgery. Downsizing of tumors is possible in most patients but only ~15% achieve complete response. If the tumor has spread to nearby organs, removal of entire

affected areas of rectum or colon and nearby organs such as prostate, bladder or uterus is recommended. After surgery, post-operative chemotherapy with standard regimen of oxaliplatin and fluoropyrimidines is recommended for high risk cancer to reduce recurrence and metastasis. Recurrence after curative surgery majorly affects survival in CRC. A 16 year study followed 188 patients who underwent surgery for rectal adenocarcinoma, 53 patients developed disease again with staggering 44.6% recurrence rates at 5 years (Farhat et al., 2019). In case of locally recurrent metastatic disease with resectable tumors, surgery followed by chemotherapy is standard of care. For patients with unresectable metastatic tumors, the goal is maximum shrinkage of tumors with systemic radio- or chemotherapy followed by surgery if successful. Unfortunately, many of the late-stage metastasis cannot be treated with surgery, so systemic chemotherapy is only used to prolong survival (Punt, Koopman, & Vermeulen, 2017).

1.2.4.2 Chemotherapy and radiotherapy are widely used in CRC

Neoadjuvant (pre-operative) and adjuvant (post-operative) radiotherapy or chemotherapy or a combination of both is standard of care for stage II and stage III CRC. Radiotherapy is frequently used before surgery to downsize tumor staging with standard doses of 45-50 gray in 25-28 fractions. A Dutch study experimented with reducing this dose as it is associated with toxicity and achieved success with short-course radiotherapy of 5 gray in 5 fractions along with total mesorectal excision. Radiotherapy has been successful in reducing local recurrence and improving survival rates in low risk, resectable stage II and stage III cancers (Glynne-Jones et al., 2017; Kapiteijn et al., 2001; Sauer et al., 2004). Chemotherapeutic fluoropyrimidines (5-Fluorouracil or capecitabine) are used concomitantly as a radiation sensitizer. Chemotherapy agents approved in CRC include the single agent fluoropyrimidines, which remains a backbone in CRC, along with different combinations of irinotecan, oxaliplatin, and trifluridine/ tipiracil. Chemotherapeutic agents are chemical drugs that inhibit the proliferation of cancer cells (and normal cells) including but not limiting to DNA-damaging drugs, competitive analogues of natural building blocks of RNA and DNA, topoisomerase inhibitors, mitotic inhibitors and corticosteroids, etc. Irinotecan inhibits topoisomerase I enzyme leading to DNA damage, while oxaliplatin and cisplatin form DNA-adducts that block replication and transcription. Fluoropyrimidines affect purine and

pyrimidine synthesis, and cause DNA fragmentation by inhibiting thymidylate synthase and resulting in the misincorporation of nucleotides in the DNA (Thorn et al., 2011).

Use of adjuvant chemotherapy with radiotherapy and/or antibody therapy is routinely recommended for high-risk stage III cancers along with surgery. Although less successful, this combination is also considered for high-risk stage II with lymphovascular invasion and obstructive tumors (Dekker et al., 2019). Palliative chemotherapy is opted when tumors cannot be removed and mainly serves to increase lifespan and quality of life for late stage CRC. Systemic treatment of mCRC includes several lines of chemotherapy in combination with anti-vascular endothelial growth factor (VEGF) /epidermal growth factor (EGF) biologics. Importantly, for ~15% of patients with unresectable liver metastasis, adjuvant chemotherapy can downsize the tumor and render it resectable. This is important as patients with resected metastasis have increased 5 year survival rates (~58%) (Fernandez et al., 2004). Combination of radiation with oxaliplatin and capecitabine was successful in downstaging tumors in stage II CRC (Rödel et al., 2003). Multicenter international study of oxaliplatin/ 5FU-LV in the adjuvant treatment of colon cancer (MOSAIC) study suggested that addition of post-operative oxaliplatin to fluoropyrimidines greatly improved disease-free survival for stage III CRC (André et al., 2009). A study analyzing the outcomes of several clinical trials comparing irinotecan as monotherapy or in combination with fluoropyrimidines reported increased progression-free survival (PFS) and overall survival (OS) in patients with advanced CRC. But no difference was observed between the benefits of irinotecan as monotherapy versus combination therapy (Wulaningsih et al., 2016). Nevertheless, these new chemotherapeutic regimens have increased median survival time to 20 months *versus* 7 months with fluoropyrimidines alone, with treatment response rates ranging between 39% to 55% (Goldberg et al., 2004; Weitz et al., 2005). However, adjuvant chemotherapy must be catered to patient-specific and disease-specific markers. For example, stage II MSI-high tumors do not benefit from adjuvant chemotherapy. Moreover, the predictive value for chemotherapy in stage III MSI colon cancer is arguable and needs further validation. Additionally, patients with stage III MSI tumors are recommended oxaliplatin-based chemotherapy as some studies have demonstrated a lack of benefit from fluoropyrimidine monotherapy (Kawakami, Zaanan, & Sinicrope, 2015).

Unfortunately, only a fraction of CRC patients respond to systemic chemotherapy and there is frequent recurrence (Punt et al., 2017). More studies are needed to better assess biomarkers that can predict the innate and acquired resistance mechanisms. Expression of *TP53* gene and transporters such as SLC29A1, ATP-binding cassette sub-family genes (*ABCG2* and *ABCC3*) are associated with drug resistance to 5-fluorouracil (Thorn et al., 2011). Genetic variants with decreased activity of two enzymes Uridine diphosphate GlucuronosylTransferase 1A1 (UGT1A1) and DPD (dihydropyrimidine dehydrogenase) that are involved in metabolism of irinotecan and 5-fluorouracil, are being clinically investigated for increased toxicity to chemotherapy (Falvella et al., 2015). Chemotherapy is also associated with significant side effects; particularly addition of oxaliplatin increases the development of sensory neuropathy, myelosuppression and gastrointestinal toxicities. Studies have tried to limit toxicity, including 3 months with oxaliplatin-based regimen, which was shown to be as effective as the standard 6 months in stage III CRC (Ramos-Esquivel, 2018). Therefore, while there is an added benefit to patients with chemotherapy, reassessment of current criteria for selection of patients and better predictive biomarkers are needed to increase its efficacy and improve patient well-being.

1.2.4.3 Anti-EGFR and VEGF are the only approved targeted therapies for CRC

Targeted therapy can work by directly affecting tumor-promoting factors such as proliferation, immune evasion, angiogenesis, survival, etc. Various pathways are attractive targets for targeted therapy in CRC, including TGF-β/SMAD, EGF/EGFR, VEGF, WNT/β-catenin, hepatocyte growth factor (HGF)/ hepatocyte growth factor receptor (c-MET/HGFR), Notch, IGF/IGFR, etc., (Y. H. Xie, Chen, & Fang, 2020). In addition, targeted inhibition of the RAS/RAF/MEK and PI3K/AKT/MTOR pathways are widely being analyzed in preclinical and clinical studies for CRC. Small molecules, such as kinase inhibitors, proteasome inhibitors, and adenosine triphosphate (ATP)-competitive inhibitors, target specific intracellular molecules within cells. For targets on the extracellular cell surface, monoclonal antibodies or therapeutic antibodies successfully inhibit their expression and/or activity. The first food and drug administration (FDA)-approved CRC targeted therapies were the monoclonal antibodies cetuximab and bevacizumab, that target EGFR and VEGF, respectively. The benefit for adjuvant chemotherapy is enhanced by addition of anti-

EGFR or anti-VEGF therapies in the mCRC setting, based on tumor-specific and patient-specific factors such as those outlined below.

Receptor tyrosine kinases such as the EGFR are overexpressed in many cancers including lung, colorectal and breast (Y. H. Xie et al., 2020). EGFR contains a ligand-binding site on the extracellular surface, a transmembrane domain, and an intracellular domain through which it initiates a signaling cascade that activates mediators such as RAS-RAF, PI3K-AKT, phospholipase C-γ (PLC-γ), signal transducer and activator of transcription 3 (STAT-3), etc. EGFR signaling pathway is linked to myriad cellular functions such as proliferation, autophagy, metabolism, metastasis, motility, etc. Cetuximab binds to the extracellular domain of EGFR, thereby inhibiting ligand binding, inducing rapid internalization and degradation of the receptor-antibody complex (Okada et al., 2017). Cetuximab increased the PFS when administered with chemotherapy in mCRC (Cunningham et al., 2004), but efficacy was limited to RAS wild-type tumors (Van Cutsem et al., 2009). In patients with wild-type KRAS tumors initially considered to have unresectable liver metastasis, preoperative cetuximab with chemotherapy greatly increased the resection rates with improved OS compared to chemotherapy arm alone (NCT01564810). Cetuximab is murine-based and could trigger antibody-dependent cell toxicity, and so the humanized panitumumab was developed to overcome this. Similar to cetuximab, combination of panitumumab with chemotherapy improved PFS in mCRC (Douillard et al., 2014).

Angiogenesis is a key hallmark of cancer and is defined as the formation of new blood vessels from existing vessels, which contributes to tumor progression and initiation by promoting growth and metastasis. VEGF ligands and their cognate RTK, VEGFR, play a central role in this process. As tumors grow, the distance from existing vascular supply increases resulting in dearth of oxygen supply. This creates a demand for new blood vessels to supply oxygen and metabolites to rapidly proliferating tumor cells. Hypoxic tumor cells produce pro-angiogenic factors including VEGF, triggering an 'angiogenic switch' leading to accelerated tumor blood vessel formation and leaky endothelial barrier (Seeber, Gunsilius, Gastl, & Pircher, 2018). The VEGF family is also implicated in modifying the tumor microenvironment, metastasis and motility of endothelial cells. Activation of VEGFR leads to activation of RAS/RAF, PI3K/AKT, and PLC-γ signaling pathways and production of several inflammatory cytokines (Y. H. Xie et al., 2020). VEGFR and VEGF

expression are elevated in serum, tissues and vasculature of CRC patients, and correlates with poor prognosis (Martins et al., 2013; Okita et al., 2009; N. R. Smith et al., 2010). Bevacizumab is a humanized monoclonal antibody against VEGF. The prolonged median survival of mCRC patients by combining oxaliplatin or irinotecan with fluorouracil, capecitabine, and leucovorin, is further improved by addition of bevacizumab to this regimen (Hurwitz et al., 2004; Saltz et al., 2008). Maintaining treatment for longer during disease progression further improved therapeutic success in patients (Grothey et al., 2008). Two other therapeutic options aflibercept and ramucirumab were also successful in prolonging survival in clinical trials (Tabernero et al., 2015; Van Cutsem et al., 2012). Aflibercept is a recombinant fusion protein of extracellular domains of VEGFR-1 and -2 that blocks binding of VEGF-A, -B, and another VEGF ligand placental growth factor (PIGF) to their cognate receptors, whereas ramucirumab is a humanized VEGFR-2 monoclonal antibody. Current trials are investigating the optimal patient-specific regimen with unresectable liver metastasis CRC. In this study, patients without *RAS/RAF* mutations are assigned doublet chemotherapy with bevacizumab or panitumumab, whereas tumors harboring *RAS/RAF* mutations were assigned bevacizumab with triple chemotherapy (Punt et al., 2017).

While monoclonal antibodies have proved successful in therapy, escalating costs are problematic. Another drawback of this line of therapy is that many tumors do not respond to anti-EGFR therapy. A major determinant of intrinsic resistance is *RAS* mutations (De Roock et al., 2010; Siddiqui & Piperdi, 2010), but some *RAS* wild-type tumors also display resistance. *BRAF* mutation is also associated with poor response to anti-EGFR therapy. One mechanism of acquired resistance is decreased expression of EGFR in cells refractory to cetuximab (Derer et al., 2012; van Houdt et al., 2010b). Compensatory activation of MAPK and phosphatidylinositol-3-kinase (PI3K) pathways downstream of IGF, c-MET, human epidermal growth factor receptor 2 (HER2) receptors, and *EGFR* mutations have also been reported to affect anti-EGFR efficacy (Y. H. Xie et al., 2020). In one study analyzing mCRC patients treated with cetuximab and irinotecan, IGF-1 positive tumors were associated with reduced OS and PFS compared to IGF-1 negative tumors (Scartozzi et al., 2012). Reduced expression of EGFR ligands such as epiregulin and amphiregulin are also associated with reduced efficacy of cetuximab (Khambata-Ford et al., 2007). Bevacizumab therapy is associated with increased risk of hypertension, proteinuria and thromboembolic side effects (Grothey et al., 2008; Hurwitz et al., 2004). Like EGFR therapy, anti-VEGF therapy is

associated with several resistance mechanisms. Namely, overexpression of PIGF, HGF, fibroblast growth factor (FGF) were found in bevacizumab-treated CRC patients (Kopetz et al., 2010), and could contribute to resistance. In line with this, Aflibercept that blocks both PIGF and VEGF performed better than bevacizumab in CRC patient-derived xenograft models (Chiron et al., 2014). Similarly, lower serum angiopoietin is associated with better prognosis in bevacizumab-treated CRC patients (Goede et al., 2010). Vanucizumab, a bispecific monoclonal antibody targeting VEGF-A and angiopoietin-2 had encouraging results in phase I clinical trials (Hidalgo et al., 2018). Overexpression and activation of c-MET signaling pathway is also associated with anti-VEGF resistance. Co-inhibition of VEGF and c-Met led to a significant decrease in tumor growth in xenograft models (X. Chen et al., 2018; Jahangiri et al., 2013). Although treatment of mCRC with anti-VEGF antibody and chemotherapy has prolonged survival after surgical resection, many eventually develop recurrences, warranting the need for alternative therapeutic options (Yasuno et al., 2019).

1.2.4.4 Immunotherapy for CRC is in its early stages of development

Immune cells such as activated T cells and natural killer (NK) cells are capable of recognizing antigens on the surface of cancer cells and mounting an anti-tumor response. Immune cells have a variety of activating and inhibitory receptors on their cell surfaces that recognize the major histocompatibility complex I (MHC-I) located on normal cells or MHC-II on antigen presenting cells (APCs). Lack of MHC-I on cancer cells trigger the activation of inhibitory receptors of NK cells. Whereas, immunogenic peptides from tumor cells are presented as antigens on MHC-II by the APCs such as dendritic cells. Upon activation of NK or T cells, they release cytotoxic granules such as granzyme and perforins, and pro-inflammatory cytokines such as interferon-γ (IFN-γ) and tumor necrosis factor (TNF-α) marking the tumor cells for programmed cell death (Gonzalez, Hagerling, & Werb, 2018). Certain homeostatic mechanisms exist to prevent unnecessary damage from immune cells including two checkpoint molecules programmed cell death protein-1 (PD-1) and cytotoxic T-lymphocyte-associated protein-4 (CTLA-4)present on T cell surfaces that negatively regulate its function. Engagement of PD-1 with its receptor PD-L1 on cancer, stromal and mesenchymal cells (in the tumor microenvironment) results in the downregulation of T-cell activity and time spent in contact with APC. Engagement of CTLA-4 downregulates production

of pro-inflammatory cytokines required for T cell activity. It also inhibits T cell activation by preventing the binding of B7 costimulatory family on APCs to cluster of differentiation 28 (CD28) "costimulating" receptor on T cells (Topalian, Drake, & Pardoll, 2015). NK- and T-cell infiltration within the tumor and the stroma of CRC, especially the regulatory T cell population is associated with favorable outcomes (Galon, 2006; X. Zhang, Kelaria, Kerstetter, & Wang, 2015). The PD-1 expressing regulatory T cells are involved in the immune suppressive functions of cytotoxic T and NK cells (Ahmadzadeh et al., 2009; Juneja et al., 2017; Y. Liu et al., 2017). Notably, preclinical studies demonstrated that administration of antibodies against CTLA-4 or PD-1 *in vivo* resulted in tumor regression (Juneja et al., 2017; Leach, Krummel, & Allison, 1996).

Immune checkpoint therapies are aimed at increasing the cytotoxic activity of T- or NK cells towards tumor cells. MSI-H tumors benefit best from immunotherapy. These tumors are associated with high mutational burden, elevated production of neoantigens and higher levels of infiltrating T lymphocytes (Passardi, Canale, Valgiusti, & Ulivi, 2017). A phase II clinical study (NCT01876511) reported that pembrolizumab, a humanized PD-1 immunoglobulin G (IgG4) inhibitor was efficacious in prolonging survival (40% response rate and 78% PFS) in MMR-deficient and MSI-H tumors compared to MMR repair-proficient tumors (0% response rate and 11% PFS). A subsequent phase I study further attested to this result and pembrolizumab had an acceptable safety profile (NCT02054806). The landmark KEYNOTE-164 study evaluated its efficacy in patients who had received chemotherapy with or without anti-VEGF/EGFR therapy. Pembrolizumab improved OS and response rates in MMR-deficient/MSI-H mCRC (Le et al., 2020). An ongoing trial for mCRC tested another PD-1 antibody Nivolumab, in patients previously treated with or were intolerant to chemotherapy. A significant portion of the patients responded to the therapy, with responses lasting a year or longer. Patients who responded to the therapy had disease control for ~12 weeks or longer (Overman et al., 2017). These results were further improved by combining Nivolumab with anti-CTLA-4 antibody ipilimumab, with drastically improved response rates and 12-month PFS rates of 71%. A follow-up report showed that 84% patients achieved disease control, with OS of 83% (NCT02060188). Several other novel PD-1/PDL-1 inhibitors are currently undergoing clinical trials for determining safety and efficacy in many solid tumors including CRC (Y. H. Xie et al., 2020). Other immune checkpoint targets of interest are T cell immunoglobulin and mucin domain containing protein- 3 (TIM-3) and T cell-

derived lymphocyte activation gene 3 (LAG-3), both are associated with poor prognosis in CRC and suppressing T cell function (X. Yu et al., 2019; Zhou et al., 2015). Unfortunately, immunotherapy has been only partially successful in CRC and has failed in patients with MSS or MMR-proficient CRC. New strategies are being tried to improve efficacy of immunotherapy including radiotherapy and bispecific antibody therapy. Radiotherapy is expected to increase tumor-specific antigens and MHC-I expression on tumor cells. Interestingly, radiotherapy provided a benefit only in the combination arm (PD-1 and CTLA-4) in melanoma, as CTLA-4 therapy alone led to resistance due to PD-1 upregulation (Twyman-Saint Victor et al., 2015). This approach is currently being tested in clinical trials for MSS-CRC (NCT03104439, NCT03007407, and NCT02888743). Bispecific antibodies such as the RG7802 or RO6958688 are capable of binding carcinoembryonic antigen (CEA) on tumor cells and CD3 on T cells, thereby facilitating T cell recognition of tumor cells. Two clinical trials observed anti-tumor activity with manageable safety profiles using RO6958688 as monotherapy or in combination with anti-PD-1 antibody (NCT02324257 and NCT02650713). Further research is needed to determine the efficacy of immune checkpoint inhibitors in early stage disease, or in patients without MSI but display immune cell infiltration.

1.2.4.5 Other therapeutic avenues are yet to achieve widespread success

Recent advances in research have helped identify new druggable pathways in CRC including immunotherapy, inhibitors of cell signaling kinases, β-catenin destabilizers, etc. Some of these efforts are described below. Most CRC tumors that are mutated for *BRAF* exhibit point mutations at codon 600 (valine changed to glutamic acid), which results in constitutive activation of the MAPK pathway. As previously mentioned, BRAF-mutant tumors are associated with poor prognosis, are MSI-high and refractory to adjuvant chemotherapy. However, BRAF kinase inhibitors which are successful in melanomas (Chapman et al., 2011), are ineffective in CRC as monotherapy (Ducreux et al., 2019). BRAF inhibitors resulted in paradoxical activation of extracellular signal-regulated kinase 1/2 (ERK 1/2) in RAS-mutant cancers and resulted in RAF dimerization that reactivates RAF (A. D. Cox, Fesik, Kimmelman, Luo, & Der, 2014). Similarly, MEK inhibitors are ineffective as monotherapy due to several resistance mechanisms and crosstalk from other pathways (Temraz, Mukherji, & Shamseddine, 2015). This can be due to upregulation

of RTK expression or upstream regulators that reactivate ERK in RAS-mutant cancer cells (A. D. Cox et al., 2014). Therefore, ERK inhibitors were developed to overcome resistance to RAF/MEK inhibitors and have shown promise in reducing tumor growth of KRAS, BRAF or NRAS-mutant xenograft models (Morris et al., 2013). Identification of *BRAF* mutations is required to cater therapy in these patients, as prognosis is often poor for anti-EGFR therapy (De Roock et al., 2010). Several studies have highlighted the benefit of combining BRAF inhibitors (encorafenib) and binimetinib (MEK inhibitor) with cetuximab in *BRAF*-mutant mCRC (NCT02928224, BEACON trial) which was recently approved by the FDA. In addition to MAPK pathway inhibitors, two clinical trials have been launched to test the efficacy and maximum tolerated dose of copanlisib, a PI3K inhibitor (NCT03735628, NCT03711058). Currently, we are awaiting the results of two phase II clinical trials using Akt inhibitor MK-2206 which showed pre-clinical activity in CRC (NCT01802320, NCT01186705) (Agarwal et al., 2014).

Several studies have reported that c-Met/HGF is overexpressed in CRC (Y. H. Xie et al., 2020). Savolitinib, a selective Met inhibitor had a decent tolerability profile in patients with solid tumors (Gan et al., 2019), and is currently being tested in phase II CRC trial (NCT03592641). Another non-selective FDA-approved Met inhibitor crizotinib which also targets the anaplastic lymphoma kinase (ALK), recepteur d'origine Nantais (RON) and ROS (ROS proto-oncogene 1, receptor tyrosine kinase) receptors is also being tested in CRC (NCT02510001, NCT03792568). Merestinib, a non-selective inhibitor of AXL, MET, ROS1, discoidin domain receptor (DDR) and fms like tyrosine kinase 3 (FLT3), in combination with the VEGF monoclonal antibody Ramucirumab, has just completed phase I for advanced cancers including CRC. It was found to have a tolerable safety profile and efficacy, and the dose required for phase II study was determined (He et al., 2019).

An actively studied compound in the clinic is regorafenib. It is a multikinase inhibitor of VEGFR, tyrosine kinase with immunoglobulin-like and EGF-like domains 2 (TIE2), platelet derived growth factor receptor-β (PDGFR-β) which successfully impacts angiogenesis (Dhillon, 2018). It was approved for use as a single agent in refractory CRC that do not respond to systemic therapies (Grothey et al., 2013). Insulin-like growth factor receptor-type 1 (IGF-1R) activation is associated with resistance to anti-EGFR therapy (Ma et al., 2016), and CRC progression (Vigneri et al., 2017).

A phase II clinical study with robatumumab, a monoclonal antibody against IGF-1R seemed to have a partial response in chemotherapy-refractory CRC patients (Lin et al., 2014). Another IGF-1R antibody, ganitumab, was well tolerated when administered with chemotherapeutic regimen in *KRAS*-mutant CRC (NCT00813605).

Several other pathways are being exploited in therapy. A few inhibitors targeting the β-catenin/WNT pathway are being tested in the clinic for mCRC including WNT-974 and LGK-974, palmitoyltransferase inhibitors that interfere with processing and secretion of WNT ligands (NCT02278133, NCT01351103). One group of compounds that were found to reduce the risk for CRC include the nonsteroidal anti-inflammatory drugs (NSAIDs), which target the cyclooxygenase enzymes (COX-1 and COX-2). Studies have shown that long-term intake of COX-2 inhibitors such as celecoxib was associated with reduced adenoma incidence (Bertagnolli et al., 2006). Current clinical trials are testing COX inhibitors with anti-PD-L1 in MMR-deficient/MSI-H CRC (NCT03638297). Vitamin D is being assessed for co-treatment with chemotherapy for mCRC (SUNSHINE trial). Despite the discovery of many new targets, most of them have had poor success. More studies need to focus on biomarker identifications to stratify patients into different prognostic subgroups based on their therapeutic response. One such prognostic group is tumors with *KRAS* mutations, which are frequently associated with therapeutic relapse and resistance.

1.3 Mutant RAS isoforms are major drivers of human cancers including CRC

RAS mutations are early genetic events that drive tumorigenesis. Despite identification of several cancer-associated genes, mutant *RAS* remains amongst the most common oncogenes observed in nearly 30% of all human cancers (COSMIC database). Continuous expression of RAS is often necessary for cancer maintenance, as knockdown of RAS impairs tumorigenicity, suggesting an "addiction" to mutant *RAS* (Brummelkamp, Bernards, & Agami, 2002; Chin et al., 1999). Nearly three decades ago, the transforming ability of Harvey and Kirsten rat sarcoma viruses was attributed to the cellular genes *HRAS* and *KRAS*, respectively, that are converted to oncogenes. *RAS* mutant alleles were soon discovered in many human cancers. Several reports published that the mutant *HRAS* allele transformed cells that were previously immortalized by Myc, simian virus

40 (SV40) large T antigen or adenovirus E1A oncogenes (Newbold & Overell, 1983). This suggested a multi-step model of tumorigenesis and indicated that RAS can transform cells only if they have undergone predisposing alterations. In line with this, inducible expression of mutant allele $Kras^{G12V}$ *in vivo* did not alter intestinal cell homeostasis on its own, but required the loss of *Apc* gene to predispose cells to transformation by mutant KRAS (Land, Parada, & Weinberg, 1983; Sansom et al., 2006). Around the same time, it was also determined that several carcinogens, such as ionizing radiations, chemicals, etc., induced tumors that harbored *RAS* mutations (Balmain & Pragnell, 1983; Guerrero, Villasante, Corces, & Pellicer, 1984).

The three *RAS* genes (*KRAS*, *HRAS* and *NRAS*) are not equally mutated in human cancers, *KRAS* is most mutated (~86%), followed by *NRAS* (~11%) and *HRAS* (~3%) (A. D. Cox et al., 2014). Amongst the three major cancer types that frequently harbor *RAS* mutations, the majority (~95%) of pancreatic ductal tumors (PDAC) and many lung adenocarcinomas (~30%) exhibit mutations only in the *KRAS* isoform, whereas CRC tumors comprise both *KRAS* mutations (~45%) and *NRAS* mutations (~7.5%). Importance of the KRAS isoform in CRC was analyzed *in vitro* by comparing tumorigenic properties among cell lines expressing the three isoforms of RAS. HCT116 and DLD-1 human CRC cells expressing oncogenic $KRAS^{G13D}$ exhibited accelerated proliferation, and anoikis-resistance compared to $HRAS^{G12V}$- and $NRAS^{G12V}$-expressing cells (Keller et al., 2007). Similar observations were made *in vivo,* as mice expressing mutant $Kras^{G12D}$ in the colonic epithelium demonstrated hyperplasia and aberrant MAPK signaling, which was absent in $Nras^{G12D}$-expressing mice, suggesting isoform-specific differences in CRC progression (Haigis et al., 2008). Cancer-associated *RAS* mutations are single-point substitutions, and predominantly occur at hotspot codons 12, 31 and 61 (~98% of tumors). Specific point mutations are associated with different types of cancer. For example, nearly all *RAS* mutations in pancreatic and lung tumors are at codon 12, whereas in CRC, mutations seem to preferentially occur at codon 12, with a smaller proportion (~20%) occurring at codon 13, followed by codons 61 and 146, according to cBioPortal metastatic CRC dataset memorial sloan-kettering cancer center (MSKCC) dataset, (Yaeger et al., 2018). *KRAS* is predominantly mutated at codon 12, *HRAS* at codon 12 followed by codons 61 and 13 respectively, whereas there is a preference for codon 61 in *NRAS*. There are also differences in the type of amino acid substitutions at codon 12 or 13. For example, glycine is most frequently changed to glutamate (G12D or G13D) in CRC and (G12D) in pancreatic cancers,

followed by glycine to valine (G12V) substitution. In lung cancers, there is a preference for codon 12 to be mutated from glycine to cysteine (G12C). It was previously thought that mutations have similar outcomes in cancer, but it is becoming increasingly evident that they differentially impact survival. This was demonstrated in the "RASCAL" study which collected global data on colorectal tumor genotypes and disease outcomes from over 2000 patients (Andreyev et al., 2001). The study revealed that *KRAS* mutations are associated with poor survival, and notably, stage III patients with *KRAS* mutations have a higher risk of relapse or death. The study also revealed that $KRAS^{G12V}$ were the most common mutations and associated with more aggressive tumors. Therefore, therapeutic approaches need to be catered not only to RAS isoforms but also to the type of mutations.

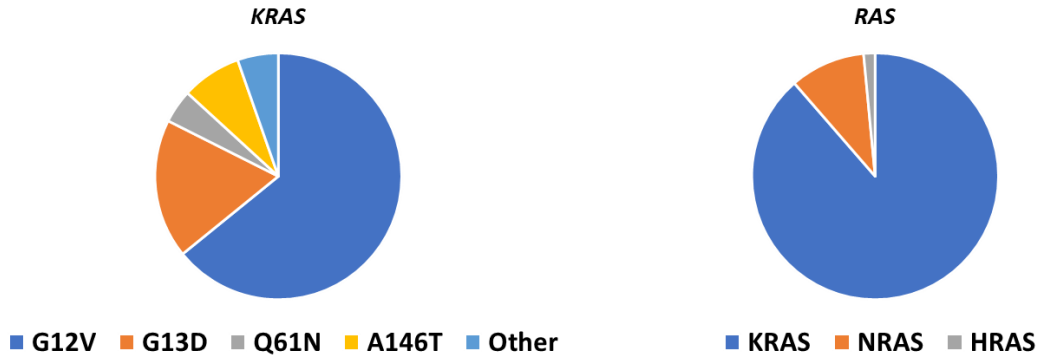

Figure 1.5. Summary of *RAS* mutations in Colorectal cancers

Graph depicts the proportion of CRC cases that exhibit mutations in the hotspot codons of KAS isoform (12, 13, 61 and 146) compared to the other codons (left). Graph depict the proportion of CRC cases mutated for the three RAS isoforms. Data were obtained from cBioPortal database, by combining the following colorectal adenocarcinoma datasets- TCGA, Pan cancer Atlas and Metastatic MSKCC, Cancer cell 2018 (Total 1728 samples).

1.4 Decades of research provide insights into RAS structure, regulation and localization

The *RAS* genes code for ~21 kilodalton (kDa) proteins (HRAS, NRAS and two splice variants of KRAS-KRAS4A and KRAS4B). These isoforms share ~82-90% sequence identity. Although they share significant functional similarity, evidence suggest isoform-specific functions (Quinlan & Settleman, 2009). All isoforms are widely present in cells, with KRAS being ubiquitous in nearly all cell types. Knockout of the *Kras* isoform, but not *Hras* or *Nras*, was shown to be essential for normal development in mice (Johnson et al., 1997). Ras is a small GTPase member of a large

superfamily of low-molecular weight GTPases that act as molecular switches that are active when guanosine 5′ triphosphate (GTP)-bound and inactive when guanosine 5′ diphosphate (GDP)-bound. Guanine nucleotide exchange factors (GEFs) such as son of sevenless-1 and -2 (SOS1 and SOS2) are proteins that promote GDP dissociation and GTP binding. RAS has low intrinsic GTPase activity, so GTP to GDP conversion is catalyzed by GTPase activating proteins (GAPs) such as neurofibromatosis 1 (NF1) and p120GAP (Hobbs, Der, & Rossman, 2016). This regulation by GAP is lacking in cells expressing mutant alleles of RAS, which remain constitutively GTP-bound. Codon-12 mutations show complete insensitivity to GAP-mediated hydrolysis. Whereas mutations at codon 61 and codon 13 (key catalytic residues) exhibit reduced GAP insensitivity compared to codon-12 mutants, but accelerated rate of nucleotide exchange with preferential GTP binding compared to RAS wild-type proteins (M. J. Smith, Neel, & Ikura, 2013).

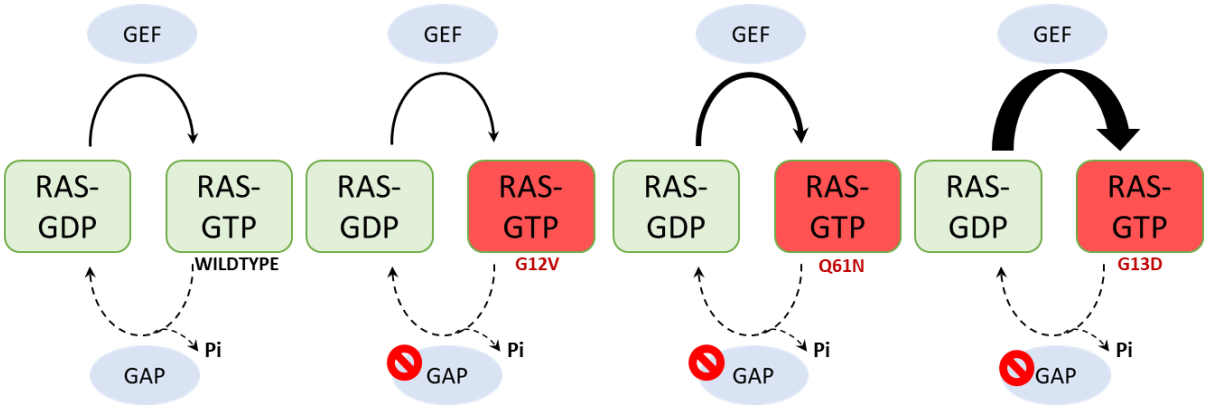

Figure 1.6. Proposed mechanism of constitutive activation of RAS mutants
As cellular levels of GTP/GDP are at millimolar concentrations, RAS is persistently nucleotide bound. RAS proteins have low intrinsic GTPase activity and nucleotide exchange capabilities, which are stimulated by family of proteins called GTPase activating proteins (GAPs) and guanine nucleotide exchange factors (GEFs), respectively RAS mutated at codons 12, 13 and 61 are constitutively GTP bound. Codon 12 mutants display insensitivity to GAP, whereas codon 61 mutants have reduced GAP sensitivity and intrinsic hydrolysis, but also increased GEF activity compared to wildtype RAS. Similarly, codon 13 mutants exhibit reduced GAP-mediated hydrolysis but also a huge increase in GEF activity compared to wildtype RAS. (M. J. Smith et al., 2013)

Small GTP-binding proteins possess a classic catalytic G-domain that contains two dynamic switch I (residues 30-40) and switch II (residues 60-76) regions that undergo conformational changes with GDP-GTP cycling. Switch I and II are crucial for interaction of RAS with its effectors and regulators. The γ-phosphate of GTP interacts with two residues at T35 and G60

causing a shift in the orientation of switch II (Karnoub & Weinberg, 2008). These two residues are amongst the most conserved residues in the GTPase family, suggesting shared mechanisms of GTP binding. The G-domain is identical between the RAS isoforms in the effector lobe 1 (residues 1-86), but there exist some variations (~82% sequence similarity) in allosteric lobe 2 (residues 87-167). Lobe 1 contains the active site including the switch I and II regions, nucleotide-binding residues, GTP hydrolysis and the phosphate-binding loop (residues 10-17). Lobe 2 contains the membrane interacting portions, allosteric residues and helix regions that facilitate binding to membrane phospholipids (Buhrman et al., 2011). Most differences between the isoforms are attributed to the C-terminal ends of the protein and located within the hypervariable regions (HVR) containing the cysteine CAAX motif required for farnesylation, and the upstream cysteine residues required for palmitoylation. These differences explain the isoform specific post-translational processing of RAS (Castellano & Santos, 2011; Hancock, Magee, Childs, & Marshall, 1989), which could in turn selectively alter effector binding due to different subcellular localizations (Hancock, 2003). RAS isoforms terminate with a CAAX tetrapeptide motif that is required for a series of post-translational lipid modifications that tether RAS to the membrane. The reaction is catalyzed by farnesyltransferase (FTase) that results in the addition of a terminal farnesylated cysteine, which undergoes further processing by isoprenylcysteine methyltransferase, and removal of the AAX peptide sequence. Farnesyltransferase inhibitors (FTI) block all of the above processes, and RAS remains in the cytosol, unable to activate its downstream targets. Indeed, inhibition of FTase *in vivo* resulted in the regression of $Hras^{G12V}$-driven tumors suggesting that membrane tethering is essential for Ras biological activity (Kohl et al., 1995). For KRAS4A and NRAS, an alternate 20-carbon isoprenylation is added via geranylgeranyltransferase (GGTase) which compensates for the lack of FTase activity. RAS proteins then shuttle to the plasma membrane (PM) via two routes depending on second set of targeting signals located adjacent to farnesylated cysteine. A final post-processing step results in the addition of two palmitoyl long-chain fatty acid groups to the cysteine residues upstream of CAAX motif in HRAS, and a single palmitic acid in KRAS4A and NRAS isoforms at the PM that further stabilizes the PM interaction. Palmitoylated isoforms enter the exocytic pathway, trafficking to the PM via the trans Golgi network (TGN). In-frame deletion mutations involving one or more of these cysteines affected membrane localization, lipid binding and transforming ability of mutant Hras, linking post-translational modifications of Ras to its biological activity (B. M. Willumsen, Norris, Papageorge,

Hubbert, & Lowy, 1984; Berthe M. Willumsen, Christensen, Hubbert, Papageorge, & Lowy, 1984). However, KRAS4B isoforms bypass TGN and are not palmitoylated due to contiguous C-terminal lysine residues that facilitate direct membrane anchoring (Karnoub & Weinberg, 2008). The process and enzymes targeting post-translational modifications of RAS are exploited for therapy.

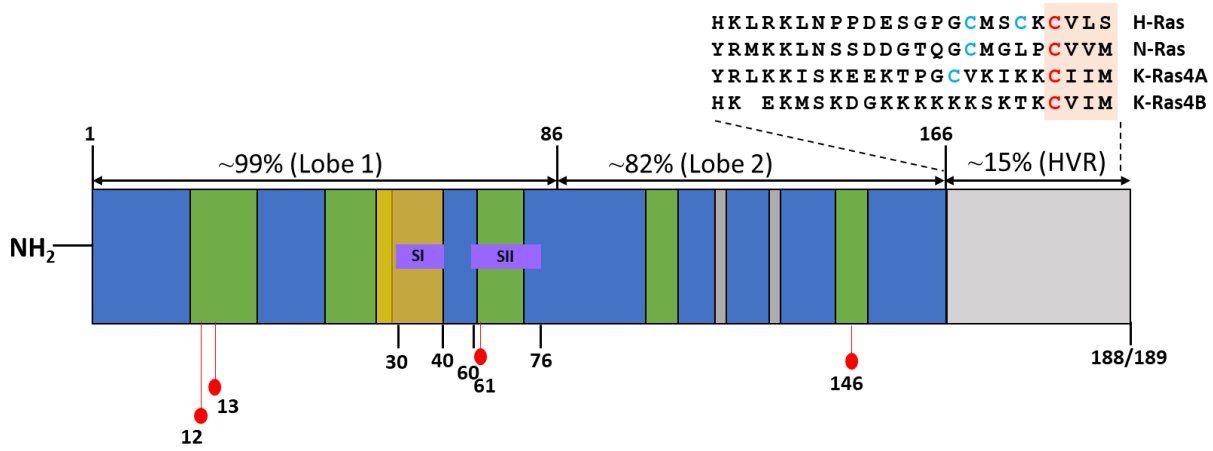

Figure 1.7. Primary structure of RAS isoforms

Lobe 1 also known as effector lobe (residues 1-86) is highly similar between the RAS isoforms. Lobe 2 also known as allosteric lobe (residues 87-167) is ~82% similar between isoforms. Together these lobes are referred to as G-domain which are mostly similar between the four isoforms. The most variable regions (~15%) between the isoforms are at the C-terminal known as hypervariable region (HVR). The unique amino acid residues are depicted on top for each isoform, C residue (in red) refers to farnesylated cysteine and C residue (in blue) refers to palmitoylated cysteine. The last four residues in the HVR (in orange square) is the CAAX motif required for plasma membrane (PM) targeting. Residues highlighted (in grey) are essential for PM binding/trafficking. Residues highlighted (in green) are essential for Mg(II)/nucleotide binding. Residues (in yellow) are required for downstream effector binding. Switch I (SI) domain consisting of residues 30-40 are necessary for interaction with GAPs and effectors, while Switch II (SII) comprising of residues 60-76 are necessary for interaction with GEFs. SI and SII domains in lobe 1 undergo conformational changes upon GTP-GDP binding. The red lollipops represent the hotspot mutations in metastatic CRC dataset MSKCC (Yaeger et al., 2018) *from cBioPortal. Majority (~98%) of RAS mutations in CRC occur at these four residues. The height of the lollipop correlates with the mutation frequency associated with that codon in CRC.*

The PM contains myriad microdomains (Prior et al., 2001). Quantitative electron microscopic (EM) analysis of PM shows that Hras is predominantly located at lipid-rafts when GDP-bound and is associated with non-raft regions when GTP-bound. GTP-loading therefore regulates the lateral segregation of Hras in the PM. Galectin-1 is found in a complex with the HVR domain of activated

Hras and Kras isoforms. This could be crucial for this lateral segregation process, as knockdown of galectin-1 prevents clustering of $Hras^{G12V}$ in the PM (Prior, Muncke, Parton, & Hancock, 2003). On the other hand, Kras is associated with non-raft regions whether GTP- or GDP-bound. This study also demonstrated that activated Kras and Hras are located at non-overlapping non-raft microdomains. Different subcellular localizations of RAS could account for different effector binding and signaling between isoforms. RAS activation leads to membrane recruitment and activation of downstream effector RAF-1 kinase (Downward, 2003). Consistent with previous studies, Raf-1 activation was significantly more in non-raft fractions expressing $Hras^{G12V}$ compared to $Hras^{G12V}$ associated with lipid rafts (Prior et al., 2001). Besides PM, evidences suggest that activated Ras isoforms are associated with other subcellular compartments such as endosomes and TGN (Hancock, 2003). Activated Hras targeted to endosomal and Golgi compartment are capable of activating downstream effectors including c-Jun N-terminal kinase (Jnk), PI3K, and Raf-1, with varied efficacies (Chiu et al., 2002). Given that HRAS and NRAS are stably expressed on Golgi membranes, and KRAS and HRAS are found on endosomal membranes, differences in signaling outputs between isoforms could also be attributed to differences in subcellular localization.

1.5 The wide effector web of oncogenic RAS

Typically, activation of cell surface RTKs, such as EGFR, PDGFR, by their ligands, result in autophosphorylation and binding of the adaptor protein, growth factor receptor bound protein 2 (GRB2). GRB2 binds SOS1 and SOS2, which translocate to the PM upon RTK activation. Close proximity of RAS to SOS on the intracellular side of the PM stimulates GTP-binding on RAS (Downward, 2003). RAS proteins control various cellular functions and signaling pathways that regulate normal cell proliferation and survival. In cells expressing mutated *RAS*, constitutive signaling fuels malignant phenotypes such as uncontrolled proliferation, enhanced motility, formation of new blood vessels to facilitate angiogenesis, etc. RAS-GTP preferentially binds to RAS binding domain (RBD) or RAS association (RA)-domain-containing effectors. More than 10 such effector families have been identified downstream of RAS, some of well-studied effectors are discussed below.

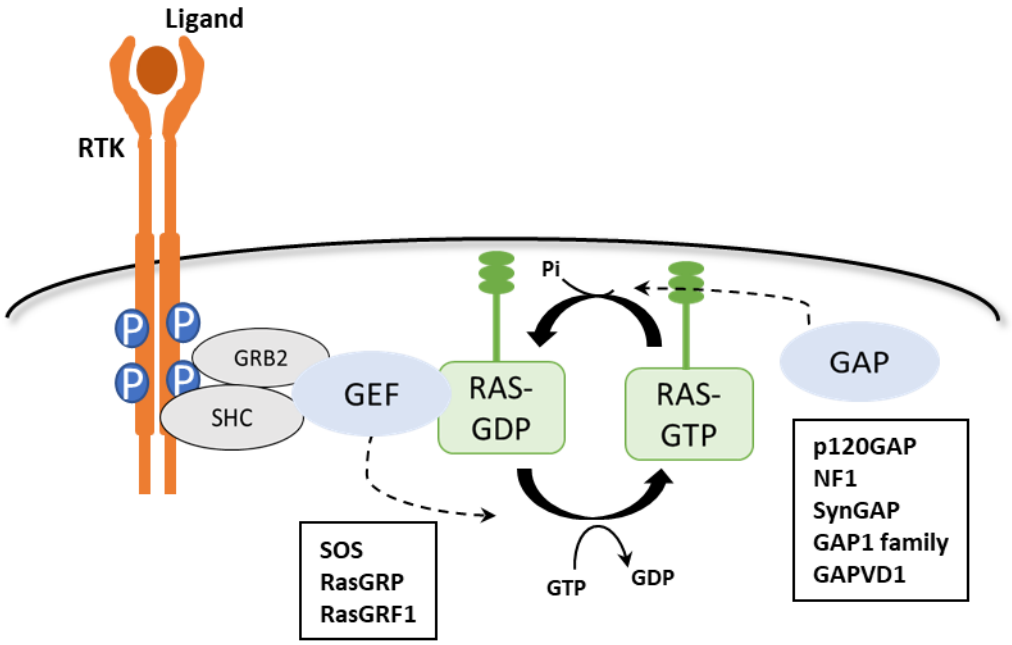

Figure 1.8. Upstream activation of wildtype RAS

When unstimulated, RAS is bound to GDP and inactive. Receptor tyrosine kinases (RTKs) are located at cell membranes where their extracellular domains bind ligands, this information is then relayed to intracellular secondary messengers to signal to cells to perform basic functions such as differentiation, survival, cell division, etc. Upon activation of receptors such as EGFR by their cognate ligands epidermal growth factor (EGF), RTKs become autophosphorylated (P) on several tyrosine residues on the intracellular side of cell membranes. These act as recognition sites for adaptor proteins such as SHC and GRB2. GRB2 then recruits RAS-GEF, SOS1 to cell membranes where they encounter GDP-bound RAS. As GTPs are ten-fold excess of GDP, SOS1 facilitates exchange of GDP for GTP to generate active RAS. To turn off RAS activation, GAP stimulates the hydrolysis of GTP to GDP. The known RAS-GEFs and GAPs are indicated in boxes.

1.5.1 Activation of MAPK pathway is a dominant feature of mutant RAS

The serine/threonine kinase RAF was the first Ras effector to be characterized. Activated RAS binds to and recruits three RAF isoforms, namely ARAF, BRAF, and CRAF, to the PM via a conserved RBD and cysteine-rich domains at the N-terminal region of RAF (Chong, Lee, & Guan, 2001; Chong, Vikis, & Guan, 2003; Marais, Light, Paterson, & Marshall, 1995), following which RAF kinases are regulated via multiple mechanisms that involve phosphorylation. Ser338, Tyr341, Tyr491 and Ser494 are four activating phosphorylation sites on CRAF that are RAS-inducible (Chong et al., 2003). Maximal phosphorylation of ARAF and CRAF at Tyr341 by both janus

activated kinase (JAK) and SRC (Wan et al., 2004), and at Ser338 by p21 activated kinase (PAK) are dependent on activated RAS. By contrast, BRAF is constitutively phosphorylated at S445, which is further increased in the presence of active RAS (Chong et al., 2001). CRAF kinase activity is also dependent on other residues including T491 and S494 in the activation loop of RAF kinase domain. Substitutions of T491/S494 in CRAF and the corresponding residues T598/S601 in BRAF, results in constitutive kinase activity and increased sensitivity to RAS activation. *In vitro*, a $BRAF^{V600E}$ mutant had ~500-fold increase in kinase activity compared to wild-type protein. BRAF mutants with elevated kinase activities increased ERK phosphorylation to levels comparable to activated RAS^{G12V} (Wan et al., 2004). This study also reported that the oncogenic mutation of BRAF does not require the segmental phosphorylation events that wild-type protein relies on for full functioning. Upon activation, RAF binds to and phosphorylates MEK1 and MEK2 at two key serine residues at positions 218 and 221. In turn, they bind and phosphorylate their *bonafide* substrates ERK1/2 (Roux & Blenis, 2004). ERK1/2 proteins are phosphorylated at dual sites (Thr202 and Tyr204 in ERK1 and Thr183 and Tyr185 in ERK2), and mutation of these sites curbs ERK 1/2 activity. ERKs are proline-directed serine/threonine kinases that require a proline at positions +1 and −2 relative to the site of phosphorylation in their substrates, with a consensus of PxS/TP or simply S/TP, where x is any amino acid (Eblen, 2018).

A significant proportion of pERK 1/2 translocates to the nucleus upon activation to regulate several transcription factors. ERK also activates an ever growing list of cytosolic proteins that regulate many cellular functions including cytoskeleton, cell adhesion, cell signaling, apoptosis, etc. (Ünal, Uhlitz, & Blüthgen, 2017; Yoon & Seger, 2006). Amongst the ERK substrates are the family of serine/threonine kinases RSK namely (RSK1, RSK2, RSK3, RSK4). RSK contains C-terminally located D domain that is responsible for docking and activation by ERK1/2. All isoforms contain six key phosphorylation residues, mutation of four of these sites are crucial for RSK1 activation (S221, S363, S380, and T573). Although the exact mechanisms are unclear, ERK1/2 are thought to phosphorylate RSK1 on T573, S363 and T359 (Roux & Blenis, 2004). Additionally, ERK-mediated recruitment of RSK to the PM may also result in the phosphorylation of S363 and S380 residues by other membrane-associated kinases. Substrates of RSK are implicated in a wide variety of cellular processes, including several transcription factors such as immediate early response genes, ribosomal protein S6, cell cycle regulating protein $p27^{kip1}$, cAMP Response Element Binding Protein (CREB), and tumor suppressor liver kinase B1 (LKB1).

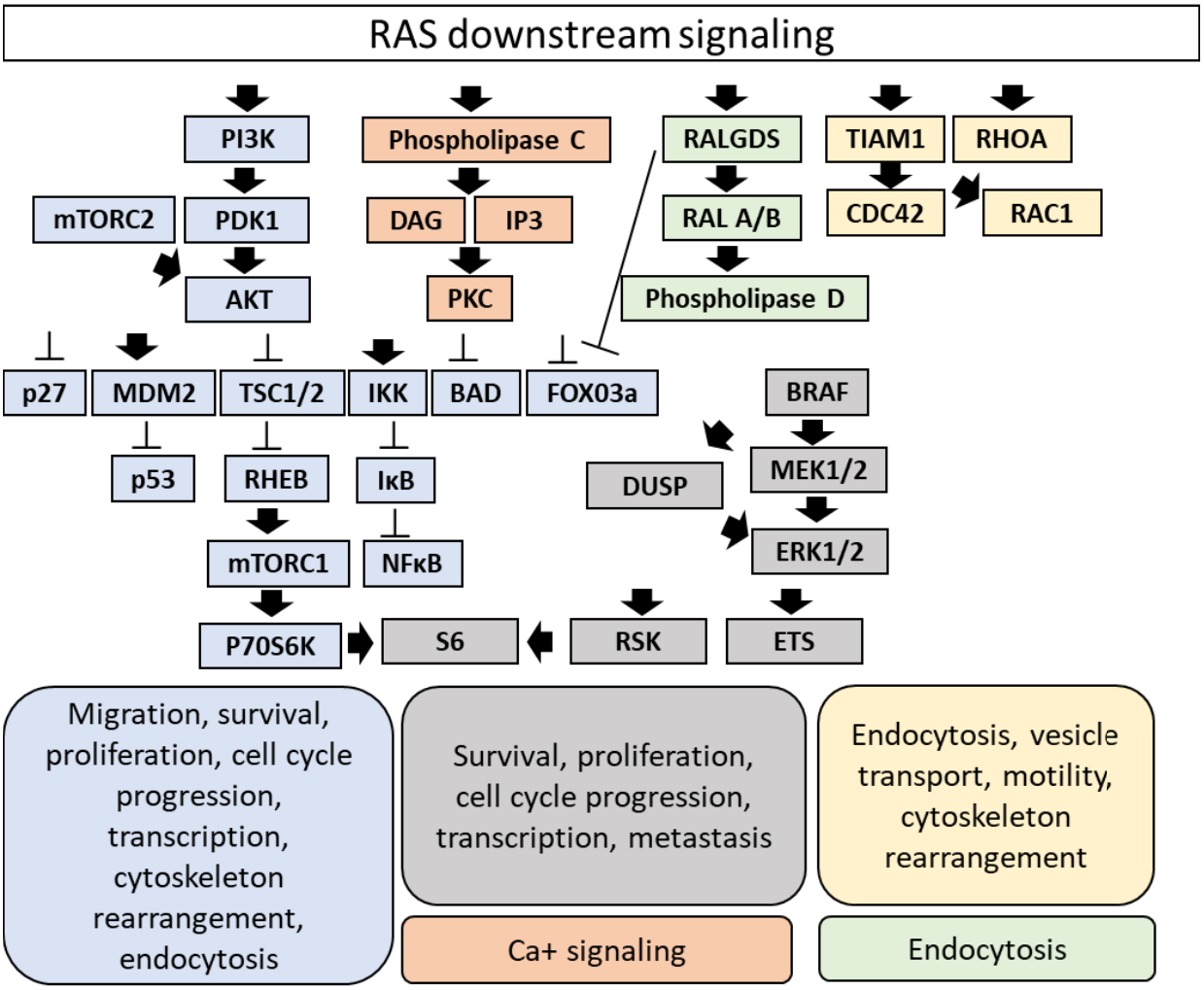

Figure 1.9. Myriad downstream signaling cascades of active RAS

Once active, RAS-GTP binds direct downstream effectors containing RAS binding domain (RBD) or RAS association (RA) domain. Several downstream signaling proteins are upregulated indirectly owing to the processes upregulated by mutant RAS. The most well-known signaling pathways are depicted here. The biological functions associated with the pathways and effectors are described below. The pathways and their effectors are color-differentiated broadly based on their major cellular functions.

Termination of ERK signaling is regulated by dual-specificity phosphatases (DUSPs), also known as mitogen-activated protein kinase phosphatases (MKP) family, containing a docking domain that binds to ERK1/2. DUSPs are transcriptionally induced in response to ERK activation. ERK activation also phosphorylates and stabilizes DUSP4 protein (Kucharska, Rushworth, Staples, Morrice, & Keyse, 2009). Different isoforms of DUSPs are rapidly upregulated upon cellular transformation with oncogenic BRAF and KRAS in intestinal epithelial cells, and cancer cell lines

driven by *RAS* mutations including CRC (Buffet et al., 2017; Cagnol & Rivard, 2013; Yun et al., 2009b). Loss of nuclear ERK activity correlates with DUSP4 expression in colorectal cancer lines. DUSP4 expression was inhibited with the MEK1/2 inhibitor UO126 suggesting that DUSPs are induced as a part of negative feedback loop of ERK signaling. Currently, several components of the MAPK pathway including DUSP, MEK, ERK and RAF are being evaluated in the clinic for CRC therapy. Some of these efforts are discussed under efforts to target RAS-mutant cancers.

1.5.2 Activation of the PI3K pathway

RAS directly interacts with the RBD domain of the catalytic p110 subunit of type I PI3K. The importance of this interaction is underlined by the fact that mutations of *PIKCA*, which codes for the catalytic subunit, is frequently observed in sporadic CRC. PI3K is recruited to the PM via the p85 regulatory subunit, which recognize tyrosine-phosphorylated adaptor proteins. There, PI3K phosphorylates phosphatidylinositol-4,5-bisphosphate (PtdIns(4,5)P_2) to produce phosphatidylinositol-3,4,5-trisphosphate (PtdIns(3,4,5)P_3), a second messenger that binds downstream effector molecules with pleckstrin homology (PH) domains. The PTEN tumor suppressor acts as a phosphatase for PtdIns(3,4,5)P_3 and PtdIns(3,4)P_2, effectively inhibiting PI3K signaling (Malek et al., 2017). Inactivating *PTEN* mutations are frequent events in cancers, including CRC, resulting in constitutive PI3K signaling. PI3K proteins also have a scaffolding role, and function as adaptors to the formation of protein-protein complexes involved in several biological roles (Bilanges, Posor, & Vanhaesebroeck, 2019). PDK1 (phosphoinositide-dependent kinase 1) is a master serine/threonine kinase of the PI3K pathway that is important for activation of large number of downstream AGC kinase family including the protein kinase C (PKC) isoforms, $p70^{S6K}$ also known as S6 Kinase 1 (S6K1), RSK, serum glucocorticoid kinase (SGK), etc. (Scheid, Parsons, & Woodgett, 2005). Another key effector of this pathway is AKT, which is recruited via PtdIns(3,4,5)P_3 or PtdIns(3,4)P_2 to the PM, where it is activated by phosphorylation at T308 (by PDK1) and S473 (by mechanistic target of rapamycin complex 2 [mTORC2]). More than 100 effectors of AKT have been identified including apoptosis inducers (Bcl-2-associated death promoter [BAD]), cell cycle mediators (p27 and p21), forkhead box O (FOXO) transcription factors, etc. (Bilanges et al., 2019). Notably, AKT phosphorylation of the (tuberous sclerosis complex) TSC2 protein activates mTORC1.

The mTORC1 pathway is a key mediator of cell growth and metabolism, protein synthesis, autophagy, amongst other functions. Known mTORC1 phosphorylated substrates include S6K1 and the eIF4E-binding proteins (4E-BP1 and 4E-BP2) (Y. Yu et al., 2011). Inhibiting mTOR activity using inhibitors such as rapamycin and OSI027 or *via* RNA interference, diminished the viability and *in vivo* tumor growth of KRAS-mutant CRC (Fritsche-Guenther et al., 2018; Y. J. Zhang et al., 2009). mTORC1 is required for the formation of intestinal polyps in a mouse model of FAP. Notably, these studies showed that mTORC1 contributed to the CIN model of CRC pathogenesis (Aoki, Tamai, Horiike, Oshima, & Taketo, 2003). Early in CRC tumorigenesis, $Apc^{min/+}$ mice displayed upregulated mTOR signaling. Long-term treatment with rapamycin prolonged survival and inhibited intestinal neoplasia (Koehl et al., 2010). Importance of PI3K signaling in tumor growth was demonstrated in an *in vivo* model of KRAS-driven tumorigenesis, where tumor growth was sustained by persistent PI3K signaling even after the loss of oncogenic RAS (K. H. Lim & Counter, 2005). Although monotherapy with PI3K inhibitors have not been successful in clinic, combination strategies that simultaneously downregulate PI3K and MAPK signaling have shown promise in curbing growth of KRAS-mutant CRC cell lines (Ebi et al., 2011). Similar to negative regulation of ERK signaling by DUSPs, two phosphoproteomic studies identified GRB10 as negative regulator of PI3K, MAPK and mTORC1 signaling (Hsu et al., 2011; Y. Yu et al., 2011). Similar to MAPK pathway, many components of the PI3K pathway are being evaluated in the clinic for CRC therapy, and dual inhibition of PI3K and MAPK effectors present a potential strategy to overcome resistance to MEK inhibitors. Some of these efforts are discussed in a later chapter.

1.5.3 Other RAS signaling pathways

A third well-studied effector pathway of RAS is the Ral-GEF family comprising of RAL guanine nucleotide dissociation stimulator (RALGDS), RALGDS-like gene (RGL1), RGL2/RIF and RGL3, through them RAS activates the RAS-like GTPases (RAL), RALA and RALB which are active when bound to GTP and inactive when bound to GDP (Moghadam et al., 2017). Active RAS binds and recruits RAL-GEFs to RALA and RALB, which enables RAL-GTP to activate effectors such as phospholipase D1 and RAL binding protein 1 (RALBP1). This initiates a cascade

of multiple downstream effectors as RALBP1 serves as a scaffolding protein. RALBP1 exhibits RhoGAP-like activity towards CDC42 and RAC, these in turn regulate critical functions, such as filipodia formation and membrane ruffling, respectively, enabling cell migration. RAL effectors Sec5 and Exo84 are also involved in the regulation of exocytosis (Neel et al., 2011). Small GTPases RALA an RALB are activated in CRC lines and patient tumors. Downregulation of RALA using RNA interference reduced anchorage-independent growth of human CRC cells via a RALBP1-dependent mechanism (Martin, Samuel, Routh, Der, & Yeh, 2011). Impeding RALGEF activation of RAL GTPases also inhibited mutant RAS-mediated growth on soft agar, suggesting that RALGEFs are crucial for RAS-transformation (Hamad et al., 2002).

Phospholipase Cε is yet another effector of RAS signaling, which has two RA domains (one of which strongly binds RAS-GTP) and N-terminal CDC25 GEF domain which acts as an upstream activator of small GTPases (Harden, Hicks, & Sondek, 2009). *In vitro*, mutant RAS bound to and stimulated PLCε activity (Kelley, Reks, Ondrako, & Smrcka, 2001). PLC isoforms hydrolyze membrane phospholipids to generate inositol triphosphate and diacylglycerol. Through these effectors, RAS activation is linked to calcium mobilization and PKC activation. The significance of PLCε in CRC tumorigenesis is highlighted by using $Apc^{Min/+}$ lacking PLCε$^{-/-}$, which displayed markedly reduced adenoma formation, tumor progression, viability, proliferation, and attenuation of angiogenesis (M. Li, Edamatsu, Kitazawa, Kitazawa, & Kataoka, 2009).

Another major downstream signaling pathway of active RAS that deserves a special mention is the RAC pathway. RAC1 is activated by two ways, either by binding to PI3K, or by T lymphoma invasion and metastasis-inducing protein 1 (TIAM1). Mice lacking *Tiam1* were found to be resistant to mutant Ras-induced skin tumors, establishing a role of Tiam1 in tumor imitation and progression (Malliri et al., 2002). RAC is a member of the Rho subfamily of related GTPases that includes Ras homolog family member A (RHOA) and cell division cycle 42 (CDC42), with defined roles in cytoskeleton modelling. RHO family GTPases are implicated in cellular process such as motility, membrane and vesicular trafficking, adhesion, cell cycle regulation, etc. Overexpression of RAC1 in human CRC xenograft model accelerated tumorigenesis in mice, while inhibition of RAC1 suppressed tumor formation, highlighting the importance of RAC1 in tumor growth (Espina et al., 2008). Other mouse models have also shown that PI3K-mediated

Rac1 activation was necessary for KRAS-mediated pancreatic tumorigenesis (Wu et al., 2014). In conclusion, signaling networks downstream of mutant RAS are wide, complex and dynamic and further research will likely uncover other novel, targetable effector pathways of RAS. Future research will likely use computational and systemic approaches to model how integration of multiple RAS effector pathways will influence the biological output or therapeutic resistance to inhibitors.

1.6 Mutant RAS regulates myriad tumorigenic properties

Through the wide web of downstream effectors, mutant RAS promotes crucial cellular functions that promote tumor initiation and progression. Some of the classical RAS-mediated tumorigenic properties are discussed below.

1.6.1 Proliferation and survival

Cell cycle progression is controlled by several cyclin-dependent protein kinases. Microinjections of anti-Ras antibodies to suppress Ras signaling inhibited proliferation of cycling cells, G_0/G_1 cell cycle phase transition, and progression through G_1 phase (Dobrowolski, Harter, & Stacey, 1994). A study using mutant-specific sgRNA against oncogenic KRAS introduced indels in the mutated nucleotide region in human CRC lines. Compared to WT KRAS sgRNAs, mutant KRAS targeting sgRNAs specifically reduced the proliferation of KRAS-mutant CRC and PDAC cell lines, suggesting that KRAS is crucial for cancer proliferation (W. Lee, Lee, Jun, Lee, & Bang, 2018). NIH3T3 cells expressing dominant-negative form of Ras (RAS^{S17N}) inhibited cell proliferation and prevented progression through the S phase of cell cycle (Aktas, Cai, & Cooper, 1997). Cell cycle progression in RAS-transformed cells are mediated via ERK activation and its nuclear translocation. Consistent with this, activation of the members of erythroblast transformation specific (ETS) family of transcription factors (ELK-1, FOS, c-JUN, c-MYC) enable the expression of key cell-cycle regulatory proteins such as cyclin D1 (Yordy & Muise-Helmericks, 2000). Stabilized c-FOS expression via sustained ERK activation leads to activation of genes involved in G1 progression. ERK signaling besides suppressing retinoblastoma (RB) pathway and $p27^{KIP1}$, can also inhibit other negative cell cycle regulators including FOXO3a, SRY-related HMG-box (SOX6), JUN-D, growth arrest and DNA-damage-inducible protein 45 alpha (GADD45A), and transducer of ERBB2 1 (TOB1). This way, RAS can link growth factor signaling to cell cycle

machinery (Aktas et al., 1997; Eblen, 2018). Inactivation of FOXO3a is also a key step in promoting cell survival. Inhibiting ERK-mediated FOXO3a phosphorylated reduced tumorigenesis and increased apoptosis (J.-Y. Yang et al., 2008). Other ERK targets act as positive regulators of cell survival. They include myeloid leukemia cell 1 (MCL-1) and BIM, members of BCL-2 family of apoptosis regulators. ERK-mediated degradation of BIM isoforms prevents pro-apoptotic functions. PI3K activation downstream of RAS activation is also famously associated with pro-survival effects of oncogenic KRAS. Similar to ERK, AKT inhibits pro-apoptotic factors BCL-2 family members BAD and BAX. AKT also phosphorylates and activates murine double minute 2 (MDM2), negating the effects of p53. In addition to these mechanisms, PI3K mediates cell survival through other means (Duronio, 2008). Therefore, RAS promotes proliferation via multiple mechanisms including activation of cell cycle, transcriptional upregulation of growth factors, and inhibition of DNA-damage checkpoint.

1.6.2 Cytoskeleton re-organization and motility

The majority of human cancers are of epithelial origin and display a loss of cell polarity and tissue organization. Epithelial cell polarity is tightly regulated and has tumor suppressive functions. Hence, many of the proteins involved in this process are downregulated in cancers. Microarray profiling revealed a strong epithelial-mesenchymal transition (EMT) signature amongst the most differentially expressed genes associated with mutant $HRAS^{G12V}$ when compared to wild-type RAS in the human CRC cell line CACO-2 (Joyce, Cantarella, Isella, Medico, & Pintzas, 2009). The loss of E-cadherin, one of the key components of adherens junctions, is a classical feature of EMT, a process by which cancer cells lose epithelial properties and gain mesenchymal features. TGF-β in combination with RAS signaling promotes invasion and metastasis by activating the EMT process (Janda et al., 2002; Royer & Lu, 2011). TGF-β induced EMT only in cells transformed with mutant RAS and not wild-type RAS. These cells exhibited upregulation of the mesenchymal markers N-cadherin and vimentin, besides downregulation of the epithelial marker E-cadherin (Arase et al., 2017; Janda et al., 2002). Using RAS oncogenes that specifically interacted with PI3K or MAPK effectors or via specific signaling pathway inhibitors, TGF-β induced EMT was shown to be dependent on MAPK signaling. During EMT, genes necessary for epithelial state are kept repressed by induction of transcription factors such zinc finger E-box

binding homeobox 1 (ZEB1), twist-related protein 1 (TWIST), SNAIL, etc. KRAS-dependent lung cancer line treated with TGFβ1 reduced expression of E-cadherin and this was inversely associated with ZEB1 (Singh et al., 2009). In line with this, other studies demonstrated that ZEB1-driven EMT is a crucial event in KRAS-mutant lung cancer and PDAC tumorigenesis. Additionally, ZEB1 expression was also found to correlate with poor outcomes and advanced tumor grades (Arner, Du, & Brekken, 2019). Using *in vivo* models expressing pancreas specific KRAS and p53 mutations, features of EMT was identified as an early event in premalignant lesions, and cells that had undergone EMT expressed high levels of Zeb1.

EMT facilitates invasion and renders a fibroblast-like morphology to cells, with detached cell clusters from primary tumor site that traversed through basement membranes (Rhim et al., 2012). Expression of $KRAS^{G12V}$ or constitutively active MEK in intestinal epithelial IEC-6 cells resulted in loss of cell-cell contacts and fibroblast-like morphology, which was rescued with the MEK inhibitor UO126 (Lemieux, Cagnol, Beaudry, Carrier, & Rivard, 2015). This phenotype was also reported in another study where Erk pathway inhibitors reversed the disruption of cell-cell junctions caused by mutant Ras (Edme, Downward, Thiery, & Boyer, 2002). This study also demonstrated that overexpression of mutant Ras^{G12V} was sufficient to induce cell motility. Notably, co-expression of active Rac and Mek also promoted cell motility suggesting that both of these are implicated downstream of mutant Ras (Edme et al., 2002). Low-adhesion cells have reduced actin stress fibers, which refers to actin fibers between focal adhesions and cytoplasm that regulate cell contractility. RhoA activation and downregulation of Rho effector-ROCK in Ras-transformed cells inhibits formation of actin stress fibers and this contributes to increased motility (Sahai, Olson, & Marshall, 2001). Expressing either oncogenic KRAS, HRAS or BRAF in CACO-2 CRC cells, increased the migration and invasion ability compared to parental CACO-2 cells. This was reversed by inhibiting RHOA or RAC1 expression. Whereas knockout of the mutant $KRAS^{G13D}$ abrogated migration compared to parental DLD-1 cells. Notably, $KRAS^{G12V}$-expressing CACO-2 cells exhibited filipodia-like formation which was dependent on activated CDC42 (Makrodouli et al., 2011). Collectively the data points to a concerted role of RhoA, RAC1 and CDC42 in cell motility mediated by RAS.

Anoikis refers to the ability of normal epithelial cells that are usually dependent on extracellular matrix (ECM) for adhesion, to undergo suspension-induced apoptosis when detached, presumably evolved as a means for the body to get rid of unwanted cells. Gaining resistance to anoikis is a prerequisite for development of carcinoma and promotes a survival advantage during metastasis to distant sites within the body. Several studies have shown that expression of mutant RAS isoforms imparts epithelial cells with adherence-independent growth ability on soft agar (McFall et al., 2001). Expression of activated forms of MEK1 and MEK2 in IEC-6 also induced anchorage-independent growth, implicating MAPK pathway in anoikis resistance (Voisin et al., 2008). Blocking MAPK activation with the MEK 1/2 inhibitor U0126 only partially inhibited anoikis, suggesting involvement of other pathways in this process. In line with this, activation of SGK1 kinase was shown to be required for cell survival upon detachment from ECM in both RAS-transformed breast cancer cell line MCF10A and CRC cells (Mason et al., 2016). Epithelial cells maintain cell-cell contacts via lateral and apical cell surfaces. In Ras-transformed eye-imaginal discs of *Drosophila*, reduced expression of adhesion proteins such as E-cadherin, Neural Cell Adhesion Molecule, Armadillo, etc., was dependent on expression of Scribble. Scribble is a cell polarity regulator identified as a tumor suppressor protein in *Drosophila* (Waghmare & Kango-Singh, 2016). RAS-mediated transformation of MCF10A cells resulted in loss of cell adhesion proteins and disruption of cobblestone morphology of epithelial cells, which was reverted with Scribble expression. Knockdown of Scribble expression in RAS-transformed MCF10A cells produced filipodia-like protrusions and increased invasion, and Scribble levels was regulated by ERK signaling. Rescuing scribble expression in RAS-transformed cells also inhibited anoikis resistance (Dow et al., 2008). Although far from complete, large body of work has helped us understand the various processes such as EMT and anoikis by which oncogenic RAS endows metastatic potential to tumor cells.

1.6.3 Metabolic reprogramming

Decades ago, the 'Warburg effect' was described whereby cancer cells use glycolytic metabolism and reduced oxidative phosphorylation even in the presence of sufficient oxygen levels. Glucose transporter 1, GLUT1 (*SLC2A1*) is a glucose importer that is upregulated in isogenic CRC cells expressing mutant *KRAS* or *BRAF* genes, compared to wild-type counterparts, which conferred

growth advantage in low-glucose environments. Notably, culturing cells in low-glucose media gave rise to colonies that were mutated for KRAS (Yun et al., 2009b). Glutamine is another major energy source for tumor growth and anchorage-independent growth of KRAS-mutant HCT116 cells. It fuels the tricarboxylic acid (TCA) cycle, increases glucose consumption and adds to the glycolytic intermediates of the pentose phosphate pathway (Weinberg et al., 2010). This study also showed that disruption of mitochondrial function and ROS generation by reducing the expression of Transcription factor A, mitochondrial (TFAM), significantly affected KRAS-mediated tumorigenesis. Dependence on glutamine and glucose by KRAS-transformed cells was also demonstrated in KRAS-mutant MDA-MB-231 and PDAC cells, whose proliferation was limited in media limited for these nutrients (Gaglio et al., 2011; Son et al., 2013). This was further supported by the finding that these cells expressed high levels of metabolic genes such as enolase (ENO 1/2), phosphoglycerate kinase (PGK), pyruvate kinase M2 (PKM2) and lactate dehydrogenase A (LDHA), glutamate oxaloacetate transaminase 1 (GOT1), and malic enzyme 1 (ME1). A significant proportion of the consumed glucose is shunted away from TCA cycle in KRAS-transformed mouse and human cells and converted to lactate, consistent with a high rate of lactate secretion in cancer cells, which is considered as a classical hallmark of cancer. The changes observed in metabolic enzymes in KRAS-mutant cells were also recapitulated in human CRC tissues, including an upregulation in GLUT1 and the glutamine transporter SLC1A5 (Josiah et al., 2016; Toda et al., 2017). Besides enzymes implicated in glycolytic and glutamine metabolism, KRAS-mutant expressing CRC cells, such as DLD-1, also displayed quantifiable differences in phosphoserine biosynthesis pathway. An extensive whole-proteome profiling of normal, adenoma and adenocarcinoma matched clinical CRC tissues demonstrated that CRC progression is associated with changes in proteins belonging to several metabolic pathways including oxidative phosphorylation (OXPHOS), fatty acid metabolism, glucose import, and solute transporters for sugars or amino acids (Wiśniewski et al., 2015).

Macropinocytosis is a highly conserved endocytic process through which cells take up nutrients from the extracellular milieu via macropinosomes (Recouvreux & Commisso, 2017b). *KRAS* mutation increases the rate of macropinocytosis in cancer cells, as shown by several studies (Bar-Sagi & Feramisco, 1986; Commisso et al., 2013a; Tajiri et al., 2017). Recent reports show that increasing the rate of macropinocytosis aid cancer cells to adapt to the increasing demand for

nutrient supply required for tumor growth. Indeed, rate of macropinocytosis was elevated in glucose-addicted cells (Hodakoski et al., 2019b). Amino acid sources such as albumin and other proteins which are internalized via this process are degraded, and incorporated into TCA, acetyl-coenzyme A, glutamine, and serine/glycine metabolic pathways (Commisso et al., 2013b). Internalized proteins are degraded to amino acids such as alanine, which supports cell growth in low-glucose conditions by supplying to TCA intermediates and gluconeogenesis. Plasma membrane v-ATPase and bicarbonate transporter SLC4A7 play important roles in this process. Mutant RAS alters plasma membrane localization of v-ATPase and SLC4A7 expression in various cancer cell lines and human PDAC tissues. *In vivo* knockdown of SLC4A7 expression curbed mutant-RAS driven PDAC tumor growth. Depletion of v-ATPase also reduced the plasma membrane localization of RAC1 (Ramirez, Hauser, Vucic, & Bar-Sagi, 2019). A related study showed that lack of RAC1-activating guanine-exchange factor, dedicator of cytokinesis 1 (DOCK1) expression, inhibited the growth-advantage of KRAS-transformed cells in low-glutamine medium. Notably, DOCK1-selective inhibitor successfully inhibited macropinocytosis (Tajiri et al., 2017). Similarly, pretreating glucose-starved cells with RAC1 inhibitor also affected macropinocytosis uptake. Interestingly, inhibiting macropinocytosis with RAC1 inhibitor or macropinocytosis inhibitor EIPA selectively affected cells under glucose-starvation compared to complete growth media (Hodakoski et al., 2019b).

Autophagy is a mechanism that is utilized by cells to survive under nutrient stress, via a process of degrading unnecessary cellular components that are made available for reutilization (A. D. Cox et al., 2014). Classically, autophagy was thought to be non-selective process but it is now being increasingly appreciated as a selective process involving engulfment of specific cargoes (Kaur & Debnath, 2015). Autophagy-mediated degradation of proteins, lipids and glycogen produces amino acids, fatty acids and glucose, respectively, which can be used for glycolysis, TCA pathways and other energy production pathways. Several studies have reported that KRAS-mutant cells depend on autophagy to feed aggressive tumor growth (Guo et al., 2013; Kinsey et al., 2019; Lock et al., 2011). Expression of mutant $Hras^{G12V}$ or $Kras^{G12V}$ increased the basal rate of autophagy as measured by membrane-translocation and proteolytic processing of the autophagosome marker LC3. Viability of Ras-transformed cells were selectively affected upon starvation, only in cells lacking the essential autophagy-related (Atg) proteins Atg5 and Atg7 or p62 (Guo et al., 2011).

Inhibition of the MAPK pathway led to increased autophagic flux in KRAS-mutant PDA cells by increasing the phosphorylation of autophagic mediators Unc-51-like Kinase 1 (ULK1) and AMP-activated protein kinase (AMPK). Consistent with these results, co-treatment with combinations of trametinib (MEK1/2 inhibitor) with inhibiting autophagy (either by using the inhibitor chloroquine or by using cells expressing dominant-negative autophagy-related protein ATG4B) had synergistic anti-proliferative effects. The combined therapy was also successful in mediating tumor regression in NRAS-mutant, KRAS-mutant and BRAF-mutant melanoma, lung and CRC cells (Kinsey et al., 2019). Autophagy is also essential for mitochondrial functions. Indeed, *Ras*-mutated cells lacking autophagy-mediators (Atg5, Atg7, p62) displayed abnormal mitochondria and reduced levels of selective TCA metabolites that are produced at the mitochondria. Notably, oxygen consumption rate and ATP production due to mitochondrial respiration was also reduced in autophagy-depleted Ras-transformed cells (Guo et al., 2011). In summary, RAS-transformed cells support tumor growth in low-nutrient microenvironments by upregulating several nutrient-uptake pathways that can be therapeutically exploited.

1.6.4 Angiogenesis

In cancer, an "angiogenic switch" is continually ON to enable normally quiescent vasculature to sprout new blood vessels at an accelerated rate and sustain tumor growth by catering to the increasing demand for oxygen and nutrients. The blood vessels within the tumor microenvironment are activated by a mix of pro-angiogenic inducers that result in aberrant vessel branching and blood flow, enlarged vessels, leaky endothelium and increased endothelial cell proliferation (Hanahan & Weinberg, 2011). One of the most potent angiogenesis-stimulating growth factor is VEGF, which is also the prime target for anti-angiogenic therapy in CRC. In pancreatic tumor tissues, a strong correlation was observed between *KRAS* mutations and high VEGF expression (Ikeda et al., 2001). In CRC, patients with high VEGF expression had lower survival rates than those with lower VEGF expression (Ellis, Takahashi, Liu, & Shaheen, 2000). The first observation that mutant RAS oncogenes stimulate angiogenesis came from an early *in vivo* study, that showed that in addition to hyperplasia, activated Ras resulted in hypervascularized tumor tissues (Kranenburg, Gebbink, & Voest, 2004). One classic mechanism by which RAS modulates angiogenesis is by upregulating the expression of VEGF. Several studies show that in

CRC cells, oncogenic Ras is instrumental to increased expression of VEGF-A via multiple transcriptional and translational mechanisms. Further, downregulation of VEGF expression inhibited Ras-induced tumorigenic potential *in vivo*. Functionally, VEGF expression and other angiogenic factors in RAS-transformed cells stimulated the invasion and endotube formation of HUVEC endothelial cells in coculture experiments (Matsuo et al., 2009). Moreover, endothelial cell proliferation was enhanced upon addition of conditioned media from VEGF-overexpressed CRC cells. Notably, inhibition of VEGFR-2 kinase inhibitors reduced liver metastasis burden and tumor vasculature, and increased survival in mice injected with CT26 colon carcinoma cells (Ellis et al., 2000).

Another mechanism by which activated RAS mediates angiogenesis is by modifying the ECM in tumor microenvironment (Mathias et al., 2010). Activated Ras has been known to increase the expression of matrix metalloproteases (MMP-2, MMP-1 and MMP-9) and urokinase plasminogen activator (uPA) (Paciucci, Torà, Díaz, & Real, 1998), that act to breakdown the ECM. The uPA receptor (uPAR) localized plasmin formation to the cell surface, which facilitates tumor cell migration through ECM and basement membranes. Alternatively, uPA-uPAR complex on endothelial cells could promote the migration of developing sprouts through the ECM (Kranenburg et al., 2004). A third mechanism by which mutant RAS modulates angiogenesis is by inhibiting the expression of anti-angiogenic factors. One such negative regulators are thrombospodins, TSP-1 and TSP-2, which have important roles in tissue remodeling, metastasis, angiogenesis, wound healing, and inflammation. While the roles of TSP in angiogenesis and tumor growth remains controversial, several studies have pointed to an inhibitory role of TSP in blood vessel formation, angiogenesis and metastasis. Therefore, angiogenesis and metastasis seem to be mediated by a fine balance of pro-angiogenic VEGF and inhibitory factors, such as TSP (Gutierrez, Suckow, Lawler, Ploplis, & Castellino, 2003; Maeda et al., 2000; Tokunaga et al., 1999). TSP-1 expression is repressed in dysplastic regions undergoing extensive neovascularization in a mouse model of intestinal adenoma (Gutierrez et al., 2003). CRC is one of the best studied angiogenesis-dependent solid tumors, and it successfully responds to anti-angiogenic therapy. As previously discussed, many of these agents targeting either VEGF or their cognate receptors VEGFR are a part of conventional therapy for CRC. However, due to resistance mechanisms to anti-angiogenesis therapy and motivated by the clinical success of this line of therapy in colorectal tumors, several

new angiogenic agents are being developed or tested for metastatic CRC as discussed in an earlier section (Riechelmann & Grothey, 2017).

1.7 Targeting KRAS-mutant colorectal cancers is a challenging task

1.7.1 Direct inhibition of RAS

Targeting RAS-driven cancers is a multifaceted approach with direct and indirect means for curbing the activity of the oncogene. Direct inhibition of RAS has been extremely challenging thus far, thereby labeling mutant RAS as "undruggable". As RAS is a GTP-binding protein, early attempts consisted in the design of nucleotide-competitive inhibitors, similar to ATP-competitive inhibitors that successfully target several protein kinases. However, GTP is the most abundant intracellular nucleotide and binds with very high affinities to RAS, overriding the efficacy of GTP-competitive inhibitors (A. D. Cox et al., 2014). Another key requirement for RAS function is the post-translational mechanism that targets RAS to the PM. Two FTase inhibitors, lonafarnib and tipifarnib, have advanced to phase III clinical trials but lacked antitumor activity in RAS-driven colon or pancreatic cancers. This was attributed to compensatory mechanisms, such as alternative prenylation that ensures membrane localization of RAS in the absence of FTase enzyme (A. D. Cox et al., 2014). The compounds deltarasin and deltazinone reduce membrane-associated RAS by inhibiting guanine nucleotide dissociation inhibitor like solubilization factor or phosphodiesterase-6 delta (PDEδ). PDEδ is a membrane transport protein that can bind KRAS and modulates the membrane localization of KRAS. Deltarasin and deltazinone affected RAS-mediated tumorigenesis *in vitro* (Papke et al., 2016) and *in vivo* (G. Zimmermann et al., 2013). Other approaches being considered include the pan-RAS inhibitor (RAS-IN-3144) and the anti-sense oligonucleotide (AZD4785), the latter being tested in the clinic for KRAS-mutant lung cancers (Ryan & Corcoran, 2018).

While there is a dearth of drug-binding pockets on the surface of RAS, several attempts to identify direct binding inhibitors have been partially successful. Compounds SCH-53870, SCH53239 and SCH-54292, bind to a hydrophobic pocket near the switch II region, and interfere with GDP-GTP nucleotide exchange of RAS. However, these molecules are not very stable due to the presence of hydroxylamine and are associated with dose-limiting toxicity (A. D. Cox et al., 2014; Peri et al., 2005). Another group of direct inhibitors called MCP compounds identified in yeast two-hybrid

studies target the RAS-RAF interaction. One such compound, MCP110, successfully inhibited the PM localization of Raf to sites of activated Ras, but its potency is low with no structural information available on Ras binding (González-Pérez et al., 2010). Nuclear magnetic resonance studies have shown that active RAS exists in two conformational states, state 1 binds GEFs while state 2 binds effector proteins. The Zn^{2+} cyclen compounds selectively binds and stabilizes state 1, shifting the equilibrium and preventing the effector binding of RAS. However, cyclen compounds are not drug-like and not viable for *in vivo* studies (A. D. Cox et al., 2014; Rosnizeck et al., 2010). Further, two groups reported on KRAS4B binding compounds including DCAI, although weak binders they prevented RAS-SOS1 interaction and SOS-1 mediated nucleotide exchange. Little is known about the efficacy of these molecules against mutant RAS (A. D. Cox et al., 2014).

Work by the Shokat lab identified a previously unknown binding site in the $KRAS^{G12C}$ isoform (Ostrem, Peters, Sos, Wells, & Shokat, 2013), but other isoforms remain undruggable by this approach. Using a novel approach, thiol-reactive small compounds were identified that selectively bound mutant $KRAS^{G12C}$ isoform compared to wild-type KRAS. Biochemical studies show that the compound binds to a switch-II associated pocket, adjacent to cysteine at codon 12, which was not reported in other RAS structures. The compound selectively affected the viability of $KRAS^{G12C}$-positive lung cancer cell lines, and inhibited RAS activity by interfering with SOS-catalyzed nucleotide exchange and effector binding. Second, the compounds preferentially and irreversibly bind to RAS-GDP than RAS-GTP, suggesting that the success of this approach requires the cycling of mutant RAS between their nucleotide-bound states (Sheridan, 2020). Other compounds such as derivatives of brefeldin A and YM-254890 bind and stabilize the GDP-bound state of RAS. A recent switch-II binding inhibitor, ARS-1620, exhibited potent activity against $KRAS^{G12C}$-mutant cell lines versus control cells lacking the mutation. This study also demonstrated the therapeutic potential of ARS-1620 *in vivo*. Only xenografts established from $KRAS^{G12C}$- mutant tumors were sensitive to the drug. Moreover, a wide panel of $KRAS^{G12C}$, but not other KRAS mutant isoforms were differentially sensitive to the drug in 3D spheroids (Janes et al., 2018). Two direct covalent inhibitors of $KRAS^{G12C}$, AMG 510 and MRTX849, are in human clinical trials for KRAS-mutant lung tumors, but only a partial response is observed (Hata & Shaw, 2020; Sheridan, 2020). Prior experience with clinical inhibition of the MAPK pathway had taught

us that tumor cells re-adapt via multitude of feedback mechanisms to restore signaling. In line with this, a recent study employed single cell sequencing to identify resistance drivers in heterogeneous cell populations that responded differentially to $KRAS^{G12C}$ inhibitors (Xue et al., 2020). Cells adapted to the inhibitor by upregulating EGFR pathway signaling, upregulating the expression of Aurora kinase A, and upregulating the protein or mRNA expression of KRAS. Taken together $KRAS^{G12C}$ inhibitors are promising but should be considered in rational combinations with other inhibitors to improve efficacy.

1.7.2 Indirect inhibition of RAS

The current standard first-line therapy for RAS-mutated tumors consist of chemotherapy plus bevacizumab (Holch, Stintzing, & Heinemann, 2016). This is because testing CRC patients is obligatory for *KRAS*, *NRAS* and *BRAF*-mutations, as they are refractory to anti-EGFR therapy (Misale et al., 2012). Given the wide network of effectors downstream of RAS, targeting the signaling pathway effectors and availability of several protein kinase inhibitors have the potential to affect several aspects of KRAS-mediated malignancy. The MAPK pathway is not a linear cascade but consists of feedback mechanisms at multiple levels that complicate therapeutic efficiency. However, using RAF inhibitors (vemurafenib, dabrafenib or encorafenib) or MEK inhibitors (trametinib and selumetinib) in the clinic for KRAS-driven cancers either alone or in combination with chemotherapy have not been successful enough to warrant FDA approval, mainly due to resistance mechanisms that involve RAF1 and ERK re-activation, as mentioned previously. Several preclinical studies have tested MEK inhibitors with drugs targeting other pathways such as SHP-2/SOS, EGFR tyrosine kinase activity, Janus kinase, autophagy, etc., highlighting the potential for combination therapy in KRAS-mutant cancer (Drosten & Barbacid, 2020; Ryan & Corcoran, 2018). In mouse models of KRAS-mutant lung cancer, NVP-BEZ235, a dual pan-PI3K and mTOR inhibitor treatment alone did inhibit tumor growth, but tumor regression was achieved with cotargeting with MEK inhibitors (Engelman et al., 2008). However, co-targeting MEK and PI3K activities in the clinic are met with significant toxicities.

Several preclinical studies have established the importance of targeting autophagy downstream of mutant RAS (Mancias & Kimmelman, 2011). Autophagy inhibitors (chloroquine and its derivative

hydroxychloroquine) are already in clinical use and are now being tested in various cancers including pancreatic cancers (A. D. Cox et al., 2014; Ryan & Corcoran, 2018). Targeting glutamine dependency in KRAS-mutant cancers has shown preclinical potential by development of glutaminase enzyme inhibitor CB-839 (Mukhopadhyay et al., 2020). CB-839 is being tested in the clinic for many solid tumors, but not for KRAS-mutant CRC. KRAS-mutant cells were selectively lethal to oxidized form of vitamin C, which entered cells in a GLUT1-dependent manner. KRAS mutant cells were associated with more GLUT1 expression (Yun et al., 2015). Hence, vitamin C is currently being tested in several mCRC clinical trials.

Synthetic lethal approach has gained significant attention over other approaches, with the intention of finding 'Achilles heel' targets specific for mutant over wild-type RAS. Using siRNA or shRNA libraries in cells addicted or not to the KRAS oncogene, several synthetic lethal effectors, such as cell cycle and survival genes [baculoviral IAP repeat containing 5 (*BIRC5)* or survivin, anaphase-promoting complex/cyclosome (*APC/C)*, Wilms' tumor 1 (*WT1)*, *BCL-xL*], transcriptional factors [guanine adenine thymine adenine binding protein 2 (*GATA2)* and *SNAI2*], etc., have been identified (A. D. Cox et al., 2014). Notably, TANK-binding kinase 1 (*TBK1)* was identified as synthetic lethal in an shRNA screen for cell lines expressing mutant KRAS compared to wild-type counterpart. Loss of TBK1 expression reduced tumor growth of KRAS-mutant xenografts *in vivo*, and BCL-xL was deemed important for survival of TBK1-sensitive lung cancer cells (Barbie et al., 2009). Subsequently, studies have been divisive on the differential essentiality of TBK1 for KRAS-mutant CRC, lung and pancreatic cell lines (Muvaffak et al., 2014; Z. Zhu et al., 2014). However, combined MEK and TBK1 inhibitors (Z. Zhu et al., 2014) or MEK with BCL-xL (Corcoran et al., 2013) were successful in reducing survival of KRAS-mutant tumors. With the development of pooled CRISPR/Cas9 libraries, the search for RAS-specific synthetic lethal pathways have been uplifted. Using this new technology, five genes [Ras-converting enzyme 1 (*RCE1)*, Isoprenylcysteine Carboxyl Methyltransferase *(ICMT)*, *RAF1*, *SHOC2* and *P*tdIns(3,4,5)P3-dependent Rac exchanger 1 *(PREX1)*] were found essential in the context of oncogenic RAS in acute myeloid leukemia cells (Tim Wang et al., 2017). Other groups have applied this principle to other KRAS-mutant cancers, including CRC (Yau et al., 2017). In this study, genetic knockdown or small molecule inhibition of metabolic genes (*NADK, SUCLA2* and *KHK)* was selectively lethal to KRAS-mutant compared to KRAS wild-type xenografts. Notably,

the essentiality of these genes was identified *in vivo,* but not *in vitro*, highlighting the importance of tumor microenvironment to identify new therapeutic targets. As a positive control in such CRISPR screens, the KRAS-mutant cells were sensitive to loss of expression of the driving oncogene. These screens also have the additional advantage of identifying novel tumor suppressor pathways (Huang et al., 2019). Thus, new advancements in technology and recent achievements in identifying multiple direct and indirect inhibitors of mutant RAS activity, has instilled a cautious optimism to find better and effective ways to curb the oncogenic potential of RAS.

1.8 Probing cancer cell-surface proteomes for therapeutic targets

Proteins at the cell surface are attractive and accessible targets for immunotherapy. They are especially convenient for the design of monoclonal antibodies, which do not permeate plasma membrane, unlike small molecule inhibitors. A comprehensive mutational profiling of cell-surface coding genes in a panel of CRC lines uncovered several novel RTKs that could be targeted in CRC (Donnard et al., 2014). RTKs play very important roles in cancer, and their increased activity in tumorigenesis is often attributed to gene duplications, overexpression, point mutations, etc. (Casaletto & McClatchey, 2012). Identification of RTKs has significantly accelerated the race for targeted cancer therapies, enabling the development of monoclonal antibodies and tyrosine kinase inhibitors against several cell surface receptors, including EGFR, VEGFR, c-MET, etc. (Gschwind, Fischer, & Ullrich, 2004). A growing body of evidence suggests that RTKs are subject to spatial regulation in cancers. This is a concept that is vastly underappreciated and could likely affect the response or sensitivity to targeted therapies (Casaletto & McClatchey, 2012). For example, modulating the expression of oncogenic KRAS in human and mouse intestinal cells altered cell-surface EGFR levels and diminished sensitivity to cetuximab and EGF stimulation (Derer et al., 2012; van Houdt et al., 2010b). Analysis of whole membrane proteomes of clinically matched normal *versus* adenoma and carcinoma CRC tissues revealed that protein fractions corresponding to integral PM compartments were downregulated in cancer *versus* normal cells. Beyond RTKs, expression of solute transporters for uptake of sugars and amino acids were also upregulated in cancer cells suggesting that cell-surface proteins play critical roles in CRC progression (Wiśniewski et al., 2015). Similar observations were made in an isogenic model that progressed form normal cells to oncogenic $HRas^{G12V}$-transformed cells and ultimately metastasis.

Interestingly, in this model, the majority of genes altered enroute to malignancy belonged to the PM compartment. Notably, a network of genes involved ECM regulation such as collagens and laminins are amongst the most significant RAS-induced cell surface protein changes (Danielsson et al., 2013). Other reports have also shown that mutant RAS alters cell surface expression of cathepsin B (Cavallo-Medved et al., 2003), SLC1A5 (Toda et al., 2017), and GLUT1 (Pupo, Avanzato, Middonti, Bussolino, & Lanzetti, 2019). GLUT1 and SLC1A5 along with other cell-surface proteins were also identified differentially expressed by isolating and quantifying cell-surface proteins associated with CRC progression in other studies (de Wit et al., 2012; Wiśniewski et al., 2015).

Using a similar methodology, several interesting cell surface proteins were quantified as differentially expressed in KRAS-transformed MCF10A breast epithelial cell line *versus* isogenic controls (Ye et al., 2016). As previously seen, a majority of cell-surface changes mediated by mutant KRAS at the cell surfaces were downregulated. Notably, majority of these KRAS-mediated changes were rescued by MAPK pathway inhibition and not PI3K pathway, consistent with some studies in the literature that suggest that MAPK is the more dominant transforming pathway downstream of mutant RAS (Donnard et al., 2014). Furthermore, this study also highlighted the potential for combining the surfaceome approach with CRISPR/Cas9 technology and antibody phage display, to identify functional cell surface proteins that can be therapeutically exploited. Consistent with the aforementioned loss of EGFR expression in KRAS-mutant cells, sgRNA-mediated knockout of EGFR selectively affected viability of KRAS-wildtype rather than mutant MCF10A cells. Integrin Beta 5 (ITGB5) and CUB domain-containing protein 1 (CDCP1) were new interesting candidates, overexpressed on cell-surfaces of KRAS-transformed MCF10A, and identified as essential for cell proliferation via CRISPR assay. Other studies have also reported that CDCP1 is overexpressed in many solid cancers and could be therapeutically targeted (Leroy et al., 2015). Collectively, all these studies point to the potential of using cell surface proteomics to identify new "druggable" proteins that contribute to tumorigenesis. This is important as the limited targeted therapeutic options are associated with resistance mechanisms in KRAS-mutated CRC.

1.8.1 Most popular techniques employed for isolating cell surface proteins

Historically, isolation of cell surface proteins was carried out using fractionation and centrifugation techniques which were associated with low yields and cross-contamination from other organelles (Elschenbroich, Kim, Medin, & Kislinger, 2010). These drawbacks paved the way for the development of relatively 'new' techniques, most popular choices are the cell surface biotinylation (CSB) and chemical capture of cell surface glycoproteins. CSB involves selective, covalent labelling of proteins with biotin reagents, which are captured post-lysis onto streptavidin-coated solid surfaces. These biotin reagents consist of biotin moiety, a spacer (with or without cleavable linker unit), and a reactive moiety that interacts with certain chemical groups in proteins. Most used biotin reagent of this type is the sulfo- N-hydroxysulfosuccinimide (NHS) -esters, which selectively label proteins on exposed lysine residues, a feature that is abundant in most proteins. Sulfo-NHS-LC-biotin has been successfully applied to isolate cell surface proteins in combination with quantitative proteomics from several cell types *in vitro* and *in vivo* (Elschenbroich et al., 2010). The advantage of using chemoproteomics to quantify accessible cell-surface proteins clinically is well demonstrated by *in vivo* biotinylation of mice bearing A20 B-cell lymphoma. This study uncovered a promising therapeutic target bone marrow stromal antigen 2 (BST-2) that is selectively located at lymphoma blood vessels. Inhibition of BST-2 with monoclonal antibodies reduced growth of lymphoma xenografts (Schliemann et al., 2010). This technique was also successfully employed to quantify differential PM-associated proteins, and identify several cell receptors and cell adhesion molecules in metastatic *versus* primary CRC cells (Luque-García et al., 2010).

Comparison of different biotinylation methods to quantify cell surface proteins produced the most reproducible and high purity (~68%) results with amino-oxy-biotin (Weekes et al., 2010). Majority of cell surface proteins are glycosylated, and this is exploited by another labeling strategy called cell surface capture (CSC). CSC introduces an aldehyde group to sialic acid side chains of glycan residues on PM proteins by a selective periodate-enabled oxidation step. The next step is aniline-catalyzed oxime ligation reaction to stably attach amino-oxy-biotin to the aldehyde group. The success of using this reagent with proteomics was demonstrated in a model of Ras-induced senescence. A significant number of cell-surface proteins were enriched (~78% purity) and Notch1 was identified as upregulated at the cell surfaces of senescent cells. Novel non-canonical signaling

by Notch contributed to many facets of oncogene-induced senescence (Hoare et al., 2016). The protocol used to isolate biotinylated cell-surface proteins by either sulfo-NHS-biotin ester or amino-oxy-biotin was significantly improved to obtain consistently high yields and purity of PM proteins. While sulfo-NHS-biotin isolated more total PM proteins (~49%), amino-oxy-biotin had the highest purity of PM proteins *versus* intracellular proteins (~74%). This study successfully developed a reliable and reproducible protocol for routine isolation of PM proteins (Hörmann et al., 2016). Altogether, significant advancements in the labeling strategies combined with mass spectrometry has facilitated the quantification of several druggable cell surface proteins.

2 Altered levels of copper in the pathology of genetic diseases including cancer

Metal ions are vital for several cellular functions. They are essential for biochemical reactions and serve as cofactors to many biological processes, including transcription, DNA repair and enzymatic activity. The importance of trace metals in biology is further highlighted by the fact that altering their levels leads to several human disorders including cancer (C. R. Ferreira & Gahl, 2017; Serra, Columbano, Ammarah, Mazzone, & Menga, 2020). Several studies have reported that serum copper (Cu) levels and ceruloplasmin (CP) oxidase activity are increased in tumor tissues compared to matched control, in various types of cancer including lung, breast, gastrointestinal, and prostate (Habib, Dembinski, & Stitch, 1980; Linder, Moor, & Wright, 1981; Nayak, Bhat, Upadhyay, & Udupa, 2003; Rizk & Sky-Peck, 1984; Turecký, Kalina, Uhlíková, Námerová, & Krizko, 1984). CP is a serum glycoprotein consisting of six-seven copper atoms per protein, which utilizes 90% of dietary Cu for its activity. Linder *et al*., showed that activity and production of Cp is increased in rats with tumors (Linder, Bryant, Lim, Scott, & Moor, 1979), and the rate of intestinal Cu absorption is increased in tumor-bearing rats compared to normal rats (Cohen, Illowsky, & Linder, 1979). Using radioactive labelled Cu^{64}, the same group demonstrated that Cu-bound to Cp was readily taken up by tumor cells with similar uptake kinetics as unconjugated Cu, suggesting copper-bound Cp could be a potential Cu source for cellular uptake. Notably, tumor tissues absorbed the bulk of radiolabeled Cu compared to normal tissues, suggesting an accelerated import of Cu to tumors (C. H. Campbell, Brown, & Linder, 1981). Abnormal levels of Cu are also a consequence of inherited genetic disorders such as Wilson's, Menkes, Occipital horn syndrome which are lethal in children if not intervened early. Clinical manifestations of Wilson's disease

include abnormal accumulation of Cu in liver and brain, with decreased CP and Cu levels in the blood serum for both Wilson's and Menkes disease. In Menkes patients, activities of Cu-dependent enzymes are diminished due to defective incorporation of Cu. The genes implicated in these disorders were discovered to be copper-exporting *ATP7B* (Wilson's disease) and the closely related *ATP7A* (Menkes disease) (C. R. Ferreira & Gahl, 2017). Given its role in regulating the activity of ferroxidases, Cp and hephaestin, mice deficient for dietary copper exhibited classical symptoms of anemia that can be reversed by Cu-supplementation (Tao Wang et al., 2018). Consequently, iron homeostasis and distribution are affected in the absence of Cu. CP is required for the release of iron from reticuloendothelial storage sites. CP is also essential for the oxidation of ferrous to ferric iron facilitating incorporation into the iron transport protein transferrin (C. R. Ferreira & Gahl, 2017). Interestingly, rats fed with a diet rich in iron had impaired growth and exhibited low serum and tissue Cu levels, which was reversed by Cu supplementation (Ha, Doguer, Wang, Flores, & Collins, 2016), suggesting an overlap in iron-copper metabolism. Owing to the fact that brain contains high levels of Cu, Cu is involved in the pathogenesis of neurological disorders including Alzheimer's, Parkinson's disease, amyotrophic lateral sclerosis and Huntington disease (Desai & Kaler, 2008). Therefore, disruption of metal ion homeostasis can contribute to serious metabolic disorders, and their roles in tumor biology is an understudied subject.

2.1 Cu-binding proteins play diverse biological roles in mammalian cells

While copper deficiency leads to incomplete growth, excess copper can be damaging to cells. Systemic copper deficiency resulted in anemia and stunted body growth of rats (Ha et al., 2016). Free Cu generates hydroxy radicals and reactive oxygen species (ROS) that are responsible for lipid peroxidation in membranes, direct oxidation of proteins, and cleavage of DNA and RNA. When present in excess, it can also compete with other essential metals such as ferrous-Sulfur clusters and zinc (Zn), affecting structure and/or activity of metalloproteins (Festa & Thiele, 2011). Notably, excess Cu can interfere with the activity and structure of Zn-dependent p53 protein (Tassabehji, VanLandingham, & Levenson, 2005). Copper can exist in oxidized Cu(II) and reduced Cu(I) states enabling its use as a cofactor in redox chemistry. They serve as sites of electron transfer between proteins and catalyze the activity of cuproenzymes required for growth

and development. Copper is required for myriad cellular functions ranging from neurotransmitter production, mitochondrial respiration, pigment formation, and connective tissue strength, to name a few. Studies have shown that levels or activity of cuproenzymes, implicated in some of these biological functions, including CP, copper/zinc superoxide dismutase (SOD1), cytochrome c oxidase (CCO), and lysyl oxidase (LOX) could serve as clinical markers for copper deficiency (Desai & Kaler, 2008). Amongst the clinical features of Wilson patients, mitochondria are often observed as swollen and disorganized. Other *in vivo* models have shown that exposure excess Cu or chronic Cu-deficiency exhibit irregular mitochondria morphology (J R Prohaska, Downing, & Lukasewycz, 1983; L. Zeng, Ai, Zhang, & Li, 2020). Mitochondria contains two major cuproenzymes - CCO and SOD1. SOD1 converts superoxide anions to peroxide, playing critical roles in ROS scavenging. Cu-deficient rats displayed reduced activity and levels of SOD1 in various tissues, suggesting post-transcriptional regulation of SOD1 by Cu (Joseph R Prohaska, Geissler, Brokate, & Broderius, 2003). CCO is located at the inner membrane of mitochondria and is required for the mitochondrial ETC activity and ATP production. Copper deficiency or overloading affected the activity and expression of CCO and interfered with mitochondrial respiration (Sokol, Devereaux, O'Brien, Khandwala, & Loehr, 1993; H. Zeng, Saari, & Johnson, 2007). Another Cu-dependent oxidase enzyme LOX is required for formation and stabilization of connective tissue. Their primary role is to convert lysine residues in collagen and elastin to reactive aldehydes during ECM remodeling. Cu-dependent tyrosinase regulates pigmentation and melanin production. Activity of both LOX and tyrosinase are defective in Menkes patients (C. R. Ferreira & Gahl, 2017), and the associated mice model (Y. Wang, Zhu, Weisman, Gitlin, & Petris, 2012), displaying clinical symptoms of connective tissue malformation and hypopigmentation patches. Some of the well-known Cu-binding proteins and their roles in biology are listed below.

Table 1.2. Summary of Cu-binding proteins and enzymes in humans and their biological functions

ENZYME/PROTEIN	FUNCTION
Cytochrome c oxidase (CCO)	Mitochondrial oxidative phosphorylation, ATP production
Cu/Zn superoxide dismutase (SOD1)	Free radical detoxification

Tyrosinase	Melanin synthesis, pigmentation
Ceruloplasmin (CP)	Ferroxidase: Fe loading onto transferrin, anemia
Lysyl oxidase (LOX)	Crosslinking of collagen and elastin, cell-cell contact, ECM modeling
Lysyl oxidase-like proteins (LOXL)	E cadherin silencing and EMT, ECM modeling
Hephaestin	Ferroxidase for ferroportin-mediated iron efflux, iron anemia
Dopamine β–hydroxylase	Norepinephrine synthesis
Copper amine oxidase (SSAO)	Deamination of primary amines to aldehyde, immune response. Fat metabolism
Diamine oxidases	Degrade histamine
Peptidylglycine α-aminating monooxygenase	Activation/maturation of neuropeptides
X-linked inhibitor of apoptosis protein (XIAP)	Inhibitor of apoptosis, inhibition of caspases
Glucose oxidase	Pentose phosphate pathway oxidoreductase
Coagulation factors V and VIII	Blood coagulation, Hemophilia
Mitogen activated kinase (MEK) 1/2	Signal transduction, activation of MAPK pathway
Amyloid precursor protein	Neuronal development, associated with Alzheimer's disease
Antioxidant Protein 1 (ATOX1)	Metallochaperone that delivers Cu to ATP7A/ATP7B, aids in cuproenzyme maturation and cu export
ATP7A	Cu export, cuproenzyme maturation and Cu loading

CTR1	High-affinity cellular import
CCS	Metallochaperone transfer Cu to SOD1
COX17	Metallochaperone that transfer Cu to SCO1 and COX11 in mitochondria for delivery to cytochrome c oxidase
Glutathione (GSH)	Metallochaperone transfers Cu to MT, Cu detoxification
Metallothionein (MT)	Sequesters Cu in cytoplasm, Cu detoxification

2.2 Charting the trajectory of Cu in the body

2.2.1 Cellular Cu uptake mechanisms

Dietary Cu is primarily absorbed through the mucosal wall of enterocytes in the small intestine. In portal circulation, Cu(II) is carried by the albumin-histidine complex (containing ~18% total Cu), and is released as Cu-histidine serving as a donor of Cu for tissues along with CP and α2-macroglobulin (containing ~12% total Cu), another major source of exchangeable Cu. The remaining exchangeable Cu is bound to CP. Except for the liver, both CP and histidine are said to release Cu at the cell surface and not penetrate the PM (Harris, 2000; van den Berghe & Klomp, 2009). One mode of high-affinity (K_m~1-5 μM) transport of Cu through PM of intestinal epithelial cells or other cells is via an importer CTR1 (*SLC31A1*) that is well-conserved from yeast to humans (Öhrvik & Thiele, 2014). Strains lacking *SLC31A1*-equivalent homologues had difficulty to grow in low-Cu conditions (Nevitt, Ohrvik, & Thiele, 2012). Mice lacking *Ctr1* die *in utero*, and display severe developmental deficits (Kuo, Zhou, Cosco, & Gitschier, 2001). CTR1 is a heavily glycosylated PM protein, with serine and methionine-rich residues and repeats of MX3M motifs (Harris, 2000). Mutational and functional studies in yeast reveal that MX3M motif in Ctr1 is critical for Cu uptake, suggesting a Cu(I) coordination state affinity for methionine residues during importation (B.-E. Kim, Nevitt, & Thiele, 2008). CTR1 forms a multimeric pore on the PM and requires reduction of Cu(II) to Cu(I), and so its maximal activity is dependent on Cu/Fe (iron) metalloreductases STEAPs (Nevitt et al., 2012; Öhrvik & Thiele, 2014). Intestinal knockout of *Ctr1* in mice, affected post-natal growth and iron metabolism implicating the importance of CTR1 in absorption of dietary Cu (B.-E. Kim et al., 2008).

However, we lack more information on the regulatory process that drives Cu(I) transport from the diet through CTR1 located at the apical surfaces of brush border microvilli in IEC. Adding to the complexity is that CTR1 is located at apical cell membranes only in suckling mice but is relatively more intracellular in adult mice (Lutsenko, Barnes, Bartee, & Dmitriev, 2007). Located in duodenal enterocytes, is another potential Cu importer- the divalent metal transporter 1 (DMT1). Although its primary role is in iron uptake, DMT1 has affinity to several other metals including Cu. In several models including CRC line CACO-2 and *Drosophila melanogaster*, loss of DMT1 function resulted in Cu intracellular limitation. However, patients with *DMT1* mutations exhibited defects in iron metabolism with no apparent defects in Cu levels, questioning the role of this pathway in Cu uptake (van den Berghe & Klomp, 2009). Although evidence is weak for the role of CTR2 in Cu importation, in the absence of CTR1, several studies state that the CTR1-related CTR2 can also transport Cu(I) across membranes. Notably, mRNA levels of CTR2 is low compared to CTR1, especially in the intestines. CTR2 is more readily located at the membranes of vacuoles and intracellular vesicles such as endosomes and lysosomes, but expression of cell-surface directed Ctr2 does rescue growth defective phenotype of yeast strains lacking Ctr1 in low Cu conditions. Cell-surface import of Cu by CTR2 is ~20-fold less than CTR1 (van den Berghe & Klomp, 2009). Similar to the functional requirement of CTR1 on six-transmembrane epithelial antigen of the prostate (STEAP), phenotype rescue by Ctr2 in low Cu conditions was dependent on the expression of yeast ferroreductase, Fre6 (Rees & Thiele, 2007). Studies in mice also show the existence of an additional low-affinity (K_m ~ 10 μM) Cu uptake pathway that is not yet characterized (B.-E. Kim et al., 2008). This suggests existence of multiple mechanisms of Cu uptake besides the high affinity importer, CTR1.

2.2.2 Intracellular transport of Cu by chaperones

Once inside cells, Cu binds to cytosolic proteins such as ATOX1, copper chaperone for SOD1 (CCS), and C oxidase 17 copper chaperone (COX17) rapidly as free Cu is toxic to cells. The current understanding is that Cu moves between organelles and via cell membranes bound to Cu-delivering proteins. Yeast studies have demonstrated that metallochaperones function to prevent intracellular scavenging of Cu, and enable Cu availability for Cu-dependent functional proteins (T. D. Rae, Schmidt, Pufahl, Culotta, & O'Halloran, 1999). This suggests that free Cu ions in cells

are highly limited, and cuproenzymes are not activated by free Cu ions. Cox17 was initially identified in yeast as necessary for mitochondrial respiratory complex IV (CCO) assembly and can bind up to four Cu(I) atoms. Cox17 along with Cox11 and synthesis of cytochrome c oxidase (Sco 1/2) proteins are essential for copper transfer to CCO in mitochondria (Horng, Cobine, Maxfield, Carr, & Winge, 2004). Without Cu as cofactor, SOD1 is catalytically inactive and SOD1-deficient cells are unable to protect themselves against oxidative stress. Cu-chaperone CCS is structurally similar to SOD1 and transfers Cu to SOD1 via direct physical interaction (B.-E. Kim et al., 2008; T. D. Rae et al., 1999). Although yeast strains lacking Ccs are defective in SOD1 activity, this is overcome by exogenous Cu suggesting additional Ccs-independent mode(s) of SOD1 activation by Cu (T. D. Rae et al., 1999). Another Cu chaperone glutathione (GSH) has been shown to load Cu onto apo-SOD1 (Harris, 2000). ATOX1 delivers Cu(I) to the secretory compartment, where it binds to metal-binding domain (MBD) repeats with the consensus GMTCXXC motif at the N-terminal segments of copper exporters ATP7A and ATP7B (Wernimont, Huffman, Lamb, O'Halloran, & Rosenzweig, 2000). It was shown using yeast homologue of ATP7A/ATP7B, Ccc2, which is located at the outer membranes of TGN, that it receives Cu (I) ions from ATOX. Cu ions are then pumped into the compartment by Ccc2 via unknown mechanisms for loading onto cuproenzymes (Banci, Bertini, Chasapis, Rosato, & Tenori, 2007). Once inside the secretory lumen, the steps needed to load Cu onto apoenzymes in unclear. Studies using Cp show that apoenzymes traversing the secretory pathway may acquire Cu directly without local Cu-chaperones (B.-E. Kim et al., 2008). *Atp7a* and *Atox1* knockout mice display decreased SOD3 activity and expression, supporting the role of these Cu-chaperones in regulating the function of cuproenzymes in TGN (Jeney et al., 2005; Qin, Itoh, Jeney, Ushio-Fukai, & Fukai, 2006). Furthermore, activity of essential enzymes such as CCO, CP, dopamine-beta-hydroxylase, and tyrosinase are deficient in mice lacking *Atox1* or *Atp7a* (I Hamza et al., 2001; Hunt, 1974; Phillips, Camakaris, & Danks, 1986). ATP7B can also deliver Cu to apo-CP (Terada et al., 1998). Consequently, yeast strains lacking ctr1 or ctr3 are respiratory-deficient, oxidative stress-sensitive and iron deficient, suggesting a dearth of intracellular Cu levels to support these functions (Rees & Thiele, 2007).

Most of the Cu in intestinal cells is tightly bound to cysteine-rich Cu-chaperones such as metallothionein (MTs) and GSH (Hunt & Port, 1979). Cu(I) bound to GSH is present at high

intracellular concentrations and could potentially convey Cu to MTs. Both these chaperones play a crucial role in intracellular metal detoxification (Calvo, Jung, & Meloni, 2017; A. M. Ferreira, Ciriolo, Marcocci, & Rotilio, 1993; Harris, 2000). Levels of cellular GSH correlate with rate of Cu uptake and exchangeable pool of Cu. Gsh levels are altered in Cu-deficient rats and required for biliary excretion of Cu. Besides MTs, GSH is also implicated in Cu transfer to other apo-enzymes including CP, SOD1, and hemocyanin (Harris, 2000). Reducing Gsh levels in Cu-deficient rats increased intracellular Cu levels in hepatocytes which were not bioavailable to circulation, suggesting that in liver GSH serves to mobilize Cu stores for systemic supply (Nevitt et al., 2012). Mammalian MTs are composed of various isoforms, the major isoforms MT-1 and MT-2, predominantly bind Cu, but also have affinity for other metals including Zn and cadmium. Interestingly, MT binding to Zn is readily exchanged for Cu, when sufficiently amount of the metals are present (Gudekar et al., 2020). MT increase in several tissues, including the intestines, in response to systemic changes in Cu levels (Calvo et al., 2017; Kelly & Palmiter, 1996). Mice lacking Mt in the *Atp7a*-mutant background, lacked Cu tolerance compared to Mt-sufficient littermates. Loss of Mt and Atp7a collectively accumulated Cu levels, and loss of Mt alone altered Cu homeostasis. Similar results are observed in cultured cells lacking MTs *in vitro*. Growth defect of ATP7A/MT-deficient cells were rescued by chelating Cu with bathocuproine disulfonate (BCS), suggesting that MTs are critical to protecting cells from cuproptosis (Gudekar et al., 2020; Kelly & Palmiter, 1996). Taken together several Cu-binding proteins play a concerted role in maintaining Cu bioavailability and delivery within cellular compartments, but there are lot of gaps in our understanding of Cu homeostasis in cells (B.E. Kim et al., 2008).

2.2.3 Exporting Cu out of cells

Interestingly, *Atp7a* and *Atox1* knockout mice accumulate Cu in the intestine and kidney but lack Cu in brain and liver and exhibit post-natal lethality and mortality. This Cu accumulation in intestines has been shown to be due to a defect in Cu egress out of cell and not uptake, resulting in Cu deficiency in other organs (I Hamza et al., 2001; Hunt, 1974; Packman, 1987; Phillips et al., 1986). The *in vivo* results were recapitulated in IEC-6 cells, wherein knockdown of Atp7a hyperaccumulated Cu (Gulec & Collins, 2014). This suggests that ATP7A is essential for supplying diet-sourced Cu out of the intestines to other organs that utilize Cu. While ATP7A is

implicated in the biosynthesis of various metalloenzymes in the TGN, excess Cu causes the translocation of ATP7A to cell periphery (M J Petris & Mercer, 1999; M J Petris et al., 1996). As previously mentioned, excess Cu is a ROS inducer and ATP7A-overexpressing cells had an increased propensity to resist cuproptosis (excess Cu-ion induced cell apoptosis). Cu-resistant variants of chinese hamster ovary (CHO) cells maintained low intracellular Cu even in the presence of high exogenous Cu. This was attributed to overexpression of ATP7A and an increased rate of Cu efflux (Camakaris et al., 1995). This cell-surface localization of ATP7A due to changes in intracellular Cu is abolished in *Atox1* mutants, suggesting a role for ATOX1 in this process (Iqbal Hamza, Prohaska, & Gitlin, 2003). This way ATP7A plays a major role in shuttling Cu through epithelial and endothelial barriers, thereby regulating processes such as intestinal and renal absorption of Cu and Cu transport across blood brain barriers (Lenartowicz et al., 2015). Similar shuttling mechanisms have been reported for ATP7B, Cu-exporter implicated in the Wilson's disease (Lutsenko et al., 2007; Tuo Wang & Guo, 2006). ATP7B expression is relatively lower than ATP7A and is most abundant in liver and less so in the kidneys, placenta, intestines and brain (Tuo Wang & Guo, 2006). Liver is a major Cu storage organ (Chun, Catterton, Kim, Lee, & Kim, 2017), and CP is synthesized and secreted by the liver. Therefore, hepatic Cu is redistributed to the plasma by ATP7B via its regulation of Cu loading and maturation of CP in secretory vesicles. In line with this, introduction of a full-length ATP7B in the rat model of Wilson's disease rescued the excess Cu-accumulated in liver. These studies also showed that ATP7B regulates the excretion of copper from bile (Terada et al., 1999). Taken together, ATP7A and ATP7B proteins play mutually exclusive functions of copper loading in the secretory compartment and copper export from cells, both these functions are also critically dependent on the ATOX1 Cu chaperone protein. Physiologically, symptoms of Menkes disease arise due to the inability of ATP7A to pump Cu across basolateral membrane of intestinal epithelial cells disrupting systemic Cu supply, highlighting the importance of Cu efflux role of ATP7A.

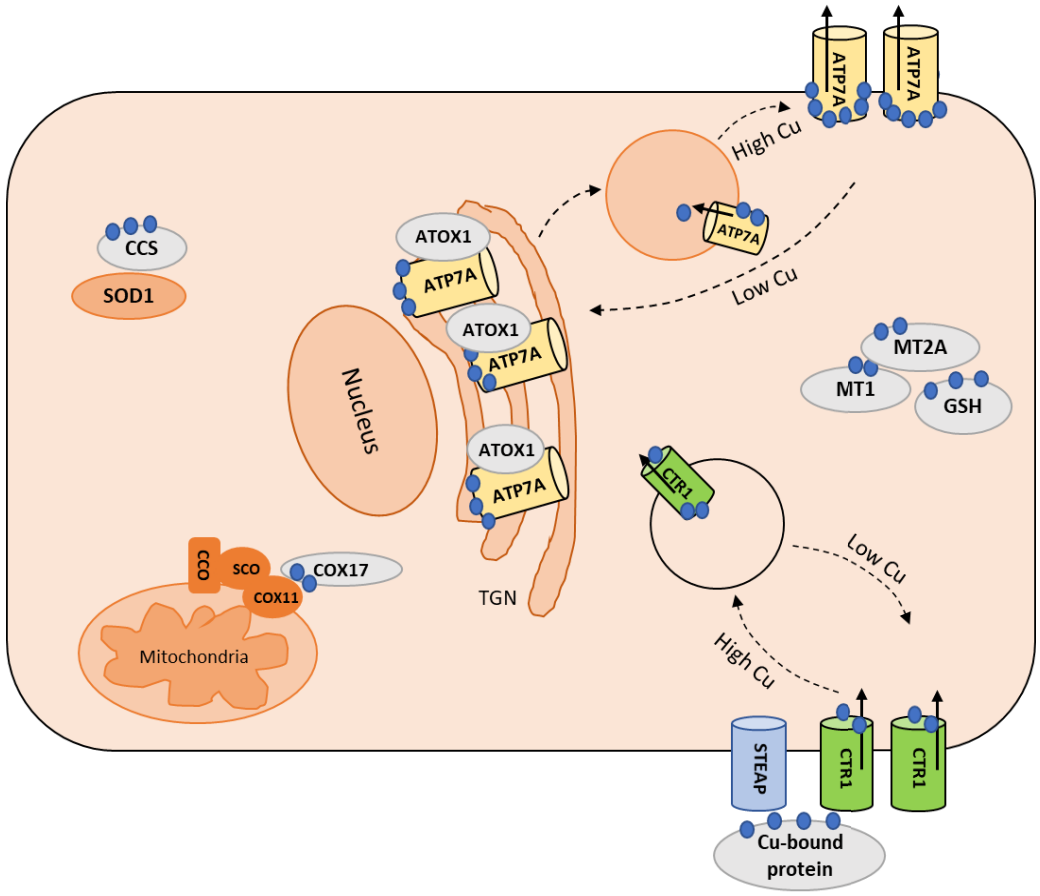

Figure 1.10. Schematic representation of Cu homeostasis in intestinal epithelial cells (IEC)
Cu (blue circles) is absorbed by the intestines bound to proteins such as albumin, ceruloplasmin in serum. Cu is primarily imported into cells as Cu(I) by high-affinity CTR1 importer, a process dependent on STEAP family of metalloreductases which reduce Cu(II) to Cu(I). If intracellular Cu increases, CTR1 is downregulated via endocytosis into vesicles to reduce Cu importation. Alternatively, cell-surface CTR1 increases during Cu starvation. CTR1 or the related Cu importer CTR2 are also thought to mobilize Cu from intracellular vesicles. Once inside, Cu is carried to respective compartments by Cu-binding chaperones (grey circles). COX17 transports Cu to SCO and COX11 complexes in mitochondria driving Cu supply to electron transport chain (ETC) enzyme cytochrome c oxidase (CCO). CCS chaperone supplies Cu to the antioxidant enzyme Cu/Zn superoxide dismutase (SOD1). ATOX1 transports Cu to Cu-exporting ATP7A and ATP7B proteins in the secretory compartments of trans-Golgi network (TGN). ATP7A and ATP7B imports Cu into secretory vesicles for loading onto cuproenzymes. If intracellular Cu increases, ATP7A translocate from TGN to cell periphery via vesicles to export Cu to extracellular milieu. Alternatively, Cu starvation decreases cell-surface associated ATP7A. Intracellular exchangeable pools of Cu are likely stored in glutathione (GSH) and metallothionein (MT) which are also crucial for metal detoxification.

2.2.4 Potential intracellular stores of Cu

The mechanisms regulating Cu reserves inside cells needs more investigation. Intriguingly, Cu that enters hepatocytes become absorbed in cells and only ~40% is subject to efflux. While a significant portion is bound to Cu-chaperones as discussed above, evidence suggests that Cu is also likely stored in intracellular compartments. It is thought that intracellular Cu-derived from CP localize into two distinct compartments- endosomes and clathrin-coated vesicles that merged to lysosomes. This suggests that vesicular Cu is a dynamic Cu-transporting organelle inside cells (Davidson, McOrmond, & Harris, 1994; Harris, 2000). Yeast vacuoles are somewhat functional to mammalian lysosomes. Indeed, studies in yeast show that ctr2 and fre6 metalloreductase work in a concerted fashion to mobilize Cu stores from vacuoles to the cytosol via undefined mechanisms (Rees & Thiele, 2007). In mammalian cells, CTR2 and CTR1 localize to intracellular organelles such as lysosomes and endosomes, but it is yet to be determined if they are functional (B.-E. Kim et al., 2008). However, CTR2 mediated Cu transport from lysosomes to cytosol is being considered as a possible theory after degradation of Cu-containing proteins in the lysosomes (Polishchuk & Polishchuk, 2016). By imaging cells lacking CTR2 with Cu-fluorescent sensors researchers showed that Cu accumulated in late endosomes. This study also established a role for CTR1 in mobilizing Cu stores out of endosomes (Öhrvik et al., 2013). CTR1 could also be implicated in mobilizing Cu stores from endosomes to cytosol, and this could be one of the possible explanations as to why intestinal cells lacking Ctr1 hyperaccumulate Cu (Nose, Kim, & Thiele, 2006). MTs have been implicated in the storage and delivery of Cu to lysosomes. It is proposed that the acidic environment of lysosomes would favor the degradation of MT and displacement of Cu (Polishchuk & Polishchuk, 2016). Similarly, yeast mitochondria were reported to contain significantly higher unbound-Cu levels, more than the amount that is required for functioning of Cu-dependent cuproenzymes. This Cu pool is dynamic and responds to changes in cytosolic Cu levels. Addition of exogenous Cu further augments the endogenous Cu pools of mitochondria (Baker, Cobine, & Leary, 2017; Cobine, Ojeda, Rigby, & Winge, 2004). Overall, while some minimal lines of evidence suggest the existence of intracellular Cu-storing organelles, more studies are needed to fortify this theory.

2.3 Different ways of regulating Cu-homeostasis proteins by fluctuating Cu levels

The mRNA coding for CTR1 do not seem to change as an indicator of Cu status. However, cells deal with excess Cu by stimulating the endocytosis of cell surface CTR1 into endocytic vesicles, reducing further Cu importation (Michael J Petris, Smith, Lee, & Thiele, 2003). Inhibiting clathrin-dependent endocytosis prevented CTR1 internalization. Other studies have implicated macropinocytosis in the degradation of cell surface CTR1 (Holzer & Howell, 2006). CTR1 internalization is proportional to increasing doses of Cu and silver [Ag(I) is isoelectric to Cu(I)], but not Zn or Fe. These experiments also suggest that although there is steady-state expression of CTR1 at the cell surface, their levels are constitutively recycled between endocytic vesicles and the PM. Alternatively, CTR1 is increased in the intestines of Cu-deficient mice (Chun et al., 2017). Chaperone CCS is regulated at the level of protein degradation via a 26S proteasome-dependent mechanism. In cultured mammalian cells or rodent models, CCS levels are inversely correlated to Cu levels. Rats fed with Cu-deficient diets accumulate CCS levels in liver and erythrocytes, which does not correspond to mRNA levels (Bertinato & L'Abbé, 2003). Similarly, cells treated with copper chelator also increased CCS levels and stability (half-life ~22 h). In both the cases, addition of exogenous Cu and not Fe or Zn prevented the increase of CCS. Alternatively, exogenous Cu reduced CCS levels (half-life ~6 h). In an opposite manner, Cu levels also regulate basolateral membrane-associated Cu-dependent protein called hephaestin in colon carcinoma cells. Cells with low Cu levels exhibit low hephaestin levels (Nittis & Gitlin, 2004). In IEC-6 cells, exogenous Cu increased Atp7a protein levels and not mRNA in a dose-dependent manner. The increase in Atp7a levels was attributed to increased stability in presence of Cu (half-life ~41 h) and degraded under conditions of Cu-deprivation via the proteasome pathway. The increase in Atp7a in IEC-6 was specific to Cu and Ag, but not to other metals (Chun et al., 2017; L. Xie & Collins, 2013). Although ATP7A transcript changes are generally not thought to change with respect to Cu levels, one study showed that CHO cells chronically exposed to Cu and selected for cuproptosis-resistance increased both Atp7a mRNA and protein levels (Camakaris et al., 1995). MTs are regulated transcriptionally and induced by metal regulatory transcription factor 1 (MTF-1) transcription factor in response to heavy metals (Gudekar et al., 2020). In IEC-6 cells which accumulated Cu upon Atp7a knockdown, expression of Mt1a increased in parallel (Gulec & Collins, 2014). Other *in vitro* and *in vivo* models of Cu accumulation also demonstrate increased transcript levels of MT genes- Mt1a and Mt2a, to deal with Cu-toxicity (Packman, 1987; L. Xie & Collins, 2013). Overall, several Cu-

dependent proteins and genes are regulated in response to fluctuations in intracellular Cu levels, and these changes can be used for indirect assessment of Cu levels.

2.4 Structural regulation of ATP7A

ATP7A and ATP7B are Cu exporters and are classified as members of P-type ATPase family based on their conserved functional domains. They are essentially ATP-driven membrane pumps. In the context of Cu, high-affinity metal binding triggers the translocation of ATP7A or ATP7B to the cell surface and subsequent release to the cell exterior, a process that is driven by the energy produced during ATP hydrolysis (Lutsenko et al., 2007). ATP7A and ATP7B share a structural core consisting of eight transmembrane-spanning segments (TMS). The N-terminal tail contains six repetitive MBD with metal-binding motif GMxCxxC (where x is any amino acid), that serve as Cu-coordinating ligands for Cu(I) binding. They also contain protruding cytosolic and soluble domains including an N-domain with an ATP-binding site, catalytic P-domain undergoing phosphorylation and A-domain with the conserved TGE motif required for dephosphorylation and terminating the catalytic process (Lutsenko et al., 2007; Skjørringe et al., 2017). The central step in the catalytic process is the transfer of γ-phosphate from ATP to the invariant aspartic acid residue in DKTG motif of the P domain, resulting in a transient phosphorylated-intermediate. Completion of the autophosphorylation process and ATP hydrolysis (ATP to ADP conversion) causes a conformational change that places the Cu-bound TMS in an outward-facing, low-affinity state. After Cu release, ATP7A is dephosphorylated and returns to the inward-facing conformation. The Cu-chaperone ATOX1 interacts with the N-terminal MBD via the CxxC motif. The translocation of ATP7A from TGN to cytosolic vesicles and to the PM, is eventually returned to the TGN when Cu levels are restored to manageable levels. At the TGN, a similar mechanism of ATP-driven process is proposed for Cu delivery into the secretory lumen for utilization by cuproenzymes.

Analysis of disease-associated mutations and *in vitro* studies using mutant *ATP7A* and *ATP7B* reveal that several structural elements are necessary for their function. 1) TMS 3 was found to be essential for movement from the endoplasmic reticulum to TGN, 2) MBD segments 5 and 6 are necessary for the functional activity, 3) C-terminal dileucine motifs (residues 1487–1488), and 4)

phosphatase motif (TGE motif, residues 873–878 in the A domain) are necessary for retrieval of ATP7A to endosomes as these mutants are essentially trapped in the PM, 5) highly conserved CPC residues 1000–1002 from the TMS 6 and, 6) a phosphorylation motif (DKTG; residues 1044–1047) are essential for Cu-induced PM trafficking, 7) a C-terminal PDZ motif ($D^{1497}TAL^{1500}$ residues) along with di-leucine motif ensures apical membrane expression of ATP7A (Yi & Kaler, 2014). In addition, nine amino acids $F^{37}AFDNVGYE^{45}$ in N terminus of ATP7B were shown to be essential for TGN retention in low Cu, and for targeting to apical membranes of hepatocytes during high Cu conditions. Certain invariant residues in the N-domain that are critical for coordination of ATP differ between ATP7A and ATP7B and are indicated in Figure 2.2 (Braiterman et al., 2009; Lutsenko et al., 2007).

The importance of phosphorylation in regulating trafficking and activity of Cu-ATPases has been suggested, after the observation that human ATP7A and ATP7B are phosphorylated on serine residues *in vitro* and *in vivo* (Veldhuis et al., 2009). Several studies have demonstrated evidence of phosphorylation of human and yeast ATP7A by AKT2 and PKA kinases (Sudhahar et al., 2018; Valverde et al., 2008). A global study to identify phosphosites in human and hamster ATP7A identified 21 novel phosphosites. Although a subset of the sites was phosphorylated in response to Cu, only mutations of serine residues 1469 or 1432 at the C-terminal region abrogated Cu-responsive trafficking to the PM without affecting TGN localization (Veldhuis et al., 2009). A wide-panel of patient-derived *ATP7A* mutants displayed defective post-TGN localization in response to Cu. A vast majority of these mutations are present in the P domains which regulate phosphorylation, suggesting the importance of this domain in the catalytic function of ATP7A (Skjørringe et al., 2017). Another feature of ATP7A is that it is heavily glycosylated and runs as diffuse bands (Yueyong Liu, Pilankatta, Hatori, Lewis, & Inesi, 2010; Yamaguchi, Heiny, Suzuki, & Gitlin, 1996). Therefore, inhibiting this post-translational modification with glycosidase or tunicamycin altered the mobility of ATP7A and it appears as a sharp band in gels. Intriguingly, ATP7B does not seem to be glycosylated in these experiments. This seems consistent with presence of N-linked glycosylation motifs in ATP7A but not in ATP7B. These motifs are in the cytosolic loops between TMS 1 & 3 and TMS 5 & 6 which are likely exposed to the extracellular milieu when ATP7A is PM localized. Pulse chase experiments show that ATP7A is converted to a complex, higher molecular weight glycosylated protein after synthesis, consistent with ATP7A

localization at the TGN (Yamaguchi et al., 1996). The importance of this post-translational modification in proper localization and thus functioning of ATP7A is demonstrated by the mutant variant A1364D from the clinical model of Menkes disease, which exhibited a defect in glycosylation, and was consequently mislocalized to endoplasmic reticulum (B.-E. Kim & Petris, 2007). However, very little is known about the post-translational modifications and their effect on ATP7A activity as more sophisticated studies are lacking.

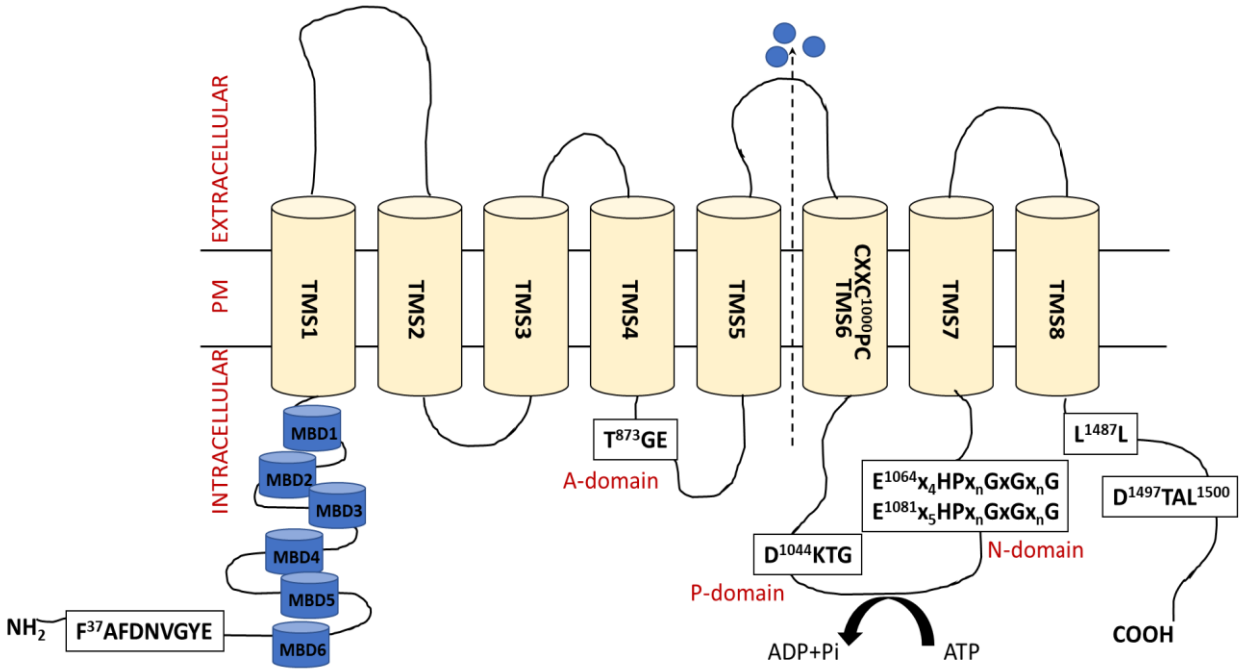

Figure 1.11. Schematic representation of structure of Cu-ATPases

ATP7A/ATP7B have eight transmembrane spanning segments (TMS) [yellow cylinders] located at the plasma membrane (PM) or trans-Golgi network membranes. Located at the N-terminal region are the metal binding domains (MBD) [blue cylinders] with the metal binding motifs GMxCxxC which bind Cu ions (blue circles) or ATOX1 on the intracellular side. A-domain also known as phosphatase domain is characterized by TGE motif that is critical for dephosphorylation and turning off efflux activity. P-domain with the conserved DKTG motifs is required for ATP-driven phosphorylation. N-domain is crucial for nucleotide (ATP) binding. Together P and N domains drive ATP hydrolysis and conformational changes that facilitate Cu export. The critical invariant residues for ATP coordination are indicated for ATP7B (top) and ATP7A (bottom). PDZ motif ($D^{1497}TAL^{1500}$) and $F^{37}AFDNVGYE^{45}$ residues at the C-, and N-terminals are required for correct localization of ATP7A and ATP7B respectively.

2.5 Myriad roles of Cu -regulating proteins in tumorigenesis

Transcriptome analysis revealed that several Cu homeostasis genes (CHGs) including *SLC31A1*, *ATP7A*, *SOD1*, *SOD2, SCO1, COX11*, *STEAP3*, *MTF1*, *MTF2*, copper metabolism domain containing 1 (*COMMD1*), etc. are increased in tumor samples compared to normal colonic tissues. Changes in mRNA levels of *SLC31A1*, *SCO1* and *COX11* are also found in CRC cells HCT116, HT-29 and CACO-2 (Barresi et al., 2016). Similar study with an extended dataset of CHGs reported that *ATOX1, LOXL,* hephaestin like 1 *(HEPHL1)* genes are overexpressed in many cancers including CRC (Blockhuys et al., 2017). Using a mice model of pancreatic islet cell carcinoma, researchers demonstrated that increased Cu in drinking water accelerated tumor growth and volume, and this was inhibited by treating the mice1 with the copper chelator, ammonium tetrathiomolybdate (TTM) (Ishida, Andreux, Poitry-Yamate, Auwerx, & Hanahan, 2013). Under such Cu-limiting conditions, the activity of rate-limiting mitochondrial ETC enzyme CCO was severely affected resulting in reduced ATP production, even in the presence of increased glycolysis levels. Similar results were obtained in another seminal study which showed the growth of *BRAF*-mutant mouse embryonic fibroblasts (MEF) is reduced in mice receiving a Cu-deficient diet compared to normal diet. The tumor growth was further reduced in the presence of TTM and a similar drug Trientine (Brady et al., 2014). Both these studies also highlight the potential for repurposing clinical copper chelators in curbing tumorigenesis.

2.5.1 CTR1 regulates ERK activation, autophagy and tumor growth

Recent work from the Donita Brady lab show that genetic ablation of *SLC31A1 (CTR1)* affected *in vitro* proliferation and *in vivo* tumorigenesis of BRAF-mutant and NRAS-mutant melanoma cell lines (Brady et al., 2014). Not only in melanomas, but growth of a BRAF-driven mice model of lung adenocarcinomas is also affected in the absence of CTR1. Similarly, BRAF-wildtype CRC cells HCT116 were relatively less sensitive to TTM compared to BRAF-mutant HT29 cells, the inhibitory effect in HT29 was rescued by Cu supplementation (Baldari et al., 2019). Attenuated tumor growth in the absence of CTR1 was attributed to reduced phosphorylated-ERK 1/2 levels in the BRAF-mutant tumors. Notably, treating mice with TTM or genetic ablation of *Ctr1 in vivo* increased survival in a mouse model of melanoma, and this correlated with reduced phosphorylated-ERK levels (Brady, Crowe, Greenberg, & Counter, 2017). Similarly, using

Drosophila melanogaster S2 and MEF cells, loss of CTR1 expression was shown to impact Ras^{G12V} or insulin/FGF signaling. Specifically, ERK signaling was affected over other effectors. Notably, Cu-chelation and not Fe-chelation affected ERK phosphorylation suggesting that lack of bioavailable Cu affected MEK1/2 activity. In line with this, MEK1 from different cellular sources was shown to bind Cu with high affinity *in vitro,* and exhibit elevated kinase activities with increasing concentrations of Cu (Turski et al., 2012). One mechanism of acquired resistance to BRAF inhibitors in the clinic is the reactivation of MEK1/2 activity. Notably, activating mutation C121S in MEK1 rendered tumors insensitive to BRAF inhibitor vemurafenib *in vivo* but remained sensitive to copper chelation (Brady et al., 2014). In line with this BRAF-mutant melanoma cells that were resistant to MEK or BRAF kinase inhibitors were inhibited by TTM. Combining TTM with vemurafenib or with a specific MEK inhibitor trametinib synergistically inhibited adherence-independent growth of BRAF-mutant A375 cells on soft agar, and the trio combination imparted the best inhibitory results (Brady et al., 2017).

Besides a novel role of Cu in activating MEK kinases, the same group also discovered a role for Cu in autophagy. A recent work showed that autophagic kinases ULK1 and ULK2 bound Cu specifically, but not other ions such as Fe or Zn. The activation of downstream effectors of ULK1, autophagic flux and formation of microtubule-associated proteins 1A/1B light chain 3B (LC3)-positive autophagosomes were inhibited when Cu levels were depleted with TTM or loss of CTR1 expression. This phenotype persisted even in the presence of amino acid deprivation which serves as a positive control for turning on ULK1-mediated downstream effector activation. Notably, CTR1 depletion affected growth of an *in vivo* model of $KRAS^{G12D}$-driven lung tumorigenesis and this correlated with decreased autophagic flux, and number of autophagosomes (Tsang et al., 2020). KRAS-mutant cells are well known to adapt to nutrient-deprived conditions by turning on autophagy. This survival advantage was lost in KRAS-mutant lung cell lines if copper levels were depleted or ULK1 is unable to bind to Cu. Overall, these results highlight the different roles mediated by Cu importation on tumor growth, and the potential to combine copper chelation with existing therapies in oncogene-driven tumors.

2.5.2 Role of ATP7A in motility, fatty acid metabolism and tumor growth

Studies demonstrating a role for ATP7A in tumorigenesis are limited. The laboratory of Micheal Petris was the first to report that CRISPR/Cas9-mediated knockout of Atp7a diminished *in vivo* growth of $HRAS^{G12V}$-transformed immortalized MEF compared to isogenic cells expressing Atp7a. Reduced tumor growth in the absence of ATP7A correlated with increased Cu accumulation, suggesting cells did not survive due to cuproptosis (S. Zhu, Shanbhag, Wang, Lee, & Petris, 2017). Another recent study by this group reported that LOX and LOX-like (LOXL) enzymes which have well documented roles in cancer growth, regulation of ECM and metastasis, depend on ATP7A for their activity. LOXL and LOX are reported to be involved in the tumorigenesis of several cancer types including but not limiting to breast, colorectal, pancreatic, *etc*. Loss of ATP7A in breast cancer cell line 4T1 and Lewis lung carcinoma cells attenuated LOXL activity, which was rescued by overexpression of ATP7A. Like the previous study on MEF, knockdown of ATP7A accumulated Cu and reduced tumor growth *in vivo*. ATP7A-knockout cells accumulated excess ROS and were hypersensitive to subtoxic concentrations of ROS-inducing hydrogen peroxide (Shanbhag et al., 2019). Similarly, studies show that an HRAS-transformed MEF cell line lacking Atp7a, which accumulated more Cu, were also sensitive to hypoxia or hydrogen peroxide (S. Zhu et al., 2017). Previously, the Petris group had shown that hypoxia can increase the expression of ATP7A and stimulate the post-TGN localization of ATP7A, which is reversed with copper chelation. Intriguingly, ATP7A overexpression correlated with HIF-1α upregulated cells, suggesting that Cu-driven localization of ATP7A could also be observed in hypoxic cells. In support of this, data from the Petris lab showed that hypoxic cells have increased levels of Cu, contaminant decreased CCS expression and increased CP activity. Similar increases in ATP7A, LOXL activity and Cu levels were made in another model of hypoxia-induced pulmonary hypertension (White et al., 2009; Zimnicka et al., 2014). This supports the nature of free Cu ions to participate in Fenton-like chemistry and further augment the already hypoxic environments of tumors by generating more ROS. Together these data suggest a role for ATP7A in regulating and protecting tumor cells from hypoxia. In IEC-6, Atp7a levels is under the transcriptional control of hypoxia transcription factor HIF-2α. Culturing IEC-6 cells with cobalt chloride or under oxygen-deprived conditions increased Atp7a mRNA levels (L. Xie & Collins, 2011). In line with the *in vitro* studies, fish pre-exposed to hypoxia were resistant to cuproptosis likely due to increased ATP7A-mediated efflux of excess Cu (L. Zeng et al., 2020). ATP7A is also

implicated in regulating the activity of semicarbazide-sensitive amine oxidase (SSAO, also known as amino-oxidase copper-containing 3 [AOC3]/vascular adhesion protein 1 [VAP-1]). In 3T3-L1 adipocytes, both SSAO activity the intracellular Cu levels are increased during differentiation. Depletion of Cu levels by TTM or lack of ATP7A expression decreased SSAO activity both in *in vivo* and *in vitro* models, suggesting the requirement of Cu-loading by ATP7A for SSAO activity (H. Yang et al., 2018). In adipocytes, lack of SSAO activity affected fuel metabolism by downregulating glycolysis, triacylglycerol and pentose phosphate pathways, while upregulating others such as cholesterol biosynthesis. This suggests that Cu-dependent SSAO is a regulator of energy utilization in adipocytes. Additionally, inhibition of VAP1 with inhibitors or knockdown reduced tumor growth and metastasis in several *in vivo* models, apparently by reducing the tumor infiltration of immunosuppressive myeloid cells (Salmi & Jalkanen, 2019). In conclusion, several lines of evidence suggest that ATP7A may regulate tumorigenesis by regulating activity of cuproenzymes in motility and metabolism, besides protecting cells from cuproptosis.

2.5.3 Role of Cu-transporters in mediating sensitivity to platinum-based chemotherapy

Interestingly, patients with advanced stage cancers including breast, lung and colon, that did not respond to chemotherapeutics such as doxorubicin and 5-fluorouracil, exhibited increased copper levels in their serum compared to the responding counterparts (Denoyer, Masaldan, La Fontaine, & Cater, 2015). This suggests that Cu could mediate resistance to chemotherapy. Increased levels of ATP7B in CRC patients post-treatment with oxaliplatin were associated with lower PFS when compared to those with lower ATP7B levels (Martinez-Balibrea et al., 2009). In the first study that demonstrated that Cu-transporters are associated with resistance to platinum-based drugs, cells were selected for resistance to cisplatin (DDP) and were coincidentally found to be resistant to cuproptosis. Interestingly, treating cells with increased concentrations of Cu reduced intracellular accumulation of DDP, and DDP-resistant cells overexpressed either ATP7A or ATP7B (Katano et al., 2002; Safaei et al., 2004). In several breast cancer cell lines, ATP7A-low expressing cells were more sensitive to DDP compared to ATP7A-high cells *in vitro* (Chisholm et al., 2016). Similarly *in vivo*, HRAS-transformed MEF knocked out for Atp7a were more sensitive to DDP and displayed reduced tumor growth compared to Atp7a-expressing tumors (S. Zhu et al., 2017). Moreover, TTM treatment had an additive effect along with DDP to increase apoptosis and inhibit

tumor growth *in vivo*. Further experiments to determine if there were differences in ATP7A and DDP localization showed that DDP-resistant cells expressing high levels of ATP7A excluded DDP from the nucleus. TTM treated cells not only reduced ATP7A levels, but also increased nuclear DDP levels (Chisholm et al., 2016). Interestingly however, although ATP7A-high cells were resistant to DDP or carboplatin, they accumulated more platinum content than ATP7A-low, sensitive cells. This suggests that instead of increased efflux of platinum drugs in a mechanism similar to Cu export during cuproptosis, Cu-ATPases might sequester the drugs and exclude them from forming DNA adducts in the nucleus (Samimi, Katano, Holzer, Safaei, & Howell, 2004).

Another set of studies point to a role of Cu-importer CTR1 in DDP-resistance. Yeast strain lacking *ctr1* displayed increased resistance to DDP, which was not observed in strains lacking other CHGs including *atx1*, *sco1*, cox17, *etc*. Whereas ATP7A levels are inversely correlated with DDP concentration, lack of ctr1 in yeast decreased intracellular DNA-DDP adducts. Interestingly, Cu and DDP treatments inhibited each other's uptake in wildtype cells, which was not observed in ctr1-deleted strains, suggesting that CTR1 is required for DDP entry into cells. Treatment with DDP also reduced ctr1 expression levels, hinting at platinum mediated CTR1 endocytosis in a mechanism similar to Cu exposure. These results were also recapitulated in mouse cell lines where degree of Ctr1 expression directly correlated with DDP sensitivity and accumulation (Ishida, Lee, Thiele, & Herskowitz, 2002). Notably treating mice with TTM increased DDP-DNA adduct levels in tumors, probably due to an increase in CTR1 PM levels which occurs after Cu depletion. Cotreatment with TTM and DDP additively decreased growth of cervical tumors compared to individual treatments, suggesting that TTM holds potential for overcoming resistance to DDP in the clinic (Ishida, McCormick, Smith-McCune, & Hanahan, 2010). Besides CTR1 and ATP7A, a few studies have also shown that Cu-chaperone ATOX1 can transiently bind DDP and undergoes degradation (Dolgova et al., 2017; Palm et al., 2011). Since the discovery of a connection between Cu levels and response to cisplatin, we have come a long way to understand the roles played by Cu-regulating proteins in mediating resistance to platinum-based therapy. But more elegant studies and detailed investigations are needed to answer critical gaps in these studies, such as mechanisms of importation of cisplatin by CTR1, and confirmation of sequestration and efflux of cisplatin from cells by ATP7A.

2.5.4 Well established roles of Cu in angiogenesis

The implication of Cu in angiogenesis gained attention when Cu salts stimulated angiogenesis and endothelial cell migration (McAuslan & Reilly, 1980). Using an *in vivo* model of cornea angiogenesis, researchers noticed that Cu levels were concentrated in cornea during neovascularization, and Cu-deficient animals were unable to stimulate cornea angiogenesis (Ziche, Jones, & Gullino, 1982). Interestingly, the same group showed that several fragments of CP, provided they contained Cu ions, were able to stimulate cornea angiogenesis (Raju, Alessandri, Ziche, & Gullino, 1982). Since then numerous studies have explored the option of using Cu chelation to inhibit angiogenesis. Using an *in vivo* model for brain tumors, researchers identified that Cu-sufficiency were necessary for formation of large vascularized carcinomas. Cu deficiency affected several parameters of angiogenesis including endothelial cell turnover, microvascular density, and vascular permeability (S. S. Brem et al., 1990). These results were reproduced in another *in vivo* study using rat glioblastoma xenografts, wherein invasiveness and pseudopodia-like extensions at the tumor-matrix border were reduced in animals treated with low Cu diet and penicillamine (S. Brem, Tsanaclis, & Zagzag, 1990). Notably, Cu can stimulate the biological activity of angiogenin, a critical factor in the formation of blood vessels (Soncin, Guitton, Cartwright, & Badet, 1997). Several preclinical studies then repurposed the use of Cu chelation as antiangiogenic therapy for cancers including head and neck cancer (C. Cox et al., 2001), hepatocellular carcinoma (J. Yoshii et al., 2001), breast cancer (Pan et al., 2002), and lung cancer (M. K. Khan et al., 2002). Although limited, some phase I clinical trials have tested or are currently testing the feasibility of Cu chelation as an antiangiogenic therapy (Denoyer et al., 2015).

2.6 Cu-targeting drugs in cancers

Anti-Cu agents such as TTM, choline tetrathiomolybdate (ATN-224), trientine, D-penicillamine have been successfully used in clinic for treating Wilson's and Menkes diseases. Several preclinical studies have shown that these agents have strong chemotherapeutic properties and that has paved way for clinical trials in cancer employing Cu chelation (Baldari, Di Rocco, & Toietta, 2020). Use of TTM and trientine have overtaken the older D-penicillamine primarily due to the latter's association with hematologic, neurological and renal toxicities. On the other hand, TTM is well tolerated during long term treatments with minimal side effects including nausea, leucopenia,

anemia which are all reversable. Several studies have demonstrated the efficacy and safety of TTM *in vivo* (G. Khan & Merajver, 2009). TTM has a different mechanism of action compared to penicillamine. The former forms a trimeric complex with Cu and Cu-binding proteins rendering it non-bioavailable. Because TTM bound to Cu-proteins remains in the plasma, measurement of serum CP levels is a relatively better surrogate for evaluating TTM efficacy compared to total Cu measurements (Gartner et al., 2009; G. Khan & Merajver, 2009). Whereas penicillamine has the potential to reduce Cu(II) to Cu(I), altering its binding to Cu-chaperones, and effectively mobilizing and clearing out Cu into the urine. In preclinical stage, TTM was very effective in reducing tumor volume, angiogenesis and distant metastasis in head and neck, and breast cancers. In phase II clinical studies in highly angiogenic, metastatic CRC (Gartner et al., 2009) and renal cell carcinoma (Redman et al., 2003). TTM was well tolerated either alone or in combination with chemotherapy. In both cases, patients receiving TTM had modest disease control, and VEGF levels correlated with disease-free progression, warranting the need to examine other regimens and approaches to improve TTM efficacy in clinic. In a phase II study, subjects with resectable, aggressive esophageal cancer were administered TTM post-treatment with chemotherapy, radiotherapy and surgery for two years. Three-year PFS and OS rates were 44% and 45% respectively. The most impressive OS and PFS results with TTM in preclinical studies were achieved in breast cancer patients with high risk for recurrence. In preclinical mouse models, TTM-mediated reduction of CP levels correlated well with decreased LOXL2, and collagen density in premetastatic lungs, suggesting that TTM can modify tumor microenvironments *in vivo* (Chan, Willis, Kornhauser, Ward, et al., 2017). Trientine was developed as an alternative to patients who were refractory to penicillamine and had milder side effects including allergies, swelling and fever. Similar to TTM, it can also affect blood vessel formation and endothelial cell migration. ATN-224 is supposed to be more stable than TTM, given that latter needs to be administered frequently (3-6 times/day). It is currently in phase III for Wilson's disease and in phase I for limited cancer studies (Baldari et al., 2020; F. Wang et al., 2010).

Another class of Cu-targeting drugs are copper complexes that induce cell death by generating ROS in cancer cells. Casiopeina III-ia is a novel Cu-compound that increased apoptosis of glioma cells and CRC cells via caspase-dependent mechanisms (Carvallo-Chaigneau et al., 2008; Trejo-Solís et al., 2012). Ionophores usually transport metal ions inside cells across biological membranes and between cellular compartments. Disulfram (DSF) is one such ionophore used in

clinical trials as an alcohol abuse drug via its irreversible inhibition of alcohol dehydrogenase. It is classified under the dithiocarbamate family, whose members induce apoptosis by increasing metal uptake including Cu (F. Wang et al., 2010). The first study to show DSF had specific anti-cancer activity against melanoma cell lines and not in control melanocytes, also demonstrated that its anti-apoptotic activity can be dramatically enhanced by combining nanomolar concentrations of DSF with Cu ions (Cen, Brayton, Shahandeh, Meyskens, & Farmer, 2004). Importantly, this effect is rescued by chelating Cu-ions. Intriguingly, DSF-Cu treatment exponentially increased intracellular concentrations of Cu compared to Cu treatments alone. DSF and Cu form complex redox reactions which were not reproduced by combining with other metal ions. It was further shown that DSF-Cu compound can inhibit proteasome activity, which mediated apoptosis in breast cancer cells MDA-MB-231. DSF-Cu induced apoptosis specifically in malignant MCF10A cells and were non-toxic to the isogenic, normal counterparts (D. Chen, Cui, Yang, & Dou, 2006). These studies also demonstrated that neither DSF nor Cu alone caused apoptosis at low doses, but the combination was dramatically toxic to cancer cells. Although National Institute of Health (NIH) national cancer institute reports that this drug is being tested in clinical trials for pancreatic, glioblastomas, and prostate cancers, more studies are needed to determine the specificity and in vivo efficacy of DSF in other cancers including CRC. Bis-(thiosemicarbazone)-Cu complexes is increased when combined with exogenous Cu, namely glyoxalbis [N4-methylthiosemicarbazonato]Cu(II) [Cu(II)(GTSM)] and diacetylbis-[N4-methylthiosemicarbazonato] Cu(II) [Cu(II)(ATSM)] selectively kill prostate cancer cells *in vitro* and *in vivo* without affecting normal epithelial cells (Cater et al., 2013). These complexes increase intracellular bioavailable Cu(II) and inhibits proteasome activity. Cu-ATSM when labeled with Cu-radioisotopes is currently being tested clinically to image hypoxic areas of tumors. Cu-ATSM rapidly diffuses into different kinds of cells and tumor tissues and selectively accumulates in reduced environments such as hypoxia. Tumor uptake of Cu-ATSM correlates with increased metastatic potential, poor prognosis, increased hypoxia and hypoxia inducing factor (HIF-1α) expression. Additionally, it acts as a theranostic agent as it is subject to radioactive decay and can be used as internal radiotherapy. Some studies have also demonstrated its anti-tumor effect *in vitro* and *in vivo* against hypoxic tumors. Notably in mice treated with ^{64}Cu-ATSM and bevacizumab, BRAF-mutant HT29 xenografts grew significantly less compared to bevacizumab only-treated mice, highlighting the potential of combining Cu-drugs with conventional therapies in CRC (Y.

Yoshii et al., 2017). Cu ionophores DSF, Cu-ATSM and Cu-GTSM are proposed to affect cell viability by inhibiting proteasome function and activity (Gaur et al., 2018). Cu in both oxidation states (I) and (II) can interact with the active site of proteasome, affecting its conformation and inducing apoptosis (Prachayasittikul, Prachayasittikul, Ruchirawat, & Prachayasittikul, 2013). Clioquinol (5-chloro-7-iodo-8-hydroxyquinoline, CQ) is another ionophore showing preference for Cu(II) and Zn(II) binding, that has been tested for clinical efficacy *in vivo* (Ding & Lind, 2009), and has a similar mechanism of action involving proteasomal system (Gaur et al., 2018; Prachayasittikul et al., 2013). Taken together, several lines of evidence suggest that drugs which modulate Cu levels could be repurposed and tested for cancer therapy. Future studies might uncover novel Cu-disrupting drugs such as small molecule inhibitors of ATP7A that could show therapeutic benefits in cancer.

3 Thesis objectives

Although mainstream therapy for CRC (surgery, chemotherapy, monoclonal antibodies against EGFR and VEGF, and immunotherapy) is partially successful in increasing disease-free survival, their efficacy is marred by poor clinical response, toxicities and resistance mechanisms. Notably, a quarter of CRC are diagnosed at metastatic stages which are aggressively associated with therapeutic resistance, warranting the need for alternative therapeutic strategies. KRAS is mutated in nearly half of CRC, frequently driving resistance against monoclonal antibodies or cell signaling inhibitors. Direct or indirect targeting of RAS has been clinically challenging due to compensatory mechanisms. Despite efforts, no new therapeutic options have been approved for resistant prone KRAS-mutant CRC thus far.

The primary goal of my thesis was to identify new therapeutic strategies against KRAS-mutant CRC. Two global proteomic studies comparing primary enterocytes with CRC adenoma or carcinoma cancer tissues identified drastic changes in the cell-surface or nuclear proteome, revealing several "druggable" protein functional classes at the cell surface (PMID: 22968445, PMID: 26245529). Cell surface proteins are an attractive compartment to look for new therapeutic targets, due to the ease of accessibility and design of monoclonal antibodies or kinase inhibitors. W**e focused on identifying new therapeutic candidates by quantifying the differential cell surface proteome of KRAS-mutant versus non-transformed intestinal cells**.

To this end, the following objectives were designed to achieve this goal: 1. Establish and optimize a reliable protocol to isolate and quantify cell surface proteins by proteomics, 2. Identify differential cell surface proteins in KRAS-mutant versus KRAS-wildtype intestinal cells, 3. Identify which of these differential cell surface proteins functionally contributed to mutant KRAS tumorigenesis by using techniques such as CRISPR-Cas9 functional screens, 4. Validate the importance and selectivity of identified cell surface candidate in tumorigenesis of various KRAS-mutant CRC cells and tissues.

This led to the identification that survival of KRAS-mutant CRC compared to the KRAS-wildtype counterparts are selectively dependent on cell surface copper exporter ATP7A. Further work revealed that copper metabolism could be targeted in KRAS-mutant CRC by copper chelators such as TTM. Growth of KRAS-mutant CRC were significantly inhibited by TTM compared to KRAS-

wildtype controls. This work was published in *Nature Communications* (Chapter 2). In chapter 3, we performed genome wide CRISPR/Cas9 screen to identify pathways that could be co-targeted to potentially increase anti-proliferative efficacy of TTM. And in chapter 4, I describe our work on the characterization of KRAS-mutant intestinal cell signaling. This led to the identification of various feedback mechanisms mediated by mutant KRAS that rendered cells independent of growth factor signaling.

Chapter 2: Copper bioavailability is a KRAS-specific vulnerability in colorectal cancer

Léo Aubert[1,#], Neethi Nandagopal[1,#], Zachary Steinhart[2], Geneviève Lavoie[1], Sami Nourreddine[1], Jacob Berman[3], Marc K. Saba-El-Leil[1], David Papadopoli[4], Sichun Lin[2], Traver Hart[5], Graham Macleod[2], Ivan Topisirovic[4], Louis Gaboury[1,6], Christoph J. Fahrni[7], Daniel Schramek[3,8], Sylvain Meloche[1,9], Stephane Angers[2,10], and Philippe P. Roux[1,6,*]

Affiliations:

[1]*Institute for Research in Immunology and Cancer (IRIC), Université de Montréal, Montreal, 2950, Chemin de la Polytechnique, Montréal, Quebec, Canada, H3T 1J4*

Léo Aubert, Neethi Nandagopal, Geneviève Lavoie, Sami Nourreddine, Marc K. Saba-El-Leil, Louis Gaboury, Sylvain Meloche & Philippe P. Roux

[2]*Department of Pharmaceutical Sciences, Leslie Dan Faculty of Pharmacy, University of Toronto, 144 College Street, Toronto, Ontario, Canada, M5S 3M2*

Zachary Steinhart, Sichun Lin, Graham Macleod & Stephane Angers

[3]*Lunenfeld-Tanenbaum Research Institute, Mount Sinai Hospital, University of Toronto, 600 University Ave., Toronto, Ontario, Canada, M5G 1X5*

Jacob Berman & Daniel Schramek

[4]*Department of Oncology, Lady Davis Institute for Medical Research, Jewish General Hospital, McGill University, 3755 Côte Sainte-Catherine Road, Montreal, Quebec, Canada H3T 1E2*

David Papadopoli & Ivan Topisirovic

[5]*MD Anderson Cancer Center, University of Texas, 515 Holcombe Blvd, Houston, Texas, USA, 77030*

Traver Hart

[6]*Department of Pathology and Cell Biology, Faculty of Medicine, Université de Montréal, Montreal, Quebec, Canada.*

Louis Gaboury & Philippe P. Roux

[7]*School of Chemistry and Biochemistry, Petit Institute for Bioengineering and Bioscience, Georgia Institute of Technology, 315 Ferst Dr NW, Atlanta, Georgia, USA, 30332*

Christoph J. Fahrni

[8]*Department of Molecular Genetics, University of Toronto, Toronto, Ontario, Canada.*

Daniel Schramek

[9]*Department of Pharmacology and Physiology, Faculty of Medicine, Université de Montréal, Montreal, Quebec, Canada.*

Sylvain Meloche

[10]*Department of Biochemistry, Faculty of Medicine, University of Toronto, Toronto, Ontario, Canada.*

Stephane Angers

Corresponding author

[*]Correspondence and requests for materials should be addressed to P.P.R. (email: philippe.roux@umontreal.ca).

1. Author contributions

These authors contributed equally: Léo Aubert, Neethi Nandagopal.

L.A. and N.N. conceived, performed and analyzed most of the experiments, and contributed with P.P.R. to the study design and writing the manuscript. G.L. carried out all retroviral infections, performed WST-1 and Annexin-V assays, and helped in confirming qPCR and IB experiments. S.N. performed and analyzed IF experiments and participated in discussions related to the overall goals of the project. Z.S., J.B., S.L., G.M., and T.H., designed, performed and analyzed CRISPR/Cas9 screens, supervised by S.A. and D.S. Both M.S.E. and S.M. supervised *in vivo* xenograft experiments, and C.J.F. helped in the design and analysis of experiments using Cu-sensing probes. D.P. performed, designed and analyzed bioenergetics experiments, under I.T. supervision. L.G. supervised IHC experiments and analyzed patient-derived data. S.A., S.M., D.S., and I.T. critically read the manuscript. P.P.R. supervised and conceived the study.

2. Abstract

Despite its importance in human cancers, including CRC, oncogenic KRAS has been extremely challenging to target therapeutically. To identify potential vulnerabilities in *KRAS*-mutated CRC, we characterize the impact of oncogenic KRAS on the cell surface of intestinal epithelial cells. Here we show that oncogenic KRAS alters the expression of a myriad of cell-surface proteins implicated in diverse biological functions and identify many potential surface-accessible therapeutic targets. Cell surface-based loss-of-function screens reveal that ATP7A, a copper-exporter upregulated by mutant KRAS, is essential for neoplastic growth. ATP7A is upregulated at the surface of KRAS-mutated CRC and protects cells from excess copper-ion toxicity. We find that *KRAS*-mutated cells acquire copper via a non-canonical mechanism involving macropinocytosis, which appears to be required to support their growth. Together, these results indicate that copper bioavailability is a KRAS-selective vulnerability that could be exploited for the treatment of *KRAS*-mutated neoplasms.

3. Introduction

CRC is one of the leading causes of cancer-related deaths worldwide (Siegel, Miller, & Jemal, 2016). CRC is a highly heterogeneous disease, composed of several biologically and clinically distinct entities that can determine the prognosis and response to therapy. Identification of subtype-specific vulnerabilities is necessary for the design of tailored treatment and improved patient outcomes (Dienstmann, Salazar, & Tabernero, 2020). In the metastatic setting, treatment options for CRC are limited, but recent advances in targeted therapies, such as antiVEGF-A and antiEGFR antibodies, have improved overall survival (Arvelo, Sojo, & Cotte, 2015; Emburgh, Sartore-bianchi, Di, Siena, & Bardelli, 2014). Unfortunately, nearly half of CRC cases harbor *KRAS* mutations, which are negative predictive markers for antiEGFR therapy (Siddiqui & Piperdi, 2010) and common drivers of innate and acquired resistance (Misale et al., 2012) (**Supplementary Fig. 2.1a**).

KRAS belongs to the RAS family of ubiquitously expressed small GTPases, which serve as a major communication hub between cell-surface receptors and intracellular signaling pathways (Prior, Lewis, & Mattos, 2012). Cancer-causing *KRAS* mutations result in aberrant activation of the RAS/MAPK pathway (P. M. Campbell & Der, 2004; Pylayeva-Gupta, Grabocka, & Bar-Sagi, 2011). This provides diverse advantages to cancer cells, such as increased proliferation and survival, macropinocytosis and altered metabolism, evasion of the immune response, alteration of the tumor microenvironment, and metastasis (Pylayeva-Gupta et al., 2011). While several decades of intense efforts have been unsuccessful to pharmacologically target oncogenic forms of KRAS (A. D. Cox et al., 2014), the recent emergence of clinical-grade $KRAS^{G12C}$ inhibitors has shown promise in the management of tumors harboring oncogenic *KRASG12C* mutations (Janes et al., 2018). However, recent reports have highlighted the partial effects of these inhibitors in patients and uncovered many mechanisms of resistance that involves compensatory pathways, such as EGFR, FGFR, AXL, and PI3K/AKT (Lou et al., 2019; Xue et al., 2020). Therefore, the development of alternative therapeutic options is still urgently needed for the efficient targeting of KRAS-addicted cancers (A. D. Cox et al., 2014).

While the intracellular signaling events modulated by KRAS are currently being evaluated as potential therapeutic targets (Takashima et al., 2013, Santana-Codina et al., 2020) much less is known about its potential impact on the cell surface. Elucidating how oncogenic KRAS modifies

the cell surface proteome (surfaceome) may improve our understanding of its complex mechanism of action, and possibly identify new attractive therapeutic targets. To achieve this, we combine both cell-surface proteomics and loss of function CRISPR screens to identify a novel candidate, the Cu-exporter ATP7A as synthetic lethal to KRAS-transformed cells. ATP7A regulates the intracellular Cu levels and tumor growth in KRAS-transformed cells. This study demonstrates that inhibiting Cu supply is an attractive therapeutic option for *KRAS*-mutant cells.

3.1 Results

3.1.1 $KRAS^{G12V}$ reprograms the intestinal cell surfaceome

To identify surfaceome changes associated with KRAS-mediated transformation in the context of CRC development, we used an isogenic intestinal epithelial cell model (IEC-6) stably expressing $KRAS^{G12V}$ (KRAS) or an empty vector (Control). IEC-6 cells normally form a confluent cobblestone-like monolayer (**Supplementary Fig. 2.1b**), but as expected, ectopic expression of $KRAS^{G12V}$ reduced cell–cell contact inhibition and confers a proliferative advantage under both adherent (**Supplementary Fig. 2.1c**) and nonadherent (**Supplementary Fig. 2.1d**) conditions. To determine the impact of oncogenic KRAS on the intestinal epithelial cell transcriptome, we performed genome-wide RNA-sequencing (RNA-seq) and identified a large number of upregulated (546) and downregulated (1225) genes (**Fig. 2.1a, Supplementary Data 1**). Using gene set enrichment analysis (GSEA) (Subramanian, Tamayo, Mootha, Mukherjee, & Ebert, 2005), we found a significant overlap with hallmark signatures associated with KRAS signaling (**Fig. 2.1b**) and MYC targets (**Supplementary Fig. 2.1e**), which are well-known KRAS downstream effectors. In addition, we found a very good correlation between our dataset and oncogenic KRAS-specific transcriptional changes occurring in CRC specimens from The Cancer Genome Atlas (TCGA) (**Fig. 2.1c**), which illustrates that the IEC-6 cell model mimics some of the validated transcriptional signature of KRAS-mutated CRC. We also performed a gene-annotation enrichment analysis using g:Profiler (Reimand et al., 2016, Wadi, Meyer, Weiser, & Stein, 2016) and found highly significant enrichments in several gene-annotations associated with the cell surface, including the terms plasma membrane and cell periphery (**Fig. 2.1d, e**). These results suggested that oncogenic KRAS regulates a transcriptional program that profoundly modifies the intestinal epithelial cell surfaceome.

To characterize changes occurring at the cell surface in response to oncogenic KRAS, we conducted a comprehensive surfaceome analysis based on the coupling of two state-of-the-art chemoproteomic approaches, cell surface biotinylation (CSB) and cell surface capture (CSC) (**Supplementary Fig. 2.2a**), with label-free quantification by liquid chromatography and tandem mass spectrometry (LC-MS/MS) (**Fig. 2.1f**). While CSB involves the labeling of free primary amine groups in cell-surface proteins with the non-permeable reagent Sulfo-NHS-LC-biotin, CSC is based on the specific labeling of cell-surface sialylated glycoproteins using aminooxy-biotin,

taking advantage of the fact that most cell-surface proteins are glycosylated. We confirmed that both surface biotinylation methods resulted in specific cell-surface labeling in IEC-6 cells, with very little evidence of intracellular biotinylation, as shown using immunofluorescence microscopy (**Supplementary Fig. 2.2b**). We found that, irrespective of the chemoproteomic method used, $KRAS^{G12V}$ expression drastically modified the cell-surface biotinylation profile of IEC-6 cells (**Fig. 2.1g**). Interestingly, we also noticed that the biotinylation pattern was very different depending on the approach used (**Fig. 2.1g**), suggesting that using both approaches in parallel may increase the coverage and yield of cell-surface proteins. After data curation to determine high-confidence cell-surface proteins (see Methods section), we identified 366 and 354 highly relevant cell-surface proteins with CSB and CSC, respectively, from which 329 were common to both datasets (**Supplementary Fig. 2.2c**). Consistent with the observed differential biotinylation patterns (**Fig. 2.1g**), we found that many proteins were exclusively found with either CSB (37) or CSC (25), indicating the complementarity of these two approaches for cell-surface proteomics. Importantly, we found a high level of reproducibility between biological replicates (**Supplementary Fig. 2.2d**) and observed a good correlation between both methods ($R^2 = 0.571$) (**Supplementary Fig. 2.2e**). Results were combined to find that 60 (~15%) and 85 (~22%) cell-surface proteins were significantly upregulated and downregulated ($P < 0.05$, unpaired one-tailed Student's *t*-test) in $KRAS^{G12V}$-transformed cells, respectively (**Fig. 2.1h, Supplementary Fig. 2.2f, Supplementary Data 2**).

To determine the involvement of transcriptional regulation in cell-surface reprogramming by $KRAS^{G12V}$, we compared both surfaceome and transcriptome datasets. We found a relatively good correlation ($R^2 = 0.531$) between both datasets (**Supplementary Fig. 2.3a**), suggesting that many changes occurring at the cell surface result from $KRAS^{G12V}$-dependent transcriptional regulation (**Fig. 2.1i**). Nevertheless, we also found a large number of cell-surface proteins whose expression did not correlate with respective transcript levels (**Fig. 2.1i, Supplementary Data 3**), suggesting the involvement of post-transcriptional mechanisms downstream of $KRAS^{G12V}$. We used immunofluorescence microscopy, flow cytometry, and immunoblotting to validate these positive (EGFR, E-cadherin, N-cadherin, and CD44) and negative (ITGB1, EphA2, TLR4, TGFBR1, and AXL) correlations (**Supplementary Fig. 2.3b, c**). Together, these data demonstrate that oncogenic KRAS reprograms the surfaceome of intestinal epithelial cells through both transcriptional and post-transcriptional mechanisms.

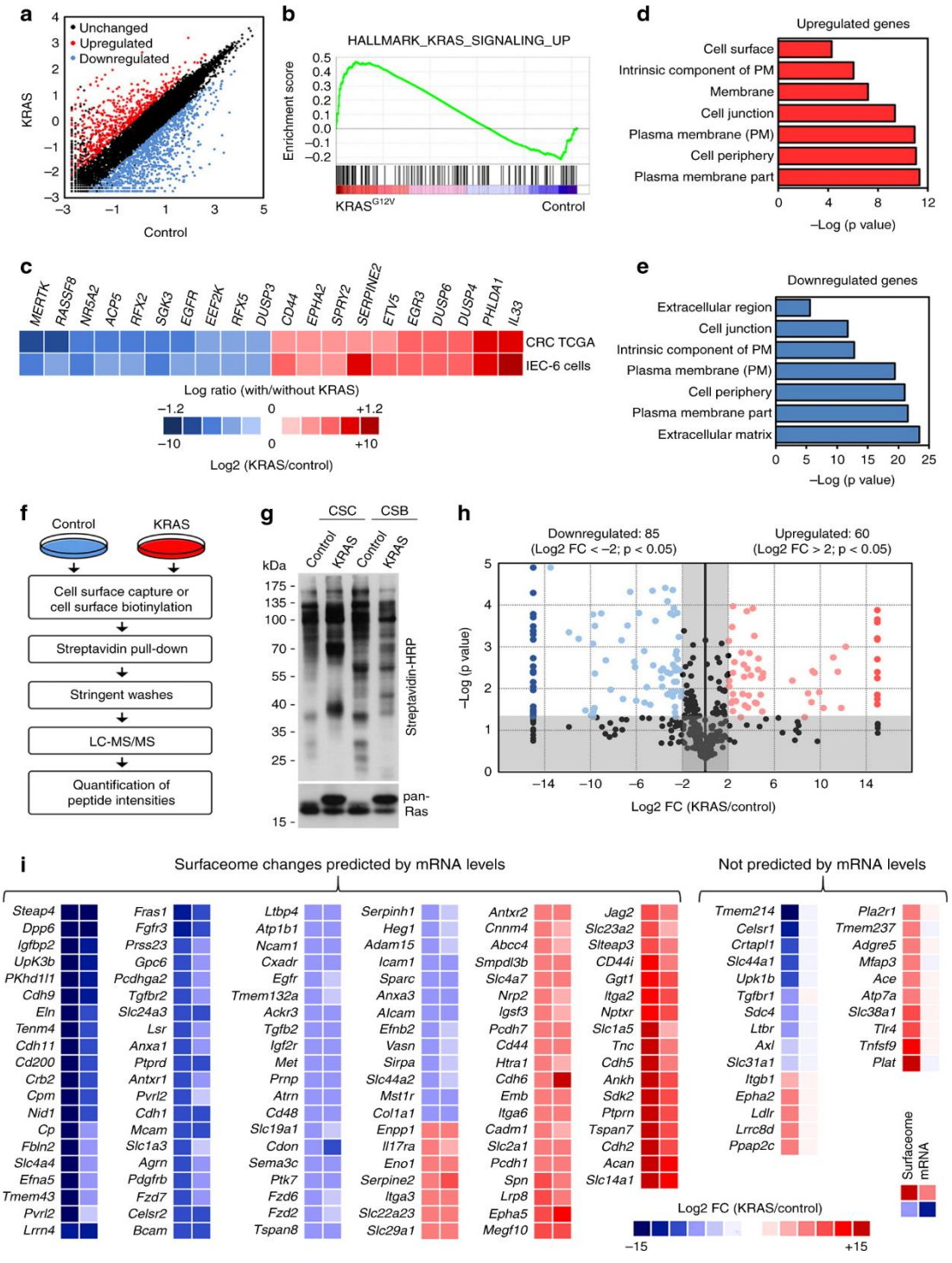

Figure 2.1. Oncogenic KRAS modifies the surfaceome of intestinal cells

(a–e) *IEC-6 cells stably expressing KRAS^{G12V} (KRAS) or empty vector (Control) were subjected to deep mRNA sequencing, and global transcriptome changes associated with KRAS^{G12V} are depicted* ***(a)***. ***(b)*** *Transcriptome data was analyzed using publicly available hallmark database in GSEA for potential enrichment of KRAS_SIGNALING_UP signature in our dataset.* ***(c)*** *Log$_2$ fold changes*

(FC) of genes known to be regulated by mutant KRAS were compared between our transcriptome and the publicly available KRAS-mutated colorectal cancer TCGA datasets. Bar charts depicting the most significant Gene ontology (GO) terms enrichment correlating with transcripts either ***(d)*** *upregulated or* ***(e)*** *downregulated by* $KRAS^{G12V}$. ***(f–i)*** *Cell surface capture (CSC) and cell surface biotinylation (CSB) were used in parallel for the purification of cell-surface proteins.* ***(f)*** *Workflow for the identification and quantification of surfaceome changes induced by* $KRAS^{G12V}$. ***(g)*** *The global cell-surface biotinylation pattern was evaluated in control and KRAS cells by immunoblotting (IB) using horseradish peroxidase (HRP)-conjugated streptavidin. Results represent N = 3 independent experiments.* ***(h)*** *Volcano plot of high-confidence surfaceome changes induced by KRASG12V. Shaded areas represent cut-off range of negative* log_{10} *(P-value) versus* log_2 *FC (KRAS/control).* ***(i)*** *Heatmap comparing the most significant surfaceome changes (first column), with respective transcriptomic changes (second column), induced by* $KRAS^{G12V}$. *For panels* ***(a, h, i)****, data are means of N = 3 independent biological replicates.* Log_2 *FC (KRAS/Control) above 2 or below −2 (4-fold) were considered as significantly upregulated (red) or downregulated (blue), respectively. P-values were determined by unpaired two-tailed Student's t-tests.* $P < 0.05$.

3.1.2 ATP7A is a synthetic lethal target for KRAS-addicted CRC

To identify cell-surface proteins that are required for the fitness of mutant KRAS-mutated cells, we carried out an in vitro loss-of-function CRISPR/Cas9 screen using a lentiviral gRNA library designed using our surfaceome results (**Fig. 2.2a, Supplementary Data 4**). In addition to genes coding for cell-surface proteins (eight gRNAs per gene), our library also included reference gRNAs targeting both essential (including *Myc*) and nonessential (including *Gpr101*) genes (Hart et al., 2015). Following KRAS gRNA-library transduction, Control and KRAS cells were allowed to grow for seven (D7) and fourteen (D14) days. Relative gRNA abundance was determined at D7 and D14 by high-throughput sequencing and compared to the initial cell populations (D0) (**Fig. 2.2a**). To increase the robustness of our findings and limit potential bias due to genetic drifts, this screen was performed on two different pairs of isogenic IEC-6 cells generated at different times. Our results show that the fold-change distribution of gRNAs targeting essential genes was significantly shifted compared to those targeting non-essential genes, indicating that the screens performed as designed (**Fig. 2.2b**). A log Bayes Factor (BF) was then calculated for each gene using the Bayesian analysis of gene essentiality (BAGEL) algorithm, which measures the confidence that knockdown or knockout of a specific gene causes a decrease in fitness (Hart & Moffat, 2016).

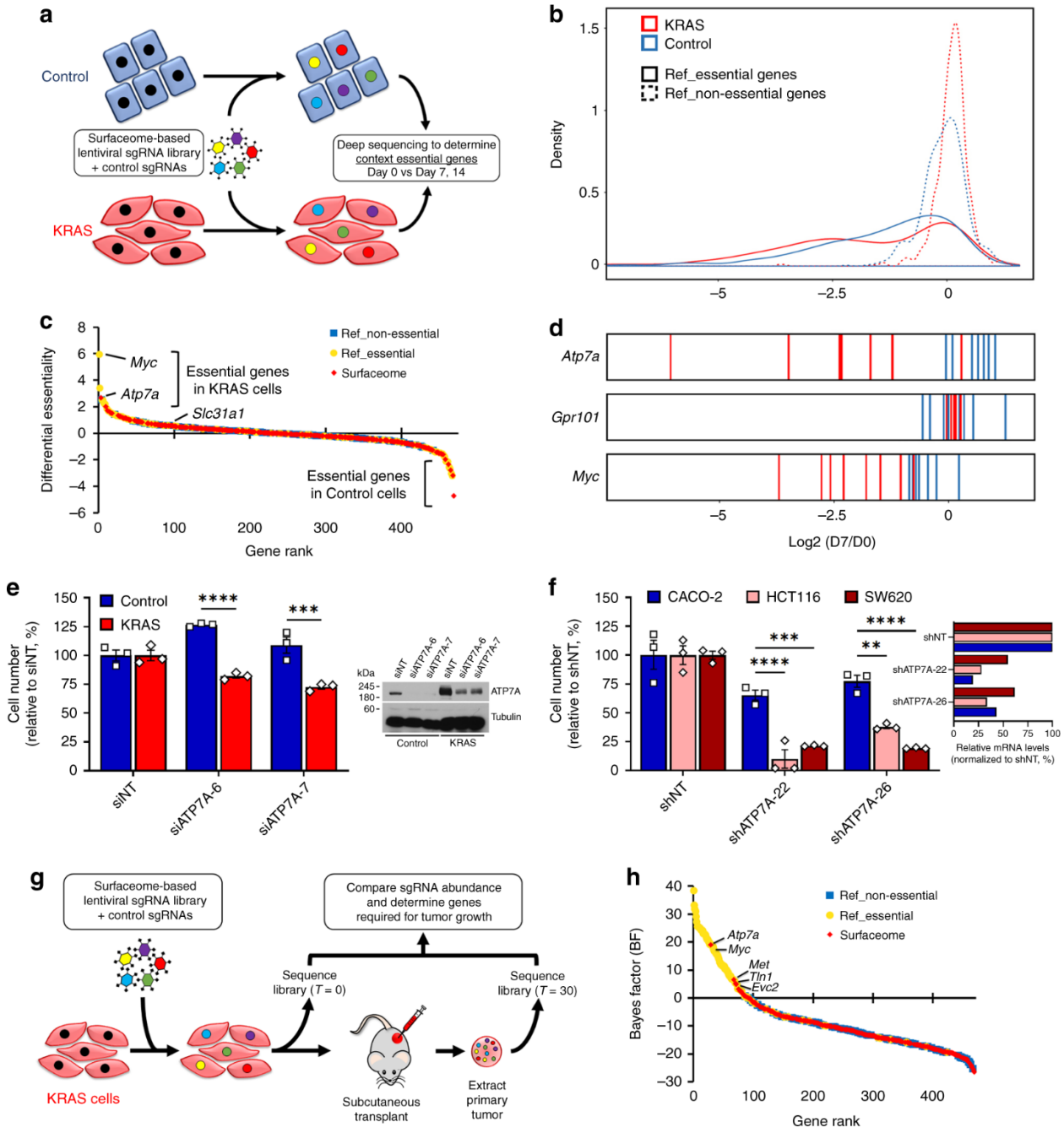

Figure 2.2. Identification of ATP7A as a vulnerability for KRAS-addicted CRC cells

(a) *Experimental design for identification of KRAS-specific vulnerabilities by in vitro CRISPR/Cas9 screening.* ***(b)*** *Graph depicting the fold-change distributions of gRNAs targeting essential (solid lines) and nonessential (dashed lines) genes at day 7 after infection of Control and KRAS cells with KRAS-library.* ***(c)*** *Waterfall graph showing differential essentiality scores between Control and KRAS cells, depicting genes coding for cell-surface proteins significantly altered by KRAS^{G12V} (red diamonds) and reference genes coding for proteins known to be essential*

(green circles) or non-essential (blue squares). ***(d)*** *Bar graphs illustrating the Log_2 FC of the eight gRNAs targeting Atp7a, the non-essential gene Gpr101 and essential gene Myc at day 7 in Control (blue) and KRAS (red) cells.* ***(e)*** *Bar chart indicating the relative cell viability of Control and KRAS cells after ATP7A knockdown. IB for ATP7A showing the efficient knockdown by RNAi (right). Data represent N = 3 independent experiments with five replicates, and N = 3 independent experiments (right). ***P = 0.0001; ****P < 0.0001.* ***(f)*** *As in* ***e,*** *CRC cells were analyzed for cell viability upon ATP7A knockdown. Graph showing the efficient knockdown of ATP7A as measured by qPCR (right). Data represent N = 3 independent experiments with seven replicates, and two technical replicates (right). ****P < 0.0001 (CACO-2 versus HCT116, shATP7A-22); ***P = 0.0008 (CACO-2 versus SW620, shATP7A-22); **P = 0.0027 (CACO-2 versus HCT116, shATP7A-26); *P < 0.0001 (CACO-2 versus SW620, shATP7A-26).* ***(g)*** *Experimental design for the identification of KRAS-specific vulnerabilities in vivo using CRISPR/Cas9.* ***(h)*** *Waterfall graph showing BF scores for genes coding for cell-surface proteins significantly regulated by $KRAS^{G12V}$ (red diamonds), or proteins that are essential (green circles) or non-essential (blue squares). For panels* ***e, f*** *center values and error bars represent mean ± SEM, and significance was determined using two-way ANOVA with post-hoc Bonferroni's multiple-comparison analysis.*

To determine potent KRAS-specific vulnerabilities, we next calculated a differential essentiality score for each gene, which is based on the difference between BF scores observed in KRAS cells and those observed in Control cells (see Methods section). Strikingly, amongst all genes originating from the surfaceome dataset, *Atp7a* was the only candidate showing specific requirement in KRAS compared to Control cells (**Fig. 2.2c, Supplementary Data 4, 5**). A closer examination of the CRISPR/Cas9 screen revealed that 7 out of 8 of gRNAs targeting *Atp7a* affected KRAS IEC-6 cells, compared to wild-type counterparts (**Fig. 2.2d, Supplementary Fig. 2.4a**). Interestingly, the relative abundance of these gRNAs was similar to those observed for the essential reference gene *Myc* (**Fig. 2.2d, Supplementary Fig. 2.4b**), while none of the gRNAs targeting the nonessential gene *Gpr101* were differentially depleted in Control and KRAS IEC-6 cells (**Fig. 2.2d, Supplementary Fig. 2.4c**). Consistent with this, the BF score of *Atp7a* reached a level similar to that of the essential reference gene *Myc* (**Supplementary Fig. 2.4d**), suggesting the discovery of a potent synthetic lethal target for KRAS-mutated cells. We tested the relative cell proliferation by RNA-interference (RNAi) in KRAS IEC-6 cells (**Fig. 2.2e**), as well as in two KRAS-mutated CRC cell lines (HCT116 and SW620) (**Fig. 2.2f**), compared to wild-type KRAS counterparts, Control IEC-6 and CACO-2, respectively. This is consistent with the differential essentiality of ATP7A in KRAS-mutant cells, as suggested by the CRISPR screens.

To assess the pathophysiological relevance of our findings, we conducted an in vivo loss-of-function CRISPR/Cas9 screen using KRAS cells xenografted into NOD SCID gamma (NSG) mice (**Fig. 2.2g**). Briefly, cells transduced with the KRAS gRNA-library were selected for one day prior to transplantation and allowed to form tumors for one-month post implantation (D30). After extraction of primary tumors, relative gRNA abundance was determined by high-throughput sequencing and compared to the initial cell population (D0). The screen results revealed four hits with significant BF, including *Atp7a*, *Met*, *Tln1,* and *Evc2* (**Fig. 2.2h, Supplementary Data 6**). Remarkably, the BF for *Atp7a* was similar to that of *Myc*, validating our *in vitro* findings (**Supplementary Fig. 2.4e**) and highlighting the essentiality of ATP7A for KRAS-mutated tumors. As indicated, we also identified Met, Tln1 (Talin 1), and Ellis van Creveld syndrome 2 (Evc2), for which previous evidence of synthetic lethality with KRAS only exist for MET (Ebi et al., 2011). To validate the involvement of ATP7A in KRAS-dependent tumor growth, we performed soft agar assays using KRAS IEC-6 (**Supplementary Fig. 2.4f**) and KRAS-mutated CRC cells (**Supplementary Fig. 2.4g**) and found that shRNA-mediated ATP7A knockdown reduced anchorage-independent growth. Collectively, these results show that ATP7A plays an essential role in the tumorigenesis of KRAS-addicted cells.

3.1.3 ATP7A protects KRAS-mutant cells from cuproptosis

Our surfaceome analysis showed that KRAS cells express high levels of ATP7A compared to Control cells, but that its cell-surface expression does not correlate with mRNA levels (**Fig. 2.1i, Supplementary Fig. 2.5a**). We confirmed this observation by immunofluorescence microscopy (**Fig. 2.3a**) and immunoblotting (**Supplementary Fig. 2.5b**), which also revealed that ATP7A is more present at the cell surface of KRAS relative to Control cells (**Fig. 2.3a, b**). ATP7A is a homeostatic copper-exporter that protects cells from Cu toxicity by maintaining adequate intracellular Cu levels (Kaler, 2011). ATP7A levels are post-transcriptionally regulated by Cu levels (L. Xie & Collins, 2013), suggesting that $KRAS^{G12V}$ cells may have increased intracellular Cu levels than Control cells. Consistent with this, we found that mRNA levels of four genes involved in intracellular Cu homeostasis (*Mt1*, *Mt2a*, *Loxl2*, and *Loxl3*) are significantly elevated in KRAS compared to Control cells (**Supplementary Fig. 2.5c**).

Depending on its kinetic accessibility, cellular Cu can be divided into a canonical, static pool (i.e., Cu bound to enzymes such as cytochrome c oxidase or SOD1) and an exchangeable, labile pool (i.e., Cu bound to chaperones such as CCS) (Morgan, Bourassa, Harankhedkar, Mccallum, & Zlatic, 2019). The latter form of Cu is more bioavailable and can participate in dynamic cell signaling pathways (Cotruvo, Aron, Ramos-Torres & Chang, 2015). We monitored protein levels of CCS, which is a well-established readout of Cu bioavailability (Chun et al., 2017; Nose et al., 2006) and whose expression is inversely correlated to bioavailable Cu levels in cells (Bertinato & L'Abbé, 2003). We found lower CCS levels in KRAS compared to Control cells (**Fig. 2.3c Supplementary Fig. 2.5d**), suggesting an increase in bioavailable Cu due to $KRAS^{G12V}$. To corroborate these findings, we used the recently developed ratiometric Cu(I)-selective fluorescent probe, crisp-17, as another readout for bioavailable Cu (Cotruvo, Aron, Ramos-Torres & Chang, 2015). The probe was first validated using the cell-permeant complex CuGTSM and a Cu(I)-specific chelator (PSP-2) (Morgan et al., 2018), which confirmed that the probe reversibly responds to changes in cellular Cu levels (**Supplementary Fig. 2.5e, f**). Using crisp-17, we found a significantly higher fluorescence ratio in KRAS IEC-6 cells compared to Control cells, upon addition of the thiol-selective oxidant 2,2′-dithiodipyridine (DTDP), suggesting an increased pool of labile Cu in KRAS cells (**Fig. 2.3d**). Consistent with this interpretation, the kinetics for returning to the basal ratio was slower in KRAS relative to Control cells, suggesting an increased depth of the bioavailable thiol-bound Cu pool in *KRAS* mutant cells. To determine whether oncogenic KRAS-mediated ATP7A upregulation provides a protective role against Cu toxicity, we subjected Control and KRAS cells to increasing concentrations of exogenous Cu. Remarkably, we found that Control cells were significantly more sensitive to increasing Cu levels compared to *KRAS*-mutant cells, and this correlated with ATP7A levels (**Fig. 2.3e, Supplementary Fig. 2.5g, k**). These results suggest that ATP7A protects *KRAS*-mutated cells from Cu toxicity. To verify if oncogenic KRAS augments bioavailable Cu levels in human CRC cells, we evaluated CCS and ATP7A levels in KRAS wild-type (CACO-2) and KRAS-mutated (HCT116, DLD-1, SW480, and SW620) cells. Compared to KRAS wild-type CRC cells, we observed that KRAS-mutated cells had low CCS levels that inversely correlated with high ATP7A levels (**Fig. 2.3f**). Consistent with this, we found that KRAS-mutated CRC cells (HCT116 and DLD-1) had a significant increase in fluorescence ratio using crisp-17 compared to wild-type KRAS cells (CACO-2), upon addition of DTDP, suggesting elevated intracellular labile Cu pools in the KRAS-mutant cells (**Fig. 2.3g**).

Additionally, inductively coupled plasma mass spectrometry (ICP-MS) analysis revealed enhanced total Cu levels in both KRAS-mutated CRC cells compared to CACO-2 (**Supplementary Fig. 2.5l**).

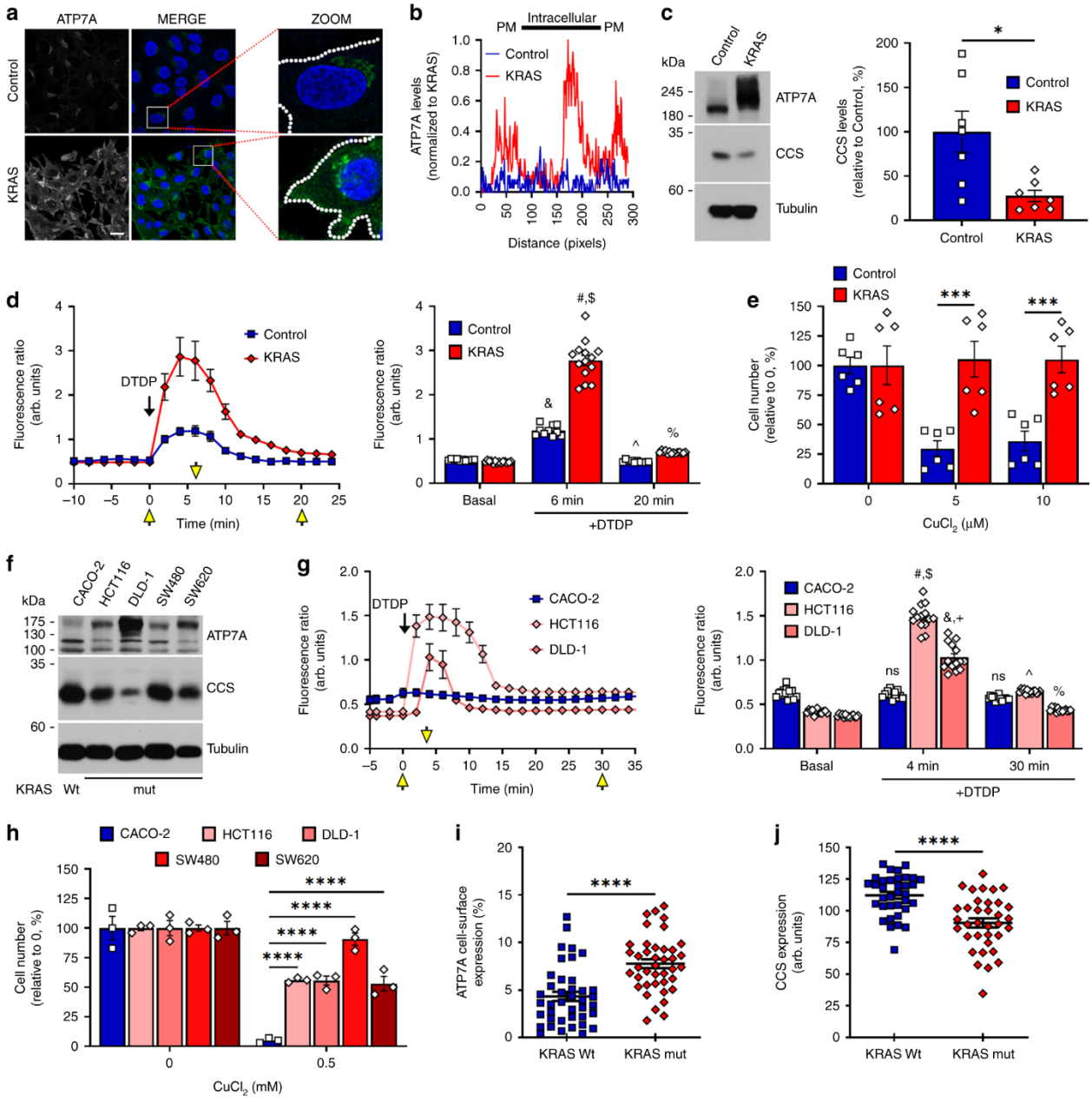

Figure 2.3. ATP7A protects KRAS-mutant cells from cuproptosis

(a) *Micrographs showing ATP7A expression (green) and DAPI (blue) in Control and KRAS cells. Scale = 20 μm, N = 3 independent experiments.* ***(b)*** *Cellular distribution profile of ATP7A as seen in a for Control (blue line) versus KRAS (red line) cells. Data were normalized to KRAS. PM plasma membrane.* ***(c)*** *IB for CCS and ATP7A expression in Control and KRAS cells, with CCS quantifications (right). All panels represent N = 7 independent experiments.*

P = 0.0110.* *(d)*** *Time-course of average crisp-17 fluorescence ratios (N = 10 cells) upon addition of DTDP at T = 0 min. Yellow arrows indicate timepoints for which quantifications are shown (right). P-values are represented as Control-basal versus DTDP (6 min) (&), Control-DTDP (6 min) versus KRAS-DTDP (6 min) (#), KRAS-basal versus DTDP (6 min) ($), Control-DTDP (6 min) versus DTDP (20 min) (^), KRAS-DTDP (6 min) versus DTDP (20 min) (%).* ***(e)*** *Graph depicting relative cell viability after CuCl2 treatment. Data represent N = 6 independent experiments.***P = 0.0002 (Control versus KRAS-5); ***P = 0.0006 (Control versus KRAS-10).* ***(f)*** *IB depicting ATP7A and CCS levels in the indicated CRC cells. Data represent N = 3 independent experiments.* ***(g)*** *As in* ***d*** *but for CRC (N = 14 cells). P-values are represented as CACO-2-basal versus DTDP (4 min) (ns), CACO-2-DTDP (4 min) versus HCT116-DTDP (4 min) (#), HCT116-basal versus DTDP (4 min) ($), CACO-2-DTDP (4 min) versus DLD-1-DTDP (4 min) (&), DLD-1-basal versus DTDP (4 min) (+), CACO-2-DTDP (4 min) versus DTDP (30 min) (ns), HCT116-DTDP (4 min) versus DTDP (30 min) (^), DLD-1-DTDP (4 min) versus DTDP (30 min) (%).* ***(h)*** *As in* ***e*** *but for CRC cells. Data represent N = 3 independent experiments.* ***(i, j)*** *Graphs represent expression of cell-surface ATP7A* ***(i)****, N = 40 random images from five patient-derived CRC tumors) and total CCS* ***(j)****, N = 35) analyzed by immunohistochemistry. For* ***c–e, g–j*** *center values and error bars represent mean ± SEM and for left panels* ***(d, g)****, mean ± SD. For* ***d, g, h*** *not-significant (ns) or ****P < 0.0001 (&, #, +, $, ^, %). Significance was determined using unpaired two-tailed Student's t-tests* ***(c, d, g, i, j)*** *or two-way ANOVA with post-hoc Bonferroni's multiple-comparison analysis* ***(e, h)****.*

According to ICP-MS data, HCT116 cells had higher Cu levels than DLD-1 cells, which correlated with the fluorescence intensity ratios in **Fig. 2.3g**. To determine if KRAS mutation and ATP7A upregulation correlates with a protective role against Cu toxicity, CRC cells were subjected to increasing concentrations of exogenous Cu. Consistent with data obtained in IEC-6 cells, we found that KRAS-mutated CRC cells had reduced sensitivity to Cu toxicity compared to wild-type counterparts (**Fig. 2.3h, Supplementary Fig. 2.5m**). We evaluated the clinical relevance of these findings by assessing ATP7A and CCS levels in CRC specimens harboring wild-type or mutant KRAS (**Supplementary Fig. 2.6**). Interestingly, while total ATP7A levels were similar between the two groups, *KRAS*-mutated samples were associated with more perinuclear and granular staining of ATP7A suggesting enhanced expression in the Golgi network (**Supplementary Fig. 2.6**) and an increase in cell-surface levels of ATP7A (**Fig. 2.3i**). We also observed that *KRAS*-mutated tumors exhibited decreased CCS levels compared to wild-type counterparts (**Fig. 2.3j, Supplementary Fig. 2.6**). Altogether, these data show that oncogenic KRAS enhances ATP7A cell-surface expression, which likely protects *KRAS*-mutated CRC cells from increased intracellular Cu levels.

3.1.4 ATP7A influences Cu-dependent tumor growth

Cu is known to influence tumor growth through the stimulation of several cuproenzymes, including CP, MEK1/2, and CCO/COX, which are associated with various biological functions (Hellman & Gitlin, 2002; Ishida, Andreux, Poitry-Yamate, Auwerx, & Hanahan, 2013; Turski et al., 2012, Horn & Barrientos, 2008). To stimulate these cuproenzymes, Cu is loaded in the secretory pathway via a process that is dependent on ATP7A (Setty et al., 2010; Shanbhag et al., 2019; Yang et al., 2018, Lutsenko, 2016). Strikingly, we found that ATP7A knockdown significantly increased CCS levels in KRAS IEC-6 cells (**Fig. 42.a**), suggesting a reduction in bioavailable Cu levels. Consistent with this, we also observed that ATP7A depletion diminished both Cp activity (**Supplementary Fig. 2.7a**) and ERK1/2 phosphorylation (**Supplementary Fig. 2.7b**). Together, these data suggest that ATP7A modulates Cu bioavailability and contributes to the activity of several cuproenzymes in mutant KRAS-addicted cells.

We then examined whether *KRAS*-mutated cells may be addicted to enhanced Cu-dependent metabolism using the Cu chelator TTM, which is currently being tested clinically against several solid tumors (G. Khan & Merajver, 2009; Lopez, Ramchandani, & Vahdat, 2019). We found that TTM treatment of KRAS cells reversed the increase of ATP7A levels (**Fig. 2.4b, Supplementary Fig. 2.7c**), increased CCS levels (**Fig. 2.4b**) and dramatically reduced the mRNA levels of four Cu-dependent genes (**Supplementary Fig. 2.7d**), suggesting reduced bioavailable Cu levels. Consistent with this, TTM significantly reduced the activity of Cu-dependent enzymes, such as Cp (**Fig. 2.4c**) and ERK1/2 phosphorylation in KRAS cells (**Fig. 2.4d, Supplementary Fig. 2.7e**), validating the decrease of bioavailable Cu pools due to Cu chelation. Interestingly, we found that KRAS cells are 30-times more sensitive to TTM (IC50~1.2 μM) as compared to Control cells (IC50~40 μM) (**Fig. 2.4e**). Similar results were obtained comparing mutant KRAS (HCT116, DLD-1) and wild-type KRAS (CACO-2) CRC cells under adherent (**Fig. 2.4f**) and non-adherent conditions (**Supplementary Fig. 2.7f**), suggesting that oncogenic KRAS increases the requirement for Cu bioavailability (Shanbhag et al., 2019).

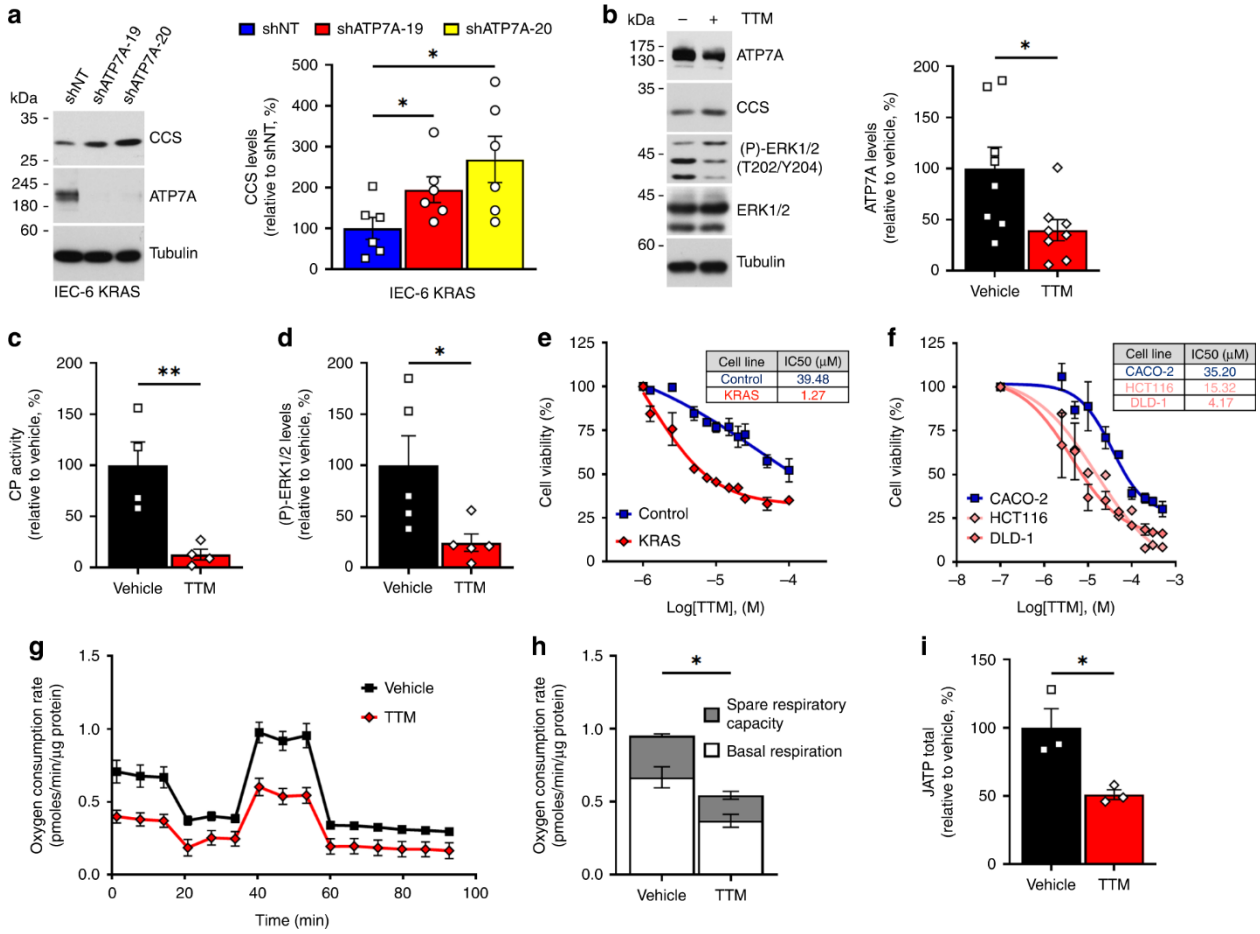

Figure 2.4. Cu chelation reduces Cu-dependent functions associated with tumor growth

(a) *IB showing CCS levels upon ATP7A knockdown with NT (nontargeting) or ATP7A shRNAs (19 and 20) in KRAS cells, with quantifications (right panel). Data represent N = 6 independent experiments. *P = 0.0460 (shNT versus shATP7A-19); *P = 0.0223 (shNT versus shATP7A-20).* ***(b–d)*** *KRAS cells were left untreated or treated with TTM for 24 h and* ***(b)*** *whole-cell lysates were analyzed by IB using antibodies against ATP7A, CCS, total and phosphorylated ERK1/2 and Tubulin. Representative IB images (**b**, left), with quantification of ATP7A levels upon TTM treatment (**b**, right). Data represent N = 8 independent experiments. *P = 0.0230.* ***(c)*** *KRAS cells were analyzed for Cp activity. Bar chart indicates relative Cp activity and data represent N = 4 independent experiments. **P = 0.0098.* ***(d)*** *As in* ***b,*** *but with quantification of phosphorylated ERK1/2 levels upon TTM treatment. Data represent N = 5 independent experiments. *P = 0.0380.* ***(e)*** *Graph depicting the viability of Control and KRAS cells in the presence or absence of TTM at indicated doses.* ***(f)*** *As in* ***e,*** *but for CACO-2, HCT116, and DLD-1. (**e**, **f**) Data are presented as relative percentage (±SEM) of living cells and represent N = 3 independent experiments with three replicates; IC50 values are indicated in adjacent table.* ***(g)*** *Mitochondrial respiration depicted by oxygen consumption rate (OCR) was measured in real-time in response to mitochondrial inhibitors oligomycin, fluoro-carbonyl cyanide phenylhydrazone (FCCP), rotenone and monensin.* ***(h)*** *Bar charts representing the mitochondrial basal respiration rates (white), *P = 0.0249; the spare respiratory capacity (SRC, gray), *P = 0.0176; and* ***(i)*** *cellular ATP*

*production rates, *P = 0.0278.* ***(g–i)*** *Data represent N = 3 independent experiments with six technical replicates. For panels* ***a–d, g–i****, center values and error bars represent mean ± standard error of the mean (SEM), and significance was determined using unpaired two-tailed Student's t-tests.*

We next examined whether TTM-mediated Cu depletion affected mitochondrial oxidative phosphorylation and concomitant ATP production in KRAS cells. We monitored oxygen consumption rate (OCR) (**Fig. 2.4g**), and found that both mitochondrial respiration (**Fig. 2.4h**) and ATP production (**Fig. 2.4i**) were significantly reduced upon TTM treatment. To determine whether ATP7A contributed to mitochondrial respiration in KRAS cells, we measured ATP levels in KRAS-mutated CRC cells (HCT116 and DLD-1) depleted for ATP7A. Interestingly, ATP7A knockdown significantly decreased ATP levels in these cells (**Supplementary Fig. 2.7g**), suggesting that ATP7A participates in Cu-loading of enzymes involved in mitochondrial oxidative phosphorylation. Consistent with these findings, we also found that ATP7A depletion significantly reduced the activity of CCO (**Supplementary Fig. 2.7h**) in *KRAS*-mutated cells, which was reported to correlate with Cu-dependent maximal mitochondrial respiration (Ishida et al., 2013). Together, our data indicate that KRAS-driven tumor growth is influenced by Cu-dependent mitochondrial respiration, which partly involves the biosynthetic role of ATP7A.

3.1.5 Macropinocytosis regulates Cu bioavailability in KRAS tumors

Our data show that oncogenic KRAS increases intracellular Cu levels, but the mechanism by which this occurs remains elusive. While CTR1 is the main Cu-importer in cells (J. Lee, Pen, Nose, & Thiele, 2002), our results demonstrate that oncogenic KRAS reduces total and cell-surface CTR1 levels in IEC-6 cells (**Supplementary Fig. 2.8a, b**), and in CRC specimens (**Supplementary Fig. 2.8c**). In addition, both *in vitro* (**Fig. 2.2c, Supplementary Fig. 2.8d**) and *in vivo* (**Fig. 2.2h, Supplementary Fig. 2.8d**) CRISPR/Cas9 screens revealed that CTR1 (*Slc31a1*) is dispensable for *KRAS*-mutated cell fitness and tumor growth. Recent studies have highlighted the importance of macropinocytosis in nutrient supply for *KRAS*-mutated cells (Commisso & Commisso, 2019), suggesting a potential alternative route for Cu uptake. Using tetramethylrhodamine (TMR)-Dextran, we confirmed that KRAS cells have enhanced rates of constitutive macropinocytosis compared to Control cells (**Fig. 2.5a**), which was inhibited by EIPA, a selective macropinocytosis

inhibitor (Koivusalo et al., 2010). Interestingly, KRAS cells were found to be more sensitive to EIPA compared to Control cells (**Fig. 2.5b**), confirming the acquired dependence of KRAS cells for macropinocytosis. To determine if macropinocytosis regulates bioavailable Cu levels, Control and KRAS cells were treated with increasing concentrations of EIPA, which appeared to preferentially increase CCS levels in KRAS compared to Control cells (**Fig. 2.5c**). Furthermore, we found that inhibition of macropinocytosis exhibited a small but statistically significant decrease in the basal fluorescence ratio of crisp-17 in KRAS cells (**Fig. 2.5d**), suggesting that macropinocytosis contributes to the supply of bioavailable Cu. Similarly, we found that EIPA treatment augmented CCS levels in KRAS-mutated compared to wild-type CRC cells (**Supplementary Fig. 2.9a**). Interestingly, we observed a decrease in ATP7A levels in response to EIPA treatment of KRAS cells (**Supplementary Fig. 2.9b**), suggesting that reducing bioavailable Cu levels inhibits ATP7A expression.

To determine if macropinocytosis contributed to Cu uptake and tumor growth *in vivo*, KRAS cells (3×10^6) were xenografted into nude mice subjected to a Cu-deficient diet (**Fig. 2.5e**). While group A received regular drinking water, groups B and C were given Cu-supplemented drinking water. Xenografted cells were allowed to grow for 2 weeks before administering EIPA (group C) or vehicle (groups A and B). As expected, we found that KRAS tumors grew significantly more in Cu-supplemented compared to Cu-deficient conditions (**Fig. 2.5f, g**). While Cu deficiency reduced serum Cp activity (**Supplementary Fig. 2.9c**), mice did not lose weight as a result of the procedure (**Supplementary Fig. 2.9d**). Interestingly, we found that KRAS tumors exposed to EIPA grew significantly less compared to vehicle (**Fig. 2.5f, g**), suggesting that inhibition of macropinocytosis and Cu uptake negatively affected tumor growth. We did not determine the impact of EIPA treatment in Cu-deficient conditions, as the combination was found to be overly detrimental to the mice. Tumors were analyzed for CCS and ATP7A expression, which revealed that EIPA treatment increased CCS (**Fig. 2.5h**) and decreased ATP7A (**Fig. 2.5i**) levels. Importantly, decreased Cu levels in EIPA-treated KRAS tumors correlated with a reduction in proliferation, as suggested by Ki67 staining (**Fig. 2.5j**), and increase in necrotic areas (**Supplementary Fig. 2.9f**). Finally, we analyzed ERK1/2 and observed an increase of its phosphorylation state in Cu-treated versus Cu-deficient KRAS tumors, which was reduced by EIPA treatment in the presence of exogenous Cu (**Supplementary Fig. 2.9e**). Collectively, these data suggest that Cu promotes KRAS tumor

growth, and that blocking macropinocytosis reduces Cu uptake, Cu-dependent signaling, as well as tumor growth.

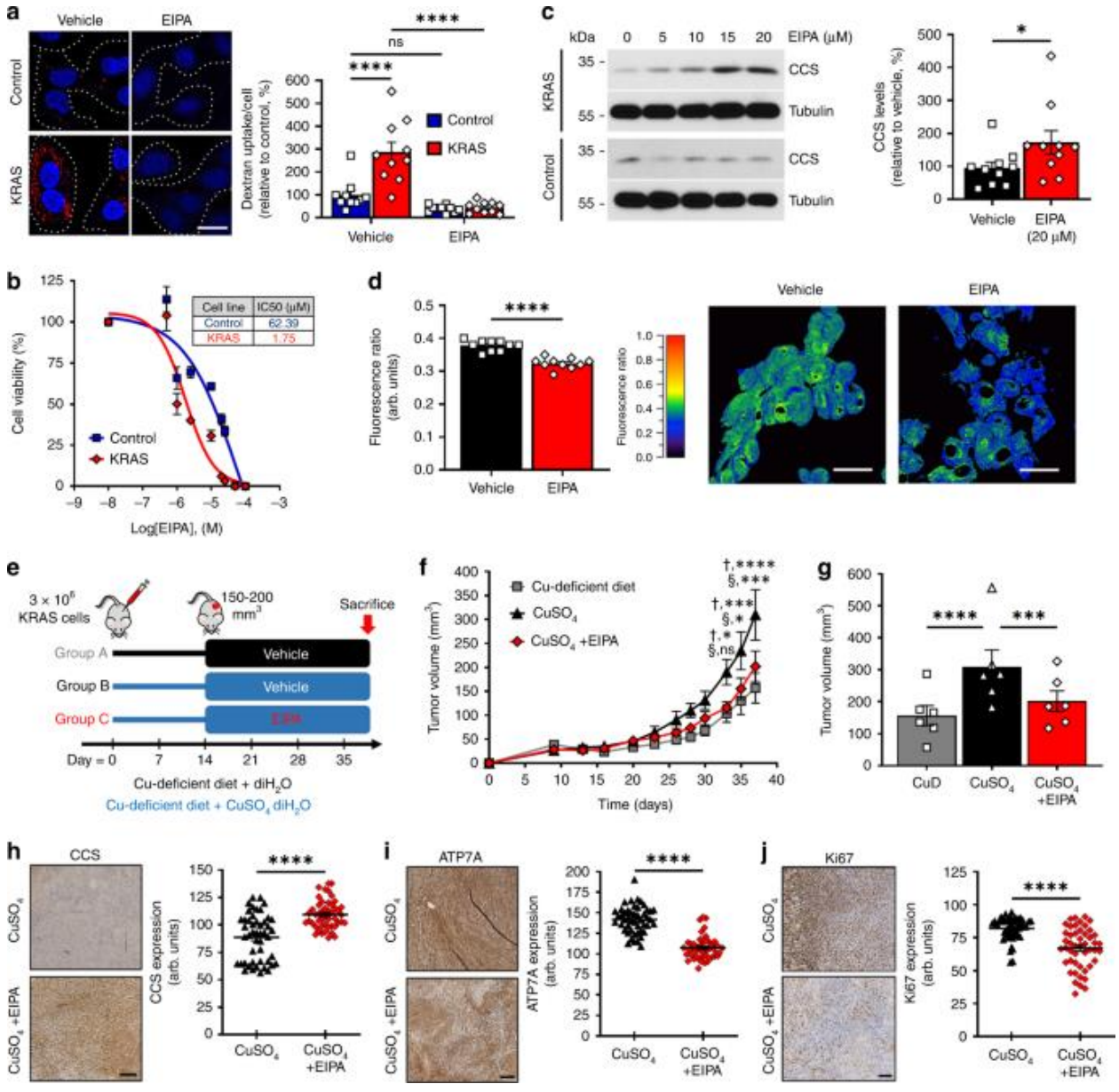

Figure 2.5. Macropinocytosis is a novel Cu supply route in mutant KRAS-driven intestinal cells

(a) *Macropinocytosis was visualized (left) and quantified (right) with TMR-dextran in Control and KRAS cells. EIPA served as negative control. White dashed lines indicate cell boundaries. Data are averaged for N > 167 cells and represent three independent experiments. ****P < 0.0001 (two-way ANOVA with post-hoc Bonferroni's multiple-comparison analysis). scale = 20 μm.* ***(b,c)*** *Control and KRAS cells were treated with EIPA at the indicated doses.* ***(b)*** *Cell viability*

graph with IC50 values in the adjacent table. Data are presented as relative percentage (±SEM) of living cells and represent N = 3 independent replicates. ***(c)*** *Cell lysates were collected, and CCS levels were analyzed by IB and quantified (right). Data represent N = 3 (left) and N = 10 (right) independent experiments. *P = 0.0336 (unpaired two-tailed Mann–Whitney t-test).* ***(d)*** *Graphs depicting average fluorescence ratios of crisp-17 for KRAS cells treated with either DMSO (vehicle) or EIPA (20 μM). Data are averaged for N = 10 cells and represent three independent experiments. Representative fluorescence intensity images are presented (right). scale = 30 μm.* ***(e)*** *In vivo protocol used to evaluate the role of macropinocytosis in Cu-dependent KRAS tumor growth. Mice injected with KRAS IEC-6 cells were provided with a Cu-deficient diet and either deionized H_2O (diH_2O) (Group A) or diH_2O with $CuSO_4$ (Groups B and C) throughout the study. After two weeks, groups A and B were treated with vehicle and group C with EIPA for three weeks. Graphs depicting* ***(f)*** *mean tumor volume over time and* ***(g)*** *mean tumor volume at the end of study (N = 6 mice). P-values between Group A and B (†, *P < 0.05; ***P < 0.001; ****P < 0.0001) and between Group B and C (§, *P < 0.05; ***P < 0.001) were determined by two-way ANOVA with post-hoc Bonferroni's multiple-comparison analysis.* ***h–j*** *Representative images (left) and quantifications (right) from immunohistochemistry profiling of mouse xenograft tissues for N = 48 CCS* ***(h)****, ATP7A* ***(i)****, and Ki67* ***(j)*** *random images from six mice per condition are depicted. scale = 250 μm. For panels* ***a–d****,* ***f–j*** *center values and error bars represent mean ± SEM. For panels* ***c****,* ***d****,* ***h–j*** **P < 0.05; ****P < 0.0001 (unpaired two-tailed Student's t-tests).*

4 Discussion

Several studies have demonstrated elevated Cu levels in tumors and sera from cancer patients (Gupte & Mumper, 2009). Interestingly, Cu levels was shown to correlate with poor prognosis and resistance to chemotherapy (Denoyer et al., 2015). Despite these observations, the mechanisms underlying Cu accumulation and tumor adaptation to excess Cu remain poorly understood. Previous studies have shown that Cu influx via the Cu-importer CTR1 plays a crucial role in mutant BRAF-driven tumor growth (Brady et al., 2014). Our findings indicate that macropinocytosis facilitates Cu entry via a noncanonical route in KRAS-mutant cells, and that CTR1 plays a negligible role in the growth of KRAS-mutant cells as suggested by the CRISPR screens. Cu likely enters cells in association with its chaperones (Inesi, 2017), such as albumin, which was also shown to act as a source of amino acids for KRAS-mutant cells (Commisso et al., 2013b). While macropinocytosis may play an even larger role in nutrient uptake, our results demonstrate that it provides bioavailable Cu required for the growth of KRAS-mutant tumors. We expect that macropinocytosis may not be the exclusive mode of Cu supply in these cells and other mechanisms such as autophagy or other low-affinity transporters could also play a role (Polishchuk & Polishchuk, 2016).

Our results show that oncogenic KRAS increases intracellular Cu levels, which promotes the stability of ATP7A as well as its cell-surface expression. While CTR1 is internalized and degraded in response to high Cu levels, ATP7A translocates to the cell-surface to export excess Cu ions (Denoyer et al., 2015). The latter mechanism is likely responsible for the increased dependency of KRAS-mutant cells towards ATP7A, suggesting that ATP7A inhibitors may specifically target KRAS-addicted cancer cells by exacerbating Cu toxicity. Interestingly, the gastric proton pump inhibitor Omeprazole was shown to inhibit ATP7A surface expression induced by excess Cu and inhibit melanogenesis (Matsui, Petris, Niki, Karaman-jurukovska, et al., 2015), but drugs that are more specific or function-blocking antibodies against ATP7A may be required to limit treatment-related toxicity.

ATP7A delivers Cu to many cuproenzymes involved in several aspects of tumorigenesis, including cell proliferation, metastasis and angiogenesis (Denoyer et al., 2015). A recent study indicated that ATP7A plays essential roles in loading LOX and LOX-like (LOXL) proteins, which have well-documented roles in tumor metastasis (Shanbhag et al., 2019). Our results suggest that KRAS-

mutant cells are addicted to high Cu levels, which is consistent with their increased sensitivity to Cu chelation. While Cu-chelating drugs are being tested against different solid cancers (Chan, Willis, Kornhauser, Mward, et al., 2017; Jain et al., 2013; M. Xu, Casio, Range, Sosa, & Counter, 2018) our results suggest that KRAS-mutated cancers may be particularly sensitive to such treatments. Cu chelation or ATP7A targeted therapy has not been exploited in CRC, but may be of particularly interest for cases where therapeutic resistance is imparted by oncogenic KRAS.

5 Methods

5.1 Cell culture, RNA interference, and viral infections

IEC-6 and CRC cell lines (CACO-2, HCT116, DLD-1, SW620, and SW480) were from ATCC and maintained at 37 °C in Dulbecco's modified Eagle's medium (DMEM) with 4.5 g/L glucose supplemented with 5% (v/v) fetal bovine serum (FBS), 100 IU/mL penicillin, and 100 µg/mL streptomycin. Cells were regularly tested by PCR to exclude mycoplasma contamination and used within 20 passages. IEC-6 cells were stably transduced with retroviral vectors encoding human KRASG12V or an empty cassette with puromycin, zeocin, or hygromycin selection markers (Addgene #9052, #1764, #1766, #18750). Retroviral particles were produced using the Phoenix cell line and antibiotic selections were performed in 5 µg/mL puromycin, 150 µg/mL hygromycin, or 100 µg/mL zeocin. Small interference RNA (siRNA)-mediated knockdown of ATP7A in IEC-6 cells was achieved by Flexitube siRNA (Qiagen) using Lipofectamine transfection reagent (ThermoFisher Scientific). Briefly, cells were transfected with 7.5 µL Lipofectamine and 75 nM siRNA in Reduced Serum OptiMEM solution, which is replaced 6 h later with regular media and let to grow for 48 h before harvesting for experiments. Short hairpin RNA (shRNA)-mediated knockdown of ATP7A was achieved using lentiviruses produced with vectors from the Mission TRC shRNA library (rat TRCN0000101812, TRCN0000101813, and human TRCN0000043173, TRCN0000043177). Cells were infected in the presence of 4 µg/mL polybrene and were selected 3 days after viral infection with 5 µg/mL (IEC-6), 3 µg/mL (CACO-2), 1.5 µg/mL (HCT116), or 2.5 µg/mL (DLD-1) puromycin.

5.2 Purification and enrichment of cell-surface proteins

Two proteomic procedures for the enrichment of cell-surface proteins were adapted from previously published methods (Weekes et al., 2010). For CSC, cells were chilled on ice, rinsed twice with ice-cold biotinylation buffer [phosphate buffered saline (PBS), pH 7.4, supplemented with 1 mM $CaCl_2$ and 0.5 mM $MgCl_2$], and then incubated with 1 mM sodium (meta)periodate (Sigma-Aldrich) at 4 °C for 30 min in the dark. The mild-oxidation reaction was quenched by addition of glycerol at a final concentration of 1 mM. Cells were then washed twice with ice-cold PBS (pH 7.4) supplemented with 5% (v/v) FBS, and biotinylated for 1 h at 4 °C with a mix of 100 µM aminooxy-biotin (Biotium Inc.) and 10 mM aniline (Sigma-Aldrich) in ice-cold PBS (pH 6.7) supplemented with 5% FBS. Cells were then washed once with ice-cold PBS pH 7.4/5% FBS,

and then once with ice-cold biotinylation buffer. Biotinylated cells were incubated in Surfaceome Lysis Buffer [noted as SLB; 1% Triton X-100, 150 mM NaCl, 10 mM Tris–HCl, pH 7.6, 5 mM iodoacetamide (Sigma-Aldrich), 1× protease inhibitor (cOmplete, without EDTA, Roche), 1 mM sodium orthovanadate (Na3VO4), and 1 mM phenylmethylsulfonyl fluoride (PMSF)] for 30 min at 4 °C. Cell debris and nuclei were removed by successive centrifugation for 10 min at 4 °C, initially at 2800 × g and then 16,000 × g. Next, biotinylated proteins were isolated from 10 mg total protein by incubating cell lysates with high-capacity streptavidin agarose resin (Thermo Fisher Scientific) for 2 h at 4 °C. Beads were washed extensively with intermittent centrifugation at 1000 × g for 5 min to eliminate all potential contaminants bound to biotinylated proteins. Three washes were performed with SLB, once with PBS pH 7.4/0.5% (w/v) sodium dodecyl sulfate (SDS), and then beads were incubated with PBS/0.5% SDS/100 mM dithiothreitol (DTT), for 20 min at RT. Further washes were performed with 6 M urea in 100 mM Tris–HCl pH 8.5, followed by incubation with 6 M urea/100 mM Tris–HCl pH 8.5/50 mM iodoacetamide, for 20 min at RT. Additional washes were performed with 6 M urea/100 mM Tris–HCl pH 8.5, PBS pH 7.4 and then water. Biotinylation efficiency was confirmed by blotting aliquots of cell lysates with streptavidin-horseradish peroxidase (HRP) (dilution 1:50,000). For proteomic analysis, beads were rinsed thrice with 50 mM ammonium bicarbonate (NH4HCO3) pH 8.5, and re-suspended in 400 µL of 50 mM NH4HCO3 pH 8.5 containing 4 µg of proteomics grade trypsin (Sigma-Aldrich), overnight at 37 °C. The proteins were further digested with an additional 4 µg trypsin for 4 h at 37 °C. The resulting tryptic peptides were then collected by centrifugation at 10,000 × g, for 10 min at RT. The beads were washed twice with MS grade water and the tryptic fractions pooled. The tryptic fractions were dried to completion in a SpeedVac and re-suspended in MS solvent (5% aqueous acetonitrile (ACN), 0.2% FA). For CSB, cells were chilled on ice, washed twice with ice-cold biotinylation buffer, and incubated with 1 mg/mL Sulfo-NHS-LC-biotin (resuspended in biotinylation buffer) for 1 h at 4 °C. The biotinylation reaction was quenched by addition of 100 mM glycine for 10 min at 4 °C, followed by two washes with ice-cold biotinylation buffer. Biotinylated cells were lysed in SLB, proteins isolated and digested for MS analysis as described above.

5.3 Mass spectrometry and database searches

Samples were loaded on a 1.5 µL C18 pre-column (Optimize Technologies) connected directly to the switching valve. They were separated on a homemade reversed-phase column (150 µm i.d. by 150 mm) with a 56-min gradient from 10 to 30% ACN/0.2% FA and a 600-nl/min flow rate on a Ultimate 3000 LC system (Eksigent, Dublin, CA) connected to an Q-Exactive Plus (Thermo Fisher Scientific, San Jose, CA). Each full MS spectrum acquired at a resolution of 70,000 was followed by 12 tandem-MS (MS–MS) spectra on the most abundant multiply charged precursor ions. Tandem-MS experiments were performed using collision-induced dissociation (CID) at a collision energy of 27%. Proteomic samples were analyzed as biological, back-to-back triplicates per condition. Peptides were identified using PEAKS 7.0 (Bioinformatics Solutions, Waterloo, ON) and peptide sequences were blasted against the Rat Uniprot database. Mass tolerances on precursor and fragment ions were 10 ppm and 0.01 Da, respectively. The false discovery rate (FDR) for peptide and protein was set to 0.5%. The minimum number of peptides per protein was set to 2, and minimum peptide length was set to ~6 amino acids. Search criteria included a static modification of cysteine residues of +57.0214 Da; a variable modification of +15.9949 Da to include potential oxidation of methionines; and a modification of +79.966 on serine, threonine, or tyrosine for the identification of phosphorylation. The data were visualized with Scaffold 4.4.6. normalized spectral abundance factors (NSAF) for the significantly upregulated or downregulated cell-surface proteins by KRAS (Log_2 FC values), for each of the replicates of CSC or CSB technique, were extracted from Scaffold 4.4.6.

5.4 Label-free quantification and data processing

Peptide precursor intensities were extracted using an integral algorithm of PEAKS® software 8.05. Proteins were then selected based on their detection in at least two replicates of the same biological condition (either Control or KRAS), with a minimum of two unique peptides, which were verified for uniqueness and leucine/isoleucine switch using the neXtProt checker (Schaeffer, Gateau, Teixeira, Michel, Zahn-zabal, & Lane, 2017) . These proteins were considered as identified with high confidence. Gene ontology cellular component (GO.CC) terms and functional annotations were queried for all identified proteins using g:profiler (http://biit.cs.ut.ee/gprofiler/index.cgi) to get an objective estimation about the number of proteins specific to the cell surface. We then manually sorted all identified proteins such that we kept those that contain at least one cell surface-

exposed domain, which could be potentially biotinylated. To do so, we analyzed proteins identified with high confidence by querying them against the UniProt online database (http://www.uniprot.org/). We then defined proteins as integral to plasma membrane proteins when they contained at least one transmembrane domain and an extracellular region (e.g., cell adhesion molecules (CAMs), RTKs), as belonging to secretory or extracellular components when they were known to be secreted and potentially interact with the cell surface (e.g., growth factors, cytokines), and as potential contaminants when they corresponded to proteins that do not possess an extracellular domain (e.g., abundant intracellular proteins that may interact with streptavidin beads, plasma membrane-tethered proteins that interact intracellularly with a biotinylated protein). Proteins were considered differentially upregulated by KRAS if $\log_2$ FC (KRAS/Control) values were ≥ 2, and downregulated if ≤ -2. Some proteins were only identified in the KRAS or Control condition, making it impossible to calculate fold-change values. Therefore, we arbitrarily assigned +15 if proteins were only present in the KRAS condition, and −15 if they were only identified in the Control condition. The value "±15" was chosen as it was higher than our highest and lowest KRAS/Control fold-change, respectively.

5.5 Inductively coupled plasma-mass spectrometry (ICP-MS)

Total Cu levels were measured by ICP-MS. Briefly, adherent cells were cultured in regular complete medium, washed once with PBS prepared in copper-free ddH2O and harvested using Accutase solution (Sigma-Aldrich). Cells were washed once more with PBS and pelleted cells were weighted. All tubes were washed in 1% ultratrace HNO3 (Sigma-Aldrich) to remove excess ions prior to use. Cu measured in the sample tubes is subtracted by background measured in a blank tube, which was treated similar to the sample tubes. Samples were digested in 0.2 mL of concentrated ultratrace HNO3 and 50 µL of 30% H_2O_2 was added to the weighted mass of solid product. The mixture was then heated at 85 °C for 2 h. After cooling, the volume was adjusted to 10 mL with Milli-Q water prior to analysis in Perkin Elmer NexION 300× ICP-MS instrument. Data are representative of three independent biological experiments.

5.6 SDS-PAGE and immunoblotting (IB)

Cells were washed twice with cold PBS (pH 7.4) and lysed in BLB lysis buffer [10 mM K3PO4, 1 mM EDTA (Ethylenediaminetetraacetic Acid), 5 mM EGTA, 10 mM MgCl2, 50 mM β-glycerophosphate, 0.5% Nonidet P-40, 0.1% Brij 35, 0.1% deoxycholic acid, 1 mM/L Na3VO4, 1 mM PMSF, and complete protease inhibitor cocktail] for 15 min at 4 °C. Lysates were centrifuged at 16,000 × g for 10 min at 4 °C, supernatants were collected and heated for 10 min at 95 °C in Laemmli buffer [50% (v/v) 4× Tris/SDS pH 6.8, 40% (v/v) glycerol, 8% (w/v) SDS, 6.2% (w/v) DTT, 2 mg Bromophenol Blue]. Alternatively, for streptavidin pull-down assays, proteins were biotinylated as described previously and eluted by heating (30 min, 95 °C) in a Laemmli buffer [50 mM Tris-HCl pH 6.8, 5% (w/v) SDS, 5% (v/v) β-mercaptoethanol, 50% (v/v) glycerol, 0.025% (w/v) Bromophenol Blue]. For IB analysis, eluates and total cell lysates were subjected to 8–12% SDS-PAGE, and resolved proteins were transferred onto polyvinylidene fluoride (PVDF) membranes. Membranes were blocked with 10 mM Tris pH 7.4, 150 mM NaCl, and 0.1% Tween 20, supplemented with 5% (w/v) dry skim milk powder, and subsequently immunoblotted with primary antibodies, diluted in 5% (w/v) dry skim milk or 5% (w/v) bovine serum albumin (BSA), overnight at 4 °C. Antibodies targeted against phosphorylated (P)-ERK1/2 (E10) (T202/Y204) (1:1000) is from Cell Signaling Technologies; Tubulin (T5618) (1:2000) from Sigma-Aldrich; Axl (C-20) (1:1000), CCS (H-7) (1:500) from Santa Cruz Biotechnology; Pan-Ras (C-4) from Abcam (1:500); ATP7A (CT77) from Betty Eipper lab (1:1000) and ATP7A (5E-10) from James Collins lab (1:2000). All secondary horseradish peroxidase (HRP)-conjugated antibodies used for immunoblotting were purchased from Chemicon. All IB data are representative of at least three independent biological experiments and were quantified using Image J. Uncropped blots corresponding to the panels presented in the Main or Supplementary Figures are included in the Source Data File (https://www.nature.com/articles/s41467-020-17549-y#Sec29), indicating the corresponding figure numbers, molecular weight markers and regions of interest for each protein.

5.7 Cell proliferation and cell counting assays

Cell proliferation in vitro was assessed colorimetrically with WST-1 reagent. Exponentially growing Control and KRAS IEC-6 cells were grown in 96-well plates in complete medium supplemented with 5% or 0.1% FBS, and the relative number of viable cells was measured at 24,

48, and 72 h. WST-1 was added 2 h prior to absorbance measurement at 450 nm using a Tecan GENios Plus microplate reader. For determination of cell viability, cells were plated in 6-well plates either in complete medium or serum-starved medium, and treated with vehicle [deionized H2O (diH2O) or DMSO], CuCl2 (diluted in diH2O), tetrathiomolybdate [TTM (Sigma-Aldrich), in 5% (v/v) DMSO/diH2O] or 5-(N-ethyl-N-isopropyl) amiloride [EIPA (Sigma-Aldrich), in DMSO] for 24 or 48 h at the indicated doses. Alternatively, cells were left to grow for an additional day in complete medium after ATP7A shRNA selection or siRNA transfection. Cells were harvested using 0.25% Trypsin-EDTA solution (Gibco) and counted with trypan blue (Gibco) to exclude dead cells.

5.8 Anchorage-independent growth assays

For anchorage-independent growth assays, equal cell numbers were resuspended in 1 mL of top agar solution [final concentration of 0.3% Noble agar (Difco) in DMEM (1×)/10% FBS and antibiotics], with or without TTM at indicated doses. This was overlaid over 1.5 mL of bottom agar solution (final concentration of 0.5% Noble agar in same medium) in a 35 mm non-TC treated culture dish. Cells were fed weekly with 1 mL of complete media, supplemented with indicated concentrations of TTM or vehicle. The number of colonies were visualized after 2 or 3 weeks by addition of 0.5 mg/mL solution of Thiazolyl Blue Tetrazolium Bromide (MTT) reagent (Sigma-Aldrich). Colonies were counted using Image J software.

5.9 Immunofluorescence microscopy

Cells were seeded in 24-well plates containing coverslips in complete medium for 24 h, then serum-starved for macropinocytosis assay. Lysine-fixable TMR-Dextran 10 kDa (Sigma-Aldrich) was added at 0.5 mg/mL to serum-free media for 30 min at 37 °C, pre-treated with DMSO or EIPA (20 μM). Cells were washed twice in ice-cold PBS pH 7.4 and fixed in 3.7% formaldehyde/ice-cold PBS for 10 min. Cells were washed thrice in ice-cold PBS, dried and mounted on microscopy slides with DAPI Vectashield (Vector laboratories). For other staining, cells were permeabilized after fixation for 10 min in PBS containing 0.3% Triton X-100 and blocked with PBS/2% FBS or BSA for 1 h. Cells were incubated for 30 min with Texas Red-Phalloidin (Invitrogen) or 1 h with AlexaFluor 488-conjugated Streptavidin (1:500) (Invitrogen) or corresponding primary

antibodies. Antibodies targeted against EGFR (C74B9) (1:200), CD44 (8E2) are from Cell Signaling Technologies (1:2000); EphA2 (C-20) (1:25), TLR4 (25) (1:50) from Santa Cruz Biotechnology; E-cadherin (36/E) (1:250), N-cadherin (32/N) (1:400) from BD Biosciences; and SLC31A1/CTR1 (NBP100-402) (1:50) from Novus Biologicals. Following PBS washes, cells were incubated for 30 min with AlexaFluor 488-conjugated secondary antibodies (Invitrogen). Images were acquired on Zeiss LSM-700 confocal laser or GE Healthcare DeltaVision imaging systems with 20× or 40× objectives, and analyzed with Zen software v2. Macropinosome quantifications and cell-areas from differential interference contrast (DIC) images were calculated using Image J software as described elsewhere (Commisso et al., 2013b).

5.10 Emission-ratiometric two-photon excitation microscopy

For the measurement of labile Cu levels, we used the crisp-17 fluorescence sensor in accordance with the published protocol (Morgan et al., 2019). Briefly, cells were grown on glass bottom culture dishes (MatTek) in complete medium and treated with or without EIPA (20 μM) for 24 h (**Fig. 2.5** experiments). Cells were then incubated with 1 μM crisp-17 in DMEM (without phenol red indicator) for 20 min and imaged at 37 °C under a humidified 5% CO2 atmosphere using a Zeiss LSM 880 two photon laser [excitation at 880 nm and emission simultaneously at 479–536 nm (ch.1) and 611–750 nm (ch.2) bandpass ranges]. Ratios were calculated as ch.2/ch.1. After imaging under basal conditions for 5–10 min, dynamic changes in intracellular Cu levels were induced by treating cells with 500 μM 2,2′-dithiodipyridine (DTDP) or 10 μM CuGTSM ionophoric complex. Copper chelation was performed with 50 μM of the high-affinity Cu chelator PSP-2 directly in imaging medium, 20 min after acquisition with CuGTSM, in accordance with the timeframes specified in the original protocol. Changes in fluorescence emission ratios for the region of interest (ROI) corresponding to the cells (cytoplasmic regions) were quantified and analyzed using Image J software (Schneider, Rasband, Eliceiri, & Instrumentation, 2017).

5.11 Flow cytometry and Annexin V staining

Cells grown on tissue culture dishes were washed with PBS and harvested with Accutase cell dissociation solution (Sigma-Aldrich) for 5 min at 37 °C. Cells (1×10^6 cells/mL) were then re-suspended in ice-cold PBS pH 7.4/1% FBS (staining buffer) and blocked in ice-cold PBS pH 7.4/5% FBS for 10 min at 4 °C, followed by two washes in staining buffer. Cells were stained with

AlexaFluor 488-conjugated Streptavidin (Invitrogen) or primary antibody for 1 h at 4 °C and washed twice with staining buffer. Primary antibodies targeted against TGFβR1/ALK-5 (1:500) is from Novus Biologicals; Integrin β1-Biotin conjugated (Ha2/5) (1:250) from BD Biosciences. Additional staining was done using AlexaFluor 488-conjugated secondary antibody for 30 min at 4 °C. For the quantification of apoptosis, adherent cells along with those in culture media were collected and washed twice with cold PBS. Cells were stained with PE (phycoerythrin)-Annexin V (BD Biosciences), according to the manufacturers' instructions, and analyzed immediately by flow cytometry. Samples were acquired using BD FACS (Fluorescence-activated cell sorting) Canto II instrument and BD FACS Diva v8.0.2 software. Data were analyzed using FlowJo v10 software, and represented as geometric mean of fluorescence is represented as mean fluorescence intensity (MFI) or percentage (%) of Annexin V positive cells.

5.12 Real-time quantitative-PCR (qPCR) analysis and RNA-sequencing

Total RNA was extracted using RNeasy mini Kit (Qiagen) and reverse-transcribed using the cDNA Reverse Transcription Kit (Applied Biosystems), as described by the manufacturer. Gene expression was determined using assays designed with the Universal Probe Library from Roche (www.universalprobelibrary.com). For each qPCR assay, a standard curve was performed to ensure that the efficacy of the assay is between 90 and 110%. The Viia7 qPCR instrument (Life Technologies) was used to detect amplification level and was programmed with an initial step of 20 s at 95 °C, followed by 40 cycles of: 1 s at 95 °C and 20 s at 60 °C. Relative expression ($RQ = 2^{-\Delta\Delta CT}$) was calculated using the Expression Suite software (Life Technologies), and normalization was done using both glyceraldehyde-3-phosphate dehydrogenase (GAPDH) and ACTB (β-Actin). Data represent average of two technical replicates from three independent biological experiments. For transcriptome analysis, total RNA was extracted using RNeasy mini Kit (Qiagen). Presence of contamination was assessed by NanoDrop (ThermoFisher Scientific) using 260/280 and 260/230 ratios. Quantification of total RNA was made by QuBit (ABI) and 500 ng of total RNA was used for library preparation. Quality of total RNA was assessed with the BioAnalyzer Nano (Agilent) and all samples had a RIN above 9.8. Library preparation was done with the KAPA mRNA-seq stranded kit (KAPA, Cat no. KK8420). Ligation was made with 9 nM final concentration of Illumina index and 10 PCR cycles was required to amplify cDNA libraries. Libraries were quantified by QuBit and BioAnalyzer. All libraries were diluted to 10 nM and

normalized by qPCR using the KAPA library quantification kit (KAPA; Cat no. KK4973). Libraries were pooled to equimolar concentration. Sequencing was performed with the Illumina Hiseq2000 using the Hiseq Reagent Kit v3 (200 cycles, paired-end) using 1.8 nM of the pooled library. Around 120 M paired-end PF reads were generated per sample. Library preparation and sequencing was made at the Institute for Research in Immunology and Cancer's (IRIC) Genomics Platform. Sequence data were mapped to the reference genome using the Illumina Casava 1.8.1 package and Refseq release 63. Expression levels of mRNA were displayed as reads per kilobase per million (RPKM), these RPKM values were used to analyze the functional enrichment of genes associated with the sequencing data by gene set enrichment analysis (GSEA). Data are representative of three independent biological experiments. RPKM values of each biological replicate were averaged for Control and KRAS conditions, and Log_2 FC (KRAS/Control) values were calculated. Transcripts were considered differentially upregulated by KRAS if log_2 FC (KRAS/Control) values were ≥ 2, and downregulated if ≤ -2 ($P < 0.05$).

Table 2.1. List of primers used

GENE NAME	SPECIES	PRIMER SEQUENCE (5' – 3')
ATP7A	HUMAN	f-atttaaggcgggaagaagga r-tctgctatcattgggggttg
Atp7a	RAT	f-tgtccctttattgtgtctacctg r-gcgctttgtaagcctgaatg
Cdh1	RAT	f-gatcctggccctcctgat r-tctttgaccaccgttctcct
Chd2	RAT	f-ccatcatcgcgatacttctg r-ccataccacgaacatgagga
Cd44	RAT	f-gtcatcaaacagaaagcaagga r-aagtcttccaccaaatgggtatt
Egfr	RAT	f-tgcaccatcgacgtctacat r-aactttgggcggctatcag
Mt1	RAT	f-actgcaaatgcacctcctg r-ggcacctttgcagacacag
Mt2a	RAT	f-tgcacctcctgcaagaaaa r-cacttgtccgaagcctcttt
Loxl2	RAT	f-gcttcggcacagctaaagag r-acctcgttgaggtggatgg
Loxl3	RAT	f-gtttctcagactccaacgtcatt r-ccacagctggtcggagtc
Slc31a1	RAT	f-ggaaccatccttatggagacac r-gaggtgggggaagctcag
Tlr4	RAT	f-ggatgatgcctctcttgcat r-tgatccatgcattggtaggtaa
Epha2	RAT	f-agaaggtcattggagcagga r-tgatagccaccggtatctcc
Itgb1	RAT	f-ctgcttctaaagttgcgatcag r-tccataaggtagtacagatcaataggg
Tgfbr1	RAT	f-aaggccaaatattcccaaca r-attttggccatcactctcaag

The heat map in **Fig. 2.1c** was generated by comparing the list of genes significantly and differentially expressed in KRAS-altered compared to KRAS-unaltered CRC specimens isolated from TCGA (594 samples) using cBioPortal platform (https//www.cbioportal.org) to the list of genes differentially expressed by KRAS in IEC-6 cells, as described above. The resulting list of common genes was further shortlisted on the genes whose expression was previously published in the literature as KRAS dependent. Primer sequences for qPCR analysis is attached.

5.13 Immunohistochemistry (IHC)

IHC staining was carried out on paraffin-embedded formalin-fixed samples using the automated Bond RX staining platform from Leica Biosystems. Sections were deparaffinised inside the immunostainer and antigen recovery was conducted using Leica Biosystems proprietary heat-induced Epitope Retrieval using low pH buffer (ER1) for 20 min. Sections were then incubated with 150 µL of each antibody at RT for 30/15 min (primary/secondary antibody, respectively). Primary antibodies targeted against Caspase-3 (1:100) and Ki-67 (1:100) are from Biocare Medical; CCS (H-7) (1:50) from Santa Cruz Biotechnology; SLC31A1/CTR1 (NBP100-402) (1:50) from Novus Biologicals; and (P)-ERK1/2 (E10) (1:400) (T202/Y204) from Cell Signaling Technologies. Detection of specific signal was acquired by using Bond Polymer DAB Refine kit (#DS9800, Leica Biosystems) or Bond Intense R Detection System (DS9263, Leica Biosystems) with a secondary Biotin-conjuguated antibody. Slides were counterstained automatically with Hematoxylin included in the detection system. Stained slides were scanned using the Hamamatsu's NanoZoomer Digital Pathology system 2HT. Virtual slides were then imported in Visiopharm Integrator System (2019.02.1.6005). Quantification was done by defining random zones of region of interest (ROI) (≥50 per condition), and determining the global intensity of DAB staining or necrotic tissue area by a custom scoring protocol by Visiopharm algorithm using HDAB-DAB color deconvolution and intensity parameters. Within the ROI, an unsupervised k-means cluster analysis was performed to separate pixels into four classes corresponding to negative, low, moderate and strong IHC staining. Mean Intensity (MI) and Area were defined for each class and a global VIS score (VS) was calculated as: VS = (MI × area) LOW + (MI × area) MOD + (MI × area) STRONG / total area of ROI. Other custom applications (APPs) were used from Visiopharm

APP center: Ki-67 APP (90004) to determine Ki-67 positive cells, HER-2 APP (90007) and GLUT-1 APP (10009) for ATP7A cell-membrane localization.

Staining of patient-derived CRC tissues was additionally scored by pathologist Dr. Louis Gaboury (Université de Montréal). Data are representative of six and five independent biological replicates for xenografts and patient tissues, respectively. In the present study, ten tissue blocks were retrieved from the archives of the pathology lab at Center Hospitalier de l'Université de Montréal (CHUM), each containing colorectal cancer that also undergone routine testing for RAS mutation. Tumor-containing tissues with sufficient intact material were randomly selected and anonymized to include five KRAS mutated cases and five KRAS wild-type cases. Five to ten unstained sections (2 μm thick) were prepared and donor blocks returned to the archives. On the one hand, each case was anonymized (or depersonalized) to maintain confidentiality, that neither age, sex, ethnicity nor any other personal information was divulgated. On the other hand, care was taken to ensure that by using these tissues there is no potential risk or benefits to the patient other than the advancement of science and knowledge on the cellular mechanisms leading to colonic cancer. Additionally, all patients signed a general consent form upon admittance authorizing the establishment to either dispose or use for research purposes of the tissues and organs removed, so an Institutional Review Board was not deemed necessary.

5.14 Mitochondrial bioenergetics analysis

Oxygen consumption rate (OCR) was measured using the XFe96 Extracellular Flux Analyzer (Seahorse, Bioscience) according to the manufacturer's protocol. Briefly, KRAS IEC-6 cells were washed twice and incubated in 200 μL of XF media containing 10 mM glucose, 2 mM glutamine, and 1 mM sodium pyruvate for 1 h at 37 °C in a CO_2-free incubator. Following the measurement of basal respiration, injections included oligomycin (1 μM), carbonyl cyanide 4-(trifluoromethoxy) phenylhydrazone (FCCP) (0.75 μM), rotenone/antimycin A (0.5 μM), and monensin (20 μM). Oligomycin inhibits ATP synthase and blocks respiration coupled to ATP production (coupled respiration). Uncoupled respiration is calculated as the difference between basal respiration and coupled respiration. FCCP uncouples the inner mitochondrial membrane, thereby allowing for the measurement of maximal oxygen consumption and maximal oxidative capacity. The addition of

rotenone (complex I inhibitor) and antimycin A (complex III inhibitor) are used to maximally perturb mitochondrial respiration. Monensin stimulates Na+ and H+ cycling across the plasma membrane, which activates glycolysis and is used to calculate maximum glycolytic capacity. OCR, extracellular acidification rate (ECAR), and proton production rate (PPR) measurements were taken before and after each injection and were used to calculate J ATP production and bioenergetic capacity as previously described (Mookerjee, Gerencser, Nicholls, & Brand, 2017). All values were normalized to protein content.

Alternatively, total ATP was measured using the ATP luminescence assay kit (Abcam). Briefly, cells were grown in complete medium supplemented with 5% FBS for 24 h, lysed and prepared according to the manufacturers' instructions prior to luminescence measurement using a Tecan GENios Plus microplate reader. All values were normalized to cell numbers. For the determination of cytochrome c oxidase (CCO) activity, KRAS cells were grown in complete medium supplemented with 5% FBS prior to incubation with 100 μM Cu for 24 h and mitochondrial extracts were prepared with the MITOISO1 mitochondria isolation kit (Sigma) according to the manufacturers' instructions. Cytochrome c oxidase activity was then measured using the CYTOCOX1 kit (Sigma) according to the manufacturers' protocol. All values were normalized to cell number.

5.15 In vivo xenotransplantation into nude mice

Throughout the study, 18 female athymic nude mice (N = 6 per condition) (Charles River stock #0490) around 8 weeks of age were subjected to a copper-deficient chow (CuD diet, TD.80388, Harlan Teklad), with either regular drinking diH2O (Group A) or supplemented with 20 mg/L CuSO4 diH2O (Sigma-Aldrich) (Group B and C). KRAS IEC-6 cells underwent screening to confirm that the cell line was free of rodent infectious agents (Mouse essential clear panel from Charles River), and 3 million cells were resuspended in PBS and injected subcutaneously in the right flank of mice at the beginning of the study. Tumors were allowed to grow until the volume reached ~150–200 mm^3 after 2 weeks into the study. Mice were randomized and administered the following treatments every 2 days: Group B vehicle (5% DMSO in diH2O) or Group C EIPA (20 mg/mL in 100 mL of vehicle) by intraperitoneal injections (i.p.) for 3 weeks. All animal procedures were performed in accordance to local animal welfare committee of the Université de

Montréal (Comité de déontologie en expérimentation animale, CDEA) in agreement with regulations of the Canadian council on animal care (CCAC). Mice were monitored periodically; tumor volume thrice per week and bodyweight once a week were recorded. Blood was collected from the saphene at the start and end of the study for Ceruloplasmin activity measurements. Mice were sacrificed at the end of the study and observed for macroscopic abnormalities, if any, and tumor tissues were excised and fixed immediately for IHC analysis. Mice were maintained under the following housing conditions: ambient temperature 22 °C, humidity control 50%, 12 h light/12 h dark cycle.

5.16 Ceruloplasmin activity assays

Blood was collected from mice (N = 6 per condition), allowed to clot and serum was used for assays on D35. Pre-treatment (D0) sera and TTM-treated sera were used as positive and negative controls respectively. Ceruloplasmin (Cp) activity was assayed and calculated according to (Schoslnsky, Lehmann, & Beeler, 1974) and adapted (Brady et al., 2014) for 96-well plates. Briefly, 3.75 µL serum was added to 37.5 µL 0.1 M sodium acetate pH 6.0 (Sigma-Aldrich) in 96-well plates and incubated at 37 °C. After 10 min, 15 µL of 2.5 mg/mL o-dianisidine dihydrochloride (Sigma-Aldrich) was added and further incubated for another 30 min at 37 °C. The reaction was stopped by adding 150 µL of 9 M sulfuric acid (Sigma-Aldrich). The absorbance was read at 540 nm with appropriate negative controls water (blank) and sample (without sodium acetate and o-dianisidine dihydrochloride). For in vitro assays, cells were treated with complete medium containing 50% FBS with or without TTM (10 µM) for 72 h. Conditioned media was collected and concentrated with Amicon Ultra-4 30MWCO (molecular weight cut-off) (Sigma-Aldrich). 50–100 µL concentrates were used for CP activity measurements, with the same protocol as above but with 750 µL of sodium acetate, 200 µL of o-dianisidine dihydrochloride for 120 min and reaction quenched by adding 2 mL of sulfuric acid. Activity was normalized to total protein content.

5.17 CRISPR/Cas9-based screens

Lentiviral gRNA library construction: genes coding for cell-surface proteins were selected based on their significant upregulation or downregulation (Log_2 FC ≥ +2 or −2) at the surface of KRAS-

mutated IEC-6 cells compared to wild-type counterparts. Rat gRNAs against selected cell-surface protein-coding genes were pooled with gRNAs against previously described reference genes that are known to be essential or nonessential to cell survival. This library, collectively referred to as KRAS-library (3732 gRNAs in total, **Supplementary Data 4**), was synthesized as 58-mer oligonucleotides and amplified by PCR in a pooled format. PCR products were then purified using the QIAquick nucleotide removal kit (Qiagen) and cloned into a modified version of the all-in-one lentiviral vector lentiCRISPRv2 using a one-step digestion and ligation reaction as previously described58. The pooled ligation reaction was purified using the QIAquick nucleotide removal kit, eluted in 23 µL ultrapure diH2O, and 2 µL of the purified ligation was transformed into 25 µL EndureTM competent cells (Lucigen) and selected using ampicillin (100 µg/mL). A total of four identical transformations were performed to yield 5000-fold representation of the library. KRAS-library plasmid DNA was harvested using the EndoFree Plasmid Maxi kit (Qiagen).

Lentivirus production and MOI testing: KRAS-library lentiviruses were produced by co-transfection of lentiviral vectors psPAX2 (4.8 µg) and pMDG.2 (3.2 µg) with KRAS-library plasmid DNA (8 µg) using the X-tremeGene TM 9 transfection reagent (Roche), as previously described (Macleod et al., 2019). Briefly, 9×10^6 HEK293T cells were seeded per 15 cm plate 24 h prior to transfection in 10% FBS in DMEM medium, then transfected with the above-mentioned transfection mixture according to the manufacturer's protocol. Twenty-four hours after transfection, the medium was removed and replaced with fresh medium (DMEM, 1% BSA, 1% Penicillin/Streptomycin). Forty-eight hours of post-transfection, virus containing medium was harvested, filtered (0.45 µm), and stored at −80 °C. KRAS-library viral titers in pWZL-hygro IEC-6 or pWZL-hygro-$KRAS^{G12V}$ cells was determined by infecting the cells with a titration of KRAS-library lentivirus in the presence of polybrene (8 µg/mL). Twenty-four hours after infection, medium was replaced with fresh media containing 4 µg/mL puromycin and selected for 48 h. The multiplicity of infection (MOI) was determined 72 h post-infection by comparing the percent of survival of infected cells to non-infected control cells (Hart et al., 2017).

5.17.1 KRAS-library CRISPR/Cas9 screening

21 million pWZL-hygro IEC-6 or pWZL-hygro-KRASG12V cells were infected with KRAS-library lentivirus at a MOI ~0.3 and selected with puromycin (1500-fold coverage after selection). Seventy-two hours of post-infection, selected cells were harvested, mixed and split into three replicates of 2 million cells to maintain 500-fold library coverage. Cells were passaged every 3–4 days as needed, and 4–5 million cells were collected for genomic DNA extraction at day 0 (D0), day 7 (D7), and day 14 (D14). Genomic DNA was extracted from cell pellets using the Purelink genomic DNA mini kit (Invitrogen). Integrated library gRNAs were amplified via two stage PCR: PCR-1 to enrich gRNA regions in the genome and PCR-2 to amplify gRNA with Illumina TruSeq adapters with i5 and i7 indices (MacLeod et al. 2019). Three 50 μL PCR-1 reactions (1 μg gDNA each) were performed for each genomic DNA sample and then pooled. For PCR-2, 5 μL of pooled PCR-1 were amplified, using unique i5 and i7 index primer combinations for each individual sample in 50 μL reactions. PCR product was separated on 2% agarose gel, and 200 bp bands and excised and purified using the PureLink™ Quick Gel Extraction and PCR Purification Combo Kit (Invitrogen) eluting in 30 μL volume. Recovered DNA was quantified using a Nanodrop and 2 μL was electrophoresed on a 2% agarose gel to ensure a clean 200 bp band was recovered. Next-generation sequencing was performed at the Lunenfeld–Tanembaum Research Institute Sequencing facility as previously described59. Libraries were sequenced to a minimum depth of 1×10^6 reads per sample on an Illumina NextSeq550 and FASTQ files were aligned to the gRNA library using MaGeck (version 0.5.3) using default parameters. For each gene in the screen, experimental condition (Control and KRAS), and timepoint, Bayes factors (BF) were calculated using the BAGEL algorithm including the 100 training non-essential and essential genes present in the library (Hart & Moffat, 2016). BF represents a confidence measure and considers the FC of all gRNAs targeting the same gene. A positive BF signifies that the gene affects cell fitness and negative BF signifies that the gene is dispensable to cell fitness. BF were normalized across samples within each screen using the preProcesscore R package before comparison. Differential essentiality scores were calculated after subtracting the BF of KRAS from Control and presented as or Log_2 FC. If $\text{Log}_2 \text{FC} \geq 2$, genes were considered differentially essential to KRAS cells. Only genes with positive BF were considered for differential essentiality. The results from two in vitro screens using two pairs of isogenic IEC-6 cells with/without mutant-KRAS were combined to represent the mean differential essentiality scores in **Fig. 2.2c** and **Supplementary Data 5**.

In vivo CRISPR/Cas9 screening: pWZL-Hygromycin-KRASG12V IEC-6 cells (21 million cells) were transduced at a MOI ~0.3 with the KRAS-library gRNAs, and transduced cells were selected with 4 μg/mL puromycin for 2 days. A D0 sample was collected on the following day. NOD/SCID/gamma (NSG) mice (N = 9) were injected with 1 million cells each (250,000 cells × 4 injections), mixed 1:1 with matrigel containing growth factors (Corning #354234). The resulting 36 tumors were harvested after 4 weeks (D30) when they reached ~1 cm^3 and assigned randomly to 3 × 12 tumors. DNA from 12 tumors was purified (Qiagen DNEasy Blood and Tissue kit) and pooled to obtain a ~600× coverage/triplicate, which was compared to the 600× D0 sample. Essentiality scores were determined from the BF.

5.18 Statistical analyses

For surfaceome and transcriptome analysis, an unpaired one-tailed Student's t-test was applied to the mean $\log_2$ FC values and selected as differentially expressed if $P < 0.05$. For all relevant panels unless specified, center values and error bars represent means ± SEM and *P*-values were determined by unpaired two-tailed Student's t-tests. ns: not significant; *$P < 0.05$, **$P < 0.01$; ***$P < 0.001$; ****$P < 0.0001$. For **Figs. (2.2e, f, 2.3e, h, 2.5a**), and **Supplementary Figs. (2.5k, m, 2.7f)**, two-way ANOVA with post-hoc Bonferroni's multiple-comparison analysis were used between groups. ns: not significant; **$P < 0.01$; ***$P < 0.001$; ****$P < 0.0001$. In **Fig. 2.5f, g** with mean tumor volume (mm^3) ± SEM, *P*-values between Group A and B (†) F(DFn,DFd) = 30.55(11,126) and between Group B and C (§) F(DFn,DFd) = 37.79(11,127) were determined by two-way ANOVA with post-hoc Bonferroni's multiple-comparison analysis. Coefficient correlation (R^2) were calculated in Excel by comparing the means (of three replicates) of $\log_2$ (FC values) for CSC versus CSB (**Supplementary Fig. 2.2e**), or transcriptome versus surfaceome (**Supplementary Fig. 2.3a**). Pearson correlation coefficient (ρ) and NSAF values (**Supplementary Fig. 2.2d**) were extracted from Scaffold database. Statistical measurements were made on distinct samples using both Graph Pad PRISM v8.4.2 and Microsoft Excel softwares.

5.19 Data availability

The raw datasets of surfaceomics (**Supplementary Data 2 and 3**), transcriptomics (**Supplementary Data 1 and 2**) and CRISPR analyses (**Supplementary Data 4–6)** are available as supplementary information in https://www.nature.com/articles/s41467-020-17549-y#Sec28. Surfaceomics data (corresponding to **Supplementary Data 2**) has been deposited in ProteomeXchange through partner MassIVE as a complete submission and assigned MSV000085560 and PXD019625. The data can be downloaded from ftp://MSV000085560@massive.ucsd.edu. TCGA data used for generating heat map in Fig. 1c and Kaplan–Meier plot in **Supplementary Fig. 2.1a** are available from cBioportal (https://www.cbioportal.org/study/summary?id=coadread_tcga_pan_can_atlas_2018). GSEA graphs presented in **Fig. 2.1b** and **Supplementary Fig. 2.1e** are available at https://www.gsea-msigdb.org/gsea/msigdb/cards/HALLMARK_KRAS_SIGNALING_UP and https://www.gsea-msigdb.org/gsea/msigdb/cards/HALLMARK_MYC_TARGETS_V1, respectively.

5.20 Acknowledgements

We thank all lab members who contributed in discussions and manuscript preparation. Proteomic analyses were performed by the Center for Advanced Proteomics Analyses (CAPCA), a Node of the Canadian Genomic Innovation Network that is supported by the Canadian Government through Genome Canada. IEC-6 cells were provided by Dr. Nathalie Rivard (Université de Sherbrooke), and pWZL-Hygromycin vector by Dr. Gerardo Ferbeyre (Université de Montréal). ATP7A polyclonal antibody was a gift from Dr. Betty Eipper (University of Connecticut) and Dr. James Collins (University of Florida). We acknowledge Julie Hinsinger for the analysis of immunohistochemistry results. We are thankful to Christian Charbonneau and Jennifer Huber for their expertise with bio-imaging techniques and transcriptome analysis, respectively. We are grateful for the time and expertise of Kim Levesque, Myriam Métivier-Bélisle and other personnel at the IRIC animal facility for mouse xenograft experiments. We benefited from the personnel at IRIC's Genomics Core Facility for RNA experiments. This work was funded by grants from the Canadian Institutes for Health Research (MOP-142374 and PJT-152995 to P.P.R), and the National Institutes of Health (R01GM067169 and R35GM136404 to C.J.F). P.P.R. is a Senior Scholar of the Fonds de la recherche du Québec—Santé (FRQS). L.A. received a Postdoctoral

Fellowship from the Cole Foundation, and N.N. was supported by Doctoral Scholarships from the FRQS and the Fonds de la recherche du Québec—Nature and Technologies (FRQNT).

7. Supplementary figures

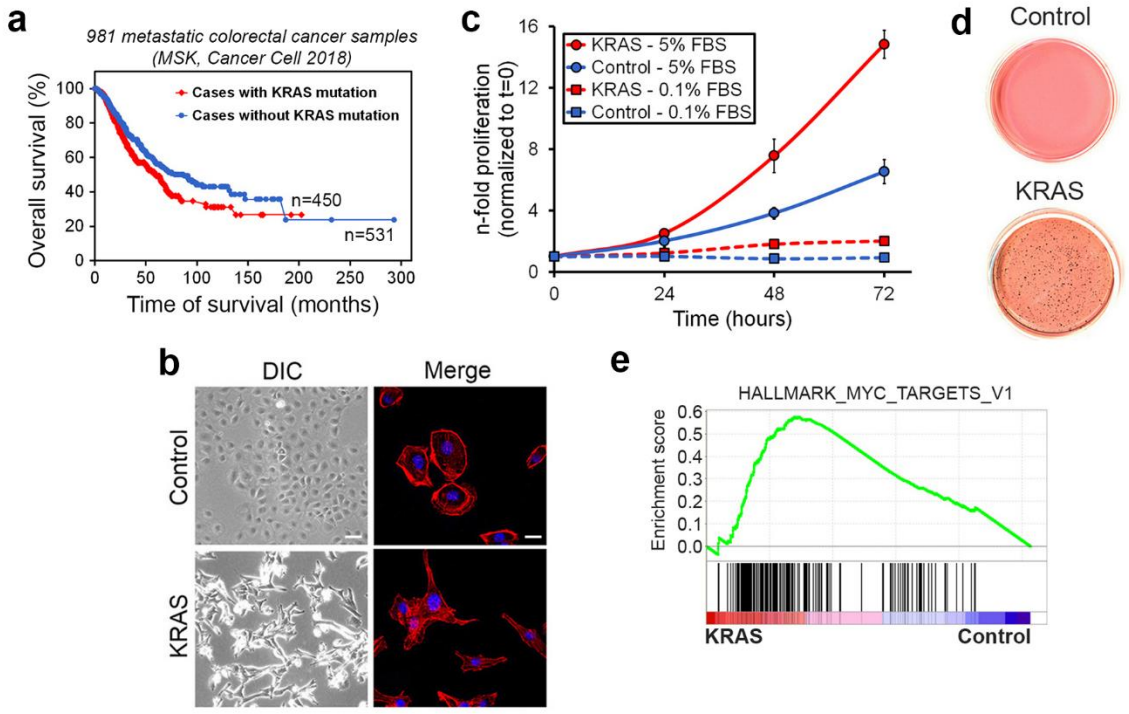

Supplementary Figure 2.1. Validation of intestinal epithelial cell model for KRAS-mediated transformation

(a) *Kaplan-Meier plot comparing overall survival of metastatic colorectal cancer patients with or without KRAS mutations from publicly available data analyzed on the cBioPortal database for Cancer Genomics (https://www.cbioportal.org/study/summary?id=crc_msk_2017).* ***(b-d)*** *Control and KRAS IEC-6 cells were analyzed for the following:* ***(b)*** *cellular phenotype with phase-contrast microscopy (DIC) [scale=10 µm], Phalloidin (red) and DAPI (blue) [scale=20 µm];* ***(c)*** *cellular proliferation using WST-1 assays in medium containing 0.1% or 5% FBS. Data were normalized to initial seeding (t=0) and expressed as mean ±SD of four replicates per condition; and* ***(d)*** *adherence-independent growth by soft agar assays. Data represent N=3 independent experiments.* ***(e)*** *Analysis of Control and KRAS IEC-6 transcriptome dataset with GSEA database correlated with upregulation of hallmark gene set "MYC_TARGETS_V1".*

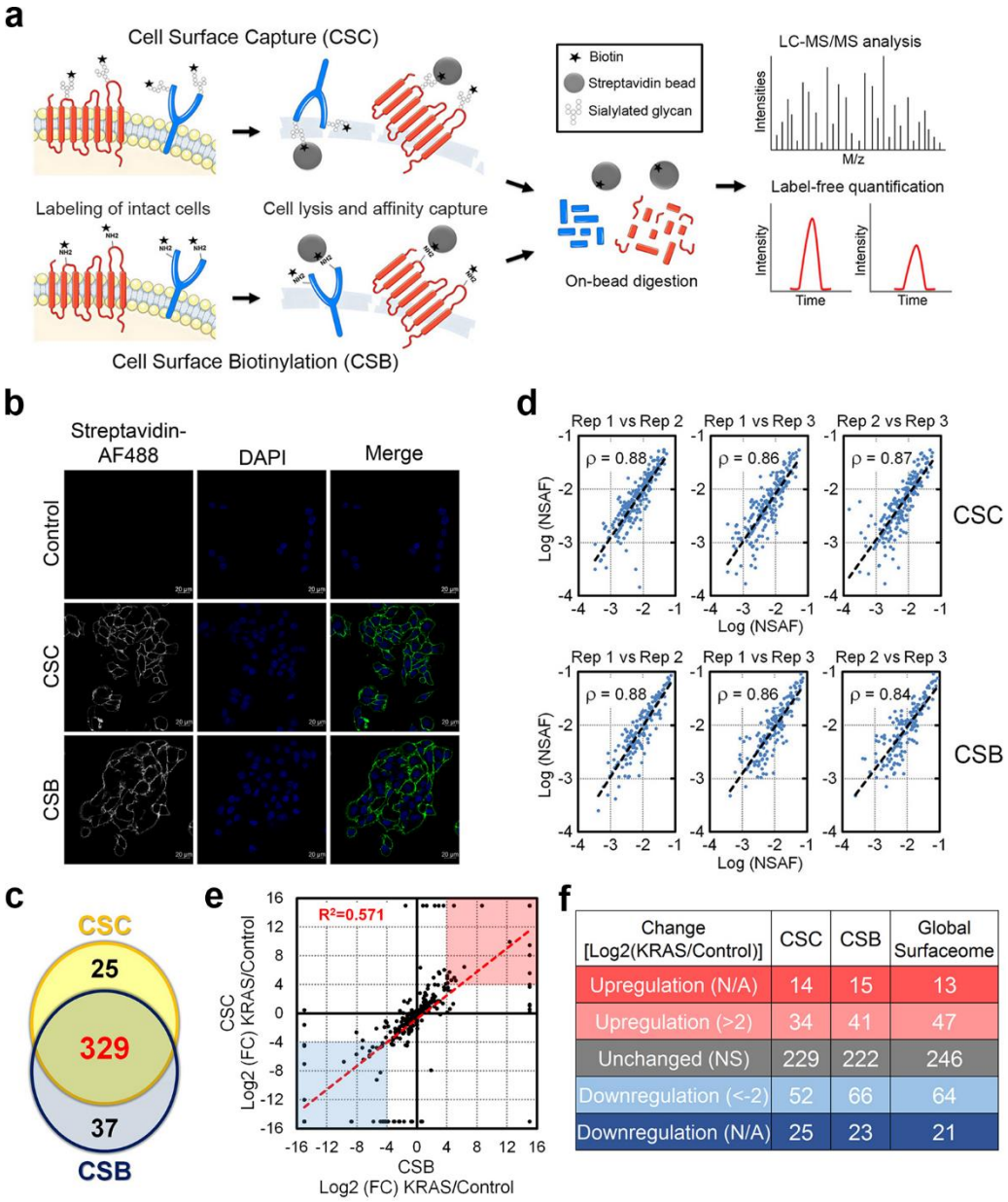

Change [Log2(KRAS/Control)]	CSC	CSB	Global Surfaceome
Upregulation (N/A)	14	15	13
Upregulation (>2)	34	41	47
Unchanged (NS)	229	222	246
Downregulation (<-2)	52	66	64
Downregulation (N/A)	25	23	21

Supplementary Figure 2.2. Validation of the surface proteomics protocol to quantify cell surface proteins

(a) *Schematic outline of the surfaceomic approach optimized for the identification and quantification of cell-surface proteins. Cell surface capture (CSC) and cell surface biotinylation (CSB) methods.* ***(b)*** *Immunofluorescence (IF) images showing the specificity of cell-surface labeling with both CSC and CSB techniques, scale=20 µm. Data represent N=3 independent experiments.* ***(c)*** *Venn diagram of all high-confidence cell-surface proteins identified in the KRAS-regulated surfaceome of IEC-6 cells, isolated using CSC or CSB.* ***(d)*** *Comparison of Normalized spectral abundance factor (NSAF) to determine the reproducibility in protein identifications between triplicates for each of the biotinylation method.* ***(e)*** *Graph deciphering the correlation between CSC and CSB for the quantification of differentially expressed cell-surface proteins by*

KRAS (R^2=0.571). Data are expressed as Log_2 FC (KRAS/Control). ***(f)*** *Table summarizing the number of proteins significantly upregulated (red) (Log_2 FC ≥ 2) or downregulated (blue) (Log_2 FC ≤ -2) at the cell-surface of IEC-6 KRAS compared to Control cells. N/A (non applicable) stands for proteins identified uniquely in Control or KRAS cells.*

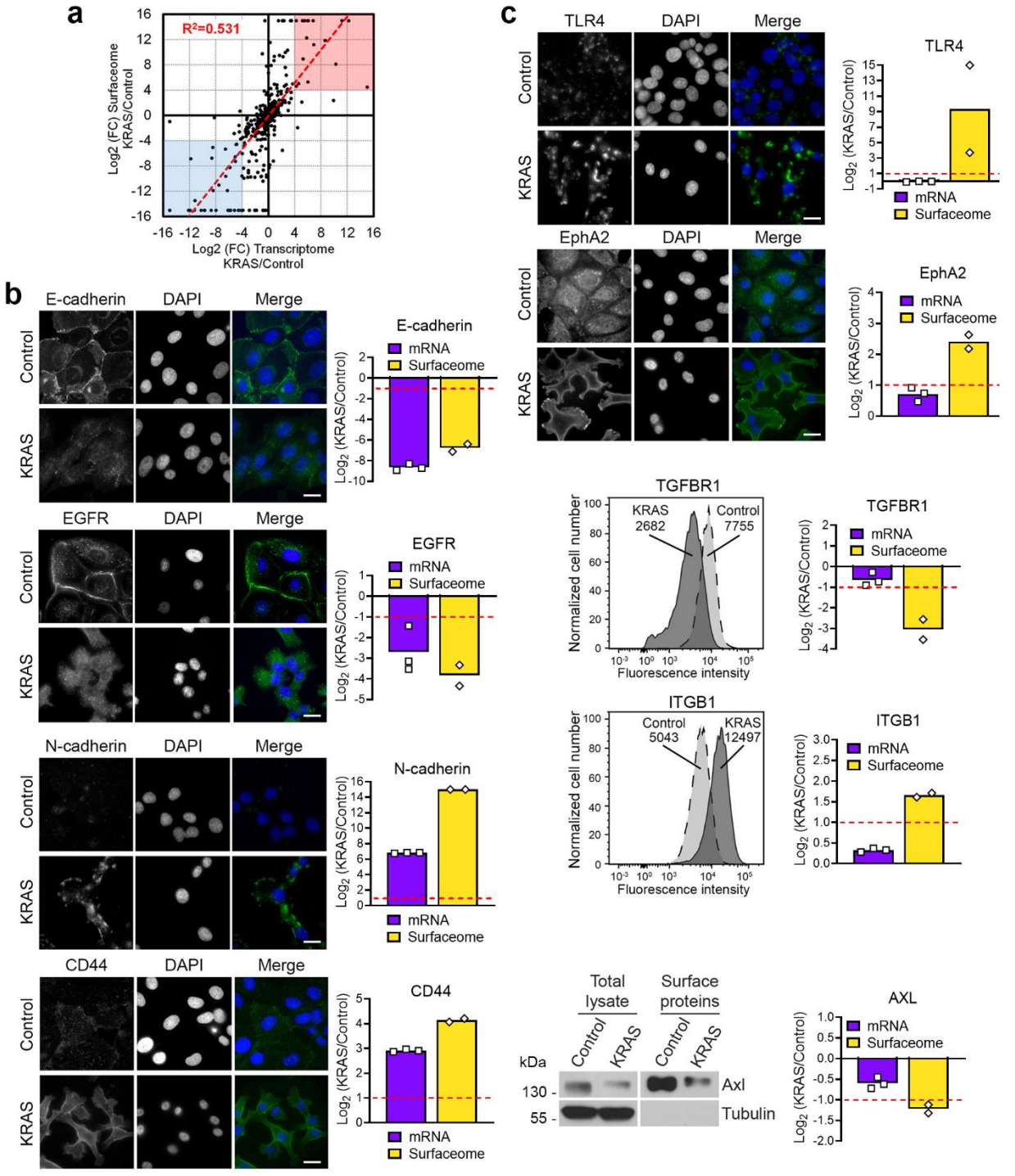
a
R²=0.531
Log2 (FC) Surfaceome KRAS/Control
Log2 (FC) Transcriptome KRAS/Control
b
E-cadherin
DAPI
Merge
Control
KRAS
mRNA
Surfaceome
Log2 (KRAS/Control)
EGFR
N-cadherin
CD44
c
TLR4
EphA2
TGFBR1
ITGB1
AXL
KRAS 2682
Control 7755
Control 5043
KRAS 12497
Normalized cell number
Fluorescence intensity
Total lysate
Surface proteins
kDa
130 -
55 -
Axl
Tubulin

Supplementary Figure 2.3. Validation of cell-surface proteins differentially modulated by mutant KRAS

(a) *Scatter plot showing the correlation between surfaceome and transcriptome datasets (R^2=0.531). Data are expressed as Log2 FC (KRAS/Control).* ***(b-c)*** *IF, flow cytometry, or immunoblot (IB) images showing the cellular localization of transcription-dependent upregulated (CDH2, CD44) or downregulated (CDH1, EGFR)* ***(b)****, and transcription-independent upregulated 6 (TLR4, EPHA2, ITGB1) or downregulated (TGFβR1, AXL) cell-surface proteins* ***(c)*** *in KRAS versus Control cells. Graphs on the right illustrate the Log_2 FC (KRAS/Control) from the transcriptome (purple) and surfaceome (yellow) datasets. Red dashed lines indicate cut-off values statistical significance. Data are expressed as means of N=3 (mRNA) or N=2 (surfaceome) independent replicates per condition. All validation data represent N=3 independent experiments, scale=17 µm.*

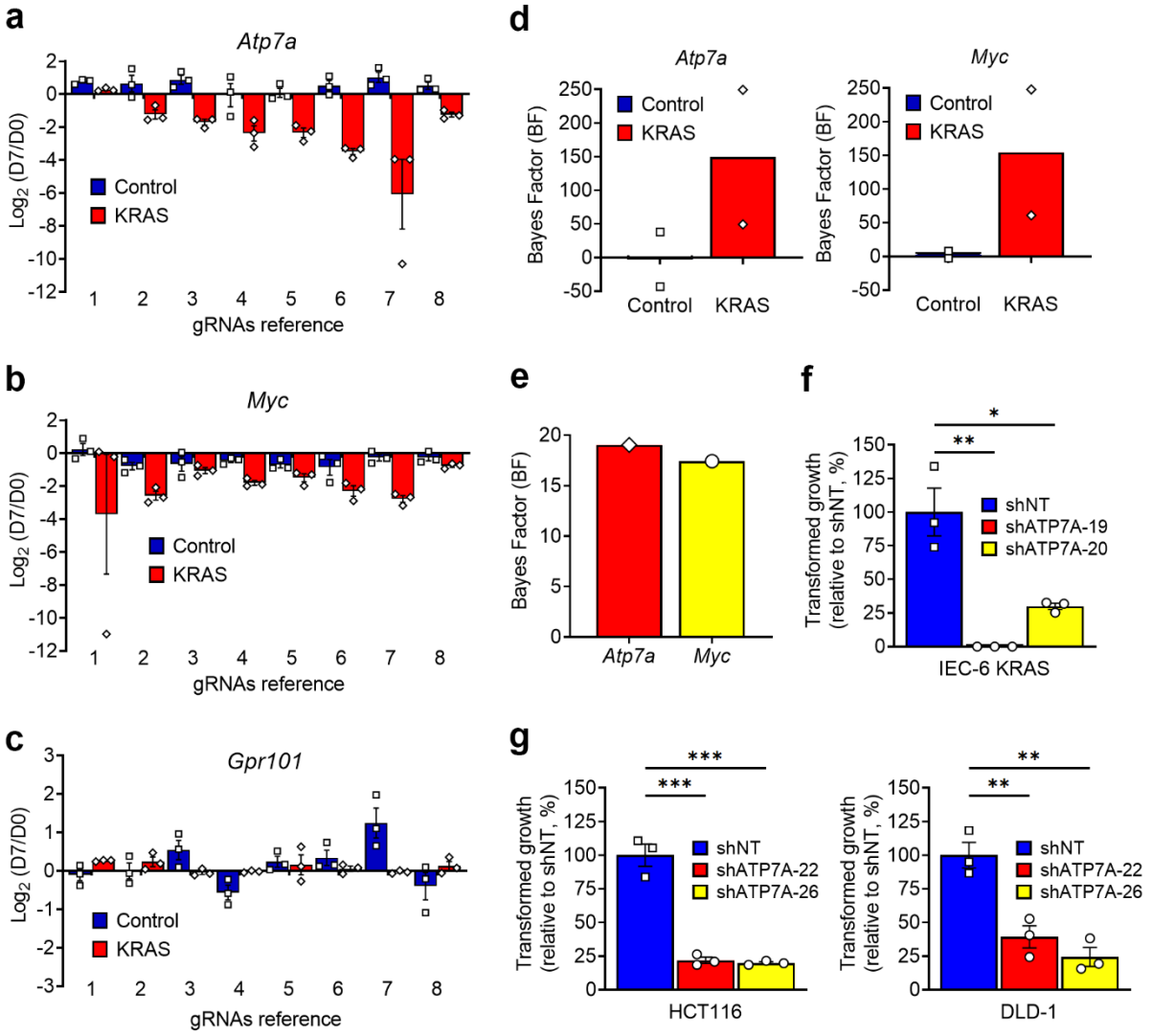

Supplementary Figure 2.4. ATP7A is essential for growth of KRAS-mutant cells

(a-c) *Graphs depicting the relative abundance of each of the eight gRNAs used in CRISPR/Cas9 screens in Control (blue) and KRAS (red) represented as Log_2 FC (Day 7/Day 0) for Atp7a* ***(a)*** *essential gene Myc* ***(b)*** *and non-essential gene Gpr101* ***(c)***. *Data represent N=3 replicates per condition and are representative of two independent CRISPR screens* ***(a-c)***. ***(d)*** *Bar graphs depicting the bayes factor (BF) scores for Atp7A (left) and Myc (right), expressed as mean of the two in vitro CRISPR/Cas9 screens in Control and KRAS cells.* ***(e)*** *Same as in* ***d****, but for in vivo CRISPR/Cas9 screen in KRAS IEC-6 xenografts.* ***(f)*** *Adherence-independent growth on soft agar for KRAS IEC-6 cells with NT or ATP7A shRNAs (19 and 20), *P=0.0174; **P=0.0049. (****g****) Same as in* ***f****, except that experiments were performed using HCT116 (left) and DLD-1 (right) with NT or ATP7A shRNAs (22 and 26), ***P=0.0008 (shNT versus shATP7A-22, HCT116); ***P=0.0006 (shNT versus shATP7A-26, HCT116); **P=0.0084 (shNT versus shATP7A-22, DLD-1); **P=0.0030 (shNT versus shATP7A-26, DLD-1). Data represent N=3 independent experiments per condition* ***(f, g)***. *Data and error bars represent mean ±SEM, and statistical significance is determined using unpaired two tailed Student's t tests. *P < 0.05; **P < 0.01; ***P < 0.001.*

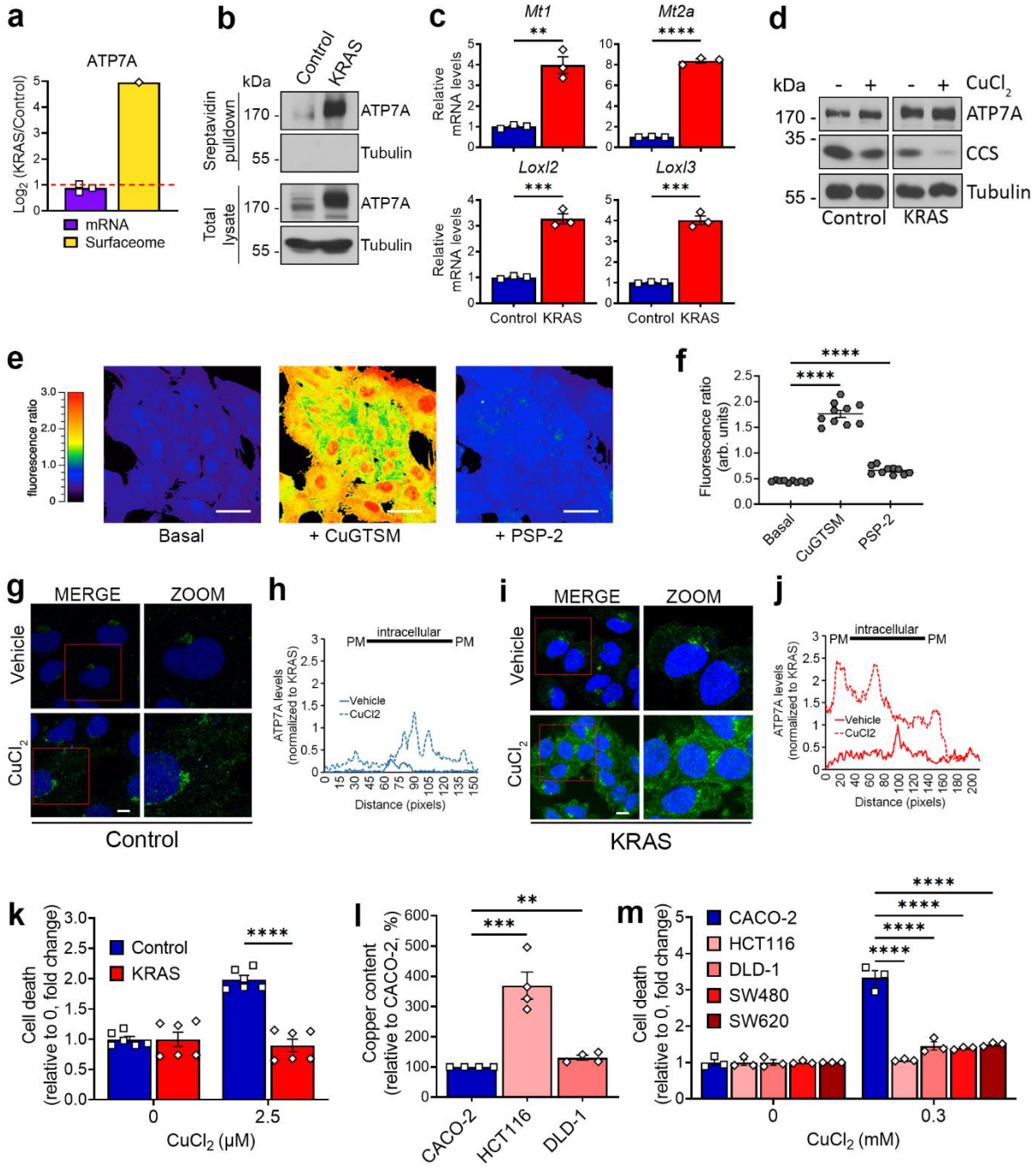

Supplementary Figure 2.5. ATP7A expression and Cu-export function are essential for survival of KRAS-mutant cells

(a) *Graph indicating the Log₂ FC (KRAS/Control) from the transcriptome (purple) and surfaceome (yellow) datasets for ATP7A. Red dashed line indicates cut-off value for statistical*

significance. Data are expressed as mean of N=3 (mRNA) or N=2 (surfaceome) independent replicates per condition. ***(b)*** *Biotinylated cell-surface proteins from Control and KRAS cells were processed for streptavidin pull-down. Eluted proteins and pre-elution lysates were analyzed by IB for ATP7A and Tubulin. Data represent N=3 independent experiments.* ***(c)*** *Relative mRNA expression levels of four Cu-dependent genes in Control and KRAS cells. Data represent N=3 independent experiments with two technical replicates.* ***(d)*** *Control and KRAS cells were treated with or without $CuCl_2$ for 24 h, and whole-cell lysates were analyzed by IB for ATP7A, CCS and Tubulin. Data represent N=3 independent experiments.* ***(e)*** *Representative images of KRAS cells incubated with the fluorescence sensor crisp-17 and left untreated (Basal), treated with CuGTSM, or treated with high-affinity Cu chelator (PSP-2) in the presence of CuGTSM. Data represent N=3 independent experiments, scale=30 µm.* ***(f)*** *Dot plot depicting the quantifications of crisp-17 fluorescence ratios averaged over N=10 cells.* ***(g-j)*** *Same as* ***d****, except that ATP7A (green) was assessed by IF with DAPI (blue). Representative images for Control* ***(g)*** *and KRAS* ***(i)*** *cells, and the corresponding graphical distribution of ATP7A levels for Control* ***(h)*** *and KRAS* ***(j)****. Data represent three random images from N=3 independent experiments, scale=10 µm. Data are normalized to untreated KRAS cells.* ***(k)*** *Control and KRAS IEC-6 were treated with the indicated doses of $CuCl_2$ for 24 h and processed for Annexin V staining by Flow cytometry. Data represent N=6 independent replicates.* ***(l)*** *Measurement of total Cu levels for the indicated CRC cells as measured by ICP-MS analysis. Data represent N=4 independent experiments, ***P=0.0010 (CACO-2 versus HCT116); **P=0.0084 (CACO-2 versus DLD-1).* ***(m)*** *Same as* ***k****, but for KRAS wild-type (CACO-2) and KRAS mutant (HCT116, DLD-1, SW480, SW620) CRC cells. Data represent N=3 independent experiments. For panels* ***(c, f, k-m)****, values and error bars represent mean ±SEM, and statistical significance is determined using unpaired two tailed Student's t tests* ***(c, f, l)*** *or two-way ANOVA with post-hoc Bonferroni's multiple comparison analysis* ***(k, m)****. **P < 0.01; ***P < 0.001; ****P < 0.0001.*

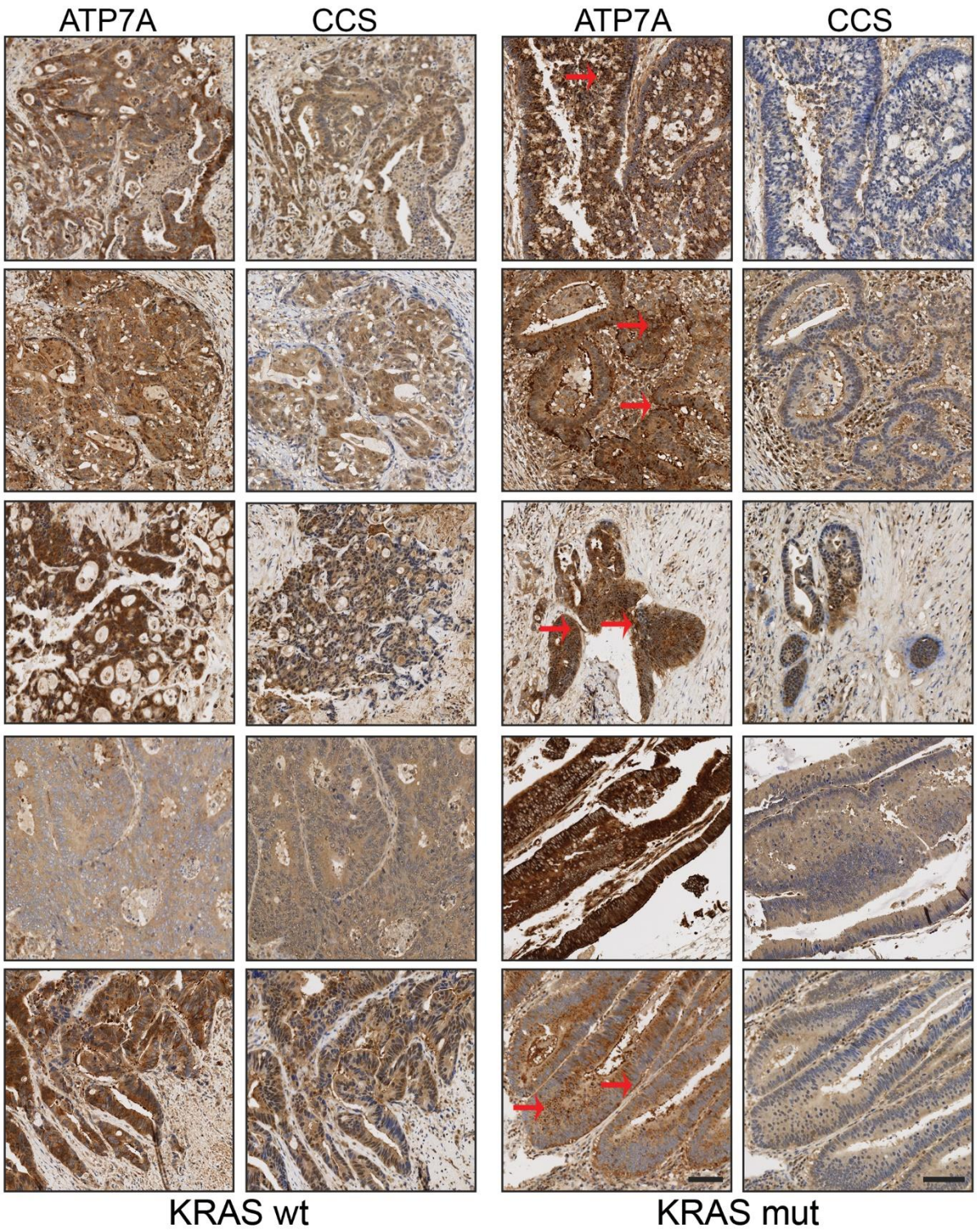
ATP7A
CCS
ATP7A
CCS
KRAS wt
KRAS mut

Supplementary Figure 2.6. ATP7A and CCS levels in KRAS wild-type and KRAS-mutant CRC tumors

Representative IHC images of ATP7A (left) and CCS (right) levels in patient derived CRC tissues with wild-type KRAS (wt) or mutant KRAS (mut) [n=5 patient tissues per 12 condition], scale=250 μm. Red arrows indicate granular staining of ATP7A in trans-Golgi network or basolateral membrane (or cell-surface) localization of ATP7A.

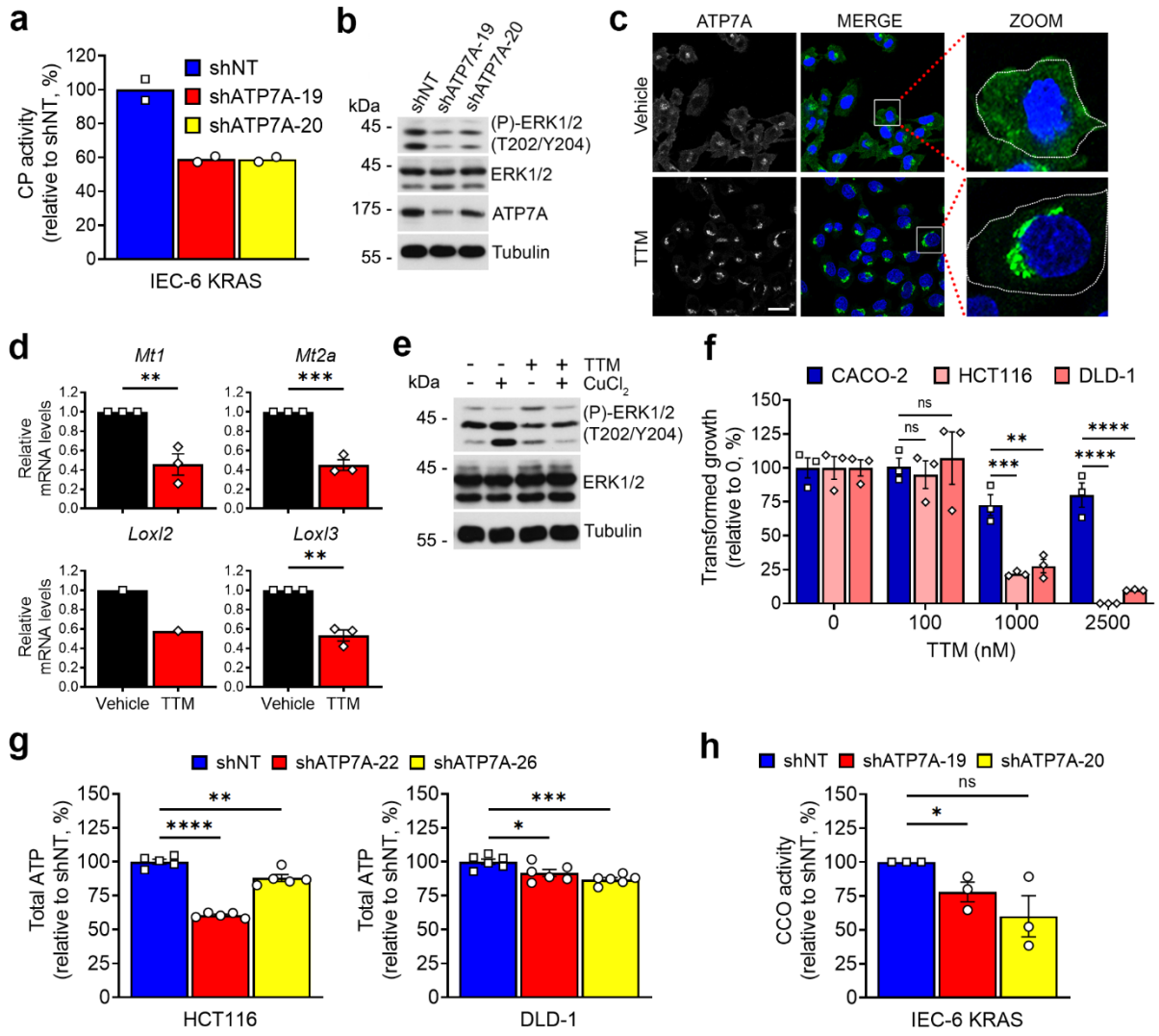

Supplementary Figure 2.7. ATP7A is required for growth and Cu-dependent functions in KRAS mutant cells

(a) *Cp activity in KRAS cells with NT or ATP7A shRNAs (19 and 20). Data is expressed as mean of N=2 independent experiments.* ***(b)*** *IB of ATP7A, Tubulin, total and phosphorylated ERK1/2 in lysates of KRAS cells with NT or ATP7A shRNAs (19 and 20). Data represent N=3 independent experiments.* ***(c)*** *KRAS cells were treated with or without TTM for 24 h, and ATP7A (green) was assessed by IF with DAPI (blue). White dashed lines indicate cell boundaries. Data represent N=3 independent experiments, scale=20 µm.* ***(d)*** *Graph depicting relative mRNA levels of Cu-dependent genes in KRAS cells treated with or without TTM for 24 h. Data are representative N=3 independent experiments with two technical replicates.* ***(e)*** *IB of total and phosphorylated ERK1/2 and Tubulin in lysates of KRAS cells untreated, treated with TTM or CuCl2, or both for 24 h. Data is representative of N=2 independent experiments.****(f)*** *Adherence independent growth on soft agar of CACO-2, HCT116 and DLD-1 cells treated with the indicated doses of TTM. Data represent*

*N=3 independent replicates per condition, ***P=0.0008 (CACO-2 versus HCT116-1000); **P=0.0027 (CACO-2 versus DLD-1-1000); ****P< 0.05; **P < 0.01; ***P < 0.001; ****P < 0.0001.*

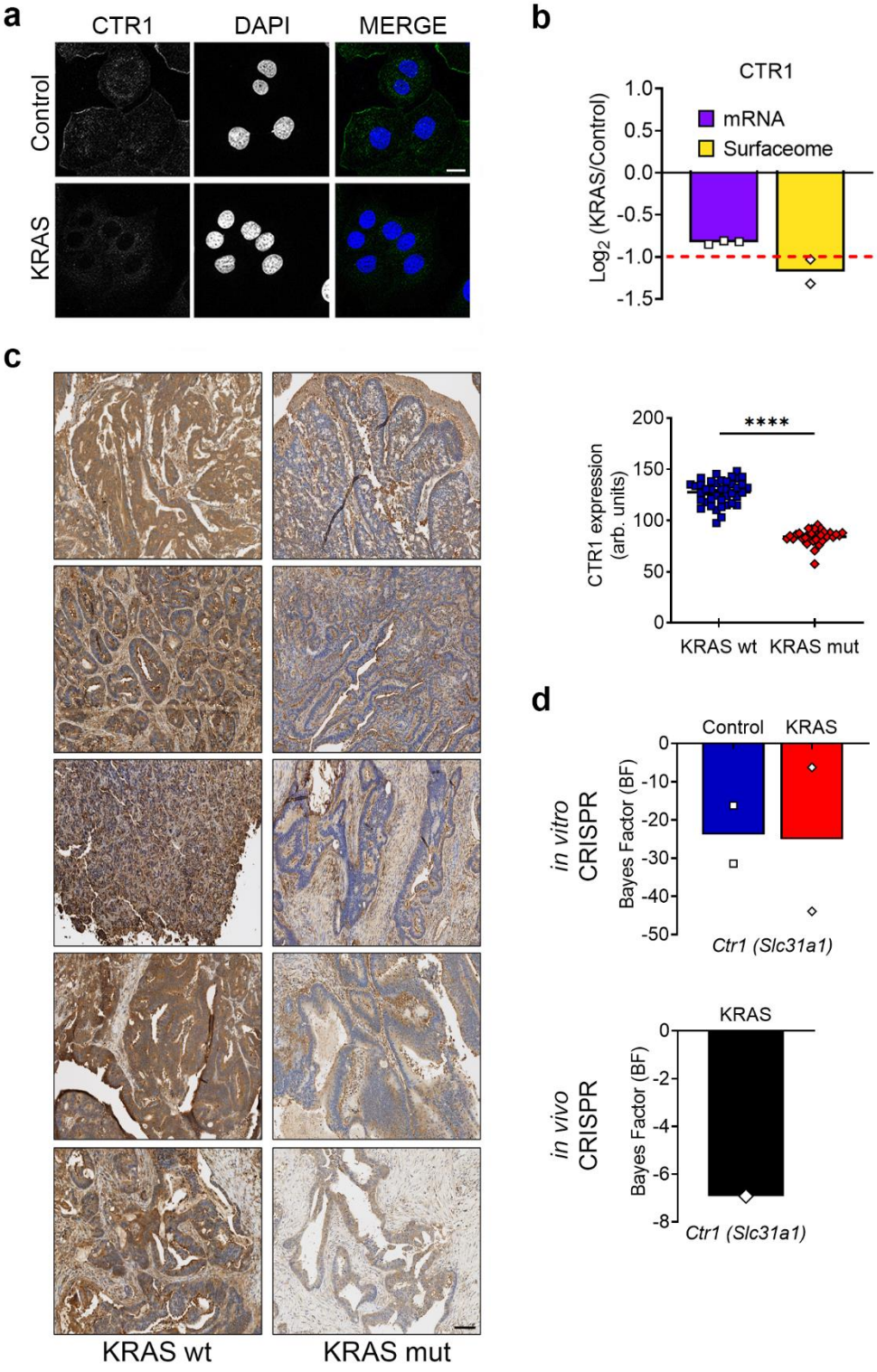
a
CTR1
DAPI
MERGE
Control
KRAS
b
CTR1
mRNA
Surfaceome
Log2 (KRAS/Control)
1.0
0.5
0.0
-0.5
-1.0
-1.5
c
KRAS wt
KRAS mut
****
CTR1 expression (arb. units)
200
150
100
50
0
KRAS wt
KRAS mut
d
in vitro CRISPR
Control
KRAS
Bayes Factor (BF)
0
-10
-20
-30
-40
-50
Ctr1 (Slc31a1)
in vivo CRISPR
KRAS
Bayes Factor (BF)
0
-2
-4
-6
-8
Ctr1 (Slc31a1)

Supplementary Figure 2.8. CTR1 is downregulated in KRAS-mutant IEC-6 cells and CRC tissues

(a) *KRAS versus Control cells were examined by IF for CTR1 (green) and DAPI (blue), scale=17 µm.* ***(b)*** *Graph indicating the Log_2 FC (KRAS/Control) from the transcriptome (purple) and surfaceome (yellow) datasets for CTR1. Red dashed line indicates cut-off value for statistical significance. Data represent N=3 (mRNA) or N=2 (surfaceome) independent replicates per condition.* ***(c)*** *Representative images (left) for CTR1 staining from IHC profiling of KRAS wt versus KRAS mut CRC patient tumors, scale=250 µm. Scatter dot plots for CTR1 levels quantified from IHC images in the indicated conditions (right). Data represent mean ±SEM of N=40 and N=32 random images from five KRAS wt and KRAS mut patient tissues, respectively. Statistical significance is determined using unpaired two-tailed Student's t test. ****$P < 0.0001$.* ***(d)*** *Bar charts representing the BF score of Ctr1 (Slc31a1) from CRISPR/Cas9 screens in KRAS versus Control IEC-6 cells (top) and in KRAS IEC-6 xenografts (bottom).*

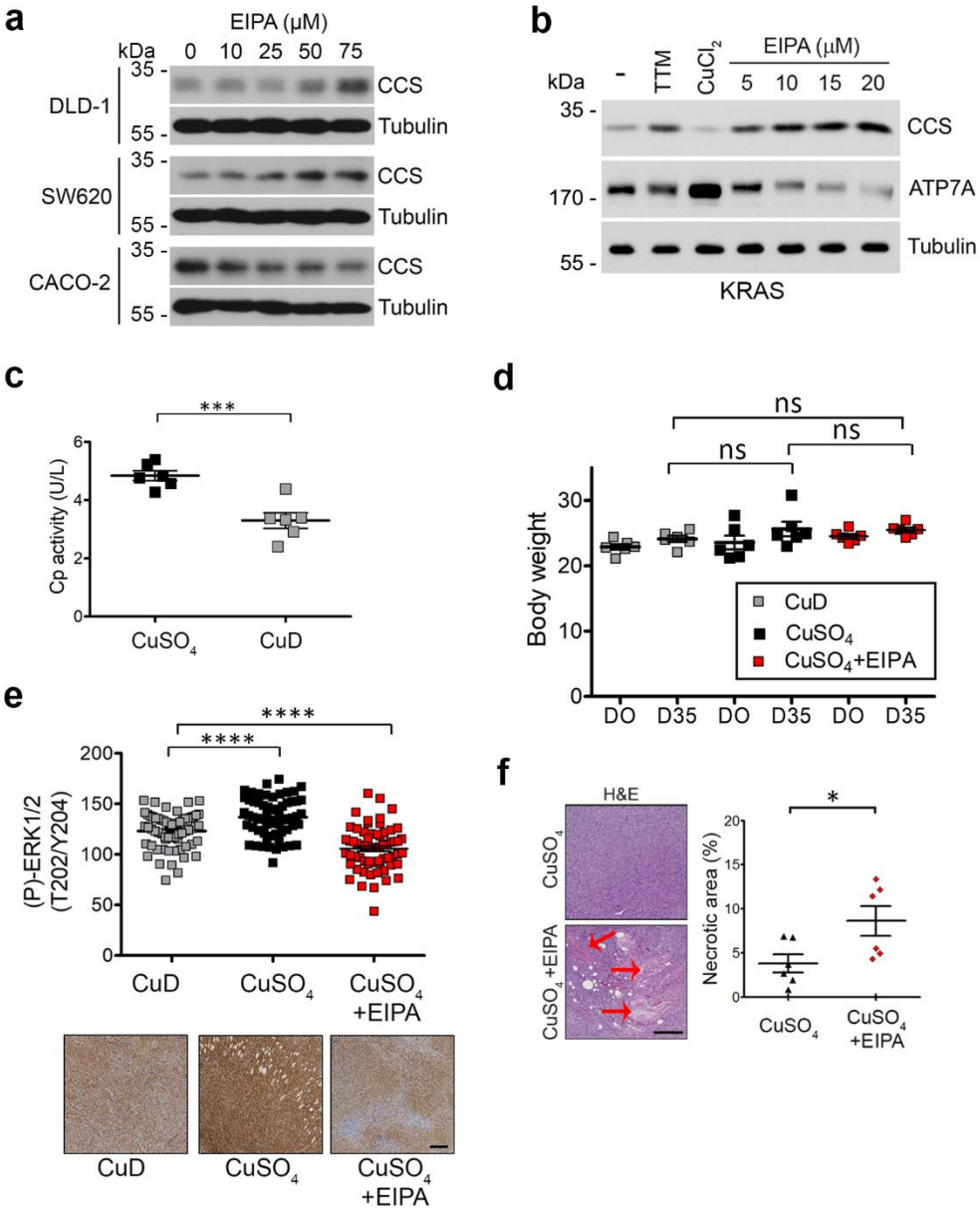

Supplementary Figure 2.9. Macropinocytosis modulates Cu levels and validation of the *in vivo* tumor growth protocol

(a) *Whole-cell lysates were collected from CRC cells after treatment with indicated doses of EIPA for 15 min, and CCS and Tubulin levels were analyzed by IB. Data represent N=3 independent experiments.* ***(b)*** *Whole-cell lysates of KRAS cells were collected after treatment with EIPA at indicated doses, TTM (10 μM) and $CuCl_2$ (100 μM) for 24 h. CCS, ATP7A and Tubulin levels were analyzed by IB. Data represent N=3 independent experiments.* ***(c)*** *Serum was collected from N=6 mice at the end of the study and Cp activity was analyzed in two technical replicates for the indicated conditions, ***P=0.0004.* ***(d)*** *Body weights were recorded in N=6 mice per condition, for the pre-treatment (D0) and post-treatment (D35) timepoints.* ***(e-f)*** *Representative IHC images*

*and quantification of phosphorylated-ERK1/2 levels **(e)** and necrotic areas **(f)** for the indicated conditions [N=63 random images from six mice per condition (e), ****P < 0.0001; N=12 images from six mice per condition **(f)**, *P=0.034], scale=250 µm. For panels **(c-f)**, values and error bars represent mean ±SEM, and statistical significance is determined using unpaired two tailed Student's t tests. ns: not significant, *P < 0.05, ***P < 0.001, ****P < 0.0001.*

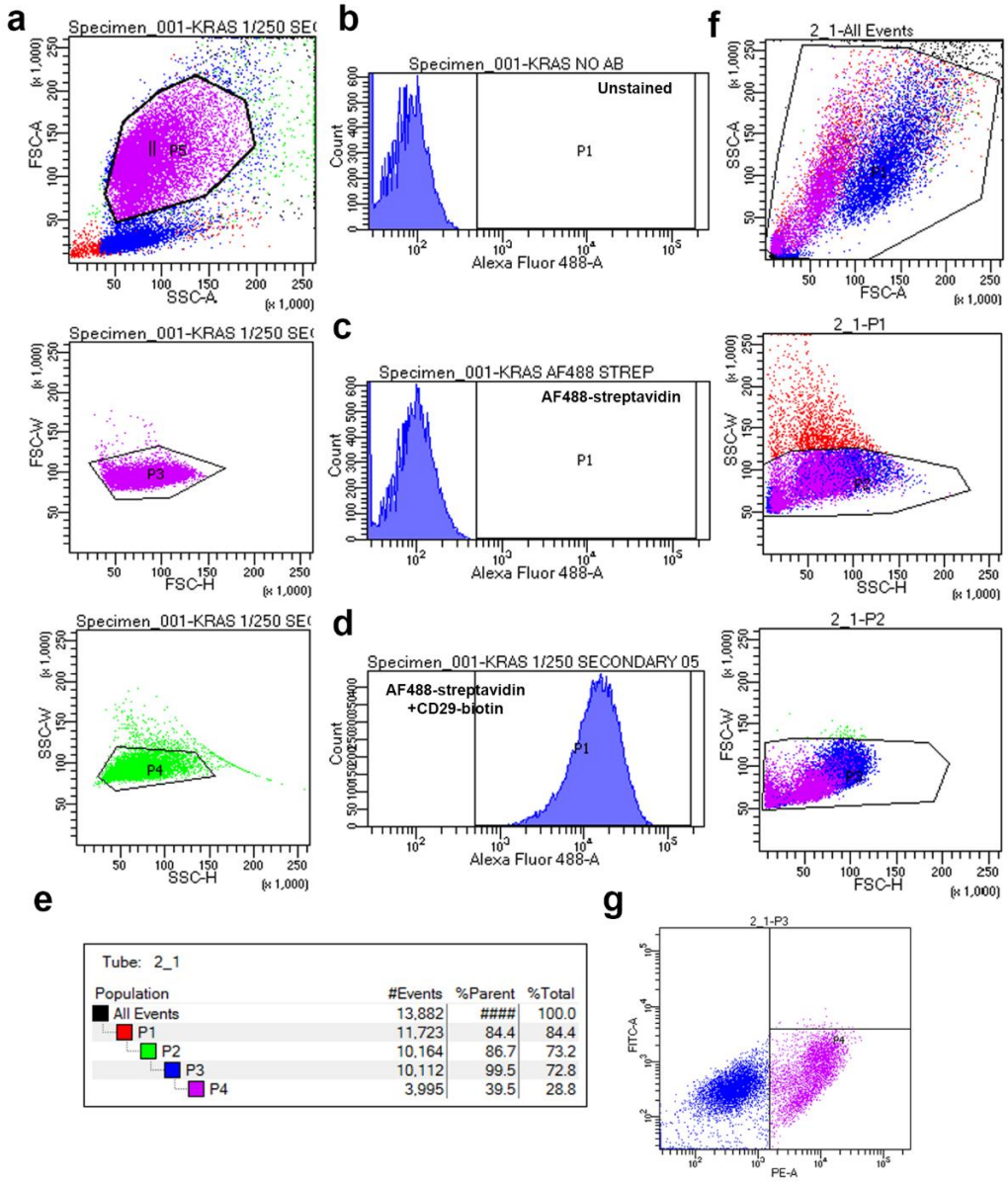

Supplementary Figure 2.10. Gating strategy for flow cytometry

(a)** For figure 2.3, P5 is first selected from FSC-A versus SSC-A plot and doublets are removed from P5 population after gating for P3 (in purple) in FSC-W versus FSC-H plot, and P4 (in green) from SSC-W versus SSC-H plot. **(b-d)** From P4, histograms (in blue) is generated and P1 is gated considering negative population in **(b)** "Unstained" control without any antibody, and in **(c)

"Alexa fluor (AF488)- streptavidin" control with secondary antibody but without primary antibody. ***(d)*** *Represents positive population with primary antibody (CD29-biotin) and secondary AF488-streptavidin antibody.* ***(e)*** *Represents gating strategy used for* ***supplementary fig. 2.5k & 2.5m. f****, Population is selected from FSC-A versus SSC-A plot as P1. From P1, doublets are removed by selecting P2 from SSC-W versus SSC-H plot and P3 from FSC-W versus FSC-H plot.* ***(g)*** *From P3 a dot plot is generated by plotting FITC-A versus PE-A, ANNEXIN-V+ cells are determined by gating for P4.*

Chapter 3: Identification of druggable pathways that may improve the therapeutic efficacy of copper chelation

1. Author contributions

The CRISPR/Cas9 screen was performed by Caroline Huard in the laboratory of Dr. Mike Tyers (IRIC). Generation of RANKS score and screen results were generated by Dr. Jasmin Coulombe-Huntington. N.N. analyzed the screen results, compared the data between conditions, prepared the graphs, generated the figures and performed the literature search to identify relevant hits. The immunoblotting experiments were also designed and performed by N.N. Philippe P. Roux conceived the idea for the screen.

2. Introduction

TTM and Trientine are clinically approved copper-lowering drugs for the treatment of congenital copper disorders, such as Wilson's disease (Baldari et al., 2020). In addition, TTM has shown significant preclinical activity in reducing tumor growth, microvessel density, tumor vascularity, and distant metastasis in several cancer models, including head and neck (Hassouneh et al., 2007), pancreatic (Ishida et al., 2013), and breast (Pan et al., 2002) cancer, as well as BRAF-mutant thyroid tumors. Although TTM treatment reduced tumor burden in BRAF-driven xenografts, tumors did not regress completely (Brady et al., 2017, 2014; M. Xu et al., 2018). However, combination of TTM and Trientine induced a prolonged anti-tumor response (Brady et al., 2014), suggesting that TTM as monotherapy is probably insufficient to completely curb tumor growth.

Limited clinical trials have attempted to test the anti-neoplastic properties of TTM in various solid cancers (Baldari et al., 2020) including hormone-refractory prostate cancer (Henry et al., 2007), metastatic renal cancer (Redman et al., 2003) and breast cancer (Jain et al., 2013). TTM was very efficient in reducing systemic copper levels within three weeks *in vivo*, as suggested by serum ceruloplasmin activity (G. Khan & Merajver, 2009; Lowndes et al., 2008). In one study with breast cancer patients, TTM increased disease-free survival rates to >67% with a median follow up of 6.7 years (Chan, Willis, Kornhauser, Ward, et al., 2017). Although stable disease and delayed progression was achieved in cancer patients treated with TTM (Lowndes et al., 2008; Pass, Brewer, Dick, Carbone, & Merajver, 2008; Redman et al., 2003), its effect as monotherapy was limited in these studies. On the positive side, several phase I studies of drug dosing have shown that long-term TTM treatments is generally well tolerated with reversible toxicities, such as mild anemia and neutropenia (G. Khan & Merajver, 2009). Notably, patients have been treated safely for 65 months with no major side effects (Chan, Willis, Kornhauser, Ward, et al., 2017).

Other studies have focused on examining the synergistic effects of TTM with other anticancer therapies. For example, TTM sensitized melanoma that are resistant to BRAF or MEK1/2 inhibitors (Brady et al., 2017, 2014), suggesting that copper chelation could be used in some instances of drug resistance. Low CTR1 and high ATP7A expression is positively correlated with cisplatin resistance. Copper chelation with TTM is known to increase levels of the copper importer CTR1 (Ishida et al., 2010), while downregulating the copper exporter ATP7A (Chisholm et al.,

2016). These studies show that TTM imparted synergistic anti-tumor effects with cisplatin by increasing intracellular platinum uptake and concentrations via CTR1- and ATP7A-dependent mechanisms (H. H. W. Chen & Kuo, 2013). Similarly, TTM sensitized breast cancer cells to the DNA-damaging drug doxorubicin (Pan, Bao, Kleer, Brewer, & Merajver, 2003). Other approaches include co-treatments with the autophagy inhibitor chloroquine (CQ), where upon TTM treatments significantly inhibited pancreatic tumor growth *in vitro* and *in vivo* (Z. Yu et al., 2019). The limited clinical activity of TTM is also likely attributed to the observation that treatment does not induce tumor cell apoptosis, as TTM appears to be cytostatic as a monotherapeutic agent (Y. J. Kim, Tsang, Anderson, Posimo, & Brady, 2020; Pan et al., 2003; Z. Yu et al., 2019). Therefore, a recent study employed high-throughput small molecule screens to identify compounds that synergized with TTM in BRAF-mutant melanomas. Pharmacological inhibition of B-cell lymphoma 2 (BCL2) family members selectively decreased the viability of cells when combined with TTM, suggesting that combination strategies may be more successful with copper chelation to better inhibit tumor growth. More preclinical studies are needed to improve the anti-tumor effects of TTM with existing therapeutic interventions, especially for aggressive, resistance-prone cancers such as KRAS-mutated CRC.

CRISPR-mediated pharmacogenetic screens can be used to identify genetic pathways that enhance or suppress activity of drugs, thus deepening our understanding of mechanism(s) of action and resistance (Jost & Weissman, 2018). It has been successfully employed to identify genes whose loss-of-function is implicated in the resistance to the BRAF inhibitor vemurafenib (Shalem et al., 2014) or ERK inhibitor SCH772984 in KRAS-mutant cells (Colic et al., 2019). Similarly, genome-wide CRISPR screens helped identify the cellular targets of newly identified drugs LB-60-OF61 (Estoppey et al., 2017) and Rigosertib (Jost et al., 2017). Using this approach in multiple cell lines, several high-confidence genes were identified, whose loss-of-function increased sensitivity to poly ADP-ribose polymerase (PARP) inhibitors (M. Zimmermann et al., 2018) or the (ataxia telangiectasia and Rad3-related) ATR checkpoint kinase inhibitor AZD6738 (C. Wang et al., 2019). Taken together, genome wide CRISPR screening is a powerful approach to better understand the specificity of a drug, the pathway(s) it targets, and identify synthetic lethal genes that could be co-targeted to improve its therapeutic efficacy.

In a previous study, we have shown that KRAS-mutant CRC are more sensitive to copper chelation by TTM compared to wild-type KRAS cells in 2D and 3D growth mediums (Aubert et al., 2020). Here, we characterized the mechanism of action of TTM and selectivity for copper chelation, and identified synthetic lethal pathways that could improve its efficacy. In collaboration with the group of Mike Tyers (Institute for Research in Immunology and Cancer), we performed a genome-wide CRISPR/Cas9 screen in NALM-6 cells (*NRAS*-mutated human pre-B-cell lymphocytic leukemia line) cultured with increasing TTM concentrations. In parallel, a similar screen was performed with the related copper chelator Trientine, enabling comparison of their mechanism of action. The screen identified several functional gene clusters, providing insights into the cellular effects of copper chelation. Additionally, we identified several genes whose loss-of-function increased or rescued the anti-proliferative effect of TTM.

3. Results and Discussion

3.1. Effect of TTM or Trientine was on-target for copper homeostasis genes

The results of the CRISPR screen indicated that the top-ranking rescue genes in all the TTM screens (2, 4, 8, 10 μM) and in the Trientine screen (500 μM) were *ATP7A* and *ATOX1*. Loss of ATP7A (Gudekar et al., 2020) and ATOX1 (I Hamza et al., 2001) have been shown to hyperaccumulate copper levels, likely explaining why cells lacking their expression overcame the inhibitory effect of copper chelation. The CRANKS (conditional robust analytics and normalization for knockout screens) score of these two genes clustered far apart from all the other genes in the screen, suggesting that the drugs were on target for inhibiting copper homeostasis (**Fig. 3.1B-E**). Several GO terms associated with copper ion export and metabolism (highlighted in blue) were indeed enriched among the genes that significantly rescued the effect of TTM or Trientine (**Fig. 3.2a**).

3.2. Copper chelation targets numerous genes involved in the electron transport chain (ETC)

The majority of genes that rescued the effect of TTM or Trientine belonged to mitochondrial electron transport chain (ETC) complex formation or activity (**Fig. 3.2b, Fig. 3.1b-e**). Many of the GO terms associated with ETC activity including ubiquinone synthesis ($P = 4.92 \times 10^{-12}$) , complex 1 activity ($P = 1.73 \times 10^{-6}$) and assembly ($P = 9.7 \times 10^{-16}$), and oxidative phosphorylation ($P = 3.98 \times 10^{-10}$) were significantly enriched amongst the top-scoring rescue genes (**Fig. 3.2a**). This rescue effect was observed in all of the TTM doses tested, however, for certain genes [ubiquinol-cytochrome c reductase complex chaperone (*UQCC2*), *UQCC1,* Ubiquinol-cytochrome c Reductase Complex III Subunit VII (*UQCRQ*), ubiquitin associated protein 2-like (*UBAP2L*), Prenyldiphosphate synthase, subunit 1 (*PDSS1*), *PDSS2*, coenzyme Q2 *(COQ2)*, *COQ7*, *SLC25A1,* bc1 synthesis like (*BCS1L*)], the scores seemed to increase with dose (**Fig. 3.2b**). String network analysis of all the rescue genes from the four TTM screens showed a strong enrichment of the mitochondrial oxidative phosphorylation pathway (**Fig. 3.2c**). Notably, several studies including ours have shown that TTM is potent inhibitor of mitochondrial complex IV activity, as CCO is a copper-dependent enzyme. As majority of cellular ATP is produced by oxidative phosphorylation rather than glycolysis (du Plessis, Agarwal, Mohanty, & van der Linde, 2015),

TTM reduced cellular ATP levels in oncogene-transformed cells (Aubert et al., 2020; Ishida et al., 2013). ETC activity comprises of five complexes I, II, II, IV and V in the inner membrane of the mitochondria (Milenkovic, Blaza, Larsson, & Hirst, 2017). In particular, genes related to the complex I (NADH:ubiquinone oxidoreductase), complex III (ubiquinol-cytochrome C oxidoreductase) and ubiquinone (coenzyme Q) electron carriers are significantly enriched in TTM-treated condition (**Fig. 3.2a**).

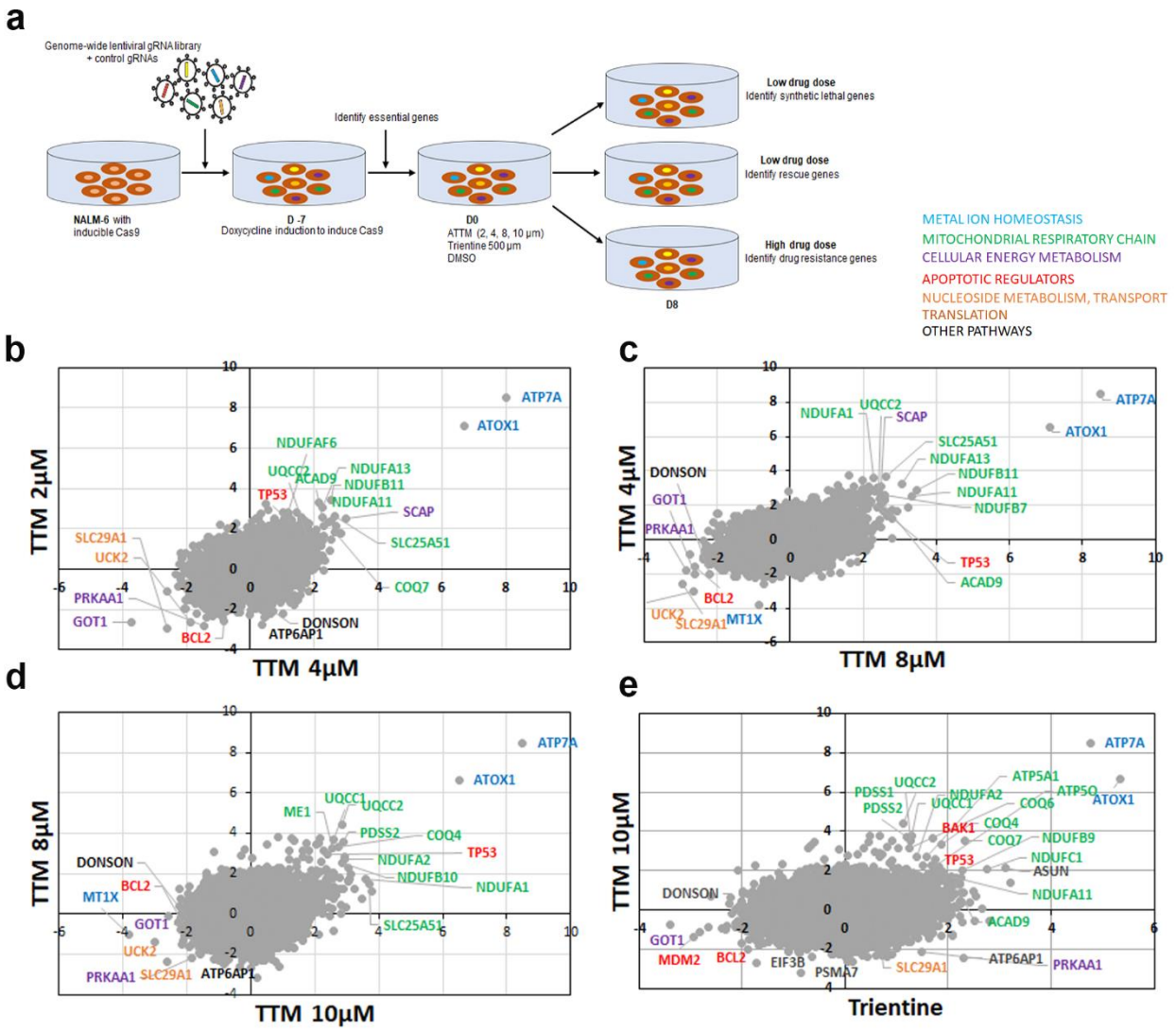

Figure 3.1. Design and results of genome-wide CRISPR-Cas9 screen to identify genes that modify cellular responses to copper chelators

(a) *Experimental design of the screen. Graphs depicting the results of the screen comparing* ***(b)*** *TTM 2 µM versus 4 µM,* ***(c)*** *TTM 4 µM versus 8 µM,* ***(d)*** *TTM 8 µM versus 10 µM,* ***(e)*** *TTM 10 µM versus Trientine 500 µM.*

Inhibition of complex I activity by a low-dose of rotenone sensitized *KRAS*-mutant cells specifically over normal cells to low-glucose conditions (Palorini, Simonetto, Cirulli, & Chiaradonna, 2013). Similarly, it was shown that restraining complex I activity by chemical inhibitors or knockdown of genes regulating complex I function [e.g. NADH:Ubiquinone oxidoreductase subunit A13 (*NDUFA13*)] increased glycolysis. Other studies have shown that cells tend to rely on glycolysis for ATP production when oxidative phosphorylation is affected (Ishida et al., 2013; Palorini et al., 2013), or vice versa (Palorini et al., 2013; Shiratori et al., 2019), suggesting that both metabolic pathways are interlinked. Therefore, our screen results indicate that knockout of complex I and III genes overcame the proliferation inhibition by TTM, likely due to compensatory activation of glycolytic pathway for cell energy production when mitochondrial ETC activity is inhibited.

To test if glycolysis is increased upon copper chelation, cells will be measured for glucose consumption and lactate production upon TTM treatments, by glucose oxidase and lactic acid assay kits respectively. Additionally, glycolytic rate can be inferred from the extracellular acidification rate (ECAR) of the surrounding media by the Seahorse extracellular flux (XF) analyzer. Glucose uptake in TTM-treated cells can also be measured using flow cytometry by adding fluorescent labelled glucose analog, 2-[N-(7-nitrobenz-2-oxa-1,3-diaxol-4-yl)amino]-2-deoxyglucose (2-NBDG or 2-deoxy-2-((7-nitro-2,1,3-benzoxadiazol-4-yl)amino)-D-glucose). Additionally, glycolytic flux can be inferred by measuring the activity of rate-limiting glycolytic enzymes. As we have previously shown that KRAS-mutant cells are more sensitive to TTM compared to KRAS-wildtype CRC, it would be interesting to determine if the rate of glucose uptake and glycolysis is relatively higher in KRAS-mutant cells upon TTM treatments. If KRAS-mutant cells exhibit enhanced adaption to glycolysis upon inhibition of oxidative phosphorylation, they might display enhanced sensitivity to low-dose glycolytic inhibitors in the presence of TTM. Cell proliferation/survival of KRAS-mutant and -wildtype cells could be measured in 2D (MTT assays) or 3D (adherence-independent growth on soft agar) growth mediums. Several chemical inhibitors of glycolysis could be tested along with a dose response of TTM and Trientine, including 2-deoxy-D-glucose, phloretin, aminooxyacetic acid, 6-aminonicotinamide, oxamate, fluoride, iodoacetate (TeSlaa & Teitell, 2014).

3.3. Aspartate metabolism may be involved in cellular responses to copper chelation

It is well known that cells lacking ETC function via inhibition of complex I or complex III are proliferation-deficient, which can be rescued by addition of pyruvate (Birsoy et al., 2015). Using a CRISPR-Cas9 screen, the Sabatini group identified that cells lacking ETC activity are dependent on aspartate synthesis via GOT1. Inhibition of cytosolic aspartate aminotransferase GOT1 enzyme synergizes with low doses of complex I inhibitor Metformin or complex III inhibitor Antimycin. Supplementation with pyruvate or glutamine, which are sources for aspartate synthesis, rescued the proliferation-defect of ETC-inhibited cells in a GOT1-dependent manner. The top-scoring synthetic lethal interactor for TTM and Trientine in our screen was GOT1. Notably, GOT1 synergy was better with lower doses of TTM (**Fig. 3.1b-e, Fig. 3.2d**). Therefore, the hypothesis is that if cells grew more dependent on GOT1 due to mitochondrial ETC inhibition by copper chelation, then inhibiting GOT1 activity could increase the anti-proliferative efficacy of TTM and Trientine.

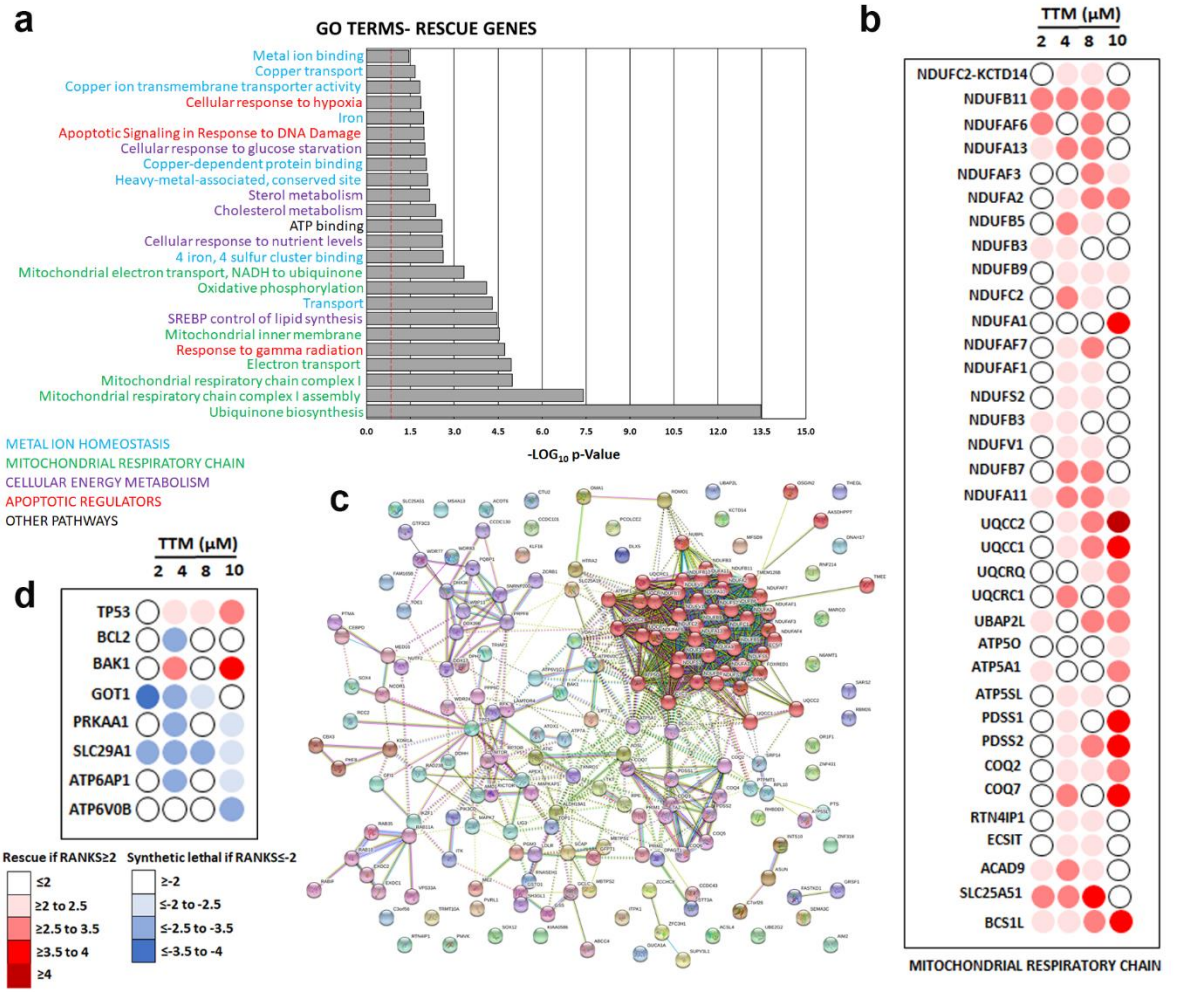

Figure 3.2. Summary of hits from the CRISPR screen that either rescues or synergizes with cellular inhibition by TTM

(a) *Gene ontology (GO) terms associated with genes that rescue anti-proliferative effect of TTM. Red line indicates cut off P value of <0.05.* ***(b)*** *Heat map depicting CRANKS score for genes regulating the mitochondrial electron transport chain (ETC) activity.* ***(c)*** *String network analysis depicting enrichment of genes associated with ETC activity amongst genes that rescue inhibitory effect of TTM.* ***(d)*** *Heat map depicting CRANKS score of apoptotic regulators (TP53, BAK1, BCL2), metabolic genes (GOT1, PRKAA1), nucleoside transporter (SLC29A1 also known as ENT1) and vesicular (H+) ATPase complex (ATP6AP1, ATP6V0B). The legend below indicates CRANKS scoring grid for genes that rescue (red), or is synthetic lethal to (blue), inhibitory effect of TTM.*

To determine if aspartate metabolism is affected upon copper chelation, we could measure aspartate levels in cells treated with TTM and Trientine by liquid chromatography-mass spectrophotometry (LC-MS). TTM treated cells could increase GOT1 activity compared to DMSO controls, which could be measured by GOT1 enzyme assay (Yoshida et al., 2020). GOT1 protein or mRNA levels could also increase in TTM-treated cells. As Glutamine or pyruvate acts as sources for aspartate production, their supplementation could potentially reverse the anti-proliferative effect of TTM. Proliferation can be measured by MTT assays with and without glutamine or pyruvate supplementation in TTM-treated cells. Additionally, it would be interesting to test if their supplementation rescues TTM-effect in cells expressing GOT1 and not in GOT1-lacking cells. Similarly, aspartate addition could be directly added to overcome the need for GOT1 activity in the presence of TTM. Along the same line of experiments, overexpression of aspartate importer SLC1A3 could also potentially rescue the inhibitory effect of TTM, specifically in aspartate-containing medium compared to medium replete of aspartate. Finally, several GOT1 inhibitors are available (Holt et al., 2018; Yoshida et al., 2020), which could be tested in concert with GOT1 knockdown for anti-proliferative synergy with increasing doses of TTM and Trientine. Cell proliferation could be measured by MTT assays and viability by Annexin V and propidium iodide (PI) quantification by flow cytometry. As KRAS transformed cells are known to increase glutamine metabolism and GOT1 expression (Son et al., 2013), it would be interesting to determine if the synergy between GOT1 inhibition with TTM could be specific to KRAS-mutant cancer cells compared to normal cells.

3.4. Copper chelation could render cells dependent on AMPK activity

Metabolic stress that reduce ATP levels are known to activate AMPK, that inhibits energy-consuming biochemical pathways (lipid and sterol synthesis, gluconeogenesis) and activates energy-producing catabolic pathways (glucose utilization, mobilization of lipid stores and autophagy) to minimize ATP consumption (Herzig & Shaw, 2018). Notably, inhibition of ETC complex I via metformin or rotenone, and inhibition of ETC complex III via antimycin A resulted in AMPK activation (Herzig & Shaw, 2018; Toyama et al., 2016). AMPK is primarily activated via phosphorylation at Thr172, which regulates its downstream target acetyl-CoA carboxylase (ACC), and this is thought to play a role in metabolic changes such as lipid synthesis in response to metformin. Studies have also shown that pharmacological inhibition of AMPK affected proliferation of pancreatic cancer cells, by blocking glucose uptake and lactate production (Hu et al., 2019). Additionally, copper chelation using TTM was shown to increase glucose consumption and AMPK activation in cancer cells, when ATP production via ETC was affected (Ishida et al., 2013). Similar observations were made in copper deficient rats, which was associated with increased AMPK activity compared to normal controls (Gybina & Prohaska, 2008). AMPK is a heterotrimeric complex composed of a catalytic α-subunit and two regulatory subunits, β and γ coded by different genes, (protein kinase AMP-activated alpha catalytic subunit) *PRKAA1* and *PRKAA2*, (protein kinase, AMP-activated, beta non-catalytic subunit) *PRKAB1* and *PRKAB2*, and (protein kinase subunit gamma-1) *PRKAG1*, *PRKAG2* and *PRKAG3* (Herzig & Shaw, 2018). In our study PRKAA1 scored as a synthetic lethal hit with TTM treatment (**Fig. 3.1b-e, Fig. 3.2d**). This suggests that AMPK activation could be critical for cells to adapt to the energy stress induced by copper chelation, and loss of AMPK could potentially synergize with TTM to curb tumor growth.

To test this hypothesis, AMPK activation could be checked in response to TTM and Trientine treatments in cancer cell lines. Phosphorylation of Thr-172 is used as a biomarker for AMPK activation, which could be analyzed upon TTM treatment compared to untreated controls. Additionally, AMPK activation is confirmed by analyzing the phosphorylation levels of bonafide downstream targets including ACC, HMG-CoA reductase (HMGCR), glycogen synthases (GYS1), eukaryotic elongation factor 2 kinase (eEF2K) (Herzig & Shaw, 2018). If AMPK is required for cell survival after copper chelation, TTM must cause a relatively greater decrease in

cell proliferation in AMPK-deficient cells compared to AMPK-sufficient cells. A similar mechanism was suggested for sensitivity to biguanides, wherein cancer cells lacking active AMPK pathway were more sensitive to the effects of complex I inhibitor metformin compared to AMPK sufficient cells (Zadra, Batista, & Loda, 2015). It would be interesting to determine if cells adapt to lower energy status post- copper chelation, by increasing glucose uptake and glycolysis in an AMPK-dependent fashion. Through methods outlined previously, TTM or Trientine-treated cells could be measured for increased rate of glycolytic flux. And if this increase in flux occurred only in AMPK-sufficient *versus* -deficient cells, we could conclude that copper deprivation increases AMPK activity to increase cellular ATP production via glycolysis to compensate for lack of ETC activity. Several inhibitors of AMPK are available namely Compound C (Hu et al., 2019), SBI-0206965 (Dite et al., 2018) and MT47-100 (Scott et al., 2015). If AMPK activity is found to be crucial for copper-deficient cells, these inhibitors could be tested for potential synergistic effects with copper chelators in several cancer cells. As literature suggests that AMPK activity could be crucial for KRAS-driven tumorigenesis (Eichner et al., 2019), and we have shown a selectivity of anti-proliferative effect of TTM for KRAS-mutant CRC, would AMPK inhibition particularly increase TTM efficacy in KRAS-mutant versus KRAS-wildtype cells?

3.5. ENT1 inhibitors could increase the efficacy of TTM

A high scoring candidate with all doses of TTM is *SLC29A1* (or ENT1, equilibrative nucleoside transporter 1) (**Fig. 3.1b-e, Fig. 3.2d**). ENT1 is a bidirectional nucleoside importer with high affinity for adenosine. It also transports Guanosine, Inosine, Hypoxanthine, and Thymidine (Boswell-Casteel & Hays, 2017). Adenosine is an ATP-derived nucleoside, which plays very important roles in hypoxia, inflammation, angiogenesis, DNA methylation, and apoptosis. More importantly, adenosine is the building block for ATP generation, and cellular uptake of adenosine via ENT1 plays a role in replenishing intracellular ATP stores (Boison & Yegutkin, 2019). The ability of ENT1 to import nucleosides is crucial for intracellular signaling (cyclic AMP, GMP), DNA and RNA synthesis, and nucleoside homeostasis (Boswell-Casteel & Hays, 2017). ENT1-knockout mice exhibit increased extracellular adenosine levels suggesting defective cellular import (Rose et al., 2011). Hypoxia or tumor microenvironments are known to increase extracellular adenosine, and evidence suggests that extracellular adenosine levels are regulated

during hypoxia via ENT1 (Eltzschig et al., 2005; Rose et al., 2011; D. Zhang, Xiong, Albensi, & Parkinson, 2011). Although intracellular adenosine metabolism is a relatively understudied process, enzymes processing adenosine levels are being considered for cancer therapy (Boison & Yegutkin, 2019). The screen results suggest that adenosine homeostasis could be altered when copper is depleted in cells, probably by providing adenosine for ATP production via ENT1 due to ETC-inhibition.

To test if ENT1 loss is synthetic lethal to TTM, proliferation of different cancer cells (expressing or lacking ENT1) will be measured upon TTM treatment. Further, a possible synergy between dose response of ENT1 inhibitors (dipyridamole, dilazep and nucleoside analog NBMPR) and TTM will be tested in cancer cells. Cell proliferation will be measured using MTT assays and cell apoptosis by quantifying Annexin V or propidium iodide using flow cytometry. Interestingly, SLC29A1 expression is increased in KRAS-dependent manner in intestinal epithelial cells compared to untransformed controls (Aubert et al., 2020). Based on this, it would be interesting to determine if ENT1 and TTM co-inhibition would have a relative or selective anti-proliferative effect on KRAS-mutant *versus* KRAS-wildtype CRC cells. Parallelly, we could determine if copper chelation increases ENT1 activity. For example, does ENT1 expression increase upon copper chelation? Although measurement of adenosine levels is tricky due to its short half-life, ENT1 activity can be measured by measuring adenosine uptake via techniques using radioactive labelled adenosine or high performance liquid chromatography (Pastor-Anglada & Pérez-Torras, 2018; Rose et al., 2011). As adenosine levels are altered in disease states including hypoxia and cancer, it is likely that adenosine levels and ENT1-mediated adenosine uptake are also altered upon copper chelation. Therefore, adenosine levels could be measured intracellularly or in extracellular milieu (in the presence or absence of ENT1 inhibitor) upon TTM treatments compared to untreated cells.

3.6. Vesicular transport could play important roles in copper chelation

Component of vesicular transport ATP6AP1 scored as synthetic lethal hit with TTM (**Fig. 3.1b,d,e, Fig. 3.2d**). Additionally, ATP6VOB also scored as synthetic lethal to 10 μM TTM dose (**Fig. 3.2d**). Studies in zebrafish showed that mutation in the vacuolar (H+) ATPase coding for the

V0D1 subunit (*ATP6V0D1)* could potentially inhibit ATP6 function and displayed a copper deficiency phenotype. *ATP6V0D1* mutants displayed decreased activity of two cuproenzymes and increased sensitivity to sub-optimal dose of copper chelator, neocuproine. Moreover, the copper-deficiency phenotype of these mutants was further enhanced with the pharmacological inhibition of Atp6 function or the loss of Atp7a expression (Madsen & Gitlin, 2008). We have shown that TTM can dramatically reduce ATP7A expression in cells (Aubert et al., 2020). In another study it was shown that the localization of ATP7A at the trans golgi network is affected when endosomal retrieval is blocked by bafilomycin A, which inhibits the vacuolar (H+) ATPase (Kalayda, Wagner, Buss, Reedijk, & Jaehde, 2008). Interestingly, the vacuolar (H+) ATPase is also implicated in the correct apical membrane localization of copper importer Ctr1 in Drosophila. In this model, loss of vacuolar (H+) ATPase also resulted in copper deficiency phenotypes like the abovementioned zebrafish model (J. Wang, Binks, Warr, & Burke, 2014). Another interesting observation is that yeasts adapt to change in pH environments by altering the expression of copper homeostasis genes, and supplementation of copper and iron ions helped them to survive under high pH environments. This suggests a role for vacuolar (H+) ATPase in iron and copper homeostasis, as it regulates the acidic pH that is optimal for yeast growth. This study also suggests that defects in acidification which are important for the secretory compartments will disrupt the copper loading onto cuproenzymes such as ceruloplasmin (yeast Fet3p) (Serrano, Bernal, Simón, & Ariño, 2004). Since vacuolar ATPase plays crucial role in the secretory compartment and intracellular trafficking, these results collectively suggest a link between proton delivery into secretory pathway and copper homeostasis. However, the mechanisms by which v type ATPase contributes to copper deficiency phenotype is still not understood.

To confirm the results of the CRISPR screen, knockdown of various subunits of v-type ATPase including ATP6AP1 and ATP6VOB to affect ATP6 activity, will be performed in many cancer cells. We need to confirm if loss of these subunits affected the expression and activity of v-ATPase by measuring H+ transport and v-ATPase activity by previously established protocols (Niikura, Takano, & Sawada, 2004). Then cells with or without functional v-ATPase will be exposed to increasing dose of TTM, to determine if loss of ATP6 expression synergized with suboptimal doses of TTM for inhibiting cellular proliferation or survival. In a similar manner, inhibitors of v-ATPases such as bafilomycin A, INDOL0, apicularen B or concanamycin (Huss & Wieczorek,

2009) can be tested for synergistic activity with TTM, by measuring cellular proliferation rates and apoptosis. Based on the suggested reference between copper homeostasis genes and v-ATPase activity in the literature, the cellular localization of copper regulating proteins such as ATP7A, CTR1, ATOX1 and CCS could be analyzed in cells expressing or lacking ATP6AP1 and ATP6VOB. This would help us to understand if v-ATPase normally regulates the compartmentalization of copper homeostasis proteins. For example, lack of functional v-ATPase could affect the ATP7A localization in the secretory vesicles, where ATP7A loads copper onto cuproenzymes. Alternatively, TTM treated cells are known to increase the expression of copper importer CTR1, and this could be prevented in cells lacking v-ATPase. Therefore, localization of copper-regulating proteins should be analyzed in cells with or without v-ATPase activity, along with TTM treatments. A further understanding of this process could be aided by experiments with or without exogenous copper in cells lacking functional v-ATPase activity. Collectively, these experiments could suggest if cell survival or adaptation to copper chelation involves v-ATPase dependent CTR1 or ATP7A localization. Additionally, activity of cuproenzymes and copper levels should be measured between cells expressing or lacking v-ATPase, either by knockdown of ATP6AP1 and ATP6VOB or using pharmacological inhibition. If cuproenzyme activity is altered in the absence of v-ATPase, this would suggest that it regulates copper loading and hence biosynthetic role of ATP7A. Taken together, if the experiments indicate that localization or function of copper dependent proteins are altered by ATP6 activity, then it could explain why loss of ATP6AP1 and ATP6VOB synergized with copper chelator TTM to further inhibit cell proliferation.

3.7. Novel role of TP53 in regulating ATP7A expression

This screen also identified an apoptotic signature as lack of functional *TP53* and *BAK1* (BCL2 Antagonist/Killer 1) rescues the anti-proliferative effect of TTM, suggesting that pro-apoptotic activity of BCL2 family and p53 is normally required for the efficacy of TTM (**Fig. 3.1b-e, Fig. 3.2d**). Further experiments with *TP53* knockdown in CRC cells led to the chance identification of previously unidentified role of p53 in regulating the expression of copper-regulating proteins ATP7A and CCS. Notably, knockdown of *TP53* led to the loss of ATP7A and CCS expression in HCT116 and DLD-1 CRC cells (**Fig. 3.3a).** Interestingly, this loss of ATP7A expression was not

rescued with addition of exogenous copper in the absence of p53 (**Fig. 3.3b)**. Some studies have suggested a role for p53 in copper-induced cellular stress response (Formigari, Gregianin, & Irato, 2013; E A Ostrakhovitch & Cherian, 2005), including regulation of copper-binding MT, which is transcriptionally induced by copper exposure (Elena A Ostrakhovitch, Olsson, von Hofsten, & Cherian, 2007). But there is a lack of understanding on the role of p53 in TTM-mediated cellular stress responses. Further, very little is known about mechanisms that regulate ATP7A levels besides copper-dependent post-transcriptional stabilization in intestinal epithelial cells (L. Xie & Collins, 2013). Therefore, it is worth exploring if p53 can transcriptionally regulate *ATP7A* and confirm if p53 can regulate *MT* in a similar manner in these cells. If these experiments show that cells lacking p53 suppress the expression of ATP7A and MT, then they should be more sensitive to addition of exogenous copper compared to controls expressing functional p53, as buffering of excess copper by these two proteins are necessary to prevent cuproptosis (Gudekar et al., 2020). Moreover, CCS decrease upon *TP53* knockdown suggests that intracellular copper levels could be modulated by p53. Further experiments are needed to directly measure copper levels by fluorescent probes or ICP-MS in cells lacking functional *TP53*. If these experiments show that copper levels were indeed perturbed upon *TP53* knockdown, and if *TP53* knockdown cells are unable to produce ATP7A and metallothionein to buffer excess copper, it could be another explanation (besides a potential anti-apoptotic role) for why cells lacking *TP53* rescued the effect of copper chelation (**Fig. 3.1b-e, Fig. 3.2d**).

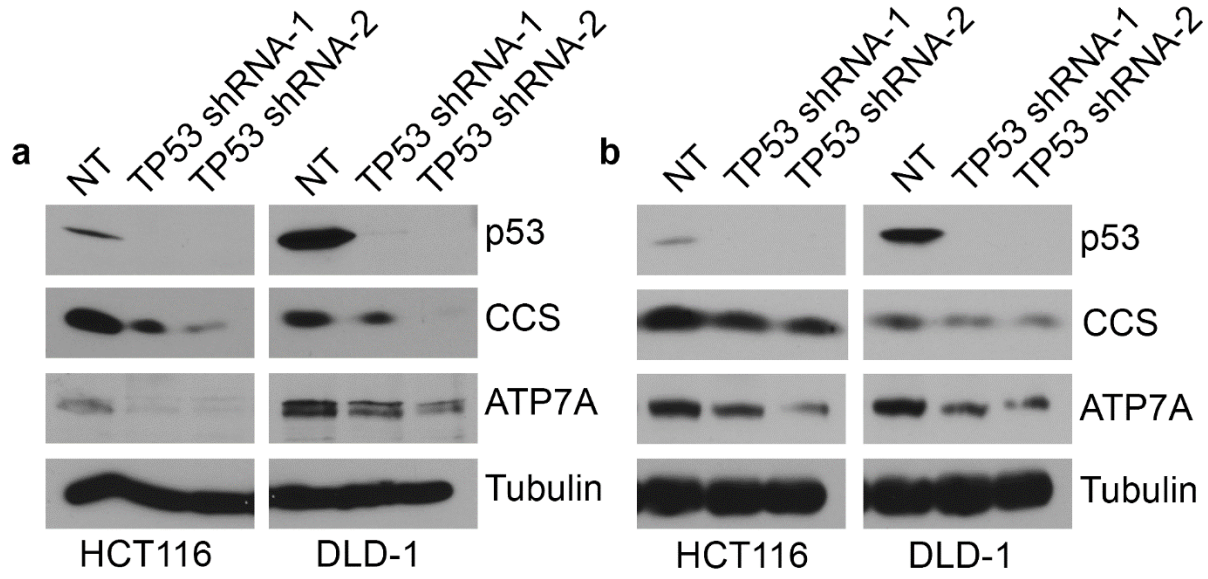

Figure 3.3. Knockdown of *TP53* reduces ATP7A and CCS levels in human CRC cells
(a, b) *Immunoblots probed for the indicated proteins upon knockdown of TP53 with two shRNA constructs and non-targeting (NT) control in KRAS-mutated HCT116 and DLD-1 colorectal cancer (CRC) cells. Immunoblots depict N=3 experiments.*

4. Conclusion

In summary, genome-wide CRISPR-Cas9 screens of TTM and Trientine treated cells suggest that these drugs are "on-target" and that the top scoring rescue genes are copper homeostasis regulating proteins. Notably, BCL2 scored as synthetic lethal target in TTM-treated (4 µM) condition, in line with the recent finding that drugs targeting the BCL2 family increased TTM efficacy in BRAF-mutant cancer cells (Y. J. Kim et al., 2020). Finally, this screen yielded several interesting synthetic lethal pathways including aspartate and adenosine metabolism, vesicular transport, that need to be thoroughly validated in the future with different techniques and in different tumor lines, for their potential to improve the anti-proliferative efficacy of TTM.

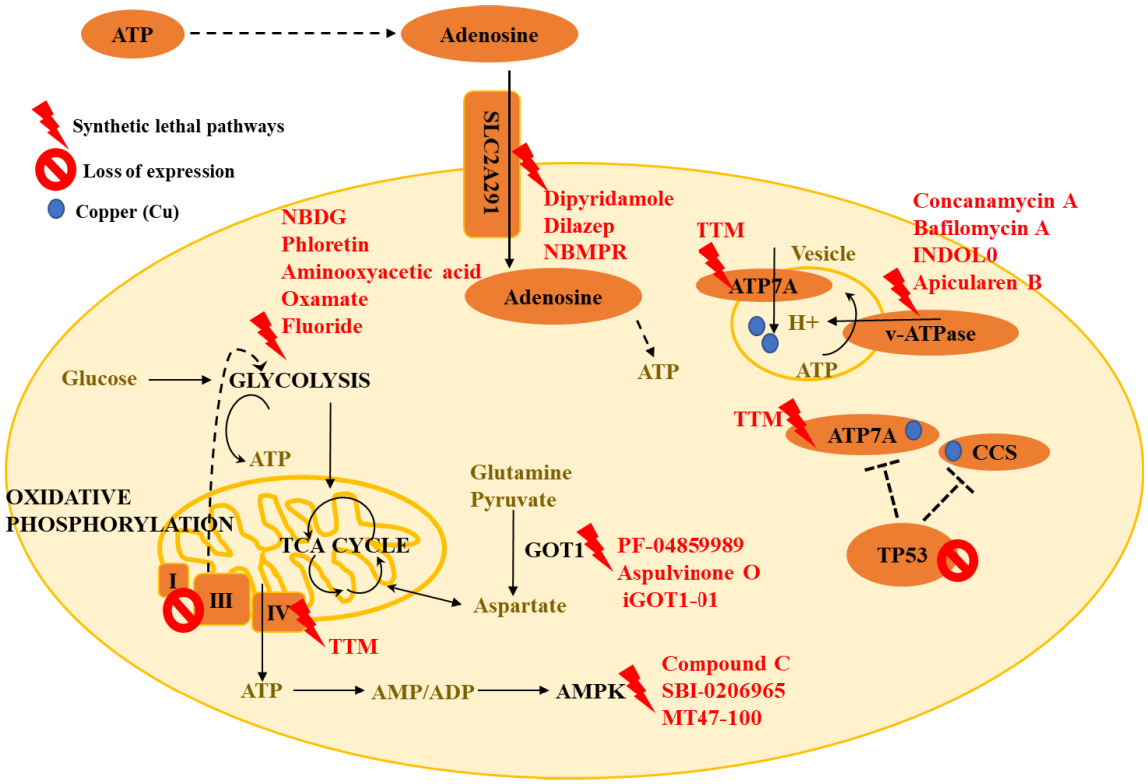

Figure 3.4. Summary of synthetic lethal pathways to improve TTM efficacy
Loss of mitochondrial ETC complex I and III are known to increase glycolysis dependency in tumor cells. Cu chelator TTM inhibit complex IV activity and ATP production of oxidative phosphorylation, which are also known to increase glycolysis dependency. SLC29A1 is an importer of adenosine and contributes to ATP metabolism. Inhibition of ETC activity increases cellular dependency of GOT1 activity, which is involved in aspartate metabolism. AMPK pathway is activated under conditions of metabolic stress to cope with low energy conditions. Mutations in Vacuolar(v)-ATPase coding genes has been shown to play a role in copper deficiency. Intracellular ATP7A and Cu trafficking mechanisms are dependent on vesicular transport. Targeting glycolysis pathway, SLC29A1, GOT1, AMPK, and v-ATPase functions could be synthetic lethal to TTM. TP53 loss affects expression of Cu-regulating proteins, ATP7A and CCS. Similarly, TTM also affects expression of ATP7A.

5. Methods

5.1. Chemogenomic genome wide CRISPR knockout screens

NALM-6 cells expressing dox-inducible Cas9 were allowed to thaw in 10% fetal bovine serum containing complete RPMI medium, and transduced with EKO sgRNA lentiviral library (MOI=0.5) with 78,754 single-guide RNAs (sgRNAs) that targeted 19,084 RefSeq genes, 20,852 alternatively spliced exons, 3,872 predicted genes and 2,043 sgRNAs with no match to human genome to estimate noise (Bertomeu et al., 2018). Each gene in the library was targeted by ~ 10 sgRNAs. Following selection of lentiviral integration by blasticidin, cells were diluted to 400,000 cells per mL, and media was supplemented with 2 μg/mL doxycycline to induce Cas9 expression starting at day -7. Cells were subcultured at days -5 and -3 (400,000 cells per mL) in media supplemented with doxycycline. On day 0, at least 70 million cells (250 cells per sgRNA) were collected as post-doxycycline sample to determine representation of EKO library pool. Remaining cells (400,000 cells per mL) were suspended in T-75 (28 million cells, 100 cells per sgRNA) and T-175 flasks (70 million cells, 250 cells per sgRNA) treated with TTM or Trientine. TTM and Trientine were dissolved in DMSO, and concentration of solvent was adjusted to not exceed 0.1% (v/v) DMSO. Concentrations of TTM were set at 2 μM, 4 μM, 8 μM and 10 μM and were chosen to result in an intermediate-high inhibition of NALM-6 based on a dose response curve. Trientine was used at 500 μM to due to intermediate inhibition of NALM-6. Further, 70 million cells were left untreated as control sample set. Concentrations in flasks were monitored every two days and if exceeded 800,000 cells per mL, they were sub-cultured with DMSO or TTM, to maintain 28 and 70 million cells (400,000 cells per mL) in T75 or T175 respectively. At day 8, cells were pelleted and frozen with 1X PBS, and the number of population doublings were determined. The population

doubling of untreated controls were 6.76 doublings over 8 days, DMSO 0.1% controls had 6.8 doublings, 2.97, 2.08, 1.37 and 0.5 doublings for TTM 2 µM, 4 µM, 8 µM and 10 µM respectively.

5.2. Genomic DNA extractions

Genomic DNA was extracted using previously described DNA extraction protocol (Bertomeu et al., 2018). Briefly, frozen cell pellets were resuspended in TE buffer (10 mM Tris-HCl pH 8.0, 1 mM EDTA) and lysis buffer (10 mM Tris-HCl pH 8.0, 10 mM EDTA, 0.5% w/v SDS, 0.2 mg/mL proteinase K), to a total volume of 14 mL. Tubes were incubated at 55 ˚C for 3 h with intermittent mixing. 5 M NaCl was added to final concentration of 0.2 M, lysates were extracted twice with an equal volume of phenol/chloroform/isoamyl alcohol (25:24:1) pH 7.5 mixture, chloroform was then removed. RNAse A was added for overnight digestion at 37 ˚C. This was followed by phenol/chloroform extraction, DNA was precipitated using 2.5 volumes of ethanol and 1/30 volume of 3 M sodium acetate (pH 5.2). The pellet was washed with 70 % ethanol, dried and resuspended in TE in a 55 ˚C dry block and sheared by passing through 27 G needle.

5.3. Next Generation Sequencing

The sgRNA library was amplified using PCR from 462 µg of genomic DNA (this corresponds to 70 million cells) or 185 ug (corresponds to 28 million cells; same PCR recipe in 2.5X smaller volumes). The PCR recipe contained 575 µL 10X PCR buffer, 115 µl 10 mM dNTPs, 23µl 100 µM primer Outer-1, 23µl 100 µM primer Outer-2, 115 µl DMSO and 145 units of GenScript Green Taq DNA polymerase in a total volume of 5.75 mL. Multiple 100 µl reactions were setup in 96-wells on a T100 thermal cycler (BioRad, USA). PCR reaction were set as follows: 95 ˚C 5 min, 26 cycles of 35 sec at 94 ˚C, 50 sec at 52 ˚C and 40 sec at 72 ˚C, final step of 10 min at 72 ˚C after the last cycle. Completed reaction mixes were combined into a single tube and mixed well. An aliquot of 1.5 mL of each PCR reaction was concentrated 15-fold by using a 2.5X (v/v) ethanol 100 %, followed by separation on agarose gel and extraction of the 475 bp amplicon. To a second PCR reaction, illumina sequencing adapters and 6 bp indexing primers were added (10 µl of 1:20 dilution of unpurified PCR1 product, 10 µl 5X buffer Kapa, 5 µl 2.5 mM dNTPs, 1 µl of PAGE-purified equimolar premix 100 µM TruSeq Universal Adapters 0 to shuffle the constant DNA region to be sequenced, 1 µl of 100 µM PAGE-purified TruSeq Adapter with appropriate index, 1

µl DMSO and 5 units Kapa HiFi HotStart DNA polymerase to 50 µl total volume). The PCR reaction 2 were as follows: 5 min at 95 ˚C, 5 cycles of 15 sec at 95 ˚C, 30 sec at 50 ˚C and 30 sec at 72 ˚C, 5 cycles of 15 sec at 95 ˚C, 30 sec at 56 ˚C and 30 sec at 72 ˚C, followed by 5 min final step at 72 ˚C after the last cycle. The 236-245 bp amplicon were purified using solid-phase reversible immobilization (SPRI) beads (AxyPrep FragmentSelect-I Kit) using a 1:1 ratio of SPRI beads and PCR product. Quantification is by Infinite M1000 PRO microplate Reader (Tecan, Switzerland) and sgRNA were sequenced in Illumina NextSeq 500 with a single end 75 bp sequencing onto a 75 cycle high output flow cell (reading 43 bp with the 23 first bp read in dark cycles) at the IRIC's genomic platform, Montreal, Canada.

5.4. Data processing and calculation of essentiality scores (CRANKS)

Illumina sequencing reads were aligned to the theoretical EKO library using Bowtie 2.2.5 software with default parameters and total read counts per sgRNA including imperfect matches were tabulated for each sample. Read counts across all untreated and 0.1 % DMSO-treated samples were added to get a single sgRNA frequency distribution averaged across the 8-day screen. The CRANKS algorithm (Condition-specific Robust Analytics and Normalization for Knockout Screens) was used to generate gene scores and FDR values, by comparing the read counts in each compound-treated sample to that in the background distribution. The minimum number reads per sgRNA (115-200) used in CRANKS was set according to the depth of coverage of the pooled background distribution. CRANKS was run under default parameters, including a minimum of 4 sgRNAs per gene passing the minimal read threshold (> 20 reads in one sample). CRANKS is an extension of the RANKS algorithm described elsewhere (Bertomeu et al., 2018).To quantify the relative abundance of each sgRNAs, the $\log_2$ ratio of sgRNA read frequency at day 8 versus day 0 is normalized to total read count ratio. To account for experimental variation in sgRNA counts, RANKS estimates *P*-value based on $\log_2$ ratio of each sgRNA compared to those of control (or non-targeting) sgRNAs. The RANKS score is the average log *P*-value for sgRNAs targeting each gene (i.e., the geometric mean of 10 sgRNAs). The *P* values for each gene is generated by comparing the RANKS score to that of a distribution of equal number of control sgRNAs for 5 million samples with FDR correction. The non-targeting sgRNAs were used as controls for calculating RANKS scores. The newer version of RANKS combines sgRNA depletion and

enrichment into a single score by averaging log(d)-log(e), where d is the fraction of control guides which are more depleted, and e is the fraction which are more enriched. If a fraction equals to zero, d or e is instead set to 1 divided by the number of control guides. In CRANKS, control sgRNAs are defined as those targeting the 500 genes immediately more essential in the given cell line than the gene itself, thereby controlling for the growth-dependent dropout and greater variance in fold-changes of essential gene-targeting sgRNAs. For genes within the top 500 most essential, all genes scored as more essential than the gene itself are used to generate the control distribution. Gene essentiality ranking in NALM-6 was determined by applying RANKS on the previous screen data (Bertomeu et al., 2018), using the non-targeting control sgRNAs as the control distribution and the default 20-read minimal sgRNA coverage, including genes with as few as a single sgRNA passing the read coverage threshold. The ranking was generated for the core set of genes in the EKO library present in RefSeq, excluding the extended part of the library, and CRANKS scores were computed for the genes within core set. CRANKS score >2 indicate that genes rescue the effect of the drug, while score <-2 indicate that genes are synergize with the drug. Only the genes that passed the cut off were selected for further analysis. GO term enrichment analysis were performed by DAVID GO (https://david.ncifcrf.gov/) or Gorilla analytical softwares (http://cbl-gorilla.cs.technion.ac.il/). To determine functional and physical protein-protein associations and networks among the enriched genes, STRING software was used (https://string-db.org/).

5.5. Immunoblotting

ATCC cell lines (HCT116, DLD-1) were cultured at 37 °C in Dulbecco's modified Eagle's medium (DMEM) with 4.5 g/L glucose, 5% (v/v) fetal bovine serum, 100 IU/mL penicillin, and 100 µg/mL streptomycin. Cells were regularly tested by PCR to exclude mycoplasma contamination. Cells were washed twice with cold PBS (pH 7.4) and lysed in BLB lysis buffer [10 mM K_3PO_4, 1 mM EDTA, 5 mM EGTA, 10 mM $MgCl_2$, 50 mM β-glycerophosphate, 0.5% Nonidet P-40, 0.1% Brij 35, 0.1% deoxycholic acid, 1 mM/L Na_3VO_4, 1 mM PMSF, and complete protease inhibitor cocktail] for 15 min at 4 °C. Lysates were centrifuged at 16,000 × g for 10 min at 4 °C, supernatants were collected and heated for 10 min at 95 °C in Laemmli buffer [50% (v/v) 4× Tris/SDS pH 6.8, 40% (v/v) glycerol, 8% (w/v) SDS, 6.2% (w/v) DTT, 2 mg Bromophenol Blue]. Total cell lysates were subjected to 8–12% SDS-PAGE, and resolved proteins were transferred onto PVDF membranes. Membranes were blocked with 10 mM Tris pH 7.4, 150 mM

NaCl, and 0.1% Tween 20, supplemented with 5% (w/v) dry skim milk powder, and subsequently immunoblotted with primary antibodies, diluted in 5% (w/v) dry skim milk or 5% (w/v) BSA, overnight at 4 °C. Antibodies targeted against Tubulin (T5618) (1:2000) from Sigma-Aldrich; CCS (H-7) (1:500) from Santa Cruz Biotechnology; ATP7A (CT77) from Betty Eipper lab (1:1000) and ATP7A (5E-10) from James Collins lab (1:2000). All secondary HRP-conjugated antibodies used for immunoblotting were purchased from Chemicon.

Chapter 4: RTK feedback inhibition underlies KRAS transformation of intestinal epithelial cells

Neethi Nandagopal[1], Léo Aubert[1], Philippe P. Roux[1, 2, *]

[1]Institute for Research in Immunology and Cancer (IRIC), Université de Montréal, Montreal, Quebec, Canada

[2]Department of Pathology and Cell Biology, Faculty of Medicine, Université de Montréal, Montreal, Quebec, Canada.

*Correspondence and requests for materials should be addressed to P.P.R. (email: philippe.roux@umontreal.ca)

Article in preparation for Brief Reports, Small GTPases

1. Author Contribution

N.N. performed the IB experiments, analyzed the data, prepared the figures, literature survey and worked with P.P.R. to establish the study design. L.A. analyzed TCGA data and was pivotal for the organization of the manuscript. L.A. and N.N. contributed to the design, analysis and implementation of the cell surface proteomics data along with P.P.R. L.A. and N.N. analyzed the RNA sequencing data. N.N. wrote the manuscript along with P.P.R.

2. Acknowledgements

I thank my co-authors for the constructive criticisms and suggestions to improve the manuscript.

3. Funding

Our work is funded by the Canadian Institutes for Health Research (CIHR) and the Cancer Research Society (CRS). P.P.R. is a Senior Scholar of the Fonds de la recherche du Québec-Santé (FRQS). N.N. was supported by Doctoral Scholarships from the FRQS and the Fonds de la recherche du Québec-Nature and Technologies (FRQNT). L.A. received a Postdoctoral Fellowship from the Cole Foundation.

4. Abstract

KRAS is a major driver of human cancers, including ~45% of CRC. KRAS-*mutated* CRC tumors are challenging to treat and exhibit resistance to $KRAS^{G12C}$ inhibitors, anti-EGFR therapy, EGFR tyrosine kinase inhibitors, as well as MEK inhibitors. Resistance mechanisms often involve dysregulated RTK expression and/or activity. Aberrant regulation of RTK expression contributes to several aspects of tumorigenesis and impacts sensitivity to pharmacological RTK inhibitors, which are major focus of targeted therapeutics. While a lot of research has focused on the intracellular signaling events downstream of mutant KRAS, much less is known about its impact on RTK expression and signaling. Herein, we observe that $KRAS^{G12V}$-driven transcriptional program spatially regulates cell surface expression of myriad RTKs. Consequently, cells were less sensitive to growth factor stimulation, suggesting a mechanism by which mutant KRAS renders cells independent of growth factor activity. To our knowledge this is the first demonstration of a strong feedback inhibition of multiple RTKs due to KRAS transformation. Our data also suggests a novel mechanism by which mutant KRAS could mediate intrinsic resistance to RTK therapy.

Keywords

KRAS, negative feedback, ERK, RTK, receptors, colorectal cancer

5. Introduction

As direct targeting of the driving oncogene has proved to be a challenging feat in mutant KRAS-driven colorectal cancers (CRC), various attempts instead focus on its downstream signaling effectors including MAPK and PI3K kinases, which phosphorylate and regulate the activity of ERK and Akt kinases, respectively (Downward, 2003). However, MAPK inhibitors (PD184352, AZD6244) exhibit poor clinical efficacy in the treatment of metastatic CRC. One main mechanism by which tumor cells escape therapeutic inhibition is by restoring the expression and/or activation of myriad receptor tyrosine kinases (RTK). Many studies have shown that inhibition of MEK kinase or its upstream kinase RAF results in paradoxical reactivation of ERK signaling, partly due to upregulation of RTKs (Corcoran et al., 2012; Duncan et al., 2012; Kitai et al., 2016). Similarly, inhibiting ERK activation in KRAS-mutant CRC cell lines increased Akt activation which was alleviated by inhibiting the expression or activity of select RTKs. (Ebi et al., 2011). Knockdown of KRAS or MEK inhibition (by AZD6244) in KRAS-mutant cells SW837 and LoVo, increased Akt activation in IGF-1R or MET dependent manner. The idea that mutant KRAS can negatively feedback on RTK levels, which is reversed upon KRAS or MAPK inhibition is demonstrated by several other studies. Notably, treating breast cancer cells with MEK inhibitor, dynamically regulates several different RTK family members (> 15 RTK) in a MYC-dependent manner (Duncan et al., 2012). Similarly, ERBB3 is activated in a MYC-dependent manner in selumetinib (MEK inhibitor) treated KRAS-mutant colon and lung cancer cells (Sun et al., 2014). Protein tyrosine phosphatase-2 (SHP2) is an adaptor protein that links upstream RTK activation to downstream effectors such as MAPK and PI3K. KRAS-mutant cells are resistant to SHP2 inhibition contrary to KRAS wild-type cells, which is reversed by co-treatment with MEK inhibitors. SHP2 inhibitors prevented ERK reactivation following treatment with MEK inhibitors in KRAS-mutant cells, suggesting that RTK re-activation could mediate resistance to MEK inhibitors via SHP2 (Mainardi et al., 2018).

While *KRAS* mutations confer intrinsic resistance to anti-EGFR therapy (Lièvre et al., 2006), CRC tissues can acquire *KRAS* mutations that eventually contribute to secondary resistance (Misale et al., 2012). Two studies have shown that one mechanism by which mutant KRAS could reduce sensitivity to anti-EGFR antibody, cetuximab, is by spatially regulating EGFR expression in colorectal intestinal epithelial cells (Derer, Lohse, and Valerius 2013; van Houdt et al. 2010).

Similarly, deregulation of EGFR expression seems to play a role in KRAS-mediated resistance to mutant-specific inhibitors. As $KRAS^{G12C}$ inhibitors specifically bound GDP-bound form of mutant KRAS, upstream RTK activity can increase GTP-KRAS and potentially contribute to resistance to $KRAS^{G12C}$ inhibitors. Analysis of drug populations resistant to $KRAS^{G12C}$ inhibitor, ARS1620, showed that resistant cells increased expression of $KRAS^{G12C}$ that do not bind the inhibitor, in a EGFR- and SHP2-dependent manner (Hata & Shaw, 2020). These studies collectively suggest that RTK activity plays a major role in KRAS-mediated drug resistance. Therefore, understanding changes in RTK expression and/or activity in response to oncogenic KRAS will aide in predicting responses to targeted therapy.

Previously, we had established an optimized cell-surface proteomics protocol to identify and quantify differential cell surface proteins associated with KRAS-transformation of intestinal epithelial cells (IEC). We observed that majority of the RTKs were downregulated at the cell surfaces of intestinal epithelial cells due to mutant KRAS transformation. Notably, we found a negative correlation between RTK expression and *KRAS* mutation status in metastatic CRC tissues. Here we show that mutant KRAS render cells insensitive to growth factors by modulating their cell-surface receptor expression. These observations are in line with the recent finding that KRAS-mediated rescaling of ERK activity is dependent on multiple, yet undiscovered mechanisms (Gillies et al., 2020).

6. Results and Discussion

6.1. Oncogenic KRAS negatively impacts cell surface RTK expression

We had previously isolated and quantified differential cell surface proteins (surfaceome) between $KRAS^{G12V}$- transformed (KRAS) versus untransformed (Control) intestinal epithelial cells, IEC-6 (Aubert et al., 2020). Our proteomics data showed that majority of proteins in the RTK family, were significantly downregulated in the cell surfaces of KRAS relative to Controls (**Fig. 4.1a**). To determine the influence of KRAS-mediated transcriptional program on the cell surfaceome of transformed cells, we had performed RNA sequencing to quantify KRAS-mutant specific global transcriptomic changes in IEC-6. Our data showed that majority of the RTK-coding mRNAs were significantly downregulated in KRAS cells, suggesting that mutant KRAS transcriptionally regulates cell surface receptor levels (**Fig. 4.1b**). Of note, Egfr was downregulated at the cell surfaces due to mutant KRAS in colorectal intestinal epithelial cells, confirming previous findings (Derer et al. 2012; van Houdt et al. 2010). Transcriptomic data showed that other RTKs, including those not identified in the surfaceome, were also significantly downregulated (~70%) in KRAS compared to Control, whereas only ~15% of the RTKs were upregulated (**Fig. 4.1b**). Amongst the significantly upregulated RTKs by mutant KRAS, there was an enrichment of Ephrin family of receptors, namely, Epha2 and Epha5. It was shown that the RAS-MAPK pathway transcriptionally upregulates Epha2 to enable cell contractility (Hill & Hogan, 2019). Interestingly, CRC pathogenesis relies on spatial regulation of ephrin receptors, including Epha5 (Kosinski et al., 2007). Although the role of Epha5 is understudied in cancers especially in CRC, our data suggests a novel role for mutant KRAS in the regulation of Epha5 expression during intestinal cell transformation. We then questioned if the expression of RTK genes was negatively correlated with mutant *KRAS* positive CRC tissues. We analyzed the metastatic CRC specimens (1134 samples) from TCGA datasets in the cBioportal database (Yaeger et al., 2018), for the mRNA expression of significantly altered RTK genes between *KRAS*-mutant or *KRAS* wild-type samples. Similar to the IEC-6 data, *KRAS*-mutation was negatively correlated with majority of the significantly altered RTKs, while similar enrichments in Ephrin family members were observed (**Fig. 4.1c**).

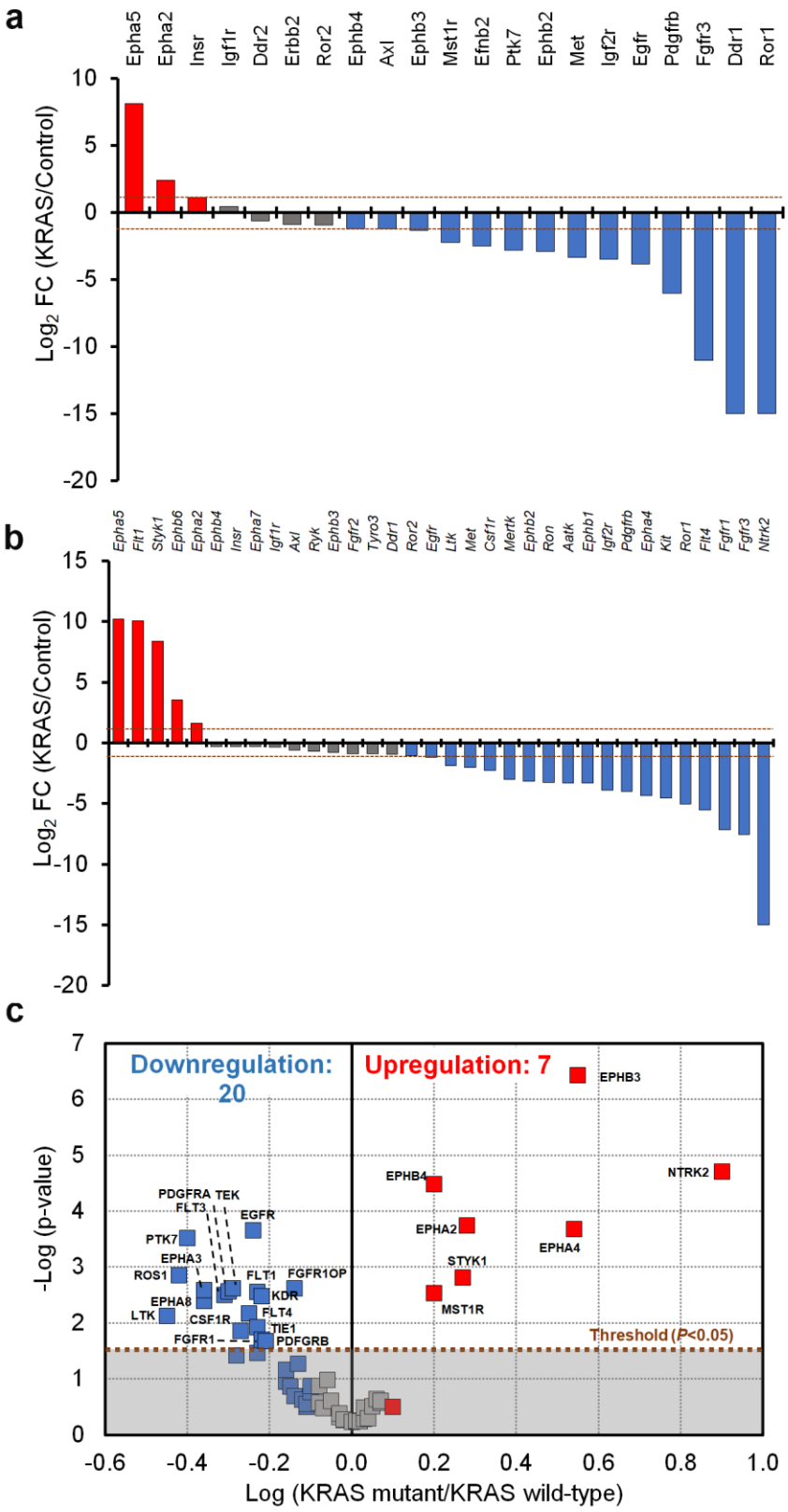
a
Epha5
Epha2
Insr
Igf1r
Ddr2
Erbb2
Ror2
Ephb4
Axl
Ephb3
Mst1r
Efnb2
Ptk7
Ephb2
Met
Igf2r
Egfr
Pdgfrb
Fgfr3
Ddr1
Ror1
Log2 FC (KRAS/Control)
b
Epha5
Flt1
Styk1
Ephb6
Epha2
Ephb4
Insr
Epha7
Igf1r
Axl
Ryk
Ephb3
Fgfr2
Tyro3
Ddr1
Ror2
Egfr
Ltk
Met
Csf1r
Mertk
Ephb2
Ron
Aatk
Ephb1
Igf2r
Pdgfrb
Epha4
Kit
Ror1
Flt4
Fgfr1
Fgfr3
Ntrk2
Log2 FC (KRAS/Control)
c
Downregulation: 20
Upregulation: 7
EPHB3
EPHB4
NTRK2
EPHA2
EPHA4
STYK1
MST1R
PDGFRA
TEK
FLT3
EGFR
PTK7
EPHA3
ROS1
FLT1
FGFR1OP
KDR
EPHA8
LTK
FLT4
CSF1R
TIE1
FGFR1
PDGFRB
Threshold (P<0.05)
-Log (p-value)
Log (KRAS mutant/KRAS wild-type)

Figure 4.1. Oncogenic KRAS negatively impacts RTK levels

(a) *Graph depicting Log_2 foldchanges (FC) of the cell surface RTK levels quantified in isogenic $KRAS^{G12V}$ (KRAS) or empty vector (Control) IEC-6 cells.* ***(b)*** *Graph depicting the Log_2 FC of mRNA levels of indicated RTKs quantified in KRAS versus Control IEC-6 cells. Dashed lines for* ***(a, b)*** *depict cut-off threshold for upregulations as Log_2 FC ≥ +1, and downregulations as Log_2 FC ≤ -1.* ***(c)*** *TCGA data from cBioportal database indicating Log FC of RTKs significantly altered in KRAS-mutant versus KRAS wild-type CRC. Grey shaded areas represent significance threshold of P<0.05. Upregulations are depicted in red, downregulations in blue and unchanged in grey. Data are normalized to Control or KRAS wild-type conditions for* ***(a, b, c)****, and depict average of N=3 replicates for* ***(a, b)****.*

Besides RTK family, we observed a significant downregulation of TGF superfamily of receptors mostly from the beta subgroup, Tgfβr2, Tgfβr3 and Tgfβr1, in both the surfaceome (**Fig. 4.2a**) and transcriptome of KRAS-mutant cells compared to KRAS wild-type cells (**Fig. 4.2b**). Although loss of TGFβ signaling is well documented in RAS-mutated CRC, TGFβ receptor levels are regulated by inactivating mutations (Kretzschmar, Doody, Timokhina, & Massagué, 1999; Trobridge et al., 2009; Y. Xu & Pasche, 2007). Here we find evidence that mutant KRAS can negatively regulate their expression levels during cellular transformation. Besides receptors, significant downregulation of TGFβ ligands is observed in KRAS-mutant cells (**Fig. 4.2b**). This could suggest a strong suppression of TGFβ signaling by KRAS, supporting the tumor suppressive role of TGFβ pathway on RAS tumorigenesis (Y. Xu & Pasche, 2007). Taken together, mutant KRAS downregulates several growth factor receptors including RTK and TGF family, suggesting remodeling of cell surfaceome in a transcriptional dependent manner.

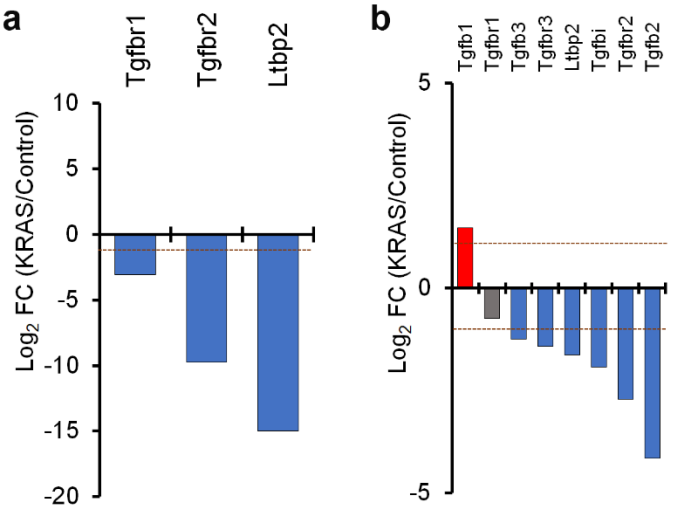

Figure 4.2. Oncogenic KRAS negatively impacts TGFβ receptor levels

(a) *Graph depicting Log_2 FC of TGFβ family receptors identified and quantified by cell surface proteomics in isogenic $KRAS^{G12V}$ (KRAS) or empty vector (Control) IEC-6 cells.* ***(b)*** *Graph depicting the Log_2 FC of mRNA levels of identified TGF family receptors and ligands in KRAS versus Control IEC-6 cells. Dashed lines for* ***(a,b)*** *depict cut off threshold of upregulated proteins or genes (red) as Log_2 FC $\geq +1$, downregulated proteins or genes (blue) as Log_2 FC ≤ -1, and unchanged genes or proteins (grey). Data are normalized to Control cells and depict average of N=3 replicates.*

6.2. Oncogenic KRAS renders cells insensitive to growth factor stimulations

In serum-starved conditions, phosphorylation would be dependent directly on oncogenic RAS activity in KRAS-mutant cell lines. We were surprised to see that $KRAS^{G12V}$ transformation of intestinal epithelial cells in serum-starved conditions did not exhibit increase the activation of Erk (phosphorylated ERK) and Akt (phosphorylated Akt) (**Fig. 4.3a**). These observations were reproduced in two other sets of isogenic IEC-6 cell pairs generated using different plasmid constructs, negating cell line or plasmid-specific effects. The negative correlation of mutant KRAS with ERK and Akt phosphorylation is also recapitulated in CRC cell lines (**Fig. 4.3b**). *KRAS*-mutated cells (HCT116, DLD-1, SW480, SW620) exhibiting reduced activation of ERK and Akt compared to KRAS-wild type, non-transformed human intestinal cells (HIEC).

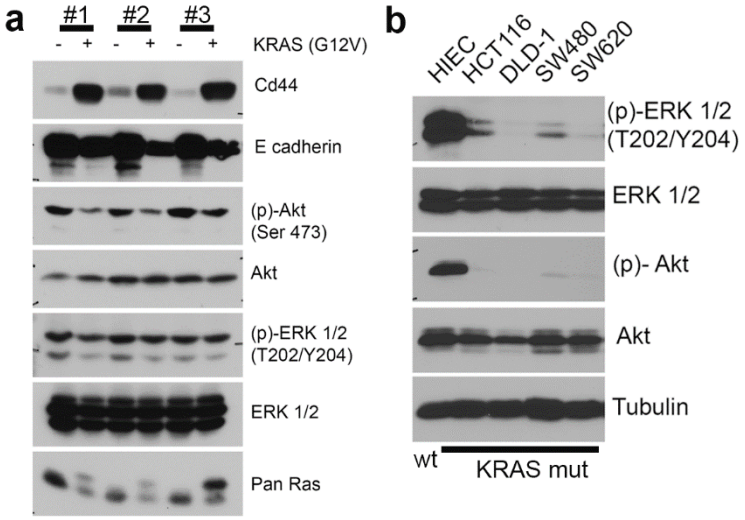

Figure 4.3. Oncogenic KRAS is negatively correlated with ERK/Akt phosphorylation

(a) *IB for phosphorylated ERK and Akt in isogenic IEC-6 cells expressing $KRAS^{G12V}$ (+) or empty vector (-) in serum-starved conditions. Data represents N=4 replicates.* ***(b)*** *IB for phosphorylated*

Akt and ERK in KRAS-mutant CRC cell lines (HCT116, DLD-1, SW480, SW620) versus KRAS wild-type control cells (HIEC). Data represent N=2.

Other studies in several KRAS-mutant cell lines, including CRC, have shown that despite significant KRAS oncogenic activity, ERK and Akt activation are minimal in the absence of growth factor stimulations (Hood et al., 2019; Tuveson et al., 2004). However, ERK and Akt phosphorylation is weak in KRAS-mutant IEC-6 when stimulated with 10% FBS (which contains a cocktail of growth factors). This is in sharp contrast with a strong Erk and Akt response in Control cells (**Fig. 4.4a**). Similarly, KRAS oncogene diminished Akt and ERK phosphorylation when stimulated with epidermal growth factor (EGF) and platelet derived growth factor (PDGF), compared to Control (**Fig. 4.4b**). Therefore, mutant KRAS restricted ERK and Akt phosphorylation in basal and growth factor-stimulated conditions. The diminished responses of KRAS-mutant cells to EGF and PDGF could be explained by the reduced expression of their cognate receptors, Egfr and Pdgfr, respectively (**Fig. 4.1a,b**). Similar diminished responses were also observed when the Tgfβ signaling pathway is activated (**Fig. 4.4c**). TGF-β receptor activation converge to induce intracellular signaling by activating and phosphorylating SMAD-2/3 transcription factors (Bellam & Pasche, 2010). In Control, stimulation with TGF-β increased Akt, ERK and Smad2/3 phosphorylation. But KRAS cells displayed relatively less Akt and Smad2/3 phosphorylation.

We also observed that KRAS cells exhibited diminished Akt phosphorylation in response to insulin stimulation, in contrast to KRAS wild-type Control. (**Fig. 4.4d**). However, the cell-surface expression of insulin receptor (Insr) was unchanged between KRAS and Control condition (**Fig. 4.1a,b**), hinting at other mechanisms. Two proteomic studies previously identified that growth factor receptor bound protein (GRB10) also known as insulin receptor-binding protein, acts as an inhibitor of insulin stimulated Akt activation (Hsu et al., 2011; Y. Yu et al., 2011). Notably, *Grb10* gene is dramatically induced in intestinal cells due to KRAS transformation (**Fig. 4.5a).** Future work will focus on determining if the reduced sensitivity to insulin in KRAS-mutant cells is mediated by negative feedback regulation by Grb10.

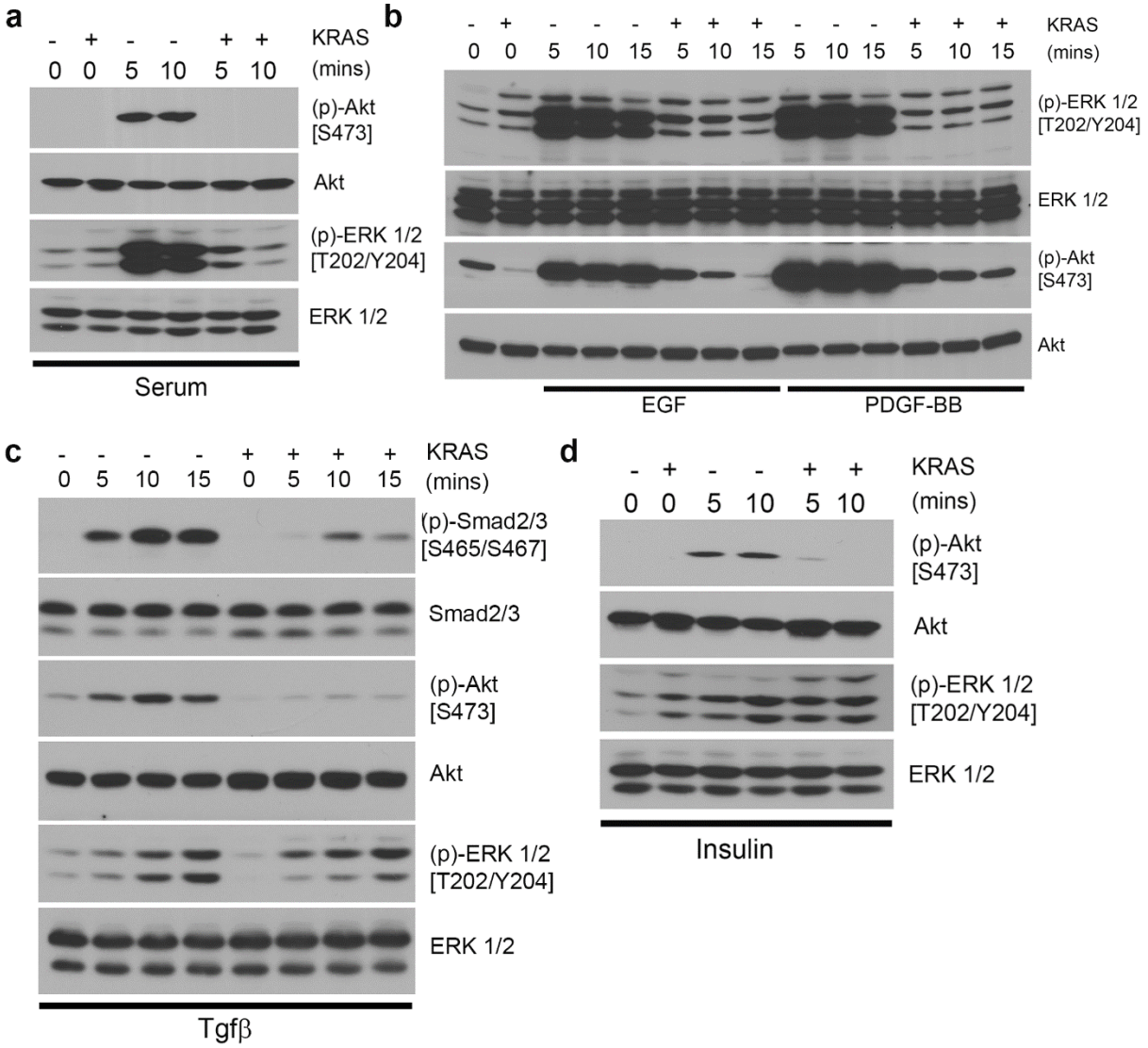

Figure 4.4. Oncogenic KRAS is negatively correlated with ERK/Akt phosphorylation
(a) *IB for phosphorylated Akt and ERK in response to 10% FBS in isogenic IEC-6 cells expressing* $KRAS^{G12V}$ *(+) or empty vector (-).* ***(b)*** *Same as in (a), but for EGF and PDGF-BB in serum-starved conditions. Same as in (b), but for TGFβ* ***(c)*** *and Insulin* ***(d)****. Data represents N=3 for* ***(a,b)*** *and N=1* ***(c,d)****.*

RTK signaling is also inhibited through negative feedback regulators namely the tumor suppressor sprouty proteins (SPRY) and sprouty-related proteins, Spred (Courtois-Cox et al., 2006; Kato et al., 2003; Shaw et al., 2007; Zhao et al., 2015). SPRY2 inhibits ERK phosphorylation downstream of several RTKs including FGFR, VEGFR, MET and EGFR signaling (Hanafusa, Torii, Yasunaga,

& Nishida, 2002; J. Lim et al., 2002; Tefft et al., 2002; Y.-W. Zhang & Vande Woude, 2013). Similarly, Mig6 (*ERRFI1*) has been shown to directly regulate the activation and expression of several RTKs including MET, EGFR and ErbB receptors (Anastasi, Lamberti, Alemà, & Segatto, 2016; Y.-W. Zhang & Vande Woude, 2013). Interestingly, modulating MIG-6 expression had detrimental effects on KRAS-or BRAF-mutant cells (Ambrogio, Barbacid, & Santamaría, 2017; Milewska et al., 2015). *Spry2*, *Spry3*, *Spred3* and *Errfi1* genes are upregulated in KRAS relative to Control (**Fig. 4.5a**). Similar anti-correlation was observed between *KRAS*-mutation and expression of these genes in TCGA CRC datasets (**Fig. 4.5b**), suggesting that the diminished responses to growth factor pathways could also be attributed to the increased expression of negative regulators of RTK signaling.

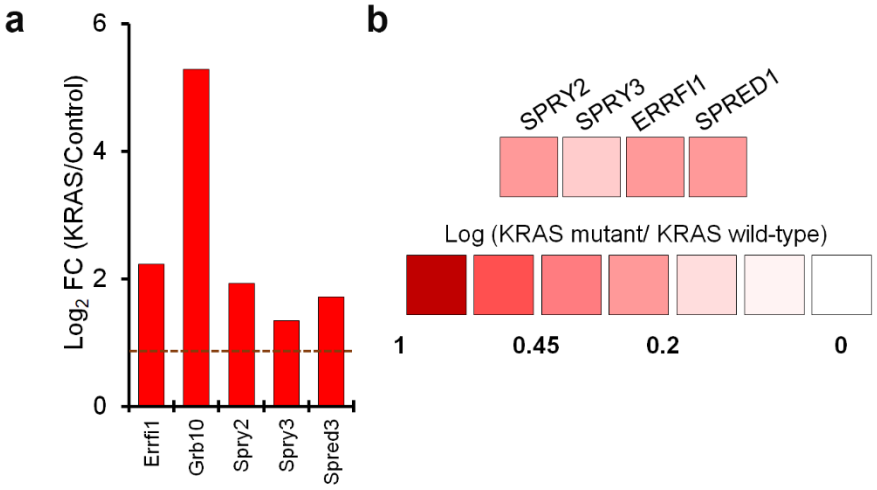

Figure 4.5. Oncogenic KRAS upregulates negative feedback regulators of RTK signaling
(a) *Log_2 FC of mRNA levels of indicated genes in isogenic IEC-6 cells expressing $KRAS^{G12V}$ (KRAS) normalized to empty vector (Control) cells. Dashed lines depict the cut off threshold of upregulated genes Log_2 FC ≥ +1. Data depicts average of N=3 replicates.* ***(b)*** *Log FC of mRNA levels of indicated genes in KRAS-mutated CRC tissues relative to KRAS wild-type from TCGA datasets.*

In conclusion, transformation of IEC by mutant KRAS activates a strong transcriptional program that repressed the expression of myriad growth factor receptors, while parallelly upregulating negative feedback regulators to rescale downstream RTK signaling. KRAS-mutant cells were dramatically less responsive to growth factor stimulations compared to wild-type counterparts. This goes against the observation that a wide-network of growth factor receptor engagement is necessary to "prime" downstream signaling of mutant RAS (Hood et al., 2019). It is possible that

KRAS regulates the intensity of ERK and Akt phosphorylation to ensure a fine balance between cellular transformation and cell death due to hyperactivation. This was demonstrated by seminal studies showing that excessive ERK signaling is toxic to cells, suggesting a "sweet spot" for effector signaling to drive transformation by mutant RAS (S. Li, Balmain, & Counter, 2018; Varmus, Unni, & Lockwood, 2016).

Although it is widely considered that oncogenic KRAS-mediated direct activation of PI3K and ERK signaling mediates intrinsic resistance to RTK inhibitors. Our data provides an alternative explanation by which oncogenic KRAS could mediate such resistance by spatially regulating growth factor receptors. To our knowledge, this is the first study to describe a global impact on the expression of several cell surface receptors, besides EGFR, by mutant KRAS. Whereas a lot of information is available on the multiple mechanisms of RTK activation during tumorigenesis (Du & Lovly, 2018), much less is known about their spatial deregulation. Deregulation of receptors including gene amplifications, overexpression and intracellular distribution can impact response to inhibitors targeting downstream effector kinases or the RTKs directly (Casaletto & McClatchey, 2012; Duncan et al., 2012), and direct inhibitors of mutant KRAS (Amodio et al., 2020). Based on our results we could predict that mutant KRAS cells could mediate intrinsic resistance to multi-kinase inhibitors such as regorafenib (EGFR, PDGFR, FGFR) which is in clinical trials for metastatic CRC (Pottier et al., 2020). This data also suggests that mutant-KRAS cells can potentially mediate resistance to MEK inhibition by restoring RTK expression, a mechanism that has been well described in several cancers including CRC (Duncan et al., 2012; Ebi et al., 2011; Kitai et al., 2016), and combination of MEK inhibitors with multikinase inhibitors could prove to be a more successful approach to curb activity of mutant KRAS.

These results have raised interesting questions that warrant more experiments. Future work will determine if KRAS cells displayed reduced activity of multiple RTKs relative to Control. Phosphorylated levels of RTKs could be measured by commercially available R&D systems Proteome Profiler Phospho-RTK Antibody Array (Amin et al., 2010). By including KRAS RNAi or MEK inhibitors as negative controls, we could determine the dynamic impact of inhibiting MAPK or RAS signaling on RTK activity. More experiments are required to test if KRAS cells displayed similar diminished responses to stimulation with other growth factors such as hepatocyte

growth factor (HGF) ligand for MET receptor, FGF-1,-2 and -9 for FGFR1 and FGFR3 receptors. As shown in (**Fig. 4.1a, b**), the expression of these receptors was downregulated due to mutant KRAS. Immunoblotting could be performed to confirm reduction of these receptors in several KRAS-mutant cells relative to KRAS wild-type cells. To test the hypothesis that negative regulators of growth factor signaling could contribute to diminished responses in KRAS cells, ERK and Akt phosphorylation in response to several growth factors (EGF, PDGF, FGF, TGFβ, Insulin) could be measured in cells with and without *Spry3*, *Spred3, Grb10* and *Errfi1* expression (via RNA interference).

7. Materials and Methods

7.1. Cell culture and viral infections

IEC-6 and CRC cell lines (HIEC, HCT116, DLD-1, SW620, and SW480) were obtained from ATCC. Cells were grown at 37 °C in DMEM with 4.5 g/L glucose supplemented with 5% (v/v) FBS, 100 IU/mL penicillin, and 100 µg/mL streptomycin. Cells were regularly tested for mycoplasma contamination and used within 20 passages. Stable cell lines from IEC-6 cells were generated with retroviral vectors encoding human *KRASG12V* or an empty cassette with puromycin, zeocin, or hygromycin selection markers (Addgene #9052, #1764, #1766, #18750). Using the Phoenix cell line, retroviral particles were produced, and antibiotic selections were performed with 5 µg/mL puromycin, 150 µg/mL hygromycin, or 100 µg/mL zeocin.

7.2. Immunoblotting (IB)

For stimulations, cells were grown on culture dishes overnight and FBS-starved for 16 h in DMEM with 100 IU/mL penicillin, and 100 µg/mL streptomycin. This was replaced with media lacking FBS and selection antibiotics but containing 25 ng/ml EGF, 100 nM Insulin, 100 ng/ml PDGF-BB or 10% FBS for the indicated times. Cells were immediately washed twice with cold PBS (pH 7.4) on ice, and lysed in BLB lysis buffer [10 mM K3PO4, 1 mM EDTA, 5 mM EGTA, 10 mM MgCl2, 50 mM β-glycerophosphate, 0.5% Nonidet P-40, 0.1% Brij 35, 0.1% deoxycholic acid, 1 mM/L Na3VO4, 1 mM PMSF, and complete protease inhibitor cocktail] for 15 min at 4 °C. Lysates were then centrifuged at 16,000 × g for 10 min at 4 °C to remove debris. The supernatants were adjusted to a concentration of 1 µg/µL and heated for 10 min at 95 °C in Laemmli buffer [50% (v/v) 4× Tris/SDS pH 6.8, 40% (v/v) glycerol, 8% (w/v) SDS, 6.2% (w/v) DTT, 2 mg Bromophenol Blue]. For analysis, 10-80 µg lysates were subjected to 8–12% SDS-PAGE, and resolved proteins were transferred onto polyvinylidene fluoride (PVDF) membranes. This was followed by blocking with 10 mM Tris pH 7.4, 150 mM NaCl, and 0.1% Tween 20, supplemented with 5% (w/v) dry skim milk powder. The blots were incubated with primary antibodies, diluted in 5% (w/v) dry skim milk or 5% (w/v) bovine serum albumin (BSA), overnight at 4 °C. Antibodies targeted against phosphorylated (p)-ERK1/2 (E10) (T202/Y204) (1:1000), CD44 (8E2) (1:1000), (p)-Akt (Ser473) (D9E) (1:1000), total Akt (1:1000) and E-Cadherin (1:1000) are from Cell Signaling Technologies; Tubulin (T5618) (1:2000) from Sigma-Aldrich; Pan-Ras (C-4) from Abcam (1:500). All secondary HRP-conjugated antibodies were purchased from Chemicon. PDGF-BB and EGF were purchased

from Thermo Fisher and Insulin from Sigma. All IB data are representative of minimum three independent biological experiments. Cell surface proteomics and RNA sequencing of IEC-6 were performed for a previous study and described in detail elsewhere (Aubert et al., 2020). TCGA dataset was obtained from cBioportal database representing metastatic CRC adenocarcinoma samples from 1134 patients (Yaeger et al., 2018).

Chapter 5: Discussion

1. Optimization of the cell surface proteomics protocol

This work began with the establishment of a reproducible protocol in the laboratory to specifically label, isolate and quantify cell surface proteins by proteomics. Prior methods including cell fractionation and colloidal silica beads are associated with more contamination from other organelles, low purity and poor yields (Elschenbroich et al., 2010). Therefore, we used two biotin-based approaches in parallel as outlined in **Fig. 2.2a**, to label and isolate cell surface proteins. These approaches were adapted from previously established protocols (Hörmann et al., 2016; Weekes et al., 2010). CSC uses aminooxy-biotin that attaches a biotin label to sialic acid side chains of glycoproteins (Y. Zeng, Ramya, Dirksen, Dawson, & Paulson, 2009), which is a common post-translational modification found on cell surface proteins (Chandler & Costello, 2016). CSB utilizes sulfo-NHS-LC-biotin to label primary amine residues such as lysine, and terminal amines of polypeptides. The timing and concentration of CSB and CSC were optimized in IEC-6 to obtain maximum staining of cell-surface proteins on intact cells at 4 ˚C to reduce the labelling of intracellular proteins. In **Fig. 5.1a**, we can observe that 30 mins of 1 mg/ml CSB produced maximum labelling of cell surface proteins with comparable intensity to 30 mins of CSC (100 mM aminooxy-biotin). We had optimized the cell lysis detergent to obtain the maximum yield of biotinylated proteins. As seen in **Fig. 5.1b**, although the amount of biotinylated proteins bound to streptavidin beads after cell lysis with three different detergents (BLB, RIPA and a Triton-based surfaceome lysis buffer WLB) did not affect CSB labelling, the yield of CSC biotinylated proteins were highest when cells were lysed with WLB lysis buffer. Using multiple techniques, we then confirmed that the selected concentrations and time point (100 mM amino-oxy-biotin and 1 mg/ml sulfo-NHC-LC-biotin, 30 mins) produced efficient labeling of cell surface proteins (**Fig. 5.1c, Fig. 2.1g, Supplementary Fig. 2.2b**). In **Fig. 5.2a,** we see that labelling with CSB or CSC is specific to cell surface-located receptors (Igf-1rβ, Epha2, Egfr) with minimum-to-no contamination from intracellular proteins (ERK 1/2, Tubulin and Nuclear Lamin A). Quantification of proteins bound to streptavidin beads following CSC and CSB labelling by LC-MS/MS mass spectrometry showed that without prior labeling the number of identified proteins was severely diminished, confirming the specificity of the protocol to isolate biotinylated cell surface proteins (**Fig. 5.2b**). Majority of

proteins isolated with CSC or CSB in the mass spectrometry were indeed associated with plasma membrane component as determined by the enrichment of GO terms (**Fig. 5.2c**).

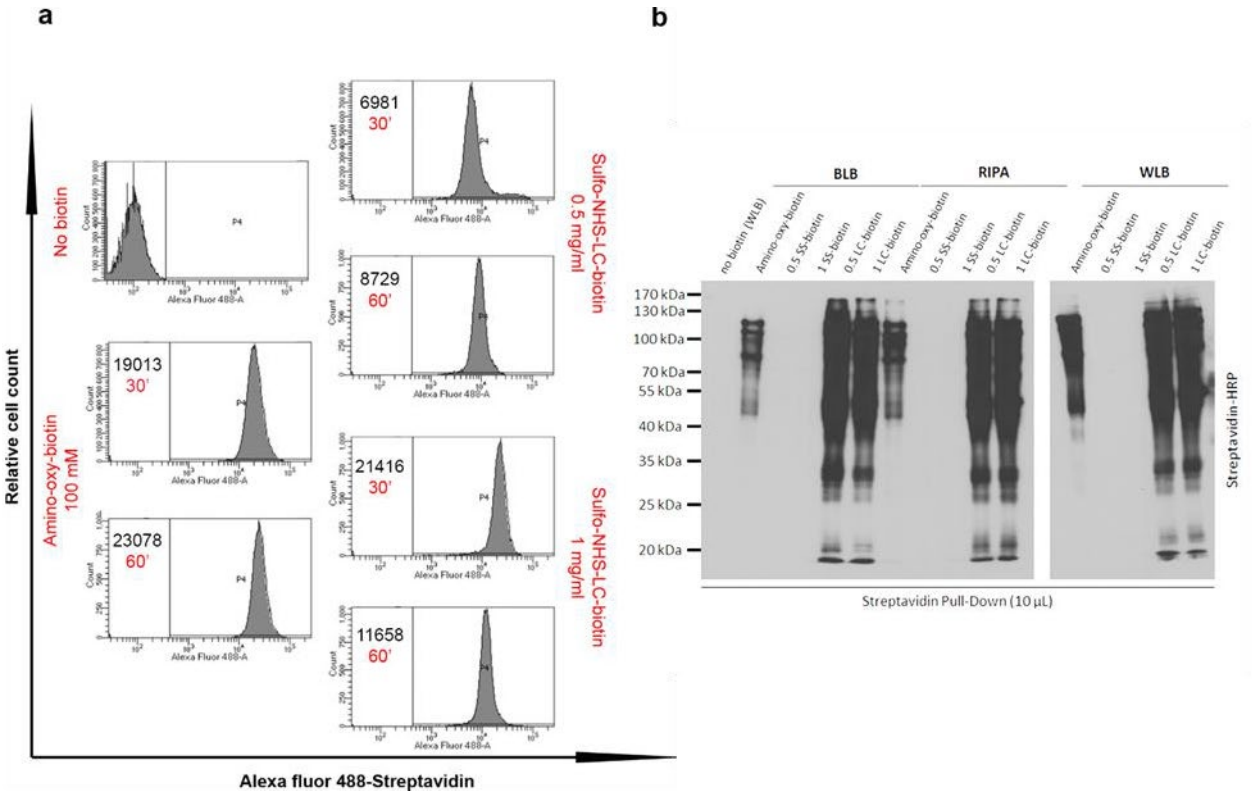

Figure 5.1. Optimization of cell surface protein biotinylation

(a) *Flow cytometry analysis of biotinylated cell surface proteins on intact cells by Alexa-fluor 488 conjugated streptavidin antibody for the indicated time points and concentrations of biotin reagents (red). The numbers on the graph indicate the median values of streptavidin-positive populations. Data represents N=3.* ***(b)*** *Immunoblot analysis of biotinylated cell surface proteins in cell lysates precipitated from streptavidin beads (Pull-Down). The biotin reagents are indicated above with 0.5 and 1 represent concentrations (mg/ml) and SS- and LC-biotin representing Sulfo-NHS-SS-biotin and Sulfo-NHS-LC-biotin respectively. BLB, RIPA and WLB represent three different cell lysis buffers, with WLB specialized for extraction of plasma membrane proteins. Data represents N=2.*

After manual curation of proteomics data, we observed that CSC and CSB yielded ~79% and ~58% purity for cell surface proteins compared to intracellular contaminants (**Fig. 5.2d**), which are comparable to the purity achieved with other studies (Elschenbroich et al., 2010; Hörmann et al., 2016). Although, majority of cell surface proteins (329) were commonly identified with both

techniques (**Supplementary Fig. 2.2c)**, each technique identified unique sets of proteins (37 for CSB and 25 for CSC) that were not identified by the other method.

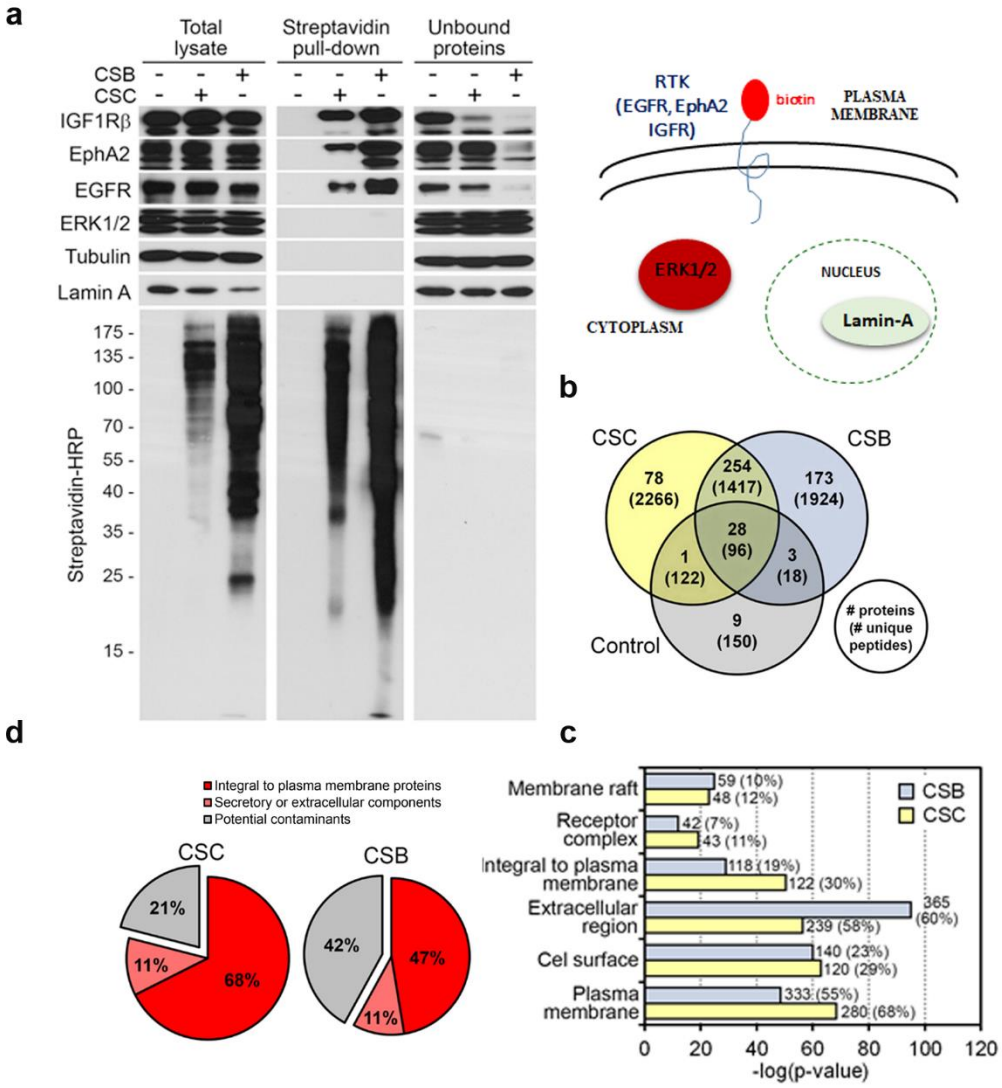

Figure 5.2. Optimization of cell surface proteomics protocol

(a) *Immunoblot analysis of proteins in the total cell lysates (before streptavidin beads addition), proteins precipitated from streptavidin beads after pull-down, and unbound fraction (proteins that did not bind streptavidin beads). Data represents N=3.* ***(b)*** *Graph depicting the number of quantified proteins by LC-MS/MS spectrometry in Control (no biotin label), CSC or CSB techniques.* ***(c)*** *Depiction of GO terms analyzed by DAVID software and enriched among the proteins identified in LC-MS/MS with CSC and CSB.* ***(d)*** *Manual curation of identified proteins by mass spectrometry for cell-surface versus intracellular proteins.*

Copper exporter ATP7A is one such candidate identified with the CSC technique and not CSB. This could be because ATP7A is hyper-glycosylated (Yueyong Liu et al., 2010), and CSC is more suited to label glycosylated proteins. The relative abundance of spectral counts indicate that cell surface proteins were differentially quantified based on the technique used (**Fig. 5.3**). Therefore, using two techniques in parallel greatly maximizes the chances of identifying maximal differences between conditions. For example, cell-surface proteins serpinE2 which has been previously shown to be increased in $KRAS^{G12V}$ transformed IEC-6 cells (Bergeron et al., 2010), and Epha5 which is transcriptionally induced by $KRAS^{G12V}$-IEC-6 (**Fig. 2.1i**), were identified as upregulated in the cell-surface proteome of $KRAS^{G12V}$ with CSB method but not with CSC.

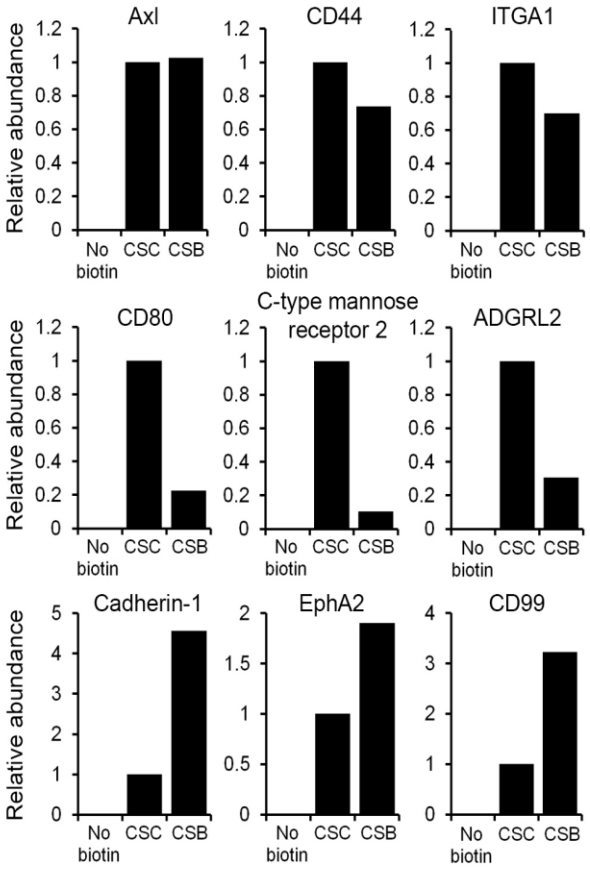

Figure 5.3: Differential enrichment of proteins based on cell surface isolation protocol used.
Spectral abundance of indicated proteins quantified by LC-MS/MS for the indicated conditions.

2. Mutant KRAS modifies the cell surfaceome by transcriptional and post-transcriptional mechanisms

We identified ~145 cell surface proteins as modified by mutant KRAS compared to untransformed control in intestinal cells (**Fig. 2.1h, Supplementary Fig. 2.2f**). Interestingly, ~15% of these changes were upregulated and ~22% were downregulated ($P < 0.05$, unpaired one-tailed Student's t-test). Transcriptomic studies have shown that oncogenic-driven cellular transformation is accompanied by downregulation of several cell-surface coding genes (Danielsson et al., 2013). Analysis of transcriptomic changes modulated by mutant $KRAS^{G12V}$ in IEC-6 by ingenuity pathway analysis (IPA) predicted that several transcription factors were upregulated in a KRAS-dependent manner (**Fig. 5.4a**). To determine the

mechanisms by which KRAS modifies the cell-surface, we compared the transcript levels of significantly altered cell-surface proteins as determined by RNA sequencing, with the cell-surface expression quantified by proteomics (**Fig. 2.1i**). We observed a modest correlation ($R^2 = 0.531$) between the transcript and cell-surface protein levels of all the significantly altered proteins (**Supplementary Fig. 2.2e**), but several cell-surface proteins were modified in a transcription-independent manner (**Fig. 2.1i**). Preliminary data suggests that percentage of cell surface proteins endocytosed in KRAS IEC-6 cells was higher than in Control (**Fig. 5.4b**). We measured the percentage of biotinylated cell surface proteins that were endocytosed by cells at 37 ºC by using cell-based L-glutathione protection assays (Cihil & Swiatecka-Urban, 2013). The preliminary date suggests increased endocytosis could be one such post-transcriptional mechanism by which mutant KRAS could modify intestinal cell surfaces during cellular transformation.

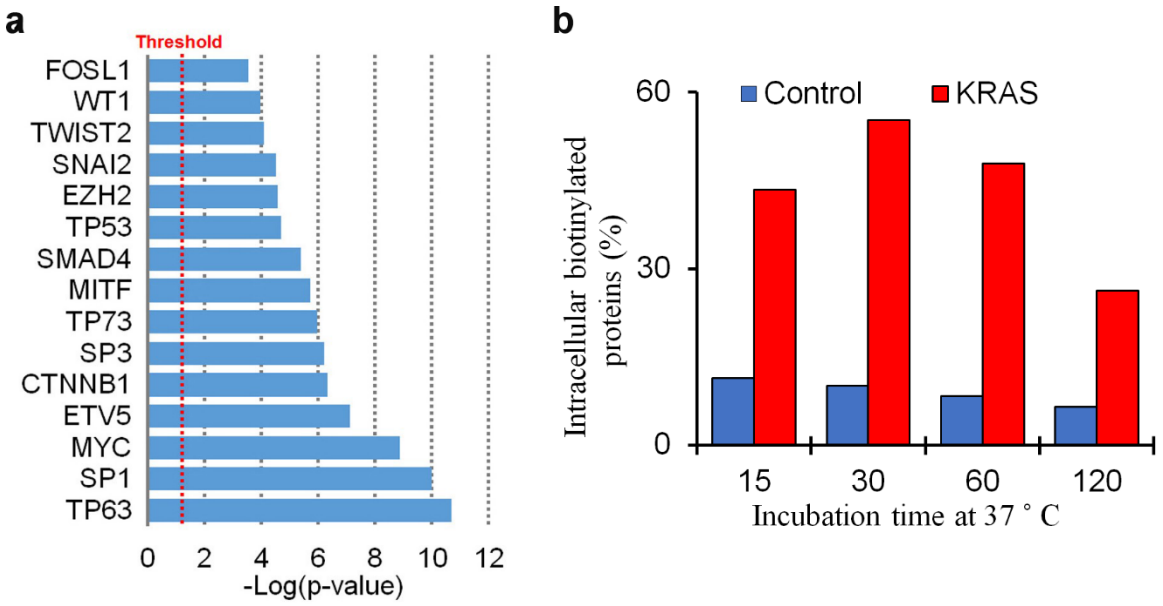

Figure 5.4. Analysis of KRAS-mediated mechanisms that could alter the cell surfaceome
(a) *Transcription factors predicted by IPA software to be upregulated in KRAS^{G12V}-transformed IEC-6 cells.* ***(b)*** *Quantification of endocytosed biotinylated cell surface proteins at 37˚C for the indicated timepoints, as measured by Alexa fluor 488 conjugated streptavidin antibody. Data is normalized to total biotinylated proteins at 0˚C before inducing endocytosis. Data represents N=2.*

Our study shows that KRAS transformation alters several different functional classes of proteins including receptors, solute carriers, cadherins, low density lipoproteins in the intestinal cell surfaceome (**Fig. 5.5**). One interesting change mediated by mutant KRAS is that majority of RTKs

are downregulated. Notably, expression of Egfr and Pdfrβ were negatively regulated by KRAS, which likely reduced cell sensitivity to their cognate ligands (**Fig. 4.1a,b and 4.4b**). Other studies have shown that EGFR expression is reduced by mutant KRAS in CRC, and this downregulation mediates resistance to anti-EGFR antibody Cetuximab (Derer et al., 2012; van Houdt et al., 2010).

Spatial deregulation of receptors through alterations in their cell surface expression or vesicular trafficking are well documented to impact tumorigenesis and underlying cytoskeletal reorganization (Casaletto & McClatchey, 2012). More studies are needed to determine the effect of how global RTK patterning in cancer can affect therapeutic responses and underlying resistance mechanisms to RTK therapy. Previous study comparing the proteome of normal intestinal cells *versus* colorectal carcinoma tissues identified several solute transporters of sugars, fatty acid and amino acids as upregulated in CRC tumorigenesis (Wiśniewski et al., 2015). Similarly, we found that majority of solute carriers are upregulated in the KRAS condition, providing an interesting insight into metabolic adaptation of KRAS-transformed cells. We had previously shown that mutant *RAS* downregulates the cell-surface expression of G-protein coupled receptors (GPCR)-type-2 vasopressin, type-1 angiotensin, and CXC type-4 chemokine receptors (Paradis et al., 2015). Herein, several members of GPCRs were downregulated in the cell surfaceome due to KRAS transformation.

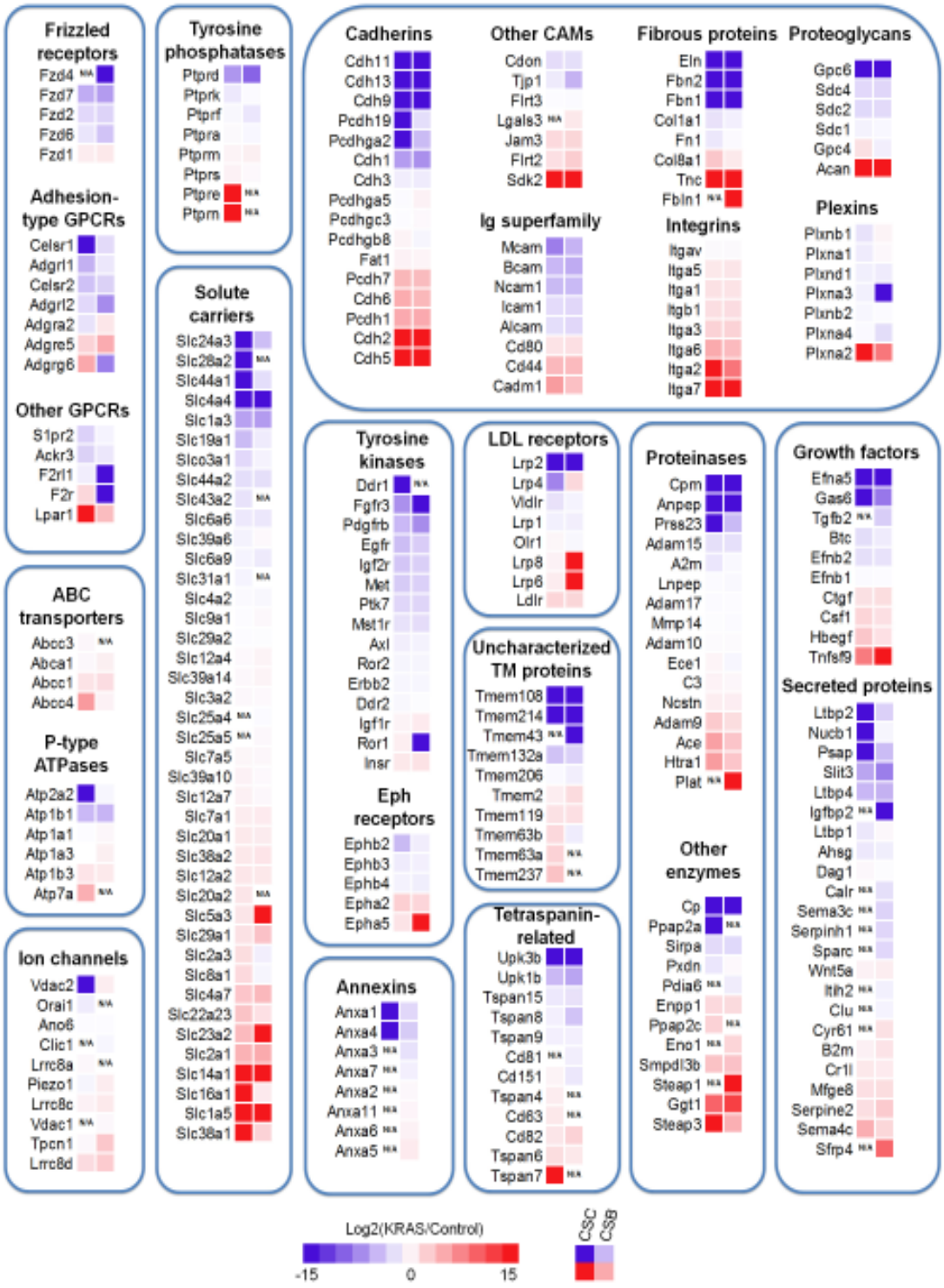
Frizzled receptors
Fzd4
Fzd7
Fzd2
Fzd6
Fzd1
Adhesion-type GPCRs
Celsr1
Adgrl1
Celsr2
Adgrl2
Adgra2
Adgre5
Adgrg6
Other GPCRs
S1pr2
Ackr3
F2rl1
F2r
Lpar1
ABC transporters
Abcc3
Abca1
Abcc1
Abcc4
P-type ATPases
Atp2a2
Atp1b1
Atp1a1
Atp1a3
Atp1b3
Atp7a
Ion channels
Vdac2
Orai1
Ano6
Clic1
Lrrc8a
Piezo1
Lrrc8c
Vdac1
Tpcn1
Lrrc8d
Tyrosine phosphatases
Ptprd
Ptprk
Ptprf
Ptpra
Ptprm
Ptprs
Ptpre
Ptprn
Solute carriers
Slc24a3
Slc28a2
Slc44a1
Slc4a4
Slc1a3
Slc19a1
Slco3a1
Slc44a2
Slc43a2
Slc6a6
Slc39a6
Slc6a9
Slc31a1
Slc4a2
Slc9a1
Slc29a2
Slc12a4
Slc39a14
Slc3a2
Slc25a4
Slc25a5
Slc7a5
Slc39a10
Slc12a7
Slc7a1
Slc20a1
Slc38a2
Slc12a2
Slc20a2
Slc5a3
Slc29a1
Slc2a3
Slc8a1
Slc4a7
Slc22a23
Slc23a2
Slc2a1
Slc14a1
Slc16a1
Slc1a5
Slc38a1
Cadherins
Cdh11
Cdh13
Cdh9
Pcdh19
Pcdhga2
Cdh1
Cdh3
Pcdhga5
Pcdhgc3
Pcdhgb8
Fat1
Pcdh7
Cdh6
Pcdh1
Cdh2
Cdh5
Other CAMs
Cdon
Tjp1
Flrt3
Lgals3
Jam3
Flrt2
Sdk2
Ig superfamily
Mcam
Bcam
Ncam1
Icam1
Alcam
Cd80
Cd44
Cadm1
Fibrous proteins
Eln
Fbn2
Fbn1
Col1a1
Fn1
Col8a1
Tnc
Fbln1
Integrins
Itgav
Itga5
Itga1
Itgb1
Itga3
Itga6
Itga2
Itga7
Proteoglycans
Gpc6
Sdc4
Sdc2
Sdc1
Gpc4
Acan
Plexins
Plxnb1
Plxna1
Plxnd1
Plxna3
Plxnb2
Plxna4
Plxna2
Tyrosine kinases
Ddr1
Fgfr3
Pdgfrb
Egfr
Igf2r
Met
Ptk7
Mst1r
Axl
Ror2
Erbb2
Ddr2
Igf1r
Ror1
Insr
Eph receptors
Ephb2
Ephb3
Ephb4
Epha2
Epha5
Annexins
Anxa1
Anxa4
Anxa3
Anxa7
Anxa2
Anxa11
Anxa6
Anxa5
LDL receptors
Lrp2
Lrp4
Vldlr
Lrp1
Olr1
Lrp8
Lrp6
Ldlr
Uncharacterized TM proteins
Tmem108
Tmem214
Tmem43
Tmem132a
Tmem206
Tmem2
Tmem119
Tmem63b
Tmem63a
Tmem237
Tetraspanin-related
Upk3b
Upk1b
Tspan15
Tspan8
Tspan9
Cd81
Cd151
Tspan4
Cd63
Cd82
Tspan6
Tspan7
Proteinases
Cpm
Anpep
Prss23
Adam15
A2m
Lnpep
Adam17
Mmp14
Adam10
Ece1
C3
Ncstn
Adam9
Ace
Htra1
Plat
Other enzymes
Cp
Ppap2a
Sirpa
Pxdn
Pdia6
Enpp1
Ppap2c
Eno1
Smpdl3b
Steap1
Ggt1
Steap3
Growth factors
Efna5
Gas6
Tgfb2
Btc
Efnb2
Efnb1
Ctgf
Csf1
Hbegf
Tnfsf9
Secreted proteins
Ltbp2
Nucb1
Psap
Slit3
Ltbp4
Igfbp2
Ltbp1
Ahsg
Dag1
Calr
Sema3c
Serpinh1
Sparc
Wnt5a
Itih2
Clu
Cyr61
B2m
Cr1l
Mfge8
Serpine2
Sema4c
Sfrp4
Log2(KRAS/Control)
-15
0
15
CSC
CSB

Figure 5.5. Different functional classes of cell surface proteins modified by mutant KRAS
Representation of significantly altered cell surface proteins by CSB or CSC technique, Log_2 FC≥ +2 is considered upregulated (red) and Log_2 FC ≤ -2 is considered downregulated (blue). P<0.05 student t tests.

3. Mutant KRAS rescales ERK and Akt activation

Although KRAS transformation increased cellular proliferation, cellular morphology and adherence-independent growth of intestinal cells (**Supplementary Fig. 2.1b-d**), we were surprised to find that phosphorylation of ERK and Akt, were not increased due to mutant KRAS activity. (**Fig. 4.3a, b**). Interestingly, stimulation with growth factors such as EGF, PDGF, insulin and Tgfβ did not dramatically augment ERK and Akt phosphorylation in KRAS-mutant cells, when compared to KRAS wild-type counterparts (**Fig. 4.4b,c,d**). While this could be attributed to the reduced RTK expression for EGF, PDGF and Tgfβ (**Fig. 4.1a, b**), Insulin receptor levels was unchanged due to mutant KRAS cells indicating other mechanisms are in play. RTK signaling is negatively regulated through feedback loops involving tumor suppressor genes sprouty genes (*SPRY-1, -2 and -4*), sprouty related genes (*SPRED-1, -2, -3*), insulin receptor-binding protein Grb10 (Hsu et al., 2011; Y. Yu et al., 2011) and mitogen-inducible gene (MIG6 or *ERRFI1*) (Du & Lovly, 2018; Y.-W. Zhang & Vande Woude, 2013). Negative regulation of RTK activity by *ERRFI1* and *SPRY2* is a delayed event and it requires transcriptional induction of these genes. We observed a strong upregulation of these genes (*Spry2*, *Spry3, Errfi1, Grb10* and *Spred3*) in KRAS compared to Control (**Fig. 4.5a,b**). Further experiments need to determine how these genes impact growth factor response in KRAS-mutant cells.

Alternatively, mutant KRAS expressing cells are reported to induce expression of *DUSP5* and *DUSP6* mRNA (Buffet et al., 2017), to "buffer" excess ERK phosphorylation (Shojaee et al., 2015; Unni et al., 2018). It was shown that KRAS transformation upregulates the expression of *DUSP* genes in IEC-6 and CRC cells in a MAPK-dependent manner, and this negatively regulates ERK phosphorylation downstream of mutant BRAF or KRAS (Buffet et al., 2017; Cagnol & Rivard, 2013; Yun et al., 2009b). ETS transcription factors, namely ETV5, can also function as a negative regulator of cell signaling by inducing DUSP expression (Mus et al., 2020; Z. Zhang et al., 2010). Analysis of transcriptomic changes specific to mutant KRAS revealed that there was a significant upregulation of Dusp gene family (*Dusp4*, *Dusp5*, *Dusp6*, *Dusp7*), and transcription factor *Etv5* (**Fig. 5.6a).** We need to perform more experiments to determine if loss of these genes would

augment basal and growth factor-stimulated ERK phosphorylation in KRAS-mutant cells. However, it is possible that KRAS-mutant cells are more sensitive to the loss of DUSP expression compared to Control cells, as unchecked ERK activity is known to be detrimental to cell survival. It was shown that loss of DUSP6 expression conferred "selective" toxicity to KRAS-mutant cells compared to KRAS-wild-type cells (Unni et al., 2018). It would be worth testing if the survival of KRAS-mutant intestinal and CRC cells is selectively dependent on the expression of DUSP family (by RNA interference or DUSP inhibitors such as BCI-215). This would also open the possibility of using DUSP inhibitors to target KRAS-mutant CRC.

Collectively, these results suggest a strong transcriptional induction of negative regulators of RAS effector signaling and RTK signaling in intestinal cells undergoing KRAS transformation. Notably, several genes from the DUSP and Sprouty family of negative feedback regulators were also upregulated in KRAS-mutant *versus* KRAS wild-type CRC tissue, as determined by the analysis of TCGA CRC specimens from cBioportal, $P<0.05$ (**Fig. 5.6b)**. Our data provides an interesting insight into the dynamic control of Akt and ERK activity in KRAS-mutant cells in response to external stimuli. Despite reduced ERK phosphorylation, KRAS-mutant cells displayed enhanced sensitivity to MAPK inhibitors, UO126 and PD184352, compared to Control. The calculated IC50 values for Control and KRAS were 40.8 μM and 0.8 μM respectively for UO126, and 1.8 μM and 0.2 μM respectively for PD184352 (**Fig. 5.6c,d**). These results are in line with another study that reported an anti-correlation between levels of phosphorylated-ERK and sensitivity to MAPK inhibition or KRAS mutations status in CRC (Yeh et al., 2009). But literature shows that releasing the negative feedback loop of ERK phosphorylation in response to MAPK pathway inhibitors contributes to therapeutic resistance. Using quantitative proteomics approach, it was shown that breast cancer cells augmented RTK expression to override loss of MEK activity (Duncan et al., 2012). Our results predict that KRAS transformed intestinal cells might behave in a similar way to MEK inhibitors by restoring cell surface RTK expression. Although this hypothesis needs to be thoroughly tested, preliminary data showed that treatment of KRAS-IEC-6 cells with MEK or PI3K inhibitors, increased Akt and ERK phosphorylation, respectively (**Fig. 5.7a**). Other studies link the increased Akt phosphorylation in MEK inhibitor-treated KRAS-mutant CRC to a compensatory increase in RTK activity (Ebi et al., 2011). Therefore, future

experiments would need to analyze if the MEK-inhibitor mediated Akt phosphorylation in **Fig. 5.7a** is due to restoration of RTK activity.

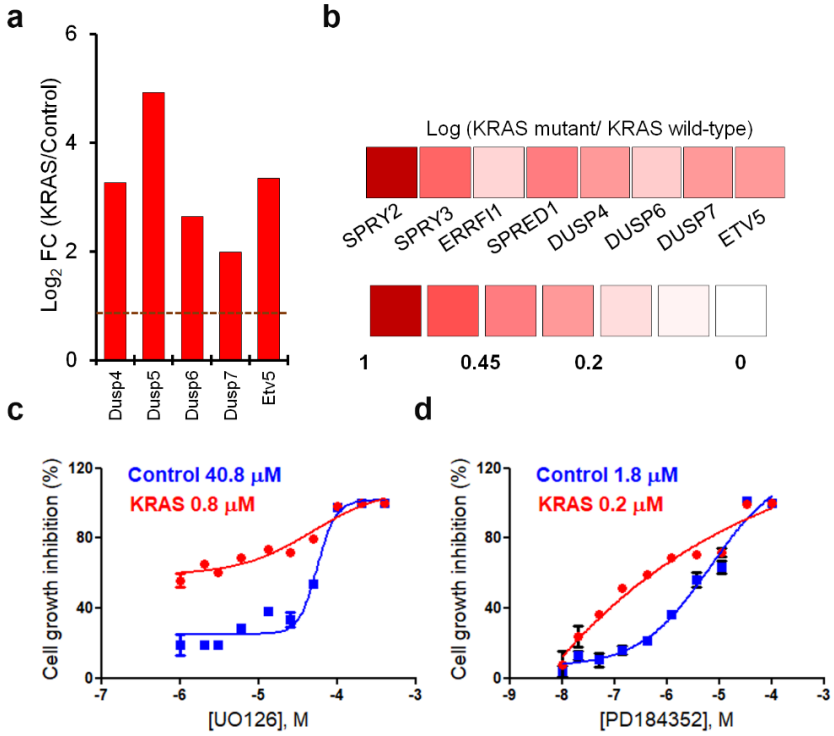

Figure 5.6. Negative regulators of cell signaling and RTK signaling

(a) *Graph depicting the Log_2 FC of mRNA levels of indicated genes in isogenic IEC-6 cells expressing $KRAS^{G12V}$ (KRAS) versus empty vector (Control). Dashed lines depict the cut off threshold of upregulated genes Log_2 FC ≥ +1. Data is normalized to Control condition and represents N=3 replicates.* ***(b)*** *TCGA data from cBioportal database indicating log foldchange (FC) of indicated genes altered in KRAS-mutant CRC relative to KRAS wild-type CRC specimens. The scale for mRNA upregulation is depicted below. Red depicts gene upregulations. HTS data quantifying proliferation of isogenic IEC-6 cells expressing $KRAS^{G12V}$ (KRAS in red) or empty vector (Control in blue) treated with increasing doses of MEK inhibitors,* ***(c)*** *UO126 and* ***(d)*** *PD184352. The calculated IC50 values are indicated on the top left corner. Data represent % inhibition of cellular proliferation quantified by luminescence readouts. Data represent average of N=2 independent screens with two technical replicates each.*

4. Myriad mechanisms of metabolic reprogramming in mutant KRAS-transformed cells

Whereas Akt and ERK phosphorylation was negatively regulated in KRAS-mutant cells, we observe a strong increase in activation of mTOR downstream effectors including S6K1, rpS6 and

4E-BP1 (**Fig. 5.7b**). Analysis of transcriptome data with gene set enrichment analysis (GSEA) database for gene classes that are overexpressed in KRAS^{G12V}-IEC-6, revealed that mTORC1 signaling is upregulated compared to untransformed Control (**Fig. 5.7c)**. Similarly, GSEA data identified enrichments of several metabolic pathways such as oxidative phosphorylation, sugar and nucleotide metabolism, fructose, galactose and glycolysis, due to oncogenic KRAS transformation (**Fig. 5.7d-h**). mTORC1 is critical regulator cellular metabolism including lipid, glucose and nucleotide metabolism (Saxton & Sabatini, 2017). Co-targeting individual metabolic pathways and mTORC1 activity successfully inhibited growth of KRAS-mutant CRC xenografts (Toda et al., 2016), implicating mTOR activity in KRAS-driven tumorigenesis.

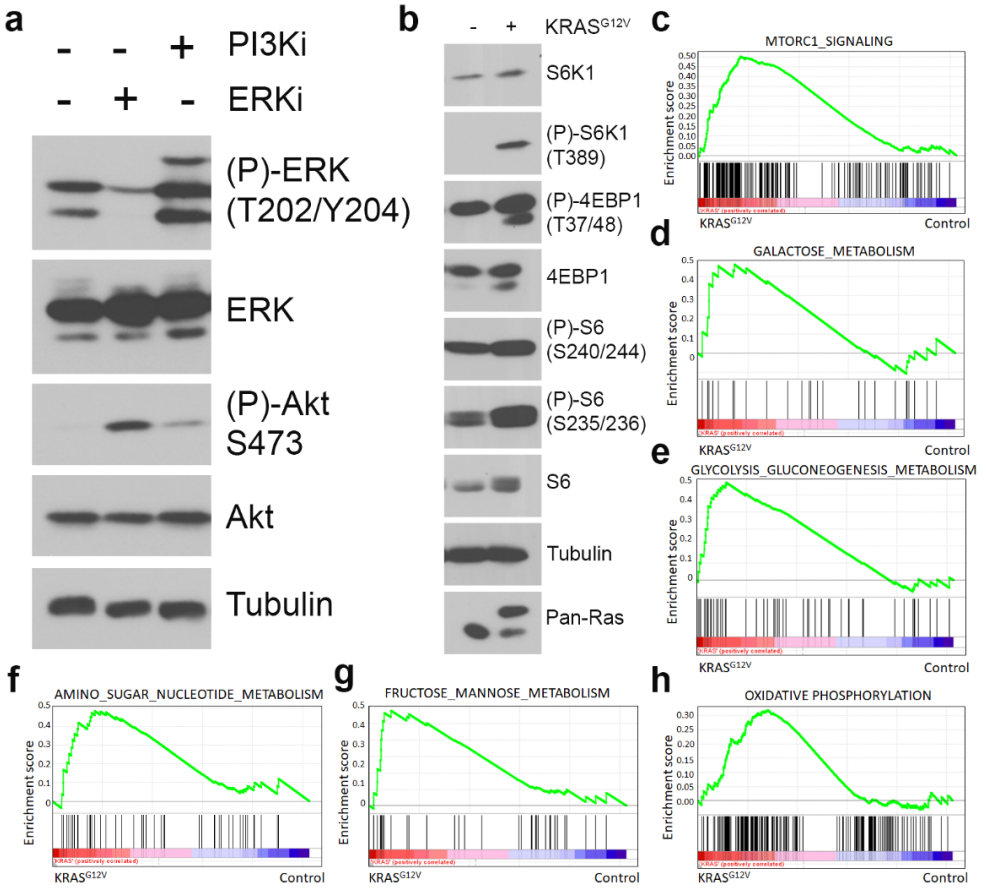

Figure 5.7. Feedback activation of cell signaling pathways and metabolic adaption in KRAS-mutant intestinal cells

(a) *Immunoblots depicting the cross-activation of ERK 1/2 and Akt phosphorylation in KRAS^{G12V}-IEC-6 cells treated with 2 µM MEK inhibitor (PD184352) and 10 µM PI3K inhibitor (LY294002) for 24 h. Data represents N=2.* ***(b)*** *Immunoblots depicting activation of downstream mTORC1 targets in Control and KRAS^{G12V}-IEC-6 cells. Data represents N=2. GSEA plots depicting*

*enrichment of **(c)** HALLMARK mTORC1 activity, **(d)** KEGG Galactose metabolism, **(e)** KEGG Glycolysis and Gluconegenesis metabolism, **(f)** KEGG Amino_Sugar_Nucleotide metabolism, **(g)** KEGG(Kyoto Encyclopedia of Genes and Genomes) Fructose and Mannose metabolism, **(h)** HALLMARK Oxidative phosphorylation in KRAS^{G12V}-IEC-6 cells compared to Control IEC-6.*

Amongst the cell surface protein changes mediated by mutant KRAS **(Fig. 5.5)**, we observe a strong upregulation of Slc2a1 and Slc2a3 (glucose importer), Slc1a5 and Slc38a1 (amino acid importer). Slc2a1 and Slc1a5 are known to be upregulated in a KRAS-dependent manner in CRC (Toda et al., 2017; Yun et al., 2009a), and Slc2a3 is predicted to be a prognostic marker for CRC (E. Kim et al., 2019). We also observed an increase rate of macropinocytosis in KRAS-IEC-6 cells, a feature that is well known to be induced by expression of mutant KRAS. Recently a better understanding of this process led to the identification of its nutrient supply role in satiating the metabolic demand caused by KRAS transformation (Recouvreux & Commisso, 2017a). A recent report demonstrated that inhibition of SLC4-family of bicarbonate transporters blocked macropinocytosis in RAS-mutant cells. In particular, SLC4A7 was significantly upregulated in RAS-dependent fashion and contributed to macropinocytosis (Ramirez et al., 2019). We observe that Slc4a7 is also upregulated in the cell surfaceome of KRAS-IEC-6 cells **(Fig. 5.5)**, and transcriptionally upregulated in KRAS-mutant CRC cells compared to KRAS-wildtype controls **(Fig. 5.8)**. However, its role in mediating macropinocytosis in these cells is yet to be determined.

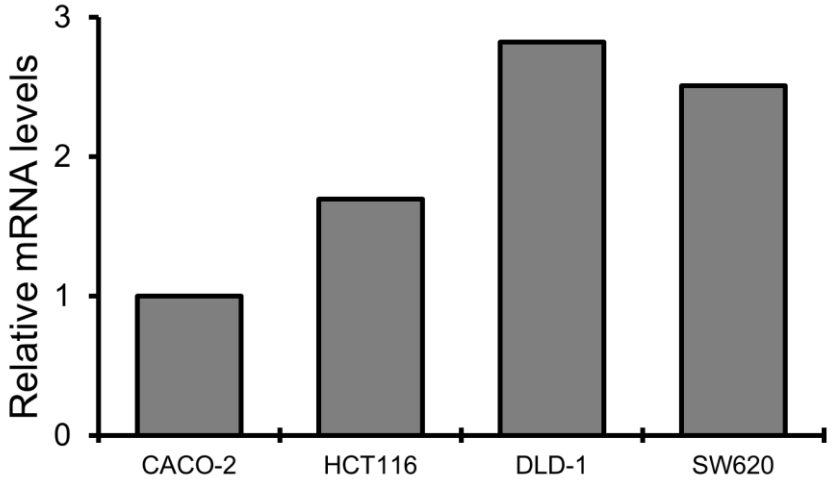

Figure 5.8. SLC4A7 expression is upregulated by mutant KRAS in CRC
SLC4A7 mRNA as quantified by RT-PCR in KRAS-mutant (HCT116, DLD-1, SW620) versus KRAS-wildtype CACO-2 cells. Data represents N=1 with two technical replicates.

Whereas a huge body of information is available on the metabolic changes mediated by oncogenic KRAS in amino acid, glycolytic and related metabolism, much less is about the impact of KRAS on micronutrients such as trace metals and vitamins. Our study identified several surface proteins including copper-regulating Ctr1, Atp7a, Steap3, magnesium-sodium related Cnnm4, Slc22a23, and calcium exporter Slc8a1 as upregulated due to KRAS-transformation in intestinal epithelial cells (**Fig. 2.1i**). This indicates that oncogenic KRAS regulates several metals ions whose neoplastic roles are increasingly appreciated (Serra et al., 2020). Exciting work from the group of Lewis Cantley reported that the micronutrient vitamin C can selectively kill KRAS or BRAF-mutant CRC (Yun et al., 2015). This has sparked interest in targeting vitamin C in CRC (Pires et al., 2018). In line with this, we found that KRAS transformation increased the expression of vitamin C importer SLC23A2 (**Fig. 2.1i**) compared to untransformed controls. Therefore, our data provides a snapshot of various well known and novel metabolic changes induced "en masse" by mutant KRAS at the transcriptome and cell surfaceome.

5. KRAS transformed cells are dependent on copper metabolism

Our data show that KRAS-transformed cells increased the expression of copper exporter Atp7a (**Fig. 2.3a, c, f, i, Supplementary Fig. 2.5a, b**). Consistent with the role of Atp7a in protecting cells from excess copper-ion induced cuproptosis, Atp7a-high KRAS-mutant cells are resistant to cuproptosis when cultured with exogenous copper (**Fig. 2.3e, h**). In a similar manner, KRAS-mutant intestinal cells are resistant to the inhibitory effects of disulfram (DSF) +copper unlike Atp7a-low Control IEC-6 cells. Cell viability was rescued with copper chelator TTM, suggesting that DSF induced cell death in copper-dependent manner (**Fig. 5.9a**) (C. Rae et al., 2013). Several studies have recently attempted to repurpose DSF for inhibiting tumor growth (Calderon-Aparicio, Cornejo, Orue, & Rieber, 2019; Ekinci, Rohondia, Khan, & Dou, 2019; H. Zhang et al., 2010), but our data suggests that KRAS-mutant cells may display resistance to DSF therapy. On the other hand, KRAS-mutant cells are significantly more sensitive to copper chelator TTM (**Fig. 5.9a, Fig. 2.4e, f, Supplementary Fig. 2.7f**), supporting the potential repurposing TTM to CRC therapy. Genome-wide CRISPR/Cas9 screens identified several synthetic lethal pathways that could be co-inhibited to increase TTM efficacy (**Fig. 3.1b-e**). Further clinical and preclinical studies are necessary to determine the use of TTM for curbing tumor growth of aggressive KRAS-mutant cancers, including combinations with existing therapeutic options for targeting KRAS pathway.

A gastric proton pump inhibitor, Omeprazole, was shown to inhibit ATP7A translocation to cell surfaces in response to exogenous copper, a process that is critical to protecting cells from cuproptosis (Matsui, Petris, Niki, Karaman-Jurukovska, et al., 2015). Another study also showed that proton pump inhibitors including esomeprazole exhibited copper-chelating activity and inhibited the copper-dependent melanogenesis process (Baek & Lee, 2015). Preliminary data showed that treatment with omeprazole reduced Atp7a expression in KRAS-mutant intestinal cells (**Fig. 5.9b**), but its effect on Atp7a localization under excess copper conditions remains needs to be tested in KRAS-mutant IEC-6. It would also be interesting to test if by inhibiting Atp7a expression and/or localization, omeprazole reversed the cuproptosis resistant-phenotype of KRAS-mutant CRC cells.

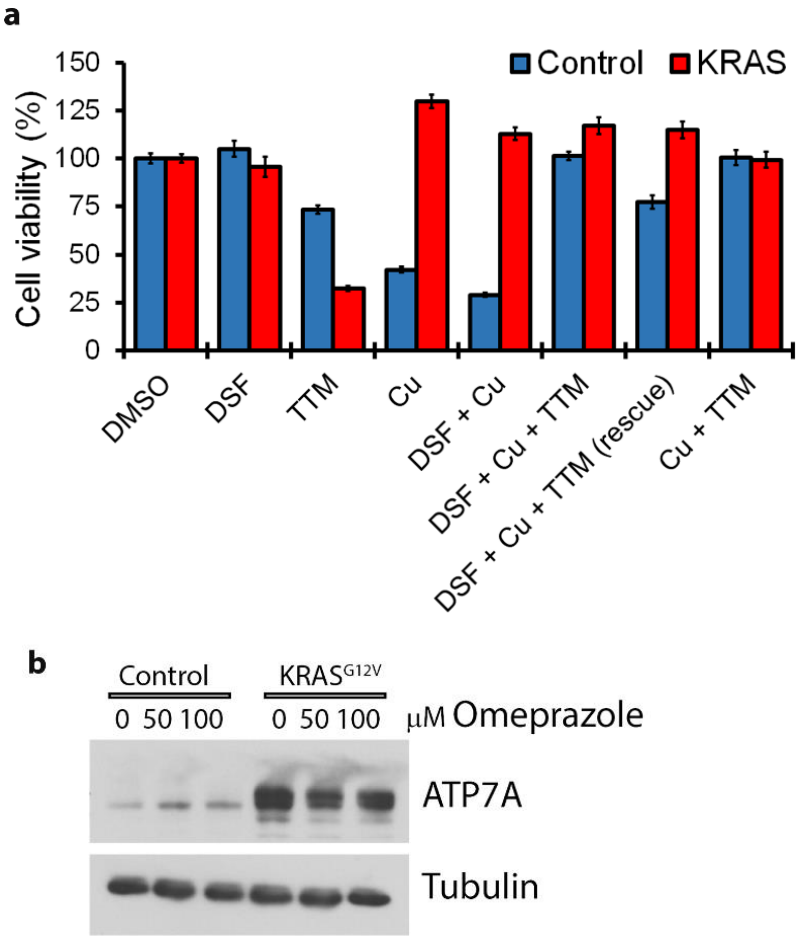

Figure 5.9. Responses of KRAS-mutant cells to Disulfram and Omeprazole

(a) *Cell viability of Control and KRAS-transformed IEC-6 treated with indicated conditions for 24 h. Disulfram (DSF) (10 nM), Copper (10 μM), TTM (10 μM). For DSF +Cu +TTM, all three are treated in combination, whereas in the rescue condition, TTM is added 2 h after DSF +Cu*

treatment. Data represents N=3. ***(b)*** *Immunoblot analysis of Control and KRAS IEC-6 lysates treated with Omeprazole (50 and 100 µM) for 24 h. Data represents N=1.*

6. KRAS transformed cells are selectively dependent on Atp7a expression

Our surfaceome-based CRISPR/Cas9 screen revealed that Atp7a knockout is synthetic lethal for KRAS-mutant intestinal epithelial and CRC cells compared to non-transformed control counterparts (**Fig. 2.2c-f, Supplementary Fig. 2.4a, d**). Loss of Atp7a did not affect the proliferation of cells in other models such as breast cancer 4T1 cells (Shanbhag et al., 2019) or $HRAS^{G12V}$-transformed MEF cells (S. Zhu et al., 2017). This could be attributed to differential regulation of ATP7A in the intestine *versus* other organs (Chun et al., 2017), or to differences in oncogene or isoform-specific signaling. Organ-specific differences in ATP7A function supported by the fact that in Menkes patients with systemic *ATP7A* mutations, some organs display copper accumulation while others exhibit copper deficiency.

The anti-proliferative effect of ATP7A loss in intestinal epithelial and CRC cells could be attributed to either of the two functions that depend on ATP7A. On the one hand, Atp7a protected KRAS-mutant cells from excess copper-induced toxicity (**Fig. 2.3e, h, Supplementary Fig. 2.5k,m**). We obtained evidence that KRAS-mutant cells had elevated levels of intracellular copper compared to KRAS-wildtype controls. Loss of ATP7A has been shown to accumulate intracellular copper levels in several cell models (Gudekar et al., 2020; Gulec & Collins, 2014; S. Zhu et al., 2017). It seems probable that accumulation of copper upon Atp7a knockout added to the already elevated copper levels in KRAS-mutant cells compared to KRAS-wildtype cells (**Fig. 2.3c, d, f, g**) explaining the differential synthetic lethality. On the other hand, ATP7A plays a biosynthetic role wherein they are responsible for copper loading onto copper-dependent enzymes in the trans-Golgi network. We observed that Atp7a knockdown or copper deprivation using TTM affected the activities of copper-dependent enzymes such CP and CCO (**Fig. 2.4b, c, d, g, Supplementary Fig. 2.7a, b, h**), suggesting that KRAS-mutant cells require the biosynthetic role of Atp7a. Therefore, it also seems likely that long term inhibition of Atp7a expression could also affect copper-dependent cellular functions such as mitochondrial respiration (mediated by CCO). These functions are critical for KRAS-tumorigenesis, likely contributing to the observed synthetic

lethality of Atp7a loss in KRAS-mutant intestinal epithelial and CRC cells compared to KRAS wildtype counterparts.

7. Multiple mechanisms to regulate ATP7A levels?

The upregulation of Atp7a in KRAS-transformed CRC and intestinal epithelial cells were observed at the protein levels (**Fig. 2.1i, Supplementary Fig. 2.5a**), with no changes in the transcript levels between KRAS-mutant and KRAS-wildtype conditions. It has been established that Atp7a expression is stabilized post-transcriptionally by copper (Chun et al., 2017; L. Xie & Collins, 2013). However, Atp7a expression is also upregulated transcriptionally by hypoxia-inducible factor HIF2α in intestinal cells and treatment with cobalt chloride to induce hypoxic environments increased Atp7a transcript levels (L. Xie & Collins, 2011) (**Fig. 5.10**). Hypoxia was shown to increase intracellular copper levels and Atp7a expression in macrophages (White et al., 2009). As hypoxia is common in tumor tissues, and is known to contribute to KRAS tumorigenesis in CRC (Kikuchi, Pino, Zeng, Shirasawa, & Chung, 2009; M. Zeng, Kikuchi, Pino, & Chung, 2010). it seems possible that hypoxic environments of CRC and other cancers could upregulate ATP7A mRNA. Other studies have also shown a protective role of Atp7a against ROS and hypoxia. Knockdown of Atp7a in MEF sensitized cells to 2% oxygen and hydrogen peroxide treatments compared to Atp7a-sufficient cells (S. Zhu et al., 2017). Thus, tumor cells could upregulate ATP7A to confer protection against hypoxia and ROS in a copper-dependent or -independent manner.

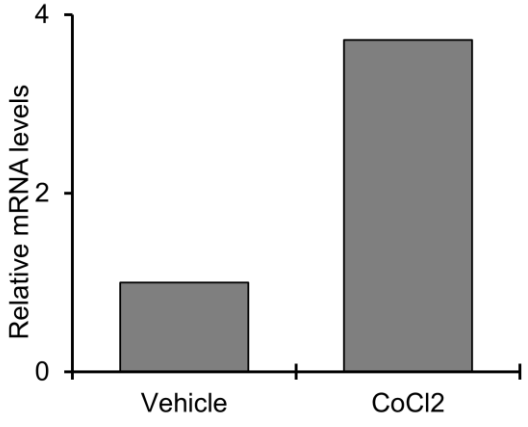

Figure 5.10. Hypoxia regulates Atp7a
RT-PCR quantification of Atp7a mRNA in wildtype IEC-6 cells treated with cobalt chloride ($CoCl_2$). Data represents N=2.

We also find preliminary evidence of a novel mechanism of ATP7A regulation involving *TP53*. *TP53* is implicated in multiple copper homeostasis mechanisms including cuproptosis and transcriptional regulation of the copper detoxification protein, metallothionein. Copper itself is known to compete with zinc to regulate p53 structure and activity (Formigari et al., 2013). *TP53* knockdown in HCT116 and DLD-1 CRC cells reduced ATP7A levels (**Fig. 3.3a**), which was not rescued by addition of exogenous copper (**Fig. 3.3b**). CCS protein was also affected with *TP53* knockdown. Further experiments are needed to determine if *TP53* affects ATP7A via transcriptional or post-transcriptional mechanisms including proteasomal degradation, as loss of *TP53* prevented the copper-dependent stabilization of ATP7A (**Fig. 3.3b**). TP53 is a regulator of cellular stress responses, and is stabilized upon DNA damage (X.-P. Zhang, Liu, & Wang, 2011). Interestingly, treatment of HCT116 with DNA-damaging drugs increased ATP7A protein levels. This increase is apparent in *TP53* wildtype HCT116 and not in *TP53* mutant DLD-1 cells (**Fig. 5.11**). Similar differential responses have been shown for anti-proliferative effect of Nutlin 3a which is selective to wildtype TP53 cells and not in TP53 mutant cells (Drakos et al., 2011). Further work needs to confirm the effect of several DNA damaging drugs on ATP7A mRNA and protein levels in several cell lines with or without *TP53* mutations. These preliminary results lead to interesting questions that need to be tested in the future. Is the increase in ATP7A expression with the DNA-damaging drugs by transcriptional, protein stabilization or via other mechanisms? Is this increase dependent on p53 activity and expression? Is this regulation of ATP7A by p53 specific to intestinal cell type? Do DNA damaging drugs modulate the levels of intracellular ionic copper which further augments ROS and DNA damage? Given that loss of p53 reduces CCS levels, is there an impact on intracellular copper levels?

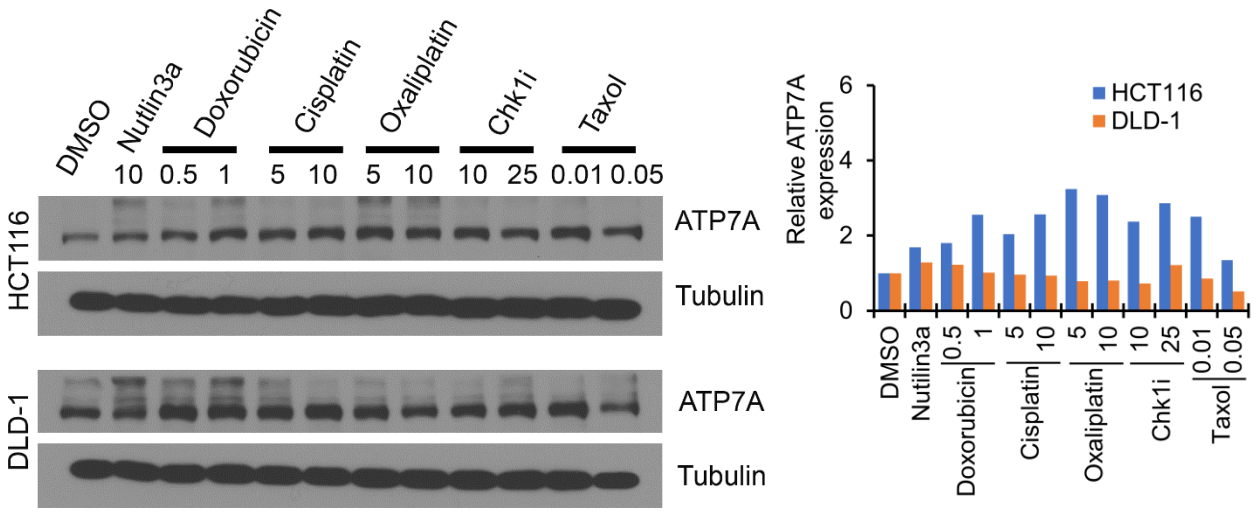

Figure 5.11. ATP7A is regulated by DNA damaging drugs

HCT116 (TP53 wildtype) and DLD-1 (TP53 mutant) are treated with the indicated concentrations of the drugs (μM) for 24 h. ATP7A protein quantifications on the right. AZD7762 is the Chk1 inhibitor used. Data represents N=1.

8. Non-canonical copper supply routes in cells

We observed that while ATP7A was overexpressed in KRAS-mutant CRC cells, CTR1 expression was significantly downregulated (**Supplementary Fig. 2.8**). CTR1 is a high-affinity copper importer in cells, whose cell surface expression is degraded in the event of excess intracellular copper (Chun et al., 2017). There have been evidences of CTR1-independent low-affinity routes for copper delivery into cells lacking CTR1 (J. Lee, Petris, & Thiele, 2002). This mechanism was also suggested for other metals such as zinc, iron and manganese. Furthermore, copper uptake through this pathway could be in the form of Cu(II) ions, whereas CTR1 uptake was Cu(I) dependent. As copper is bound to cellular copper sources- albumin and ceruloplasmin as Cu(II), it suggests that this low-affinity pathway could directly involve these copper carriers. Recent work has highlighted a novel role of macropinocytosis in delivering nutrients to KRAS-transformed cells. Several nutrients including albumin is actively taken up through this pathway and utilized for glycolysis. We thus evaluated a role for this process in regulating intracellular copper levels in KRAS mutated cells. To this effect we observed that inhibition of macropinocytosis modulated copper levels and Atp7a expression in KRAS-mutant intestinal cells (**Fig. 2.5c, d, h, i**). More studies are needed to thoroughly verify the role of macropinocytosis in copper uptake in several

KRAS-mutant CRC, and the role of CTR1 in this process needs to be validated. This could be done by measuring copper levels upon macropinocytosis inhibition in KRAS-mutant cells, with or without CTR1 expression. Moreover, other methods to inhibit macropinocytosis such as inhibition of SLC4A7, SLC4-family inhibitor 4,4'-diisothiocyanatostilbene-2,2'-disulfonate (DIDS), inhibition of v-ATPase activity with Bafilomycin A (Ramirez et al., 2019), DOCK1 inhibitor TBOPP (Tomino et al., 2018), Rac inhibitor EHT 1864 and PI3K inhibitor BKM120 (Hodakoski et al., 2019a), have to be tested in parallel to amiloride (EIPA) to thoroughly validate that macropinocytosis contributes to copper homeostasis in KRAS-mutant cells. Although our studies implicate macropinocytosis in regulating copper bioavailability in KRAS-mutant cells, we suspect that unidentified mechanisms such as autophagy or intracellular stores of copper could also play a role in this process (Polishchuk & Polishchuk, 2016).

9. Limitations

There are several limitations to this study. First, we used the rat intestinal epithelial IEC-6 cells as a model, because of the non-availability of suitable human cells that are non-cancerous and lack cancer causing mutations. For example, many studies use the human CACO-2 cells, which is wild-type for *KRAS* mutations but possess other mutations that lead to tumor formation when injected into mice. Therefore, Atp7a synthetic lethality identified in *KRAS*-mutant IEC-6 cells have been verified in several human CRC cell lines. Similarly, many of the observations made in chapters 2 and 4 such as RTK family downregulation, upregulation of amino acid and solute carriers in *KRAS*-mutant IEC-6 cells, and the potential synthetic lethal pathways with TTM identified in chapter 3, have to be verified in multiple, relevant KRAS-mutant versus KRAS wild-type human CRC models, to avoid cell-line and species-specific differences.

Another major drawback is that most of the preliminary experiments are done in *in vitro* conditions, which do not replicate the extensive features of tumor stroma. Many studies show that sensitivities to drugs differ in 2D versus 3D conditions, and therapeutics developed in 3D culture systems might stand a better chance at achieving clinical success (Devarasetty et al., 2020; Riedl et al., 2017). Some of the findings such as RTK family downregulation, synthetic lethality of ATP7A, and increased sensitivity to Cu chelator, in *KRAS*-mutated cells can be compared to KRAS wild-type counterparts in 3D organoids and tumor-stroma co-culture systems. Infact, an

earlier study observed that Atp7a knockout affected growth of $HRAS^{G12V}$-transformed MEFs only under *in vivo* but not *in vitro* conditions (S. Zhu, Shanbhag, Wang, Lee, & Petris, 2017), making the case to test the synthetic lethality of ATP7A or the efficacy of TTM by comparing several KRAS-mutant and KRAS wild-type CRC cells under *in vivo* conditions. Although we used CACO-2 (KRAS wild-type) in comparison with several KRAS-mutant lines (HCT116, DLD-1, SW620) for the ATP7A and TTM experiments, this study would benefit from including more cell lines of each genotype especially to test further hypothesis such as improving the efficacy of Cu chelating drugs and small molecule inhibitors of ATP7A. For the reasons stated above, the pathways that could be co-targeted to improve efficacy of TTM could be better tested in 3D culture systems using patient-derived organoids with or without KRAS mutation (Verissimo et al., 2016). Another drawback in our model is that transformation is achieved by $KRAS^{G12V}$ overexpression, which is not observed in human cancers that usually display *KRAS* point mutations. Therefore, animal models utilizing knock-in of oncogenic *KRAS* alleles in the intestine, or implanting tumor-derived or primary cell-derived organoids into immunocompromised mice (Jackstadt & Sansom, 2016), could serve as alternatives to KRAS-overexpression models.

Along the same lines, CRISPR screens for identifying KRAS-dependent gene essentiality or TTM-dependent synthetic lethal pathways were performed under *in vitro* conditions, with survival and proliferation as readouts. Although we had confirmed that CRISPR-mediated knockout of Atp7a affected the growth of KRAS IEC-6 both *in vivo* and *in vitro*, more experiments are needed to compare the synthetic lethality of copper depletion or ATP7A loss (either by CRISPR/Cas9 or RNAi) between multiple KRAS-mutant versus wild-type human CRC cells *in vivo.* Alternatively, we could use 3D organoids or adherence-independent growth mediums to confirm Atp7a essentiality in *KRAS*-mutated human CRC cells. Of note, Atp7a was the only candidate gene that affected survival/proliferation of KRAS IEC-6 amongst > 150 differentially expressed cell-surface proteins. Therefore, it could be worth considering if repeating the cell-surface based CRISPR/Cas9 screens with invasion or motility as readouts, could potentially lead to other therapeutically targetable cell surface proteins implicated in KRAS-driven tumorigenesis. Also, CRISPR/Cas9 screens can generate false positive hits, therefore synthetic lethal pathways identified in chapter 3 are to verified by other RNAi strategies or using small-molecule inhibitors in combination with TTM treatment. Moreover, the CRISPR/Cas9 screen to identify synthetic

lethal or rescue genes in the context of TTM efficacy was performed in *NRAS*-mutated leukemia cell line, NALM-6 which must be replaced by KRAS-mutated versus KRAS wild-type CRC cells for future experiments.

In chapter 2, CRISPR/Cas9 screens identified an anti-proliferative/survival role of loss of Atp7a expression in KRAS-mutant cells. This could be attributed to the biosynthetic or Cu exporting roles of Atp7a, which could be better dissected in future studies. Different *ATP7A* mutations exhibit differential defects, with some mutations specifically affecting the Golgi localization and biosynthetic role (Golgi mutants), and other mutations alter the cell surface localization and Cu export function under conditions of excess Cu (cell surface mutants) (Vonk et al., 2012). We could determine if re-expression of Golgi mutants or cell surface mutants rescue the proliferation and survival defects of knocking-out ATP7A expression in different KRAS-mutant CRC cells.

We showed that macropinocytosis is an alternate Cu supply route in KRAS-mutant IEC-6 cells. Our *in vivo* study showed that treating tumors with macropinocytosis inhibitor, EIPA, reduced the growth advantage of KRAS-mutant tumors in mice fed with exogenous Cu. However, it is well known that inhibiting macropinocytosis also affects the influx of crucial nutrients that drive tumorigenesis in KRAS-mutant cells, which could also explain the observed anti-proliferative effect of EIPA. Although we showed that the expression of Cu regulating proteins ATP7A and CCS, and copper levels (as measured by fluorescent sensors) are negatively regulated by EIPA, suggesting disruption of Cu levels. We should measure if uptake of radioactive-labelled Cu is disrupted due to EIPA treatments in KRAS-mutant cells. Additionally, role of macropinocytosis in modulating Cu availability needs to be confirmed in multiple KRAS-mutant CRC cells besides IEC-6 cells. Moreover, although EIPA is used frequently to inhibit macropinocytosis, it can have non-specific effects. So future experiments can be performed with other inhibitors such as RAC, PI3K and DOCK1 in addition to EIPA. Finally, although copper sensors and CCS are well studied markers of Cu bioavailability, more direct measurements of Cu levels such as ICP-MS or atomic absorption spectroscopy (AAS) could be performed in the presence of macropinocytosis inhibitors.

10. Conclusion

We have optimized and used two reproducible cell surface protein labeling approaches to quantify differential cell surface proteins in KRAS-mutant versus normal intestinal epithelial cells. We have identified several novel cell surface proteins regulated by mutant KRAS on intestinal cells, belonging to different functional families that are "druggable". Future work could focus on the role of ephrin receptor Epha5, vitamin C transporter Slc23a2, and adenosine transporter Slc29a1 on KRAS tumorigenesis, and the effect of targeting them in KRAS-mutant CRC. While the cell surfaceome was reprogrammed mostly in a transcription-dependent manner by KRAS, many of the cell-surface proteins were modulated by post-transcriptional mechanisms. This work also provided an interesting look into the spatial regulation of RTK families and cell surface receptors. CRISPR-Cas9 screens revealed that loss of Cu-exporter Atp7a is synthetic lethal to KRAS-mutated colorectal intestinal cells. Future work involves testing the anti-tumor efficacy of newly identified first-in-class small molecular inhibitors of ATP7A in KRAS-mutant cancers. Our study also revealed that KRAS-mutant colorectal cancer cells were addicted to copper metabolism and sensitive to copper chelator TTM. Therefore, more studies are needed to determine the efficacy of clinically available TTM on CRC therapy. CRISPR-Cas9 screens also provided clues on the synthetic lethal pathways that can be co-targeted with TTM to inhibitor cancer cell proliferation. Therefore, our work led to the identification of copper chelation as a novel "druggable" pathway in KRAS-mutant cells. We also show for the first time that macropinocytosis can impact copper metabolism. We hope that this thesis work can led to further studies which can test the impact of KRAS tumorigenesis in metal metabolism and test the clinical application of TTM to overcome KRAS-mediated resistance mechanisms to new and conventional CRC therapy.

AF Gazdar. (2009). Activating and resistance mutations of EGFR in non-small-cell lung cancer: role in clinical response to EGFR tyrosine kinase inhibitors. *Oncogene*, *28*(Suppl 1), S24–S31. https://doi.org/10.1038/onc.2009.198.

Agarwal, E., Chaudhuri, A., Leiphrakpam, P. D., Haferbier, K. L., Brattain, M. G., & Chowdhury, S. (2014). Akt inhibitor MK-2206 promotes anti-tumor activity and cell death by modulation of AIF and Ezrin in colorectal cancer. *BMC Cancer*, *14*(1), 1–12. https://doi.org/10.1186/1471-2407-14-145

Ahmadzadeh, M., Johnson, L. A., Heemskerk, B., Wunderlich, J. R., Dudley, M. E., White, D. E., & Rosenberg, S. A. (2009). Tumor antigen-specific CD8 T cells infiltrating the tumor express high levels of PD-1 and are functionally impaired. *Blood*, *114*(8), 1537–1544. https://doi.org/10.1182/blood-2008-12-195792

Aktas, H., Cai, H., & Cooper, G. M. (1997). Ras links growth factor signaling to the cell cycle machinery via regulation of cyclin D1 and the Cdk inhibitor p27KIP1. *Molecular and Cellular Biology*, *17*(7), 3850–3857. https://doi.org/10.1128/mcb.17.7.3850

Ambrogio, C., Barbacid, M., & Santamaría, D. (2017). In vivo oncogenic conflict triggered by co-existing KRAS and EGFR activating mutations in lung adenocarcinoma. *Oncogene*, *36*(16), 2309–2318. https://doi.org/10.1038/onc.2016.385

Amin, D. N., Sergina, N., Ahuja, D., McMahon, M., Blair, J. A., Wang, D., … Moasser, M. M. (2010). Resiliency and vulnerability in the HER2-HER3 tumorigenic driver. *Science Translational Medicine*, *2*(16), 16ra7. https://doi.org/10.1126/scitranslmed.3000389

Amodio, V., Yaeger, R., Arcella, P., Cancelliere, C., Lamba, S., Lorenzato, A., … Misale, S. (2020). EGFR Blockade Reverts Resistance to KRASG12C Inhibition in Colorectal Cancer. *Cancer Discovery*, *10*(8), 1129–1139. https://doi.org/10.1158/2159-8290.CD-20-0187

Anastasi, S., Lamberti, D., Alemà, S., & Segatto, O. (2016). Regulation of the ErbB network by the MIG6 feedback loop in physiology, tumor suppression and responses to oncogene-targeted therapeutics. *Seminars in Cell & Developmental Biology*, *50*, 115–124. https://doi.org/10.1016/j.semcdb.2015.10.001

André, T., Boni, C., Navarro, M., Tabernero, J., Hickish, T., Topham, C., … De Gramont, A. (2009). Improved overall survival with oxaliplatin, fluorouracil, and leucovorin as adjuvant treatment in stage II or III colon cancer in the MOSAIC trial. *Journal of Clinical Oncology*, *27*(19), 3109–3116. https://doi.org/10.1200/JCO.2008.20.6771

Andreyev, H. J., Norman, A. R., Cunningham, D., Oates, J., Dix, B. R., Iacopetta, B. J., … Urosevic, N. (2001). Kirsten ras mutations in patients with colorectal cancer: the "RASCAL II" study. *British Journal of Cancer*, *85*(5), 692–696. https://doi.org/10.1054/bjoc.2001.1964

Aoki, K., Tamai, Y., Horiike, S., Oshima, M., & Taketo, M. M. (2003). Colonic polyposis caused by mTOR-mediated chromosomal instability in Apc+/Δ716 Cdx2+/- compound mutant mice. *Nature Genetics*, *35*(4), 323–330. https://doi.org/10.1038/ng1265

Arase, M., Tamura, Y., Kawasaki, N., Isogaya, K., Nakaki, R., Mizutani, A., … Koinuma, D. (2017). Dynamics of chromatin accessibility during TGF-β-induced EMT of Ras-transformed mammary gland epithelial cells. *Scientific Reports*, *7*(1), 1166. https://doi.org/10.1038/s41598-017-00973-4

Arner, E. N., Du, W., & Brekken, R. A. (2019). Behind the Wheel of Epithelial Plasticity in KRAS-Driven Cancers. *Frontiers in Oncology*, *9*(October). https://doi.org/10.3389/fonc.2019.01049

Arvelo, F., Sojo, F., & Cotte, C. (2015). Biology of colorectal cancer, *9*, 520. https://doi.org/10.3332/ecancer.2015.520

Aubert, L., Nandagopal, N., Steinhart, Z., Lavoie, G., Nourreddine, S., Berman, J., … Roux, P. P. (2020). Copper bioavailability is a KRAS-specific vulnerability in colorectal cancer. *Nature Communications*, *11*(1), 3701. https://doi.org/10.1038/s41467-020-17549-y

Baek, S.-H., & Lee, S.-H. (2015). Proton pump inhibitors decrease melanogenesis in melanocytes. *Biomedical Reports*, *3*(5), 726–730. https://doi.org/10.3892/br.2015.492

Baker, Z. N., Cobine, P. A., & Leary, S. C. (2017). The mitochondrion: a central architect of copper homeostasis. *Metallomics : Integrated Biometal Science*, *9*(11), 1501–1512. https://doi.org/10.1039/c7mt00221a

Baldari, S., Di Rocco, G., Heffern, M. C., Su, T. A., Chang, C. J., & Toietta, G. (2019). Effects of Copper Chelation on BRAFV600E Positive Colon Carcinoma Cells. *Cancers*, *11*(5). https://doi.org/10.3390/cancers11050659

Baldari, S., Di Rocco, G., & Toietta, G. (2020). Current Biomedical Use of Copper Chelation Therapy. *International Journal of Molecular Sciences*, *21*(3). https://doi.org/10.3390/ijms21031069

Balmain, A., & Pragnell, I. B. (1983). Mouse skin carcinomas induced in vivo by chemical carcinogens have a transforming Harvey-ras oncogene. *Nature*, *303*(5912), 72–74. https://doi.org/10.1038/303072a0

Banci, L., Bertini, I., Chasapis, C. T., Rosato, A., & Tenori, L. (2007). Interaction of the two soluble metal-binding domains of yeast Ccc2 with copper(I)-Atx1. *Biochemical and Biophysical Research Communications*, *364*(3), 645–649. https://doi.org/10.1016/j.bbrc.2007.10.045

Bar-Sagi, D., & Feramisco, J. R. (1986). Induction of membrane ruffling and fluid-phase pinocytosis in quiescent fibroblasts by ras proteins. *Science*, *233*(4768), 1061–1068. https://doi.org/10.1126/science.3090687

Barbie, D. A., Tamayo, P., Boehm, J. S., Kim, S. Y., Moody, S. E., Dunn, I. F., … Hahn, W. C. (2009). Systematic RNA interference reveals that oncogenic KRAS-driven cancers require TBK1. *Nature*, *462*(7269), 108–112. https://doi.org/10.1038/nature08460

Barker, N., Ridgway, R. A., Van Es, J. H., Van De Wetering, M., Begthel, H., Van Den Born, M., … Clevers, H. (2009). Crypt stem cells as the cells-of-origin of intestinal cancer. *Nature*, *457*(7229), 608–611. https://doi.org/10.1038/nature07602

Barresi, V., Trovato-Salinaro, A., Spampinato, G., Musso, N., Castorina, S., Rizzarelli, E., & Condorelli, D. F. (2016). Transcriptome analysis of copper homeostasis genes reveals coordinated upregulation of SLC31A1,SCO1, and COX11 in colorectal cancer. *FEBS Open Bio*, *6*(8), 794–806. https://doi.org/10.1002/2211-5463.12060

Basu, S., Haase, G., & Ben-Ze'ev, A. (2016). Wnt signaling in cancer stem cells and colon cancer metastasis. *F1000Research*, *5*(0), 699. https://doi.org/10.12688/f1000research.7579.1

Bellam, N., & Pasche, B. (2010). TGF-β Signaling Alterations and Colon Cancer. In *Cancer treatment and research* (Vol. 155, pp. 85–103). https://doi.org/10.1007/978-1-4419-6033-7_5

Bergeron, S., Lemieux, E., Durand, V., Cagnol, S., Carrier, J. C., Lussier, J. G., … Rivard, N. (2010). The serine protease inhibitor serpinE2 is a novel target of ERK signaling involved in human colorectal tumorigenesis. *Molecular Cancer*, *9*, 271. https://doi.org/10.1186/1476-4598-9-271

Bertagnolli, M. M., Eagle, C. J., Zauber, A. G., Redston, M., Solomon, S. D., Kim, K., … Hawk, E. T. (2006). Celecoxib for the Prevention of Sporadic Colorectal Adenomas. *New England Journal of Medicine*, *355*(9), 873–884. https://doi.org/10.1056/NEJMoa061355

Bertinato, J., & L'Abbé, M. R. (2003). Copper modulates the degradation of copper chaperone for Cu,Zn superoxide dismutase by the 26 S proteosome. *The Journal of Biological Chemistry*, *278*(37), 35071–35078. https://doi.org/10.1074/jbc.M302242200

Bertomeu, T., Coulombe-Huntington, J., Chatr-Aryamontri, A., Bourdages, K. G., Coyaud, E., Raught, B., … Tyers, M. (2018). A High-Resolution Genome-Wide CRISPR/Cas9 Viability Screen Reveals Structural Features and Contextual Diversity of the Human Cell-Essential Proteome. *Molecular and Cellular Biology*, *38*(1). https://doi.org/10.1128/MCB.00302-17

Beumer, J., & Clevers, H. (2016). Regulation and plasticity of intestinal stem cells during homeostasis and regeneration. *Development (Cambridge)*, *143*(20), 3639–3649. https://doi.org/10.1242/dev.133132

Bilanges, B., Posor, Y., & Vanhaesebroeck, B. (2019). PI3K isoforms in cell signalling and vesicle trafficking. *Nature Reviews Molecular Cell Biology*, *20*(9), 515–534. https://doi.org/10.1038/s41580-019-0129-z

Birsoy, K., Wang, T., Chen, W. W., Freinkman, E., Abu-Remaileh, M., & Sabatini, D. M. (2015). An Essential Role of the Mitochondrial Electron Transport Chain in Cell Proliferation Is to Enable Aspartate Synthesis. *Cell*, *162*(3), 540–551. https://doi.org/10.1016/j.cell.2015.07.016

Biswas, S., Chytil, A., Washington, K., Romero-Gallo, J., Gorska, A. E., Wirth, P. S., … Grady, W. M. (2004). Transforming growth factor β receptor type II inactivation promotes the establishment and progression of colon cancer. *Cancer Research*, *64*(14), 4687–4692. https://doi.org/10.1158/0008-5472.CAN-03-3255

Blockhuys, S., Celauro, E., Hildesjö, C., Feizi, A., Stål, O., Fierro-González, J. C., & Wittung-Stafshede, P. (2017). Defining the human copper proteome and analysis of its expression variation in cancers. *Metallomics : Integrated Biometal Science*, *9*(2), 112–123. https://doi.org/10.1039/c6mt00202a

Boison, D., & Yegutkin, G. G. (2019). Adenosine Metabolism: Emerging Concepts for Cancer Therapy. *Cancer Cell*, *36*(6), 582–596. https://doi.org/10.1016/j.ccell.2019.10.007

Boland, C. R., & Goel, A. (2010). Microsatellite Instability in Colorectal Cancer. *Gastroenterology*, *138*(6), 2073-2087.e3. https://doi.org/10.1053/j.gastro.2009.12.064

Boswell-Casteel, R. C., & Hays, F. A. (2017). Equilibrative nucleoside transporters-A review. *Nucleosides, Nucleotides & Nucleic Acids*, *36*(1), 7–30. https://doi.org/10.1080/15257770.2016.1210805

Brady, D. C., Crowe, M. S., Greenberg, D. N., & Counter, C. M. (2017). Copper Chelation Inhibits BRAFV600E-Driven Melanomagenesis and Counters Resistance to BRAFV600E and MEK1/2 Inhibitors. *Cancer Research*, *77*(22), 6240–6252. https://doi.org/10.1158/0008-5472.CAN-16-1190

Brady, D. C., Crowe, M. S., Turski, M. L., Hobbs, G. A., Yao, X., Chaikuad, A., … Counter, C. M. (2014). Copper is required for oncogenic BRAF signalling and tumorigenesis. *Nature*, *509*(7501), 492–496. https://doi.org/10.1038/nature13180

Braiterman, L., Nyasae, L., Guo, Y., Bustos, R., Lutsenko, S., & Hubbard, A. (2009). Apical targeting and Golgi retention signals reside within a 9-amino acid sequence in the copper-ATPase, ATP7B. *American Journal of Physiology. Gastrointestinal and Liver Physiology*, *296*(2), G433-44. https://doi.org/10.1152/ajpgi.90489.2008

Bray, F., Ferlay, J., Soerjomataram, I., Siegel, R. L., Torre, L. A., & Jemal, A. (2018). Global cancer statistics 2018: GLOBOCAN estimates of incidence and mortality worldwide for 36 cancers in 185 countries. *CA: A Cancer Journal for Clinicians*, *68*(6), 394–424. https://doi.org/10.3322/caac.21492

Brem, S. S., Zagzag, D., Tsanaclis, A. M., Gately, S., Elkouby, M. P., & Brien, S. E. (1990). Inhibition of angiogenesis and tumor growth in the brain. Suppression of endothelial cell turnover by penicillamine and the depletion of copper, an angiogenic cofactor. *The American Journal of Pathology*, *137*(5), 1121–1142. Retrieved from http://www.ncbi.nlm.nih.gov/pubmed/1700617

Brem, S., Tsanaclis, A. M., & Zagzag, D. (1990). Anticopper treatment inhibits pseudopodial protrusion and the invasive spread of 9L gliosarcoma cells in the rat brain. *Neurosurgery*, *26*(3), 391–396. https://doi.org/10.1097/00006123-199003000-00003

Brenner, D. R., Weir, H. K., Demers, A. A., Ellison, L. F., Louzado, C., Shaw, A., … Canadian Cancer Statistics Advisory Committee. (2020). Projected estimates of cancer in Canada in 2020. *CMAJ : Canadian Medical Association Journal = Journal de l'Association Medicale Canadienne*, *192*(9), E199–E205. https://doi.org/10.1503/cmaj.191292

Brummelkamp, T. R., Bernards, R., & Agami, R. (2002). Stable suppression of tumorigenicity by virus-mediated RNA interference. *Cancer Cell*, *2*(3), 243–247. https://doi.org/10.1016/S1535-6108(02)00122-8

Buffet, C., Hecale-Perlemoine, K., Bricaire, L., Dumont, F., Baudry, C., Tissier, F., … Groussin, L. (2017). DUSP5 and DUSP6, two ERK specific phosphatases, are markers of a higher MAPK signaling activation in BRAF mutated thyroid cancers. *PLoS ONE*, *12*(9), 1–24. https://doi.org/10.1371/journal.pone.0184861

Buhrman, G., O′Connor, C., Zerbe, B., Kearney, B. M., Napoleon, R., Kovrigina, E. A., … Mattos, C. (2011). Analysis of Binding Site Hot Spots on the Surface of Ras GTPase. *Journal of Molecular Biology*, *413*(4), 773–789. https://doi.org/10.1016/j.jmb.2011.09.011

Cagnol, S., & Rivard, N. (2013). Oncogenic KRAS and BRAF activation of the MEK/ERK signaling pathway promotes expression of dual-specificity phosphatase 4 (DUSP4/MKP2) resulting in nuclear ERK1/2 inhibition. *Oncogene*, *32*(5), 564–576. https://doi.org/10.1038/onc.2012.88

Calderon-Aparicio, A., Cornejo, A., Orue, A., & Rieber, M. (2019). Anticancer response to disulfiram may be enhanced by co-treatment with MEK inhibitor or oxaliplatin: modulation by tetrathiomolybdate, KRAS/BRAF mutations and c-MYC/p53 status. *Ecancermedicalscience*, *13*, 890. https://doi.org/10.3332/ecancer.2019.890

Calvo, J., Jung, H., & Meloni, G. (2017). Copper metallothioneins. *IUBMB Life*, *69*(4), 236–245. https://doi.org/10.1002/iub.1618

Camakaris, J., Petris, M. J., Bailey, L., Shen, P., Lockhart, P., Glover, T. W., … Mercer, J. F. (1995). Gene amplification of the Menkes (MNK; ATP7A) P-type ATPase gene of CHO cells is associated with copper resistance and enhanced copper efflux. *Human Molecular Genetics*, *4*(11), 2117–2123. https://doi.org/10.1093/hmg/4.11.2117

Campbell, C. H., Brown, R., & Linder, M. C. (1981). Circulating ceruloplasmin is an important source of copper for normal and malignant animal cells. *Biochimica et Biophysica Acta*, *678*(1), 27–38. https://doi.org/10.1016/0304-4165(81)90044-1

Campbell, P. M., & Der, C. J. (2004). Oncogenic Ras and its role in tumor cell invasion and metastasis, *14*, 105–114. https://doi.org/10.1016/j.semcancer.2003.09.015

Carvallo-Chaigneau, F., Trejo-Solís, C., Gómez-Ruiz, C., Rodríguez-Aguilera, E., Macías-

Rosales, L., Cortés-Barberena, E., … Constantino-Casas, F. (2008). Casiopeina III-ia induces apoptosis in HCT-15 cells in vitro through caspase-dependent mechanisms and has antitumor effect in vivo. *Biometals : An International Journal on the Role of Metal Ions in Biology, Biochemistry, and Medicine*, *21*(1), 17–28. https://doi.org/10.1007/s10534-007-9089-4

Casaletto, J. B., & McClatchey, A. I. (2012). Spatial regulation of receptor tyrosine kinases in development and cancer. *Nature Reviews. Cancer*, *12*(6), 387–400. https://doi.org/10.1038/nrc3277

Castellano, E., & Santos, E. (2011). Functional specificity of ras isoforms: so similar but so different. *Genes & Cancer*, *2*(3), 216–231. https://doi.org/10.1177/1947601911408081

Cater, M. A., Pearson, H. B., Wolyniec, K., Klaver, P., Bilandzic, M., Paterson, B. M., … Haupt, Y. (2013). Increasing intracellular bioavailable copper selectively targets prostate cancer cells. *ACS Chemical Biology*, *8*(7), 1621–1631. https://doi.org/10.1021/cb400198p

Cavallo-Medved, D., Dosescu, J., Linebaugh, B. E., Sameni, M., Rudy, D., & Sloane, B. F. (2003). Mutant K-ras Regulates Cathepsin B Localization on the Surface of Human Colorectal Carcinoma Cells1. *Neoplasia (New York, N.Y.)*, *5*(6), 507–519. https://doi.org/10.1016/S1476-5586(03)80035-0

Cen, D., Brayton, D., Shahandeh, B., Meyskens, F. L., & Farmer, P. J. (2004). Disulfiram facilitates intracellular Cu uptake and induces apoptosis in human melanoma cells. *Journal of Medicinal Chemistry*, *47*(27), 6914–6920. https://doi.org/10.1021/jm049568z

Chan, N., Willis, A., Kornhauser, N., Mward, M., Lee, S. B., Nackos, E., … Vahdat, L. (2017). Influencing the tumor microenvironment: A Phase II study of copper depletion using tetrathiomolybdate in patients with breast cancer at high risk for recurrence and in preclinical models of lung metastases. *Clinical Cancer Research*, *23*(3), 666–676. https://doi.org/10.1158/1078-0432.CCR-16-1326

Chan, N., Willis, A., Kornhauser, N., Ward, M. M., Lee, S. B., Nackos, E., … Vahdat, L. (2017). Influencing the Tumor Microenvironment: A Phase II Study of Copper Depletion Using Tetrathiomolybdate in Patients with Breast Cancer at High Risk for Recurrence and in Preclinical Models of Lung Metastases. *Clinical Cancer Research : An Official Journal of the American Association for Cancer Research*, *23*(3), 666–676. https://doi.org/10.1158/1078-0432.CCR-16-1326

Chandler, K. B., & Costello, C. E. (2016). Glycomics and glycoproteomics of membrane proteins and cell-surface receptors: Present trends and future opportunities. *Electrophoresis*, *37*(11), 1407–1419. https://doi.org/10.1002/elps.201500552

Chapman, P. B., Hauschild, A., Robert, C., Haanen, J. B., Ascierto, P., Larkin, J., … McArthur, G. A. (2011). Improved Survival with Vemurafenib in Melanoma with BRAF V600E Mutation. *New England Journal of Medicine*, *364*(26), 2507–2516. https://doi.org/10.1056/NEJMoa1103782

Chen, D., Cui, Q. C., Yang, H., & Dou, Q. P. (2006). Disulfiram, a clinically used anti-alcoholism drug and copper-binding agent, induces apoptotic cell death in breast cancer cultures and xenografts via inhibition of the proteasome activity. *Cancer Research*, *66*(21), 10425–10433. https://doi.org/10.1158/0008-5472.CAN-06-2126

Chen, H. H. W., & Kuo, M. T. (2013). Overcoming platinum drug resistance with copper-lowering agents. *Anticancer Research*, *33*(10), 4157–4161. Retrieved from http://www.ncbi.nlm.nih.gov/pubmed/24122978

Chen, X., Guan, Z., Lu, J., Wang, H., Zuo, Z., Ye, F., … Teng, L. (2018). Synergistic antitumor

effects of cMet inhibitor in combination with anti-VEGF in colorectal cancer patient-derived xenograft models. *Journal of Cancer*, *9*(7), 1207–1217. https://doi.org/10.7150/jca.20964

Chin, L., Tam, A., Pomerantz, J., Wong, M., Holash, J., Bardeesy, N., … DePinho, R. A. (1999). Essential role for oncogenic ras in tumour maintenance. *Nature*, *400*(6743), 468–472. https://doi.org/10.1038/22788

Chiron, M., Bagley, R. G., Pollard, J., Mankoo, P. K., Henry, C., Vincent, L., … Bergstrom, D. A. (2014). Differential antitumor activity of aflibercept and bevacizumab in patient-derived xenograft models of colorectal cancer. *Molecular Cancer Therapeutics*, *13*(6), 1636–1644. https://doi.org/10.1158/1535-7163.MCT-13-0753

Chisholm, C. L., Wang, H., Wong, A. H. H., Vazquez-Ortiz, G., Chen, W., Xu, X., & Deng, C. X. (2016). Ammonium tetrathiomolybdate treatment targets the copper transporter ATP7A and enhances sensitivity of breast cancer to cisplatin. *Oncotarget*, *7*(51), 84439–84452. https://doi.org/10.18632/oncotarget.12992

Chiu, V. K., Bivona, T., Hach, A., Sajous, J. B., Silletti, J., Wiener, H., … Philips, M. R. (2002). Ras signalling on the endoplasmic reticulum and the Golgi. *Nature Cell Biology*, *4*(5), 343–350. https://doi.org/10.1038/ncb783

Chong, H., Lee, J., & Guan, K. L. (2001). Positive and negative regulation of Raf kinase activity and function by phosphorylation. *EMBO Journal*, *20*(14), 3716–3727. https://doi.org/10.1093/emboj/20.14.3716

Chong, H., Vikis, H. G., & Guan, K. L. (2003). Mechanisms of regulating the Raf kinase family. *Cellular Signalling*, *15*(5), 463–469. https://doi.org/10.1016/S0898-6568(02)00139-0

Chun, H., Catterton, T., Kim, H., Lee, J., & Kim, B.-E. (2017). Organ-specific regulation of ATP7A abundance is coordinated with systemic copper homeostasis. *Scientific Reports*, *7*(1), 12001. https://doi.org/10.1038/s41598-017-11961-z

Cihil, K. M., & Swiatecka-Urban, A. (2013). The Cell-based L-Glutathione Protection Assays to Study Endocytosis and Recycling of Plasma Membrane Proteins. *Journal of Visualized Experiments*, (82). https://doi.org/10.3791/50867

Cobine, P. A., Ojeda, L. D., Rigby, K. M., & Winge, D. R. (2004). Yeast contain a non-proteinaceous pool of copper in the mitochondrial matrix. *The Journal of Biological Chemistry*, *279*(14), 14447–14455. https://doi.org/10.1074/jbc.M312693200

Cohen, D. I., Illowsky, B., & Linder, M. C. (1979). Altered copper absorption in tumor-bearing and estrogen-treated rats. *The American Journal of Physiology*, *236*(3), E309-15. https://doi.org/10.1152/ajpendo.1979.236.3.E309

Colic, M., Wang, G., Zimmermann, M., Mascall, K., McLaughlin, M., Bertolet, L., … Hart, T. (2019). Identifying chemogenetic interactions from CRISPR screens with drugZ. *Genome Medicine*, *11*(1), 52. https://doi.org/10.1186/s13073-019-0665-3

Commisso, C., & Commisso, C. (2019). The pervasiveness of macropinocytosis in oncological malignancies.

Commisso, C., Davidson, S. M., Soydaner-Azeloglu, R. G., Parker, S. J., Kamphorst, J. J., Hackett, S., … Bar-Sagi, D. (2013a). Macropinocytosis of protein is an amino acid supply route in Ras-transformed cells. *Nature*, *497*(7451), 633–637. https://doi.org/10.1038/nature12138

Commisso, C., Davidson, S. M., Soydaner-Azeloglu, R. G., Parker, S. J., Kamphorst, J. J., Hackett, S., … Bar-Sagi, D. (2013b). Macropinocytosis of protein is an amino acid supply route in Ras-transformed cells. *Nature*, *497*(7451), 633–637.

https://doi.org/10.1038/nature12138
Corcoran, R. B., Cheng, K. A., Hata, A. N., Faber, A. C., Ebi, H., Coffee, E. M., … Engelman, J. A. (2013). Synthetic lethal interaction of combined BCL-XL and MEK inhibition promotes tumor regressions in KRAS mutant cancer models. *Cancer Cell*, *23*(1), 121–128. https://doi.org/10.1016/j.ccr.2012.11.007
Corcoran, R. B., Ebi, H., Turke, A. B., Coffee, E. M., Nishino, M., Cogdill, A. P., … Engelman, J. A. (2012). EGFR-mediated re-activation of MAPK signaling contributes to insensitivity of BRAF mutant colorectal cancers to RAF inhibition with vemurafenib. *Cancer Discovery*, *2*(3), 227–235. https://doi.org/10.1158/2159-8290.CD-11-0341
Costigan, D. C., & Dong, F. (2020). The extended spectrum of RAS-MAPK pathway mutations in colorectal cancer. *Genes Chromosomes and Cancer*, *59*(3), 152–159. https://doi.org/10.1002/gcc.22813
Courtois-Cox, S., Genther Williams, S. M., Reczek, E. E., Johnson, B. W., McGillicuddy, L. T., Johannessen, C. M., … Cichowski, K. (2006). A negative feedback signaling network underlies oncogene-induced senescence. *Cancer Cell*, *10*(6), 459–472. https://doi.org/10.1016/j.ccr.2006.10.003
Cox, A. D., Fesik, S. W., Kimmelman, A. C., Luo, J., & Der, C. J. (2014). Drugging the undruggable RAS: Mission Possible? *Nature Reviews. Drug Discovery*, *13*(11), 828–851. https://doi.org/10.1038/nrd4389
Cox, C., Teknos, T. N., Barrios, M., Brewer, G. J., Dick, R. D., & Merajver, S. D. (2001). The role of copper suppression as an antiangiogenic strategy in head and neck squamous cell carcinoma. *The Laryngoscope*, *111*(4 Pt 1), 696–701. https://doi.org/10.1097/00005537-200104000-00024
Cunningham, D., Humblet, Y., Siena, S., Khayat, D., Bleiberg, H., Santoro, A., … Van Cutsem, E. (2004). Cetuximab monotherapy and cetuximab plus irinotecan in irinotecan- refractory metastatic colorectal cancer. *New England Journal of Medicine*, *351*(4), 337–345. https://doi.org/10.1056/NEJMoa033025
Daaboul, H. E., & El-Sibai, M. (2018). Treatment Strategies in Colorectal Cancer. In *Colorectal Cancer - Diagnosis, Screening and Management* (Vol. i, p. 13). InTech. https://doi.org/10.5772/intechopen.71620
Danielsson, F., Skogs, M., Huss, M., Rexhepaj, E., O'Hurley, G., Klevebring, D., … Lundberg, E. (2013). Majority of differentially expressed genes are down-regulated during malignant transformation in a four-stage model. *Proceedings of the National Academy of Sciences of the United States of America*, *110*(17), 6853–6858. https://doi.org/10.1073/pnas.1216436110
Davidson, L. A., McOrmond, S. L., & Harris, E. D. (1994). Characterization of a particulate pathway for copper in K562 cells. *Biochimica et Biophysica Acta*, *1221*(1), 1–6. https://doi.org/10.1016/0167-4889(94)90208-9
De' Angelis, G. L., Bottarelli, L., Azzoni, C., De' Angelis, N., Leandro, G., Di Mario, F., … Negri, F. (2018). Microsatellite instability in colorectal cancer. *Acta Bio-Medica : Atenei Parmensis*, *89*(9-S), 97–101. https://doi.org/10.23750/abm.v89i9-S.7960
De Roock, W., Claes, B., Bernasconi, D., De Schutter, J., Biesmans, B., Fountzilas, G., … Tejpar, S. (2010). Effects of KRAS, BRAF, NRAS, and PIK3CA mutations on the efficacy of cetuximab plus chemotherapy in chemotherapy-refractory metastatic colorectal cancer: A retrospective consortium analysis. *The Lancet Oncology*, *11*(8), 753–762. https://doi.org/10.1016/S1470-2045(10)70130-3

de Wit, M., Jimenez, C. R., Carvalho, B., Belien, J. A. M., Delis-van Diemen, P. M., Mongera, S., … Fijneman, R. J. A. (2012). Cell surface proteomics identifies glucose transporter type 1 and prion protein as candidate biomarkers for colorectal adenoma-to-carcinoma progression. *Gut*, *61*(6), 855–864. https://doi.org/10.1136/gutjnl-2011-300511

Dekker, E., Tanis, P. J., Vleugels, J. L. A., Kasi, P. M., & Wallace, M. B. (2019). Colorectal cancer. *The Lancet*, *394*(10207), 1467–1480. https://doi.org/10.1016/S0140-6736(19)32319-0

Denoyer, D., Masaldan, S., La Fontaine, S., & Cater, M. A. (2015). Targeting copper in cancer therapy: "Copper That Cancer". *Metallomics : Integrated Biometal Science*, *7*(11), 1459–1476. https://doi.org/10.1039/c5mt00149h

Derer, S., Berger, S., Schlaeth, M., Schneider-Merck, T., Klausz, K., Lohse, S., … Valerius, T. (2012). Oncogenic KRAS impairs EGFR antibodies' efficiency by C/EBPβ-dependent suppression of EGFR expression. *Neoplasia (New York, N.Y.)*, *14*(3), 190–205. https://doi.org/10.1593/neo.111636

Derer, S., Lohse, S., & Valerius, T. (2013). EGFR expression levels affect the mode of action of EGFR-targeting monoclonal antibodies. *Oncoimmunology*, *2*(5), e24052. https://doi.org/10.4161/onci.24052

Desai, V., & Kaler, S. G. (2008). Role of copper in human neurological disorders. *American Journal of Clinical Nutrition*, *88*(3), 855–858. https://doi.org/10.1093/ajcn/88.3.855s

Devarasetty, M., Dominijanni, A., Herberg, S., Shelkey, E., Skardal, A., & Soker, S. (2020). Simulating the human colorectal cancer microenvironment in 3D tumor-stroma co-cultures in vitro and in vivo. *Scientific Reports*, *10*(1), 9832. https://doi.org/10.1038/s41598-020-66785-1

Dhillon, S. (2018). Regorafenib: A Review in Metastatic Colorectal Cancer. *Drugs*, *78*(11), 1133–1144. https://doi.org/10.1007/s40265-018-0938-y

Dienstmann, R., Salazar, R., & Tabernero, J. (2020). Overcoming Resistance to Anti-EGFR Therapy in.

Ding, W.-Q., & Lind, S. E. (2009). Metal ionophores - an emerging class of anticancer drugs. *IUBMB Life*, *61*(11), 1013–1018. https://doi.org/10.1002/iub.253

Dite, T. A., Langendorf, C. G., Hoque, A., Galic, S., Rebello, R. J., Ovens, A. J., … Oakhill, J. S. (2018). AMP-activated protein kinase selectively inhibited by the type II inhibitor SBI-0206965. *The Journal of Biological Chemistry*, *293*(23), 8874–8885. https://doi.org/10.1074/jbc.RA118.003547

Dobrowolski, S., Harter, M., & Stacey, D. W. (1994). Cellular ras activity is required for passage through multiple points of the G0/G1 phase in BALB/c 3T3 cells. *Molecular and Cellular Biology*, *14*(8), 5441–5449. https://doi.org/10.1128/mcb.14.8.5441

Dolgova, N. V, Yu, C., Cvitkovic, J. P., Hodak, M., Nienaber, K. H., Summers, K. L., … Dmitriev, O. Y. (2017). Binding of Copper and Cisplatin to Atox1 Is Mediated by Glutathione through the Formation of Metal-Sulfur Clusters. *Biochemistry*, *56*(24), 3129–3141. https://doi.org/10.1021/acs.biochem.7b00293

Donnard, E., Asprino, P. F., Correa, B. R., Bettoni, F., Koyama, F. C., Navarro, F. C. P., … Camargo, A. A. (2014). Mutational analysis of genes coding for cell surface proteins in colorectal cancer cell lines reveal novel altered pathways, druggable mutations and mutated epitopes for targeted therapy. *Oncotarget*, *5*(19), 9199–9213. https://doi.org/10.18632/oncotarget.2374

Douillard, J. Y., Siena, S., Cassidy, J., Tabernero, J., Burkes, R., Barugel, M., … Sidhu, R.

(2014). Final results from PRIME: Randomized phase III study of panitumumab with FOLFOX4 for first-line treatment of metastatic colorectal cancer. *Annals of Oncology*, *25*(7), 1346–1355. https://doi.org/10.1093/annonc/mdu141

Dow, L. E., Elsum, I. A., King, C. L., Kinross, K. M., Richardson, H. E., & Humbert, P. O. (2008). Loss of human Scribble cooperates with H-Ras to promote cell invasion through deregulation of MAPK signalling. *Oncogene*, *27*(46), 5988–6001. https://doi.org/10.1038/onc.2008.219

Downward, J. (2003). Targeting RAS signalling pathways in cancer therapy. *Nature Reviews Cancer*, *3*(1), 11–22. https://doi.org/10.1038/nrc969

Drosten, M., & Barbacid, M. (2020). Targeting the MAPK Pathway in KRAS-Driven Tumors. *Cancer Cell*, *37*(4), 543–550. https://doi.org/10.1016/j.ccell.2020.03.013

du Plessis, S., Agarwal, A., Mohanty, G., & van der Linde, M. (2015). Oxidative phosphorylation versus glycolysis: what fuel do spermatozoa use? *Asian Journal of Andrology*, *17*(2), 230. https://doi.org/10.4103/1008-682X.135123

Du, Z., & Lovly, C. M. (2018). Mechanisms of receptor tyrosine kinase activation in cancer. *Molecular Cancer*, *17*(1), 58. https://doi.org/10.1186/s12943-018-0782-4

Ducreux, M., Chamseddine, A., Laurent-Puig, P., Smolenschi, C., Hollebecque, A., Dartigues, P., … Gelli, M. (2019). Molecular targeted therapy of BRAF -mutant colorectal cancer. *Therapeutic Advances in Medical Oncology*, *11*(6), 175883591985649. https://doi.org/10.1177/1758835919856494

Duncan, J. S., Whittle, M. C., Nakamura, K., Abell, A. N., Midland, A. A., Zawistowski, J. S., … Johnson, G. L. (2012). Dynamic reprogramming of the kinome in response to targeted MEK inhibition in triple-negative breast cancer. *Cell*, *149*(2), 307–321. https://doi.org/10.1016/j.cell.2012.02.053

Duronio, V. (2008). The life of a cell: Apoptosis regulation by the PI3K/PKB pathway. *Biochemical Journal*, *415*(3), 333–344. https://doi.org/10.1042/BJ20081056

Ebi, H., Corcoran, R. B., Singh, A., Chen, Z., Song, Y., Lifshits, E., … Engelman, J. A. (2011). Receptor tyrosine kinases exert dominant control over PI3K signaling in human KRAS mutant colorectal cancers. *Journal of Clinical Investigation*, *121*(11), 4311–4321. https://doi.org/10.1172/JCI57909

Eblen, S. T. (2018). Extracellular-Regulated Kinases: Signaling From Ras to ERK Substrates to Control Biological Outcomes. In *Cancer Res* (Vol. 138, pp. 99–142). https://doi.org/10.1016/bs.acr.2018.02.004

Edme, N., Downward, J., Thiery, J. P., & Boyer, B. (2002). Ras induces NBT-II epithelial cell scattering through the coordinate activities of Rac and MAPK pathways. *Journal of Cell Science*, *115*(12), 2591–2601.

Eichner, L. J., Brun, S. N., Herzig, S., Young, N. P., Curtis, S. D., Shackelford, D. B., … Svensson, R. U. (2019). Genetic Analysis Reveals AMPK Is Required to Support Tumor Growth in Murine Kras-Dependent Lung Cancer Models. *Cell Metabolism*, *29*(2), 285-302.e7. https://doi.org/10.1016/j.cmet.2018.10.005

Ekinci, E., Rohondia, S., Khan, R., & Dou, Q. P. (2019). Repurposing Disulfiram as An Anti-Cancer Agent: Updated Review on Literature and Patents. *Recent Patents on Anti-Cancer Drug Discovery*, *14*(2), 113–132. https://doi.org/10.2174/1574892814666190514104035

Ellis, L. M., Takahashi, Y., Liu, W., & Shaheen, R. M. (2000). Vascular endothelial growth factor in human colon cancer: biology and therapeutic implications. *The Oncologist*, *5 Suppl 1*, 11–15. https://doi.org/10.1634/theoncologist.5-suppl_1-11

Elschenbroich, S., Kim, Y., Medin, J. a, & Kislinger, T. (2010). Isolation of cell surface proteins for mass spectrometry-based proteomics. *Expert Review of Proteomics*, *7*(1), 141–154. https://doi.org/10.1586/epr.09.97

Eltzschig, H. K., Abdulla, P., Hoffman, E., Hamilton, K. E., Daniels, D., Schönfeld, C., … Colgan, S. P. (2005). HIF-1-dependent repression of equilibrative nucleoside transporter (ENT) in hypoxia. *The Journal of Experimental Medicine*, *202*(11), 1493–1505. https://doi.org/10.1084/jem.20050177

Emburgh, B. O. Van, Sartore-bianchi, A., Di, F., Siena, S., & Bardelli, A. (2014). ScienceDirect Acquired resistance to EGFR-targeted therapies in colorectal cancer, *8*.

Engelman, J. A., Chen, L., Tan, X., Crosby, K., Guimaraes, A. R., Upadhyay, R., … Wong, K.-K. (2008). Effective use of PI3K and MEK inhibitors to treat mutant Kras G12D and PIK3CA H1047R murine lung cancers. *Nature Medicine*, *14*(12), 1351–1356. https://doi.org/10.1038/nm.1890

Espina, C., Céspedes, M. V., García-Cabezas, M. A., Del Pulgar, M. T. G., Boluda, A., Oroz, L. G., … Lacal, J. C. (2008). A critical role for Rac1 in tumor progression of human colorectal adenocarcinoma cells. *American Journal of Pathology*, *172*(1), 156–166. https://doi.org/10.2353/ajpath.2008.070561

Esteller, M. (2002). CpG island hypermethylation and tumor suppressor genes: A booming present, a brighter future. *Oncogene*, *21*(35 REV. ISS. 3), 5427–5440. https://doi.org/10.1038/sj.onc.1205600

Estoppey, D., Hewett, J. W., Guy, C. T., Harrington, E., Thomas, J. R., Schirle, M., … Hoepfner, D. (2017). Identification of a novel NAMPT inhibitor by CRISPR/Cas9 chemogenomic profiling in mammalian cells. *Scientific Reports*, *7*, 42728. https://doi.org/10.1038/srep42728

Falvella, F. S., Cheli, S., Martinetti, A., Mazzali, C., Iacovelli, R., Maggi, C., … Pietrantonio, F. (2015). DPD and UGT1A1 deficiency in colorectal cancer patients receiving triplet chemotherapy with fluoropyrimidines, oxaliplatin and irinotecan. *British Journal of Clinical Pharmacology*, *80*(3), 581–588. https://doi.org/10.1111/bcp.12631

Fang, J. Y., & Richardson, B. C. (2005). The MAPK signalling pathways and colorectal cancer. *Lancet Oncology*, *6*(5), 322–327. https://doi.org/10.1016/S1470-2045(05)70168-6

Farhat, W., Azzaza, M., Mizouni, A., Ammar, H., Ben Ltaifa, M., Lagha, S., … Ali, A. Ben. (2019). Factors predicting recurrence after curative resection for rectal cancer: A 16-year study. *World Journal of Surgical Oncology*, *17*(1), 1–10. https://doi.org/10.1186/s12957-019-1718-1

Fearon, E. R. (2011). Molecular Genetics of Colorectal Cancer. *Annual Review of Pathology: Mechanisms of Disease*, *6*(1), 479–507. https://doi.org/10.1146/annurev-pathol-011110-130235

Fernandez, F. G., Drebin, J. A., Linehan, D. C., Dehdashti, F., Siegel, B. A., Strasberg, S. M., … Pinson, C. W. (2004). Five-year survival after resection of hepatic metastases from colorectal cancer in patients screened by positron emission tomography with F-18 fluorodeoxyglucose (FDG-PET). *Annals of Surgery*, *240*(3), 438–450. https://doi.org/10.1097/01.sla.0000138076.72547.b1

Ferreira, A. M., Ciriolo, M. R., Marcocci, L., & Rotilio, G. (1993). Copper(I) transfer into metallothionein mediated by glutathione. *The Biochemical Journal*, *292 (Pt 3*, 673–676. https://doi.org/10.1042/bj2920673

Ferreira, C. R., & Gahl, W. A. (2017). Disorders of metal metabolism. *Translational Science of*

Rare Diseases, *2*(3–4), 101–139. https://doi.org/10.3233/TRD-170015
Festa, R. A., & Thiele, D. J. (2011). Copper: an essential metal in biology. *Current Biology : CB*, *21*(21), R877-83. https://doi.org/10.1016/j.cub.2011.09.040
Formigari, A., Gregianin, E., & Irato, P. (2013). The effect of zinc and the role of p53 in copper-induced cellular stress responses. *Journal of Applied Toxicology : JAT*, *33*(7), 527–536. https://doi.org/10.1002/jat.2854
Fritsche-Guenther, R., Zasada, C., Mastrobuoni, G., Royla, N., Rainer, R., Roßner, F., … Kempa, S. (2018). Alterations of mTOR signaling impact metabolic stress resistance in colorectal carcinomas with BRAF and KRAS mutations. *Scientific Reports*, *8*(1), 1–17. https://doi.org/10.1038/s41598-018-27394-1
Gaglio, D., Metallo, C. M., Gameiro, P. A., Hiller, K., Danna, L. S., Balestrieri, C., … Chiaradonna, F. (2011). Oncogenic K-Ras decouples glucose and glutamine metabolism to support cancer cell growth. *Molecular Systems Biology*, *7*(523), 523. https://doi.org/10.1038/msb.2011.56
Galon, J. (2006). Type, Density, and Location of Immune Cells Within Human Colorectal Tumors Predict Clinical Outcome. *Science*, *313*(5795), 1960–1964. https://doi.org/10.1126/science.1129139
Gan, H. K., Millward, M., Hua, Y., Qi, C., Sai, Y., Su, W., … Lickliter, J. D. (2019). First-in-human phase I study of the selective MET inhibitor, savolitinib, in patients with advanced solid tumors: Safety, pharmacokinetics, and antitumor activity. *Clinical Cancer Research*, *25*(16), 4924–4932. https://doi.org/10.1158/1078-0432.CCR-18-1189
Gartner, E. M., Griffith, K. A., Pan, Q., Brewer, G. J., Henja, G. F., Merajver, S. D., & Zalupski, M. M. (2009). A pilot trial of the anti-angiogenic copper lowering agent tetrathiomolybdate in combination with irinotecan, 5-flurouracil, and leucovorin for metastatic colorectal cancer. *Investigational New Drugs*, *27*(2), 159–165. https://doi.org/10.1007/s10637-008-9165-9
Gaur, K., Vázquez-Salgado, A., Duran-Camacho, G., Dominguez-Martinez, I., Benjamín-Rivera, J., Fernández-Vega, L., … Tinoco, A. (2018). Iron and Copper Intracellular Chelation as an Anticancer Drug Strategy. *Inorganics*, *6*(4), 126. https://doi.org/10.3390/inorganics6040126
Gillies, T. E., Pargett, M., Silva, J. M., Teragawa, C., McCormick, F., & Albeck, J. G. (2020). Oncogenic mutant RAS signaling activity is rescaled by the ERK/MAPK pathway. *BioRxiv*, 2020.02.17.952093. https://doi.org/10.1101/2020.02.17.952093
Glynne-Jones, R., Wyrwicz, L., Tiret, E., Brown, G., Rödel, C., Cervantes, A., & Arnold, D. (2017). Rectal cancer: ESMO Clinical Practice Guidelines for diagnosis, treatment and follow-up. *Annals of Oncology*, *28*(Supplement 4), iv22–iv40. https://doi.org/10.1093/annonc/mdx224
Goede, V., Coutelle, O., Neuneier, J., Reinacher-Schick, A., Schnell, R., Koslowsky, T. C., … Hacker, U. T. (2010). Identification of serum angiopoietin-2 as a biomarker for clinical outcome of colorectal cancer patients treated with bevacizumab-containing therapy. *British Journal of Cancer*, *103*(9), 1407–1414. https://doi.org/10.1038/sj.bjc.6605925
Goldberg, R. M., Sargent, D. J., Morton, R. F., Fuchs, C. S., Ramanathan, R. K., Williamson, S. K., … Alberts, S. R. (2004). A randomized controlled trial of fluorouracil plus leucovorin, irinotecan, and oxaliplatin combinations in patients with previously untreated metastatic colorectal cancer. *Journal of Clinical Oncology*, *22*(1), 23–30. https://doi.org/10.1200/JCO.2004.09.046
González-Pérez, V., Reiner, D. J., Alan, J. K., Mitchell, C., Edwards, L. J., Khazak, V., … Cox,

A. D. (2010). Genetic and functional characterization of putative Ras/Raf interaction inhibitors in C. elegans and mammalian cells. *Journal of Molecular Signaling*, *5*, 2. https://doi.org/10.1186/1750-2187-5-2

Gonzalez, H., Hagerling, C., & Werb, Z. (2018). Roles of the immune system in cancer: From tumor initiation to metastatic progression. *Genes and Development*, *32*(19–20), 1267–1284. https://doi.org/10.1101/GAD.314617.118

Grothey, A., Sugrue, M. M., Purdie, D. M., Dong, W., Sargent, D., Hedrick, E., & Kozloff, M. (2008). Bevacizumab beyond first progression is associated with prolonged overall survival in metastatic colorectal cancer: Results from a large observational cohort study (BRiTE). *Journal of Clinical Oncology*, *26*(33), 5326–5334. https://doi.org/10.1200/JCO.2008.16.3212

Grothey, A., Van Cutsem, E., Sobrero, A., Siena, S., Falcone, A., Ychou, M., … Laurent, D. (2013). Regorafenib monotherapy for previously treated metastatic colorectal cancer (CORRECT): An international, multicentre, randomised, placebo-controlled, phase 3 trial. *The Lancet*, *381*(9863), 303–312. https://doi.org/10.1016/S0140-6736(12)61900-X

Gschwind, A., Fischer, O. M., & Ullrich, A. (2004). The discovery of receptor tyrosine kinases: targets for cancer therapy. *Nature Reviews. Cancer*, *4*(5), 361–370. https://doi.org/10.1038/nrc1360

Gudekar, N., Shanbhag, V., Wang, Y., Ralle, M., Weisman, G. A., & Petris, M. J. (2020). Metallothioneins regulate ATP7A trafficking and control cell viability during copper deficiency and excess. *Scientific Reports*, *10*(1), 1–11. https://doi.org/10.1038/s41598-020-64521-3

Guerrero, I., Villasante, A., Corces, V., & Pellicer, A. (1984). Activation of a c-K-ras oncogene by somatic mutation in mouse lymphomas induced by gamma radiation. *Science*, *225*(4667), 1159–1162. https://doi.org/10.1126/science.6474169

Gulec, S., & Collins, J. F. (2014). Silencing the Menkes copper-transporting ATPase (Atp7a) gene in rat intestinal epithelial (IEC-6) cells increases iron flux via transcriptional induction of ferroportin 1 (Fpn1). *The Journal of Nutrition*, *144*(1), 12–19. https://doi.org/10.3945/jn.113.183160

Guo, J. Y., Chen, H. Y., Mathew, R., Fan, J., Strohecker, A. M., Karsli-Uzunbas, G., … White, E. (2011). Activated Ras requires autophagy to maintain oxidative metabolism and tumorigenesis. *Genes and Development*, *25*(5), 460–470. https://doi.org/10.1101/gad.2016311

Guo, J. Y., Karsli-Uzunbas, G., Mathew, R., Aisner, S. C., Kamphorst, J. J., Strohecker, A. M., … White, E. (2013). Autophagy suppresses progression of K-ras-induced lung tumors to oncocytomas and maintains lipid homeostasis. *Genes and Development*, *27*(13), 1447–1461. https://doi.org/10.1101/gad.219642.113

Gupte, A., & Mumper, R. J. (2009). Elevated copper and oxidative stress in cancer cells as a target for cancer treatment. *Cancer Treatment Reviews*, *35*(1), 32–46. https://doi.org/10.1016/j.ctrv.2008.07.004

Gutierrez, L. S., Suckow, M., Lawler, J., Ploplis, V. A., & Castellino, F. J. (2003). Thrombospondin 1--a regulator of adenoma growth and carcinoma progression in the APC(Min/+) mouse model. *Carcinogenesis*, *24*(2), 199–207. https://doi.org/10.1093/carcin/24.2.199

Gybina, A. A., & Prohaska, J. R. (2008). Copper deficiency results in AMP-activated protein kinase activation and acetylCoA carboxylase phosphorylation in rat cerebellum. *Brain*

Research, *1204*, 69–76. https://doi.org/10.1016/j.brainres.2008.01.087
Ha, J.-H., Doguer, C., Wang, X., Flores, S. R., & Collins, J. F. (2016). High-Iron Consumption Impairs Growth and Causes Copper-Deficiency Anemia in Weanling Sprague-Dawley Rats. *PloS One*, *11*(8), e0161033. https://doi.org/10.1371/journal.pone.0161033
Habib, F. K., Dembinski, T. C., & Stitch, S. R. (1980). The zinc and copper content of blood leucocytes and plasma from patients with benign and malignant prostates. *Clinica Chimica Acta; International Journal of Clinical Chemistry*, *104*(3), 329–335. https://doi.org/10.1016/0009-8981(80)90390-3
Haigis, K. M., Kendall, K. R., Wang, Y., Cheung, A., Haigis, M. C., Glickman, J. N., … Jacks, T. (2008). Differential effects of oncogenic K-Ras and N-Ras on proliferation, differentiation and tumor progression in the colon. *Nature Genetics*, *40*(5), 600–608. https://doi.org/10.1038/ng.115
Hamad, N. M., Elconin, J. H., Karnoub, A. E., Bai, W., Rich, J. N., Abraham, R. T., … Counter, C. M. (2002). Distinct requirements for Ras oncogenesis in human versus mouse cells. *Genes and Development*, *16*(16), 2045–2057. https://doi.org/10.1101/gad.993902
Hamza, I, Faisst, A., Prohaska, J., Chen, J., Gruss, P., & Gitlin, J. D. (2001). The metallochaperone Atox1 plays a critical role in perinatal copper homeostasis. *Proceedings of the National Academy of Sciences of the United States of America*, *98*(12), 6848–6852. https://doi.org/10.1073/pnas.111058498
Hamza, Iqbal, Prohaska, J., & Gitlin, J. D. (2003). Essential role for Atox1 in the copper-mediated intracellular trafficking of the Menkes ATPase. *Proceedings of the National Academy of Sciences of the United States of America*, *100*(3), 1215–1220. https://doi.org/10.1073/pnas.0336230100
Hanafusa, H., Torii, S., Yasunaga, T., & Nishida, E. (2002). Sprouty1 and Sprouty2 provide a control mechanism for the Ras/MAPK signalling pathway. *Nature Cell Biology*, *4*(11), 850–858. https://doi.org/10.1038/ncb867
Hanahan, D., & Weinberg, R. A. (2011). Hallmarks of Cancer: The Next Generation. *Cell*, *144*(5), 646–674. https://doi.org/10.1016/j.cell.2011.02.013
Hancock, J. F. (2003). Ras proteins: different signals from different locations. *Nature Reviews. Molecular Cell Biology*, *4*(5), 373–384. https://doi.org/10.1038/nrm1105
Hancock, J. F., Magee, A. I., Childs, J. E., & Marshall, C. J. (1989). All ras proteins are polyisoprenylated but only some are palmitoylated. *Cell*, *57*(7), 1167–1177. https://doi.org/10.1016/0092-8674(89)90054-8
Harden, T. K., Hicks, S. N., & Sondek, J. (2009). Phospholipase C isozymes as effectors of Ras superfamily GTPases. *Journal of Lipid Research*, *50 Suppl*, S243-8. https://doi.org/10.1194/jlr.R800045-JLR200
Harris, E. D. (2000). Cellular copper transport and metabolism. *Annual Review of Nutrition*, *20*, 291–310. https://doi.org/10.1146/annurev.nutr.20.1.291
Hart, T., Chandrashekhar, M., Aregger, M., Durocher, D., Angers, S., Moffat, J., … Brown, K. R. (2015). High-Resolution CRISPR Screens Reveal Fitness Genes and Genotype-Specific Cancer Liabilities Screens Reveal Fitness Genes. *Cell*, *163*(6), 1515–1526. https://doi.org/10.1016/j.cell.2015.11.015
Hart, T., Hin, A., Tong, Y., Chan, K., Leeuwen, J. Van, Seetharaman, A., … Andrews, B. J. (2017). Evaluation and Design of Genome-Wide CRISPR / SpCas9 Knockout Screens, *7*(August), 2719–2727. https://doi.org/10.1534/g3.117.041277
Hart, T., & Moffat, J. (2016). BAGEL : a computational framework for identifying essential

genes from pooled library screens. *BMC Bioinformatics*, 1–7. https://doi.org/10.1186/s12859-016-1015-8
Hassouneh, B., Islam, M., Nagel, T., Pan, Q., Merajver, S. D., & Teknos, T. N. (2007). Tetrathiomolybdate promotes tumor necrosis and prevents distant metastases by suppressing angiogenesis in head and neck cancer. *Molecular Cancer Therapeutics*, *6*(3), 1039–1045. https://doi.org/10.1158/1535-7163.MCT-06-0524
Hata, A. N., & Shaw, A. T. (2020). Resistance looms for KRASG12C inhibitors. *Nature Medicine*, *26*(2), 169–170. https://doi.org/10.1038/s41591-020-0765-z
He, A. R., Cohen, R. B., Denlinger, C. S., Sama, A., Birnbaum, A., Hwang, J., … Plimack, E. R. (2019). First-in-Human Phase I Study of Merestinib, an Oral Multikinase Inhibitor, in Patients with Advanced Cancer. *The Oncologist*, *24*(9), 930–942. https://doi.org/10.1634/theoncologist.2018-0411
Hellman, N. E., & Gitlin, J. D. (2002). Etabolism and, *1948*(39). https://doi.org/10.1146/annurev.nutr.22.012502.114457
Heng, H. H., Bremer, S. W., Stevens, J. B., Horne, S. D., Liu, G., Abdallah, B. Y., … Ye, C. J. (2013). Chromosomal instability (CIN): what it is and why it is crucial to cancer evolution. *Cancer Metastasis Reviews*, *32*(3–4), 325–340. https://doi.org/10.1007/s10555-013-9427-7
Henry, N. L., Dunn, R., Merjaver, S., Pan, Q., Pienta, K. J., Brewer, G., & Smith, D. C. (2007). Phase II trial of copper depletion with tetrathiomolybdate as an antiangiogenesis strategy in patients with hormone-refractory prostate cancer. *Oncology*, *71*(3–4), 168–175. https://doi.org/10.1159/000106066
Herzig, S., & Shaw, R. J. (2018). AMPK: guardian of metabolism and mitochondrial homeostasis. *Nature Reviews. Molecular Cell Biology*, *19*(2), 121–135. https://doi.org/10.1038/nrm.2017.95
Hidalgo, M., Martinez-Garcia, M., Le Tourneau, C., Massard, C., Garralda, E., Boni, V., … Krieter, O. (2018). First-in-human phase i study of single-agent vanucizumab, a first-in-class bispecific anti-angiopoietin-2/anti-vegf-a antibody, in adult patients with advanced solid tumors. *Clinical Cancer Research*, *24*(7), 1536–1545. https://doi.org/10.1158/1078-0432.CCR-17-1588
Hill, W., & Hogan, C. (2019). Normal epithelial cells trigger EphA2-dependent RasV12 cell repulsion at the single cell level. *Small GTPases*, *10*(4), 305–310. https://doi.org/10.1080/21541248.2017.1324940
Hoare, M., Ito, Y., Kang, T.-W., Weekes, M. P., Matheson, N. J., Patten, D. A., … Narita, M. (2016). NOTCH1 mediates a switch between two distinct secretomes during senescence. *Nature Cell Biology*, *18*(9), 979–992. https://doi.org/10.1038/ncb3397
Hobbs, G. A., Der, C. J., & Rossman, K. L. (2016). RAS isoforms and mutations in cancer at a glance. *Journal of Cell Science*, *129*(7), 1287–1292. https://doi.org/10.1242/jcs.182873
Hodakoski, C., Hopkins, B. D., Zhang, G., Su, T., Cheng, Z., Morris, R., … Cantley, L. C. (2019). Rac-mediated macropinocytosis of extracellular protein promotes glucose independence in non-small cell lung cancer. *Cancers*, *11*(1). https://doi.org/10.3390/cancers11010037
Holch, J., Stintzing, S., & Heinemann, V. (2016). Treatment of Metastatic Colorectal Cancer: Standard of Care and Future Perspectives. *Visceral Medicine*, *32*(3), 178–183. https://doi.org/10.1159/000446052
Holt, M. C., Assar, Z., Beheshti Zavareh, R., Lin, L., Anglin, J., Mashadova, O., … Lyssiotis, C. A. (2018). Biochemical Characterization and Structure-Based Mutational Analysis Provide

Insight into the Binding and Mechanism of Action of Novel Aspartate Aminotransferase Inhibitors. *Biochemistry*, *57*(47), 6604–6614. https://doi.org/10.1021/acs.biochem.8b00914
Holzer, A. K., & Howell, S. B. (2006). The internalization and degradation of human copper transporter 1 following cisplatin exposure. *Cancer Research*, *66*(22), 10944–10952. https://doi.org/10.1158/0008-5472.CAN-06-1710
Hood, F. E., Klinger, B., Newlaczyl, A. U., Sieber, A., Dorel, M., Oliver, S. P., … Prior, I. A. (2019). Isoform-specific Ras signaling is growth factor dependent. *Molecular Biology of the Cell*, *30*(9), 1108–1117. https://doi.org/10.1091/mbc.E18-10-0676
Hörmann, K., Stukalov, A., Müller, A. C., Heinz, L. X., Superti-Furga, G., Colinge, J., & Bennett, K. L. (2016). A Surface Biotinylation Strategy for Reproducible Plasma Membrane Protein Purification and Tracking of Genetic and Drug-Induced Alterations. *Journal of Proteome Research*, *15*(2), 647–658. https://doi.org/10.1021/acs.jproteome.5b01066
Horng, Y.-C., Cobine, P. A., Maxfield, A. B., Carr, H. S., & Winge, D. R. (2004). Specific copper transfer from the Cox17 metallochaperone to both Sco1 and Cox11 in the assembly of yeast cytochrome C oxidase. *The Journal of Biological Chemistry*, *279*(34), 35334–35340. https://doi.org/10.1074/jbc.M404747200
Hsu, P. P., Kang, S. A., Rameseder, J., Zhang, Y., Ottina, K. A., Lim, D., … Sabatini, D. M. (2011). The mTOR-regulated phosphoproteome reveals a mechanism of mTORC1-mediated inhibition of growth factor signaling. *Science (New York, N.Y.)*, *332*(6035), 1317–1322. https://doi.org/10.1126/science.1199498
Hu, M., Chen, X., Ma, L., Ma, Y., Li, Y., Song, H., … Huang, P. (2019). AMPK Inhibition Suppresses the Malignant Phenotype of Pancreatic Cancer Cells in Part by Attenuating Aerobic Glycolysis. *Journal of Cancer*, *10*(8), 1870–1878. https://doi.org/10.7150/jca.28299
Huang, J., Chen, M., Xu, E. S., Luo, L., Ma, Y., Huang, W., … Kirsch, D. G. (2019). Genome-wide CRISPR Screen to Identify Genes that Suppress Transformation in the Presence of Endogenous KrasG12D. *Scientific Reports*, *9*(1), 17220. https://doi.org/10.1038/s41598-019-53572-w
Hunt, D. M. (1974). Primary defect in copper transport underlies mottled mutants in the mouse. *Nature*, *249*(460), 852–854. https://doi.org/10.1038/249852a0
Hunt, D. M., & Port, A. E. (1979). Trace element binding in the copper deficient mottled mutants in the mouse. *Life Sciences*, *24*(16), 1453–1466. https://doi.org/10.1016/0024-3205(79)90028-6
Hurwitz, H., Fehrenbacher, L., Novotny, W., Cartwright, T., Hainsworth, J., Heim, W., … Kabbinavar, F. (2004). Bevacizumab plus Irinotecan, Fluorouracil, and Leucovorin for Metastatic Colorectal Cancer. *New England Journal of Medicine*, *350*(23), 2335–2342. https://doi.org/10.1056/NEJMoa032691
Huss, M., & Wieczorek, H. (2009). Inhibitors of V-ATPases: old and new players. *The Journal of Experimental Biology*, *212*(Pt 3), 341–346. https://doi.org/10.1242/jeb.024067
Ijspeert, J. E. G., Vermeulen, L., Meijer, G. A., & Dekker, E. (2015). Serrated neoplasia-role in colorectal carcinogenesis and clinical implications. *Nature Reviews Gastroenterology and Hepatology*, *12*(7), 401–409. https://doi.org/10.1038/nrgastro.2015.73
Ikeda, N., Nakajima, Y., Sho, M., Adachi, M., Huang, C. L., Iki, K., … Miyake, M. (2001). The association of K-ras gene mutation and vascular endothelial growth factor gene expression in pancreatic carcinoma. *Cancer*, *92*(3), 488–499. https://doi.org/10.1002/1097-

0142(20010801)92:3<488::aid-cncr1347>3.0.co;2-f
Inesi, G. (2017). Critical Review Molecular Features of Copper Binding Proteins Involved in Copper Homeostasis. https://doi.org/10.1002/iub.1590
Ishida, S., Andreux, P., Poitry-Yamate, C., Auwerx, J., & Hanahan, D. (2013). Bioavailable copper modulates oxidative phosphorylation and growth of tumors. *Proceedings of the National Academy of Sciences of the United States of America*, *110*(48), 19507–19512. https://doi.org/10.1073/pnas.1318431110
Ishida, S., Lee, J., Thiele, D. J., & Herskowitz, I. (2002). Uptake of the anticancer drug cisplatin mediated by the copper transporter Ctr1 in yeast and mammals. *Proceedings of the National Academy of Sciences of the United States of America*, *99*(22), 14298–14302. https://doi.org/10.1073/pnas.162491399
Ishida, S., McCormick, F., Smith-McCune, K., & Hanahan, D. (2010). Enhancing tumor-specific uptake of the anticancer drug cisplatin with a copper chelator. *Cancer Cell*, *17*(6), 574–583. https://doi.org/10.1016/j.ccr.2010.04.011
Jackstadt, R., & Sansom, O. J. (2016). Mouse models of intestinal cancer. *The Journal of Pathology*, *238*(2), 141–151. https://doi.org/10.1002/path.4645
Jahangiri, A., De Lay, M., Miller, L. M., Carbonell, W. S., Hu, Y.-L., Lu, K., … Aghi, M. K. (2013). Gene Expression Profile Identifies Tyrosine Kinase c-Met as a Targetable Mediator of Antiangiogenic Therapy Resistance. *Clinical Cancer Research*, *19*(7), 1773–1783. https://doi.org/10.1158/1078-0432.CCR-12-1281
Jain, S., Cohen, J., Ward, M. M., Kornhauser, N., Chuang, E., Cigler, T., … Vahdat, L. T. (2013). Tetrathiomolybdate-associated copper depletion decreases circulating endothelial progenitor cells in women with breast cancer at high risk of relapse. *Annals of Oncology : Official Journal of the European Society for Medical Oncology*, *24*(6), 1491–1498. https://doi.org/10.1093/annonc/mds654
Janda, E., Lehmann, K., Killisch, I., Jechlinger, M., Herzig, M., Downward, J., … Grünert, S. (2002). Ras and TGFβ cooperatively regulate epithelial cell plasticity and metastasis: Dissection of Ras signaling pathways. *Journal of Cell Biology*, *156*(2), 299–313. https://doi.org/10.1083/jcb.200109037
Janes, M. R., Zhang, J., Li, L.-S., Hansen, R., Peters, U., Guo, X., … Liu, Y. (2018). Targeting KRAS Mutant Cancers with a Covalent G12C-Specific Inhibitor. *Cell*, *172*(3), 578-589.e17. https://doi.org/10.1016/j.cell.2018.01.006
Jeney, V., Itoh, S., Wendt, M., Gradek, Q., Ushio-Fukai, M., Harrison, D. G., & Fukai, T. (2005). Role of antioxidant-1 in extracellular superoxide dismutase function and expression. *Circulation Research*, *96*(7), 723–729. https://doi.org/10.1161/01.RES.0000162001.57896.66
Jiang, H., Grenley, M. O., Bravo, M.-J., Blumhagen, R. Z., & Edgar, B. A. (2011). EGFR/Ras/MAPK Signaling Mediates Adult Midgut Epithelial Homeostasis and Regeneration in Drosophila. *Cell Stem Cell*, *8*(1), 84–95. https://doi.org/10.1016/j.stem.2010.11.026
Johnson, L., Greenbaum, D., Cichowski, K., Mercer, K., Murphy, E., Schmitt, E., … Jacks, T. (1997). K-ras is an essential gene in the mouse with partial functional overlap with N-ras. *Genes and Development*, *11*(19), 2468–2481. https://doi.org/10.1101/gad.11.19.2468
Josiah, E. H., Xiaojing, W., Lisa, J., Robbert, J. C. S., Irina, A. T., Jamey, D. Y., … Daniel, C. L. (2016). Oncogenic KRAS and BRAF drive metabolic reprogramming in colorectal cancer. *Molecular and Cellular Proteomics*, *15*(9), 2924–2938.

https://doi.org/10.1074/mcp.M116.058925
Jost, M., Chen, Y., Gilbert, L. A., Horlbeck, M. A., Krenning, L., Menchon, G., … Weissman, J. S. (2017). Combined CRISPRi/a-Based Chemical Genetic Screens Reveal that Rigosertib Is a Microtubule-Destabilizing Agent. *Molecular Cell*, *68*(1), 210-223.e6. https://doi.org/10.1016/j.molcel.2017.09.012
Jost, M., & Weissman, J. S. (2018). CRISPR Approaches to Small Molecule Target Identification. *ACS Chemical Biology*, *13*(2), 366–375. https://doi.org/10.1021/acschembio.7b00965
Joyce, T., Cantarella, D., Isella, C., Medico, E., & Pintzas, A. (2009). A molecular signature for Epithelial to Mesenchymal transition in a human colon cancer cell system is revealed by large-scale microarray analysis. *Clinical & Experimental Metastasis*, *26*(6), 569–587. https://doi.org/10.1007/s10585-009-9256-9
Juneja, V. R., McGuire, K. A., Manguso, R. T., LaFleur, M. W., Collins, N., Nicholas Haining, W., … Sharpe, A. H. (2017). PD-L1 on tumor cells is sufficient for immune evasion in immunogenic tumors and inhibits CD8 T cell cytotoxicity. *Journal of Experimental Medicine*, *214*(4), 895–904. https://doi.org/10.1084/jem.20160801
Kalayda, G. V, Wagner, C. H., Buss, I., Reedijk, J., & Jaehde, U. (2008). Altered localisation of the copper efflux transporters ATP7A and ATP7B associated with cisplatin resistance in human ovarian carcinoma cells. *BMC Cancer*, *8*, 175. https://doi.org/10.1186/1471-2407-8-175
Kaler, S. G. (2011). and future trends, *7*(1), 15–29. https://doi.org/10.1038/nrneurol.2010.180.ATP7A-related
Kapiteijn, E., Marijnen, C. A. M., Nagtegaal, I. D., Putter, H., Steup, W. H., Wiggers, T., … van de Velde, C. J. H. (2001). Preoperative Radiotherapy Combined with Total Mesorectal Excision for Resectable Rectal Cancer. *New England Journal of Medicine*, *345*(9), 638–646. https://doi.org/10.1056/NEJMoa010580
Karnoub, A. E., & Weinberg, R. A. (2008). Ras oncogenes: split personalities. *Nature Reviews. Molecular Cell Biology*, *9*(7), 517–531. https://doi.org/10.1038/nrm2438
Katano, K., Kondo, A., Safaei, R., Holzer, A., Samimi, G., Mishima, M., … Howell, S. B. (2002). Acquisition of resistance to cisplatin is accompanied by changes in the cellular pharmacology of copper. *Cancer Research*, *62*(22), 6559–6565. Retrieved from http://www.ncbi.nlm.nih.gov/pubmed/12438251
Kato, R., Nonami, A., Taketomi, T., Wakioka, T., Kuroiwa, A., Matsuda, Y., & Yoshimura, A. (2003). Molecular cloning of mammalian Spred-3 which suppresses tyrosine kinase-mediated Erk activation. *Biochemical and Biophysical Research Communications*, *302*(4), 767–772. https://doi.org/10.1016/s0006-291x(03)00259-6
Kaur, J., & Debnath, J. (2015). Autophagy at the crossroads of catabolism and anabolism. *Nature Reviews Molecular Cell Biology*, *16*(8), 461–472. https://doi.org/10.1038/nrm4024
Kawakami, H., Zaanan, A., & Sinicrope, F. A. (2015). Microsatellite Instability Testing and Its Role in the Management of Colorectal Cancer. *Current Treatment Options in Oncology*, *16*(7), 30. https://doi.org/10.1007/s11864-015-0348-2
Keller, J. W., Franklin, J. L., Graves-Deal, R., Friedman, D. B., Whitwell, C. W., & Coffey, R. J. (2007). Oncogenic KRAS provides a uniquely powerful and variable oncogenic contribution among RAS family members in the colonic epithelium. *Journal of Cellular Physiology*, *210*(3), 740–749. https://doi.org/10.1002/jcp.20898
Kelley, G. G., Reks, S. E., Ondrako, J. M., & Smrcka, A. V. (2001). Phospholipase Cε: A novel

Ras effector. *EMBO Journal*, *20*(4), 743–754. https://doi.org/10.1093/emboj/20.4.743
Kelly, E. J., & Palmiter, R. D. (1996). A murine model of Menkes disease reveals a physiological function of metallothionein. *Nature Genetics*, *13*(2), 219–222. https://doi.org/10.1038/ng0696-219
Khambata-Ford, S., Garrett, C. R., Meropol, N. J., Basik, M., Harbison, C. T., Wu, S., … Mauro, D. J. (2007). Expression of epiregulin and amphiregulin and K-ras mutation status predict disease control in metastatic colorectal cancer patients treated with cetuximab. *Journal of Clinical Oncology*, *25*(22), 3230–3237. https://doi.org/10.1200/JCO.2006.10.5437
Khan, G., & Merajver, S. (2009). Copper chelation in cancer therapy using tetrathiomolybdate: an evolving paradigm. *Expert Opinion on Investigational Drugs*, *18*(4), 541–548. https://doi.org/10.1517/13543780902845622
Khan, M. K., Miller, M. W., Taylor, J., Gill, N. K., Dick, R. D., Van Goled, K., … Merajver, S. D. (2002). Radiotherapy and Antiangiogenic TM in Lung Cancer. *Neoplasia*, *4*(2), 164–170. https://doi.org/10.1038/sj.neo.7900218
Kikuchi, H., Pino, M. S., Zeng, M., Shirasawa, S., & Chung, D. C. (2009). Oncogenic KRAS and BRAF differentially regulate hypoxia-inducible factor-1alpha and -2alpha in colon cancer. *Cancer Research*, *69*(21), 8499–8506. https://doi.org/10.1158/0008-5472.CAN-09-2213
Kim, B.-E., Nevitt, T., & Thiele, D. J. (2008). Mechanisms for copper acquisition, distribution and regulation. *Nature Chemical Biology*, *4*(3), 176–185. https://doi.org/10.1038/nchembio.72
Kim, B.-E., & Petris, M. J. (2007). Phenotypic diversity of Menkes disease in mottled mice is associated with defects in localisation and trafficking of the ATP7A protein. *Journal of Medical Genetics*, *44*(10), 641–646. https://doi.org/10.1136/jmg.2007.049627
Kim, E., Jung, S., Park, W. S., Lee, J.-H., Shin, R., Heo, S. C., … Chai, Y. J. (2019). Upregulation of SLC2A3 gene and prognosis in colorectal carcinoma: analysis of TCGA data. *BMC Cancer*, *19*(1), 302. https://doi.org/10.1186/s12885-019-5475-x
Kim, Y. J., Tsang, T., Anderson, G. R., Posimo, J. M., & Brady, D. C. (2020). Inhibition of BCL2 family members increases the efficacy of copper chelation in BRAFV600E-driven melanoma. *Cancer Research*, *80*(7), 1387–1400. https://doi.org/10.1158/0008-5472.CAN-19-1784
Kinsey, C. G., Camolotto, S. A., Boespflug, A. M., Guillen, K. P., Foth, M., Truong, A., … McMahon, M. (2019). Protective autophagy elicited by RAF→MEK→ERK inhibition suggests a treatment strategy for RAS-driven cancers. *Nature Medicine*, *25*(4), 620–627. https://doi.org/10.1038/s41591-019-0367-9
Kitai, H., Ebi, H., Tomida, S., Floros, K. V, Kotani, H., Adachi, Y., … Yano, S. (2016). Epithelial-to-Mesenchymal Transition Defines Feedback Activation of Receptor Tyrosine Kinase Signaling Induced by MEK Inhibition in KRAS-Mutant Lung Cancer. *Cancer Discovery*, *6*(7), 754–769. https://doi.org/10.1158/2159-8290.CD-15-1377
Kodach, L. L., Wiercinska, E., de Miranda, N. F. C. C., Bleuming, S. A., Musler, A. R., Peppelenbosch, M. P., … Hardwick, J. C. H. (2008). The Bone Morphogenetic Protein Pathway Is Inactivated in the Majority of Sporadic Colorectal Cancers. *Gastroenterology*, *134*(5), 1332–1341. https://doi.org/10.1053/j.gastro.2008.02.059
Koehl, G. E., Spitzner, M., Ousingsawat, J., Schreiber, R., Geissler, E. K., & Kunzelmann, K. (2010). Rapamycin inhibits oncogenic intestinal ion channels and neoplasia in APC Min/+ mice. *Oncogene*, *29*(10), 1553–1560. https://doi.org/10.1038/onc.2009.435

Kohl, N. E., Omer, C. A., Conner, M. W., Anthony, N. J., Davide, J. P., Desolms, S. J., … Oliff, A. (1995). Inhibition of farnesyltransferase induces regression of mammary and salivary carcinomas in ras transgenic mice. *Nature Medicine*, *1*(8), 792–797. https://doi.org/10.1038/nm0895-792

Koivusalo, M., Welch, C., Hayashi, H., Scott, C. C., Kim, M., Alexander, T., … Grinstein, S. (2010). Amiloride inhibits macropinocytosis by lowering submembranous pH and preventing Rac1 and Cdc42 signaling, *188*(4), 547–563. https://doi.org/10.1083/jcb.200908086

Kolligs, F. T., Bommer, G., & Göke, B. (2002). Wnt/beta-catenin/Tcf signaling: A critical pathway in gastrointestinal tumorigenesis. *Digestion*, *66*(3), 131–144. https://doi.org/10.1159/000066755

Kopetz, S., Hoff, P. M., Morris, J. S., Wolff, R. A., Eng, C., Glover, K. Y., … Heymach, J. V. (2010). Phase II trial of infusional fluorouracil, irinotecan, and bevacizumab for metastatic colorectal cancer: Efficacy and circulating angiogenic biomarkers associated with therapeutic resistance. *Journal of Clinical Oncology*, *28*(3), 453–459. https://doi.org/10.1200/JCO.2009.24.8252

Kosinski, C., Li, V. S. W., Chan, A. S. Y., Zhang, J., Ho, C., Tsui, W. Y., … Chen, X. (2007). Gene expression patterns of human colon tops and basal crypts and BMP antagonists as intestinal stem cell niche factors. *Proceedings of the National Academy of Sciences of the United States of America*, *104*(39), 15418–15423. https://doi.org/10.1073/pnas.0707210104

Kranenburg, O., Gebbink, M. F. B. G., & Voest, E. E. (2004). Stimulation of angiogenesis by Ras proteins. *Biochimica et Biophysica Acta*, *1654*(1), 23–37. https://doi.org/10.1016/j.bbcan.2003.09.004

Kretzschmar, M., Doody, J., Timokhina, I., & Massagué, J. (1999). A mechanism of repression of TGFbeta/ Smad signaling by oncogenic Ras. *Genes & Development*, *13*(7), 804–816. https://doi.org/10.1101/gad.13.7.804

Kucharska, A., Rushworth, L. K., Staples, C., Morrice, N. A., & Keyse, S. M. (2009). Regulation of the inducible nuclear dual-specificity phosphatase DUSP5 by ERK MAPK. *Cellular Signalling*, *21*(12), 1794–1805. https://doi.org/10.1016/j.cellsig.2009.07.015

Kuo, Y. M., Zhou, B., Cosco, D., & Gitschier, J. (2001). The copper transporter CTR1 provides an essential function in mammalian embryonic development. *Proceedings of the National Academy of Sciences of the United States of America*, *98*(12), 6836–6841. https://doi.org/10.1073/pnas.111057298

Land, H., Parada, L. F., & Weinberg, R. A. (1983). Tumorigenic conversion of primary embryo fibroblasts requires at least two cooperating oncogenes. *Nature*, *304*(5927), 596–602. https://doi.org/10.1038/304596a0

Le, D. T., Kim, T. W., van Cutsem, E., Geva, R., Jäger, D., Hara, H., … André, T. (2020). Phase II open-label study of pembrolizumab in treatment-refractory, microsatellite instability–high/mismatch repair–deficient metastatic colorectal cancer: KEYNOTE-164. *Journal of Clinical Oncology*, *38*(1), 11–19. https://doi.org/10.1200/JCO.19.02107

Leach, D. R., Krummel, M. F., & Allison, J. P. (1996). Enhancement of antitumor immunity by CTLA-4 blockade. *Science*, *271*(5256), 1734–1736. https://doi.org/10.1126/science.271.5256.1734

Leary, R. J., Lin, J. C., Cummins, J., Boca, S., Wood, L. D., Parsons, D. W., … Velculescu, V. E. (2008). Integrated analysis of homozygous deletions, focal amplifications, and sequence alterations in breast and colorectal cancers. *Proceedings of the National Academy of*

Sciences of the United States of America, *105*(42), 16224–16229. https://doi.org/10.1073/pnas.0808041105
Lee, J., Pen, M. M. O., Nose, Y., & Thiele, D. J. (2002). Biochemical Characterization of the Human Copper Transporter Ctr1 *, *277*(6), 4380–4387. https://doi.org/10.1074/jbc.M104728200
Lee, J., Petris, M. J., & Thiele, D. J. (2002). Characterization of mouse embryonic cells deficient in the ctr1 high affinity copper transporter. Identification of a Ctr1-independent copper transport system. *The Journal of Biological Chemistry*, *277*(43), 40253–40259. https://doi.org/10.1074/jbc.M208002200
Lee, W., Lee, J. H., Jun, S., Lee, J. H., & Bang, D. (2018). Selective targeting of KRAS oncogenic alleles by CRISPR/Cas9 inhibits proliferation of cancer cells. *Scientific Reports*, *8*(1), 1–7. https://doi.org/10.1038/s41598-018-30205-2
Lemieux, E., Cagnol, S., Beaudry, K., Carrier, J., & Rivard, N. (2015). Oncogenic KRAS signalling promotes the Wnt/β-catenin pathway through LRP6 in colorectal cancer. *Oncogene*, *34*(38), 4914–4927. https://doi.org/10.1038/onc.2014.416
Lenartowicz, M., Krzeptowski, W., Lipiński, P., Grzmil, P., Starzyński, R., Pierzchała, O., & Møller, L. B. (2015). Mottled Mice and Non-Mammalian Models of Menkes Disease. *Frontiers in Molecular Neuroscience*, *8*, 72. https://doi.org/10.3389/fnmol.2015.00072
Leroy, C., Shen, Q., Strande, V., Meyer, R., McLaughlin, M. E., Lezan, E., … Alex Gaither, L. (2015). CUB-domain-containing protein 1 overexpression in solid cancers promotes cancer cell growth by activating Src family kinases. *Oncogene*, *34*(44), 5593–5598. https://doi.org/10.1038/onc.2015.19
Li, M., Edamatsu, H., Kitazawa, R., Kitazawa, S., & Kataoka, T. (2009). Phospholipase Cε promotes intestinal tumorigenesis of ApcMin/+ mice through augmentation of inflammation and angiogenesis. *Carcinogenesis*, *30*(8), 1424–1432. https://doi.org/10.1093/carcin/bgp125
Li, S., Balmain, A., & Counter, C. M. (2018). A model for RAS mutation patterns in cancers: finding the sweet spot. *Nature Reviews Cancer*, *18*(12), 767–777. https://doi.org/10.1038/s41568-018-0076-6
Lièvre, A., Bachet, J.-B., Le Corre, D., Boige, V., Landi, B., Emile, J.-F., … Laurent-Puig, P. (2006). KRAS mutation status is predictive of response to cetuximab therapy in colorectal cancer. *Cancer Research*, *66*(8), 3992–3995. https://doi.org/10.1158/0008-5472.CAN-06-0191
Lim, J., Yusoff, P., Wong, E. S. M., Chandramouli, S., Lao, D.-H., Fong, C. W., & Guy, G. R. (2002). The cysteine-rich sprouty translocation domain targets mitogen-activated protein kinase inhibitory proteins to phosphatidylinositol 4,5-bisphosphate in plasma membranes. *Molecular and Cellular Biology*, *22*(22), 7953–7966. https://doi.org/10.1128/mcb.22.22.7953-7966.2002
Lim, K. H., & Counter, C. M. (2005). Reduction in the requirement of oncogenic Ras signaling to activation of PI3K/AKT pathway during tumor maintenance. *Cancer Cell*, *8*(5), 381–392. https://doi.org/10.1016/j.ccr.2005.10.014
Lin, E. H., Lenz, H. J., Saleh, M. N., Mackenzie, M. J., Knost, J. A., Pathiraja, K., … Lu, B. D. (2014). A randomized, phase II study of the anti-insulin-like growth factor receptor type 1 (IGF-1R) monoclonal antibody robatumumab (SCH 717454) in patients with advanced colorectal cancer. *Cancer Medicine*, *3*(4), 988–997. https://doi.org/10.1002/cam4.263
Linder, M. C., Bryant, R. R., Lim, S., Scott, L. E., & Moor, J. E. (1979). Ceruloplasmin elevation and synthesis in rats with transplantable tumors. *Enzyme*, *24*(2), 85–95.

https://doi.org/10.1159/000458636
Linder, M. C., Moor, J. R., & Wright, K. (1981). Ceruloplasmin assays in diagnosis and treatment of human lung, breast, and gastrointestinal cancers. *Journal of the National Cancer Institute*, *67*(2), 263–275. Retrieved from http://www.ncbi.nlm.nih.gov/pubmed/6943365
Liu, Y., Cheng, Y., Xu, Y., Wang, Z., Du, X., Li, C., … Ma, C. (2017). Increased expression of programmed cell death protein 1 on NK cells inhibits NK-cell-mediated anti-tumor function and indicates poor prognosis in digestive cancers. *Oncogene*, *36*(44), 6143–6153. https://doi.org/10.1038/onc.2017.209
Liu, Yueyong, Pilankatta, R., Hatori, Y., Lewis, D., & Inesi, G. (2010). Comparative features of copper ATPases ATP7A and ATP7B heterologously expressed in COS-1 cells. *Biochemistry*, *49*(46), 10006–10012. https://doi.org/10.1021/bi101423j
Lock, R., Roy, S., Kenific, C. M., Su, J. S., Salas, E., Ronen, S. M., & Debnath, J. (2011). Autophagy facilitates glycolysis during Ras-mediated oncogenic transformation. *Molecular Biology of the Cell*, *22*(2), 165–178. https://doi.org/10.1091/mbc.E10-06-0500
Lopez, J., Ramchandani, C. D., & Vahdat, L. (2019). Copper Depletion as a Therapeutic Strategy in Cancer, 303–330.
Lou, K., Steri, V., Ge, A. Y., Hwang, Y. C., Christopher, H., Shkedi, A. R., … Gilbert, L. A. (2019). collateral dependencies, *12*(583). https://doi.org/10.1126/scisignal.aaw9450.KRAS
Lowndes, S. A., Adams, A., Timms, A., Fisher, N., Smythe, J., Watt, S. M., … Harris, A. L. (2008). Phase I study of copper-binding agent ATN-224 in patients with advanced solid tumors. *Clinical Cancer Research : An Official Journal of the American Association for Cancer Research*, *14*(22), 7526–7534. https://doi.org/10.1158/1078-0432.CCR-08-0315
Luque-García, J. L., Martínez-Torrecuadrada, J. L., Epifano, C., Cañamero, M., Babel, I., & Casal, J. I. (2010). Differential protein expression on the cell surface of colorectal cancer cells associated to tumor metastasis. *Proteomics*, *10*(5), 940–952. https://doi.org/10.1002/pmic.200900441
Lutsenko, S. (2017). HHS Public Access, *8*(9), 840–852. https://doi.org/10.1039/c6mt00176a.Copper
Lutsenko, S., Barnes, N. L., Bartee, M. Y., & Dmitriev, O. Y. (2007). Function and regulation of human copper-transporting ATPases. *Physiological Reviews*, *87*(3), 1011–1046. https://doi.org/10.1152/physrev.00004.2006
Ma, Y., Tang, N., Thompson, R. C., Mobley, B. C., Clark, S. W., Sarkaria, J. N., & Wang, J. (2016). InsR/IGF1R Pathway Mediates Resistance to EGFR Inhibitors in Glioblastoma. *Clinical Cancer Research*, *22*(7), 1767–1776. https://doi.org/10.1158/1078-0432.CCR-15-1677
Macleod, G., Bozek, D. A., Rajakulendran, N., Weiss, S., Dirks, P. B., Angers, S., … Ahmadi, M. (2019). Genome-Wide CRISPR-Cas9 Screens Expose Genetic Vulnerabilities and Mechanisms of Temozolomide Sensitivity in Glioblastoma Stem Resource Genome-Wide CRISPR-Cas9 Screens Expose Genetic Vulnerabilities and Mechanisms of Temozolomide Sensitivity in Glioblasto. *CellReports*, *27*(3), 971-986.e9. https://doi.org/10.1016/j.celrep.2019.03.047
Madsen, E. C., & Gitlin, J. D. (2008). Zebrafish mutants calamity and catastrophe define critical pathways of gene-nutrient interactions in developmental copper metabolism. *PLoS Genetics*, *4*(11), e1000261. https://doi.org/10.1371/journal.pgen.1000261
Maeda, K., Nishiguchi, Y., Yashiro, M., Yamada, S., Onoda, N., Sawada, T., … Hirakawa, K.

(2000). Expression of vascular endothelial growth factor and thrombospondin-1 in colorectal carcinoma. *International Journal of Molecular Medicine*, *5*(4), 373–378. https://doi.org/10.3892/ijmm.5.4.373

Mainardi, S., Mulero-Sánchez, A., Prahallad, A., Germano, G., Bosma, A., Krimpenfort, P., … Bernards, R. (2018). SHP2 is required for growth of KRAS-mutant non-small-cell lung cancer in vivo. *Nature Medicine*, *24*(7), 961–967. https://doi.org/10.1038/s41591-018-0023-9

Makrodouli, E., Oikonomou, E., Koc, M., Andera, L., Sasazuki, T., Shirasawa, S., & Pintzas, A. (2011). BRAF and RAS oncogenes regulate Rho GTPase pathways to mediate migration and invasion properties in human colon cancer cells: A comparative study. *Molecular Cancer*, *10*, 1–21. https://doi.org/10.1186/1476-4598-10-118

Malek, M., Kielkowska, A., Chessa, T., Anderson, K. E., Barneda, D., Pir, P., … Stephens, L. R. (2017). PTEN Regulates PI(3,4)P2 Signaling Downstream of Class I PI3K. *Molecular Cell*, *68*(3), 566-580.e10. https://doi.org/10.1016/j.molcel.2017.09.024

Malliri, A., Van der Kammen, R. A., Clark, K., Van der Valk, M., Michiels, F., & Collard, J. G. (2002). Mice deficient in the Rac activator Tiam1 are resistant to Ras-induced skin tumours. *Nature*, *417*(6891), 867–871. https://doi.org/10.1038/nature00848

Mancias, J. D., & Kimmelman, A. C. (2011). Targeting autophagy addiction in cancer. *Oncotarget*, *2*(12), 1302–1306. https://doi.org/10.18632/oncotarget.384

Marais, R., Light, Y., Paterson, H. F., & Marshall, C. J. (1995). Ras recruits Raf-1 to the plasma membrane far activation by tyrosine phosphorylation. *EMBO Journal*, *14*(13), 3136–3145. https://doi.org/10.1002/j.1460-2075.1995.tb07316.x

Martin, T. D., Samuel, J. C., Routh, E. D., Der, C. J., & Yeh, J. J. (2011). Activation and involvement of Ral GTPases in colorectal cancer. *Cancer Research*, *71*(1), 206–215. https://doi.org/10.1158/0008-5472.CAN-10-1517

Martinez-Balibrea, E., Martínez-Cardús, A., Musulén, E., Ginés, A., Manzano, J. L., Aranda, E., … Abad, A. (2009). Increased levels of copper efflux transporter ATP7B are associated with poor outcome in colorectal cancer patients receiving oxaliplatin-based chemotherapy. *International Journal of Cancer*, *124*(12), 2905–2910. https://doi.org/10.1002/ijc.24273

Martins, S. F., Garcia, E. A., Luz, M. A. M., Pardal, F., Rodrigues, M., & Filho, A. L. (2013). Clinicopathological correlation and prognostic significance of VEGF-A, VEGF-C, VEGFR-2 and VEGFR-3 expression in Colorectal cancer. *Cancer Genomics and Proteomics*, *10*(2), 55–68.

Mason, J. A., Davison-Versagli, C. A., Leliaert, A. K., Pape, D. J., McCallister, C., Zuo, J., … Schafer, Z. T. (2016). Oncogenic Ras differentially regulates metabolism and anoikis in extracellular matrix-detached cells. *Cell Death and Differentiation*, *23*(8), 1271–1282. https://doi.org/10.1038/cdd.2016.15

Mathias, R. A., Chen, Y.-S., Wang, B., Ji, H., Kapp, E. A., Moritz, R. L., … Simpson, R. J. (2010). Extracellular remodelling during oncogenic Ras-induced epithelial-mesenchymal transition facilitates MDCK cell migration. *Journal of Proteome Research*, *9*(2), 1007–1019. https://doi.org/10.1021/pr900907g

Matsui, M. S., Petris, M. J., Niki, Y., Karaman-Jurukovska, N., Muizzuddin, N., Ichihashi, M., & Yarosh, D. B. (2015). Omeprazole, a gastric proton pump inhibitor, inhibits melanogenesis by blocking ATP7A trafficking. *The Journal of Investigative Dermatology*, *135*(3), 834–841. https://doi.org/10.1038/jid.2014.461

Matsuo, Y., Campbell, P. M., Brekken, R. A., Sung, B., Ouellette, M. M., Fleming, J. B., …

Guha, S. (2009). K-Ras promotes angiogenesis mediated by immortalized human pancreatic epithelial cells through mitogen-activated protein kinase signaling pathways. *Molecular Cancer Research : MCR*, *7*(6), 799–808. https://doi.org/10.1158/1541-7786.MCR-08-0577

McAuslan, B. R., & Reilly, W. (1980). Endothelial cell phagokinesis in response to specific metal ions. *Experimental Cell Research*, *130*(1), 147–157. https://doi.org/10.1016/0014-4827(80)90051-8

McFall, A., Ülkü, A., Lambert, Q. T., Kusa, A., Rogers-Graham, K., & Der, C. J. (2001). Oncogenic Ras Blocks Anoikis by Activation of a Novel Effector Pathway Independent of Phosphatidylinositol 3-Kinase. *Molecular and Cellular Biology*, *21*(16), 5488–5499. https://doi.org/10.1128/mcb.21.16.5488-5499.2001

Milenkovic, D., Blaza, J. N., Larsson, N.-G., & Hirst, J. (2017). The Enigma of the Respiratory Chain Supercomplex. *Cell Metabolism*, *25*(4), 765–776. https://doi.org/10.1016/j.cmet.2017.03.009

Milewska, M., Romano, D., Herrero, A., Guerriero, M. L., Birtwistle, M., Quehenberger, F., … Zebisch, A. (2015). Mitogen-Inducible Gene-6 Mediates Feedback Inhibition from Mutated BRAF towards the Epidermal Growth Factor Receptor and Thereby Limits Malignant Transformation. *PloS One*, *10*(6), e0129859. https://doi.org/10.1371/journal.pone.0129859

Misale, S., Yaeger, R., Hobor, S., Scala, E., Janakiraman, M., Liska, D., … Bardelli, A. (2012). Emergence of KRAS mutations and acquired resistance to anti-EGFR therapy in colorectal cancer. *Nature*, *486*(7404), 532–536. https://doi.org/10.1038/nature11156

Moghadam, A. R., Patrad, E., Tafsiri, E., Peng, W., Fangman, B., Pluard, T. J., … Farassati, F. (2017). Ral signaling pathway in health and cancer. *Cancer Medicine*, *6*(12), 2998–3013. https://doi.org/10.1002/cam4.1105

Mookerjee, S. A., Gerencser, A. A., Nicholls, D. G., & Brand, M. D. (2017). Quantifying intracellular rates of glycolytic and oxidative ATP production and consumption using extracellular flux, *292*, 7189–7207. https://doi.org/10.1074/jbc.M116.774471

Morgan, M. T., Bourassa, D., Harankhedkar, S., Mccallum, A. M., & Zlatic, S. A. (2019). Ratiometric two-photon microscopy reveals attomolar copper buffering in normal and Menkes mutant cells, *116*(25). https://doi.org/10.1073/pnas.1900172116

Morris, E. J., Jha, S., Restaino, C. R., Dayananth, P., Zhu, H., Cooper, A., … Samatar, A. A. (2013). Discovery of a novel ERK inhibitor with activity in models of acquired resistance to BRAF and MEK inhibitors. *Cancer Discovery*, *3*(7), 742–750. https://doi.org/10.1158/2159-8290.CD-13-0070

Moser, A. R., Pitot, H. C., & Dove, W. F. (1990). A dominant mutation that predisposes to multiple intestinal neoplasia in the mouse. *Science*, *247*(4940), 322–324. https://doi.org/10.1126/science.2296722

Mukhopadhyay, S., Goswami, D., Adiseshaiah, P. P., Burgan, W., Yi, M., Guerin, T. M., … McCormick, F. (2020). Undermining Glutaminolysis Bolsters Chemotherapy While NRF2 Promotes Chemoresistance in KRAS-Driven Pancreatic Cancers. *Cancer Research*, *80*(8), 1630–1643. https://doi.org/10.1158/0008-5472.CAN-19-1363

Munro, M. J., Wickremesekera, S. K., Peng, L., Tan, S. T., & Itinteang, T. (2018). Cancer stem cells in colorectal cancer: A review. *Journal of Clinical Pathology*, *71*(2), 110–116. https://doi.org/10.1136/jclinpath-2017-204739

Mus, L. M., Lambertz, I., Claeys, S., Kumps, C., Van Loocke, W., Van Neste, C., … Speleman, F. (2020). The ETS transcription factor ETV5 is a target of activated ALK in neuroblastoma contributing to increased tumour aggressiveness. *Scientific Reports*, *10*(1), 218.

https://doi.org/10.1038/s41598-019-57076-5
Muvaffak, A., Pan, Q., Yan, H., Fernandez, R., Lim, J., Dolinski, B., … Wang, Y. (2014). Evaluating TBK1 as a therapeutic target in cancers with activated IRF3. *Molecular Cancer Research : MCR*, *12*(7), 1055–1066. https://doi.org/10.1158/1541-7786.MCR-13-0642
Nayak, S. B., Bhat, V. R., Upadhyay, D., & Udupa, S. L. (2003). Copper and ceruloplasmin status in serum of prostate and colon cancer patients. *Indian Journal of Physiology and Pharmacology*, *47*(1), 108–110. Retrieved from http://www.ncbi.nlm.nih.gov/pubmed/12708132
Neel, N. F., Martin, T. D., Stratford, J. K., Zand, T. P., Reiner, D. J., & Der, C. J. (2011). The RalGEF-ral effector signaling network: The road less traveled for anti-ras drug discovery. *Genes and Cancer*, *2*(3), 275–287. https://doi.org/10.1177/1947601911407329
Nevitt, T., Ohrvik, H., & Thiele, D. J. (2012). Charting the travels of copper in eukaryotes from yeast to mammals. *Biochimica et Biophysica Acta*, *1823*(9), 1580–1593. https://doi.org/10.1016/j.bbamcr.2012.02.011
Newbold, R. F., & Overell, R. W. (1983). Fibroblast immortality is a prerequisite for transformation by EJ c-Ha-ras oncogene. *Nature*, *304*(5927), 648–651. https://doi.org/10.1038/304648a0
Niikura, K., Takano, M., & Sawada, M. (2004). A novel inhibitor of vacuolar ATPase, FR167356, which can discriminate between osteoclast vacuolar ATPase and lysosomal vacuolar ATPase. *British Journal of Pharmacology*, *142*(3), 558–566. https://doi.org/10.1038/sj.bjp.0705812
Nittis, T., & Gitlin, J. D. (2004). Role of copper in the proteosome-mediated degradation of the multicopper oxidase hephaestin. *The Journal of Biological Chemistry*, *279*(24), 25696–25702. https://doi.org/10.1074/jbc.M401151200
Nose, Y., Kim, B.-E., & Thiele, D. J. (2006). Ctr1 drives intestinal copper absorption and is essential for growth, iron metabolism, and neonatal cardiac function. *Cell Metabolism*, *4*(3), 235–244. https://doi.org/10.1016/j.cmet.2006.08.009
Öhrvik, H., Nose, Y., Wood, L. K., Kim, B.-E., Gleber, S.-C., Ralle, M., & Thiele, D. J. (2013). Ctr2 regulates biogenesis of a cleaved form of mammalian Ctr1 metal transporter lacking the copper- and cisplatin-binding ecto-domain. *Proceedings of the National Academy of Sciences of the United States of America*, *110*(46), E4279-88. https://doi.org/10.1073/pnas.1311749110
Öhrvik, H., & Thiele, D. J. (2014). How copper traverses cellular membranes through the mammalian copper transporter 1, Ctr1. *Annals of the New York Academy of Sciences*, *1314*(1), 32–41. https://doi.org/10.1111/nyas.12371
Oikonomou, E., Koustas, E., Goulielmaki, M., & Pintzas, A. (2014). BRAF vs RAS oncogenes: are mutations of the same pathway equal? Differential signalling and therapeutic implications. *Oncotarget*, *5*(23), 11752–11777. https://doi.org/10.18632/oncotarget.2555
Okada, Y., Kimura, T., Nakagawa, T., Okamoto, K., Fukuya, A., Goji, T., … Takayama, T. (2017). EGFR downregulation after anti-EGFR therapy predicts the antitumor effect in colorectal cancer. *Molecular Cancer Research*, *15*(10), 1445–1454. https://doi.org/10.1158/1541-7786.MCR-16-0383
Okita, N. T., Yamada, Y., Takahari, D., Hirashima, Y., Matsubara, J., Kato, K., … Shimoda, T. (2009). Vascular endothelial growth factor receptor expression as a prognostic marker for survival in colorectal cancer. *Japanese Journal of Clinical Oncology*, *39*(9), 595–600. https://doi.org/10.1093/jjco/hyp066

Ostrakhovitch, E A, & Cherian, M. G. (2005). Role of p53 and reactive oxygen species in apoptotic response to copper and zinc in epithelial breast cancer cells. *Apoptosis : An International Journal on Programmed Cell Death*, *10*(1), 111–121. https://doi.org/10.1007/s10495-005-6066-7

Ostrakhovitch, Elena A, Olsson, P.-E., von Hofsten, J., & Cherian, M. G. (2007). P53 mediated regulation of metallothionein transcription in breast cancer cells. *Journal of Cellular Biochemistry*, *102*(6), 1571–1583. https://doi.org/10.1002/jcb.21381

Ostrem, J. M., Peters, U., Sos, M. L., Wells, J. A., & Shokat, K. M. (2013). K-Ras(G12C) inhibitors allosterically control GTP affinity and effector interactions. *Nature*, *503*(7477), 548–551. https://doi.org/10.1038/nature12796

Overman, M. J., McDermott, R., Leach, J. L., Lonardi, S., Lenz, H., Morse, M. A., … André, T. (2017). Nivolumab in patients with metastatic DNA mismatch repair-deficient or microsatellite instability-high colorectal cancer (CheckMate 142): an open-label, multicentre, phase 2 study. *The Lancet Oncology*, *18*(9), 1182–1191. https://doi.org/10.1016/S1470-2045(17)30422-9

Paciucci, R., Torà, M., Díaz, V. M., & Real, F. X. (1998). The plasminogen activator system in pancreas cancer: role of t-PA in the invasive potential in vitro. *Oncogene*, *16*(5), 625–633. https://doi.org/10.1038/sj.onc.1201564

Packman, S. (1987). Regulation of copper metabolism in the mottled mouse. *Archives of Dermatology*, *123*(11), 1545-1547a. http://www.ncbi.nlm.nih.gov/pubmed/3674914

Palm, M. E., Weise, C. F., Lundin, C., Wingsle, G., Nygren, Y., Björn, E., … Wittung-Stafshede, P. (2011). Cisplatin binds human copper chaperone Atox1 and promotes unfolding in vitro. *Proceedings of the National Academy of Sciences of the United States of America*, *108*(17), 6951–6956. https://doi.org/10.1073/pnas.1012899108

Palorini, R., Simonetto, T., Cirulli, C., & Chiaradonna, F. (2013). Mitochondrial complex I inhibitors and forced oxidative phosphorylation synergize in inducing cancer cell death. *International Journal of Cell Biology*, *2013*, 243876. https://doi.org/10.1155/2013/243876

Pan, Q., Bao, L. W., Kleer, C. G., Brewer, G. J., & Merajver, S. D. (2003). Antiangiogenic tetrathiomolybdate enhances the efficacy of doxorubicin against breast carcinoma. *Molecular Cancer Therapeutics*, *2*(7), 617–622. Retrieved from http://www.ncbi.nlm.nih.gov/pubmed/12883034

Pan, Q., Kleer, C. G., van Golen, K. L., Irani, J., Bottema, K. M., Bias, C., … Merajver, S. D. (2002). Copper deficiency induced by tetrathiomolybdate suppresses tumor growth and angiogenesis. *Cancer Research*, *62*(17), 4854–4859. Retrieved from http://www.ncbi.nlm.nih.gov/pubmed/12208730

Papke, B., Murarka, S., Vogel, H. A., Martín-Gago, P., Kovacevic, M., Truxius, D. C., … Bastiaens, P. I. H. (2016). Identification of pyrazolopyridazinones as PDEδ inhibitors. *Nature Communications*, *7*, 11360. https://doi.org/10.1038/ncomms11360

Paradis, J. S., Ly, S., Blondel-Tepaz, É., Galan, J. A., Beautrait, A., Scott, M. G. H., … Bouvier, M. (2015). Receptor sequestration in response to β-arrestin-2 phosphorylation by ERK1/2 governs steady-state levels of GPCR cell-surface expression. *Proceedings of the National Academy of Sciences*, (October), 201508836. https://doi.org/10.1073/pnas.1508836112

Pass, H. I., Brewer, G. J., Dick, R., Carbone, M., & Merajver, S. (2008). A phase II trial of tetrathiomolybdate after surgery for malignant mesothelioma: final results. *The Annals of Thoracic Surgery*, *86*(2), 383–389; discussion 390. https://doi.org/10.1016/j.athoracsur.2008.03.016

Passardi, A., Canale, M., Valgiusti, M., & Ulivi, P. (2017). Immune checkpoints as a target for colorectal cancer treatment. *International Journal of Molecular Sciences*, *18*(6). https://doi.org/10.3390/ijms18061324

Pastor-Anglada, M., & Pérez-Torras, S. (2018). Who Is Who in Adenosine Transport. *Frontiers in Pharmacology*, *9*, 627. https://doi.org/10.3389/fphar.2018.00627

Peri, F., Airoldi, C., Colombo, S., Martegani, E., van Neuren, A. S., Stein, M., … Nicotra, F. (2005). Design, synthesis and biological evaluation of sugar-derived Ras inhibitors. *Chembiochem : A European Journal of Chemical Biology*, *6*(10), 1839–1848. https://doi.org/10.1002/cbic.200400420

Petris, M J, & Mercer, J. F. (1999). The Menkes protein (ATP7A; MNK) cycles via the plasma membrane both in basal and elevated extracellular copper using a C-terminal di-leucine endocytic signal. *Human Molecular Genetics*, *8*(11), 2107–2115. https://doi.org/10.1093/hmg/8.11.2107

Petris, M J, Mercer, J. F., Culvenor, J. G., Lockhart, P., Gleeson, P. A., & Camakaris, J. (1996). Ligand-regulated transport of the Menkes copper P-type ATPase efflux pump from the Golgi apparatus to the plasma membrane: a novel mechanism of regulated trafficking. *The EMBO Journal*, *15*(22), 6084–6095. Retrieved from http://www.ncbi.nlm.nih.gov/pubmed/8947031

Petris, Michael J, Smith, K., Lee, J., & Thiele, D. J. (2003). Copper-stimulated endocytosis and degradation of the human copper transporter, hCtr1. *The Journal of Biological Chemistry*, *278*(11), 9639–9646. https://doi.org/10.1074/jbc.M209455200

Phillips, M., Camakaris, J., & Danks, D. M. (1986). Comparisons of copper deficiency states in the murine mutants blotchy and brindled. Changes in copper-dependent enzyme activity in 13-day-old mice. *The Biochemical Journal*, *238*(1), 177–183. https://doi.org/10.1042/bj2380177

Pires, A. S., Marques, C. R., Encarnação, J. C., Abrantes, A. M., Marques, I. A., Laranjo, M., … Botelho, M. F. (2018). Ascorbic Acid Chemosensitizes Colorectal Cancer Cells and Synergistically Inhibits Tumor Growth. *Frontiers in Physiology*, *9*, 911. https://doi.org/10.3389/fphys.2018.00911

Polishchuk, E. V, & Polishchuk, R. S. (2016). The emerging role of lysosomes in copper homeostasis. *Metallomics : Integrated Biometal Science*, *8*(9), 853–862. https://doi.org/10.1039/c6mt00058d

Pottier, C., Fresnais, M., Gilon, M., Jérusalem, G., Longuespée, R., & Sounni, N. E. (2020). Tyrosine Kinase Inhibitors in Cancer: Breakthrough and Challenges of Targeted Therapy. *Cancers*, *12*(3). https://doi.org/10.3390/cancers12030731

Prachayasittikul, V., Prachayasittikul, S., Ruchirawat, S., & Prachayasittikul, V. (2013). 8-Hydroxyquinolines: a review of their metal chelating properties and medicinal applications. *Drug Design, Development and Therapy*, *7*, 1157–1178. https://doi.org/10.2147/DDDT.S49763

Prior, I. A., Harding, A., Yan, J., Sluimer, J., Parton, R. G., & Hancock, J. F. (2001). GTP-dependent segregation of H-ras from lipid rafts is required for biological activity. *Nature Cell Biology*, *3*(4), 368–375. https://doi.org/10.1038/35070050

Prior, I. A., Lewis, P. D., & Mattos, C. (2012). A comprehensive survey of ras mutations in cancer. *Cancer Research*, *72*(10), 2457–2467. https://doi.org/10.1158/0008-5472.CAN-11-2612

Prior, I. A., Muncke, C., Parton, R. G., & Hancock, J. F. (2003). Direct visualization of ras

proteins in spatially distinct cell surface microdomains. *Journal of Cell Biology*, *160*(2), 165–170. https://doi.org/10.1083/jcb.200209091

Prohaska, J R, Downing, S. W., & Lukasewycz, O. A. (1983). Chronic dietary copper deficiency alters biochemical and morphological properties of mouse lymphoid tissues. *The Journal of Nutrition*, *113*(8), 1583–1590. https://doi.org/10.1093/jn/113.8.1583

Prohaska, Joseph R, Geissler, J., Brokate, B., & Broderius, M. (2003). Copper, zinc-superoxide dismutase protein but not mRNA is lower in copper-deficient mice and mice lacking the copper chaperone for superoxide dismutase. *Experimental Biology and Medicine (Maywood, N.J.)*, *228*(8), 959–966. https://doi.org/10.1177/153537020322800812

Punt, C. J. A., Koopman, M., & Vermeulen, L. (2017). From tumour heterogeneity to advances in precision treatment of colorectal cancer. *Nature Reviews Clinical Oncology*, *14*(4), 235–246. https://doi.org/10.1038/nrclinonc.2016.171

Pupo, E., Avanzato, D., Middonti, E., Bussolino, F., & Lanzetti, L. (2019). KRAS-Driven Metabolic Rewiring Reveals Novel Actionable Targets in Cancer. *Frontiers in Oncology*, *9*, 848. https://doi.org/10.3389/fonc.2019.00848

Pylayeva-Gupta, Y., Grabocka, E., & Bar-Sagi, D. (2011). RAS oncogenes: weaving a tumorigenic web. *Nature Reviews. Cancer*, *11*(11), 761–774. https://doi.org/10.1038/nrc3106

Qin, Z., Itoh, S., Jeney, V., Ushio-Fukai, M., & Fukai, T. (2006). Essential role for the Menkes ATPase in activation of extracellular superoxide dismutase: implication for vascular oxidative stress. *FASEB Journal : Official Publication of the Federation of American Societies for Experimental Biology*, *20*(2), 334–336. https://doi.org/10.1096/fj.05-4564fje

Quinlan, M. P., & Settleman, J. (2009). Isoform-specific ras functions in development and cancer. *Future Oncology*, *5*(1), 105–116. https://doi.org/10.2217/14796694.5.1.105

Rae, C., Tesson, M., Babich, J. W., Boyd, M., Sorensen, A., & Mairs, R. J. (2013). The role of copper in disulfiram-induced toxicity and radiosensitization of cancer cells. *Journal of Nuclear Medicine : Official Publication, Society of Nuclear Medicine*, *54*(6), 953–960. https://doi.org/10.2967/jnumed.112.113324

Rae, T. D., Schmidt, P. J., Pufahl, R. A., Culotta, V. C., & O'Halloran, T. V. (1999). Undetectable intracellular free copper: the requirement of a copper chaperone for superoxide dismutase. *Science (New York, N.Y.)*, *284*(5415), 805–808. https://doi.org/10.1126/science.284.5415.805

Raju, K. S., Alessandri, G., Ziche, M., & Gullino, P. M. (1982). Ceruloplasmin, copper ions, and angiogenesis. *Journal of the National Cancer Institute*, *69*(5), 1183–1188. Retrieved from http://www.ncbi.nlm.nih.gov/pubmed/6182332

Ramirez, C., Hauser, A. D., Vucic, E. A., & Bar-Sagi, D. (2019). Plasma membrane V-ATPase controls oncogenic RAS-induced macropinocytosis. *Nature*, *576*(7787), 477–481. https://doi.org/10.1038/s41586-019-1831-x

Ramos-Esquivel, A. (2018). Duration of adjuvant chemotherapy for stage III colon cancer. *New England Journal of Medicine*, *379*(4), 395. https://doi.org/10.1056/NEJMc1805498

Rao, S., Setty, G., Tenza, D., Sviderskaya, E. V, Bennett, D. C., Raposo, G., & Marks, M. S. (2010). NIH Public Access, *454*(7208), 1142–1146. https://doi.org/10.1038/nature07163.Cell-specific

Recouvreux, M. V., & Commisso, C. (2017). Macropinocytosis: A Metabolic Adaptation to Nutrient Stress in Cancer. *Frontiers in Endocrinology*, *8*, 261. https://doi.org/10.3389/fendo.2017.00261

Redman, B. G., Esper, P., Pan, Q., Dunn, R. L., Hussain, H. K., Chenevert, T., … Merajver, S. D. (2003). Phase II trial of tetrathiomolybdate in patients with advanced kidney cancer. *Clinical Cancer Research : An Official Journal of the American Association for Cancer Research*, *9*(5), 1666–1672. Retrieved from http://www.ncbi.nlm.nih.gov/pubmed/12738719

Rees, E. M., & Thiele, D. J. (2007). Identification of a vacuole-associated metalloreductase and its role in Ctr2-mediated intracellular copper mobilization. *The Journal of Biological Chemistry*, *282*(30), 21629–21638. https://doi.org/10.1074/jbc.M703397200

Rhim, A. D., Mirek, E. T., Aiello, N. M., Maitra, A., Bailey, J. M., McAllister, F., … Stanger, B. Z. (2012). EMT and Dissemination Precede Pancreatic Tumor Formation. *Cell*, *148*(1–2), 349–361. https://doi.org/10.1016/j.cell.2011.11.025

Riechelmann, R., & Grothey, A. (2017). Antiangiogenic therapy for refractory colorectal cancer: current options and future strategies. *Therapeutic Advances in Medical Oncology*, *9*(2), 106–126. https://doi.org/10.1177/1758834016676703

Riedl, A., Schlederer, M., Pudelko, K., Stadler, M., Walter, S., Unterleuthner, D., … Dolznig, H. (2017). Comparison of cancer cells in 2D vs 3D culture reveals differences in AKT–mTOR–S6K signaling and drug responses. *Journal of Cell Science*, *130*(1), 203–218. https://doi.org/10.1242/jcs.188102

Rizk, S. L., & Sky-Peck, H. H. (1984). Comparison between concentrations of trace elements in normal and neoplastic human breast tissue. *Cancer Research*, *44*(11), 5390–5394. Retrieved from http://www.ncbi.nlm.nih.gov/pubmed/6488192

Rödel, C., Grabenbauer, G. G., Papadopoulos, T., Hohenberger, W., Schmoll, H. J., & Sauer, R. (2003). Phase I/II trial of capecitabine, oxaliplatin, and radiation for rectal cancer. *Journal of Clinical Oncology*, *21*(16), 3098–3104. https://doi.org/10.1200/JCO.2003.02.505

Rose, J. B., Naydenova, Z., Bang, A., Ramadan, A., Klawitter, J., Schram, K., … Coe, I. R. (2011). Absence of equilibrative nucleoside transporter 1 in ENT1 knockout mice leads to altered nucleoside levels following hypoxic challenge. *Life Sciences*, *89*(17–18), 621–630. https://doi.org/10.1016/j.lfs.2011.08.007

Rosnizeck, I. C., Graf, T., Spoerner, M., Tränkle, J., Filchtinski, D., Herrmann, C., … Kalbitzer, H. R. (2010). Stabilizing a weak binding state for effectors in the human ras protein by cyclen complexes. *Angewandte Chemie (International Ed. in English)*, *49*(22), 3830–3833. https://doi.org/10.1002/anie.200907002

Roux, P. P., & Blenis, J. (2004). ERK and p38 MAPK-Activated Protein Kinases: a Family of Protein Kinases with Diverse Biological Functions. *Microbiology and Molecular Biology Reviews*, *68*(2), 320–344. https://doi.org/10.1128/MMBR.68.2.320-344.2004

Royer, C., & Lu, X. (2011). Epithelial cell polarity: a major gatekeeper against cancer? *Cell Death and Differentiation*, *18*(9), 1470–1477. https://doi.org/10.1038/cdd.2011.60

Ryan, M. B., & Corcoran, R. B. (2018). Therapeutic strategies to target RAS-mutant cancers. *Nature Reviews. Clinical Oncology*, *15*(11), 709–720. https://doi.org/10.1038/s41571-018-0105-0

Safaei, R., Katano, K., Samimi, G., Naerdemann, W., Stevenson, J. L., Rochdi, M., & Howell, S. B. (2004). Cross-resistance to cisplatin in cells with acquired resistance to copper. *Cancer Chemotherapy and Pharmacology*, *53*(3), 239–246. https://doi.org/10.1007/s00280-003-0736-3

Sahai, E., Olson, M. F., & Marshall, C. J. (2001). Cross-talk between Ras and Rho signalling pathways in transformation favours proliferation and increased motility. *EMBO Journal*,

20(4), 755–766. https://doi.org/10.1093/emboj/20.4.755
Salmi, M., & Jalkanen, S. (2019). Vascular Adhesion Protein-1: A Cell Surface Amine Oxidase in Translation. *Antioxidants & Redox Signaling*, *30*(3), 314–332. https://doi.org/10.1089/ars.2017.7418
Saltz, L. B., Clarke, S., Díaz-Rubio, E., Scheithauer, W., Figer, A., Wong, R., … Cassidy, J. (2008). Bevacizumab in combination with oxaliplatin-based chemotherapy as first-line therapy in metastatic colorectal cancer: A randomized phase III study. *Journal of Clinical Oncology*, *26*(12), 2013–2019. https://doi.org/10.1200/JCO.2007.14.9930
Samimi, G., Katano, K., Holzer, A. K., Safaei, R., & Howell, S. B. (2004). Modulation of the cellular pharmacology of cisplatin and its analogs by the copper exporters ATP7A and ATP7B. *Molecular Pharmacology*, *66*(1), 25–32. https://doi.org/10.1124/mol.66.1.25
Sansom, O. J., Meniel, V., Wilkins, J. A., Cole, A. M., Oien, K. A., Marsh, V., … Clarke, A. R. (2006). Loss of Apc allows phenotypic manifestation of the transforming properties of an endogenous K-ras oncogene in vivo. *Proceedings of the National Academy of Sciences of the United States of America*, *103*(38), 14122–14127. https://doi.org/10.1073/pnas.0604130103
Sauer, R., Becker, H., Hohenberger, W., Rödel, C., Wittekind, C., Fietkau, R., … Raab, R. (2004). Preoperative versus postoperative chemoradiotherapy for rectal cancer. *New England Journal of Medicine*, *351*(17), 1731–1740. https://doi.org/10.1056/NEJMoa040694
Saxton, R. A., & Sabatini, D. M. (2017). mTOR Signaling in Growth, Metabolism, and Disease. *Cell*, *168*(6), 960–976. https://doi.org/10.1016/j.cell.2017.02.004
Scartozzi, M., Giampieri, R., Maccaroni, E., Mandolesi, A., Giustini, L., Silva, R., … Cascinu, S. (2012). Analysis of HER-3, insulin growth factor-1, nuclear factor-kB and epidermal growth factor receptor gene copy number in the prediction of clinical outcome for K-RAS wild-type colorectal cancer patients receiving irinotecan-cetuximab. *Annals of Oncology*, *23*(7), 1706–1712. https://doi.org/10.1093/annonc/mdr558
Scheid, M. P., Parsons, M., & Woodgett, J. R. (2005). Phosphoinositide-Dependent Phosphorylation of PDK1 Regulates Nuclear Translocation. *Molecular and Cellular Biology*, *25*(6), 2347–2363. https://doi.org/10.1128/mcb.25.6.2347-2363.2005
Schliemann, C., Roesli, C., Kamada, H., Borgia, B., Fugmann, T., Klapper, W., & Neri, D. (2010). In vivo biotinylation of the vasculature in B-cell lymphoma identifies BST-2 as a target for antibody-based therapy. *Blood*, *115*(3), 736–744. https://doi.org/10.1182/blood-2009-08-239004
Schneider, C. A., Rasband, W. S., Eliceiri, K. W., & Instrumentation, C. (2017). NIH Image to ImageJ : 25 years of Image Analysis, *9*(7), 671–675.
Schoslnsky, K. H., Lehmann, H. P., & Beeler, M. F. (1974). Measurement of Ceruloplasmin from Its Oxidase Activity in Serum by Use of o-Dianisidine Dihydrochioride furic acid are used, *20*(12), 1556–1563.
Schwitalla, S., Fingerle, A. A., Cammareri, P., Nebelsiek, T., Göktuna, S. I., Ziegler, P. K., … Greten, F. R. (2013). Intestinal tumorigenesis initiated by dedifferentiation and acquisition of stem-cell-like properties. *Cell*, *152*(1–2), 25–38. https://doi.org/10.1016/j.cell.2012.12.012
Scott, J. W., Galic, S., Graham, K. L., Foitzik, R., Ling, N. X. Y., Dite, T. A., … Oakhill, J. S. (2015). Inhibition of AMP-Activated Protein Kinase at the Allosteric Drug-Binding Site Promotes Islet Insulin Release. *Chemistry & Biology*, *22*(6), 705–711. https://doi.org/10.1016/j.chembiol.2015.05.011

Seeber, A., Gunsilius, E., Gastl, G., & Pircher, A. (2018). Anti-Angiogenics: Their Value in Colorectal Cancer Therapy. *Oncology Research and Treatment*, *41*(4), 188–193. https://doi.org/10.1159/000488301

Serra, M., Columbano, A., Ammarah, U., Mazzone, M., & Menga, A. (2020). Understanding Metal Dynamics Between Cancer Cells and Macrophages: Competition or Synergism? *Frontiers in Oncology*, *10*, 646. https://doi.org/10.3389/fonc.2020.00646

Serrano, R., Bernal, D., Simón, E., & Ariño, J. (2004). Copper and iron are the limiting factors for growth of the yeast Saccharomyces cerevisiae in an alkaline environment. *The Journal of Biological Chemistry*, *279*(19), 19698–19704. https://doi.org/10.1074/jbc.M313746200

Shalem, O., Sanjana, N. E., Hartenian, E., Shi, X., Scott, D. A., Mikkelson, T., … Zhang, F. (2014). Genome-scale CRISPR-Cas9 knockout screening in human cells. *Science (New York, N.Y.)*, *343*(6166), 84–87. https://doi.org/10.1126/science.1247005

Shanbhag, V., Jasmer-McDonald, K., Zhu, S., Martin, A. L., Gudekar, N., Khan, A., … Petris, M. J. (2019). ATP7A delivers copper to the lysyl oxidase family of enzymes and promotes tumorigenesis and metastasis. *Proceedings of the National Academy of Sciences of the United States of America*, *116*(14), 6836–6841. https://doi.org/10.1073/pnas.1817473116

Shaw, A. T., Meissner, A., Dowdle, J. A., Crowley, D., Magendantz, M., Ouyang, C., … Jacks, T. (2007). Sprouty-2 regulates oncogenic K-ras in lung development and tumorigenesis. *Genes & Development*, *21*(6), 694–707. https://doi.org/10.1101/gad.1526207

Sheridan, C. (2020). Grail of RAS cancer drugs within reach. *Nature Biotechnology*, *38*(1), 6–8. https://doi.org/10.1038/s41587-019-0382-x

Shiratori, R., Furuichi, K., Yamaguchi, M., Miyazaki, N., Aoki, H., Chibana, H., … Aoki, S. (2019). Glycolytic suppression dramatically changes the intracellular metabolic profile of multiple cancer cell lines in a mitochondrial metabolism-dependent manner. *Scientific Reports*, *9*(1), 18699. https://doi.org/10.1038/s41598-019-55296-3

Shojaee, S., Caeser, R., Buchner, M., Park, E., Swaminathan, S., Hurtz, C., … Müschen, M. (2015). Erk Negative Feedback Control Enables Pre-B Cell Transformation and Represents a Therapeutic Target in Acute Lymphoblastic Leukemia. *Cancer Cell*, *28*(1), 114–128. https://doi.org/10.1016/j.ccell.2015.05.008

Siddiqui, A. D., & Piperdi, B. (2010). KRAS Mutation in Colon Cancer: A Marker of Resistance to EGFR-I Therapy. *Annals of Surgical Oncology*, *17*(4), 1168–1176. https://doi.org/10.1245/s10434-009-0811-z

Siegel, R. L., Miller, K. D., & Jemal, A. (2016). Cancer Statistics , 2016, *66*(1), 7–30. https://doi.org/10.3322/caac.21332.

Singh, A., Greninger, P., Rhodes, D., Koopman, L., Violette, S., Bardeesy, N., & Settleman, J. (2009). A Gene Expression Signature Associated with "K-Ras Addiction" Reveals Regulators of EMT and Tumor Cell Survival. *Cancer Cell*, *15*(6), 489–500. https://doi.org/10.1016/j.ccr.2009.03.022

Skjørringe, T., Pedersen, P. A., Thorborg, S. S., Nissen, P., Gourdon, P., & Møller, L. B. (2017). Characterization of ATP7A missense mutants suggests a correlation between intracellular trafficking and severity of Menkes disease. *Scientific Reports*, *7*(1), 1–18. https://doi.org/10.1038/s41598-017-00618-6

Smith, M. J., Neel, B. G., & Ikura, M. (2013). NMR-based functional profiling of RASopathies and oncogenic RAS mutations. *Proceedings of the National Academy of Sciences of the United States of America*, *110*(12), 4574–4579. https://doi.org/10.1073/pnas.1218173110

Smith, N. R., Baker, D., James, N. H., Ratcliffe, K., Jenkins, M., Ashton, S. E., … Womack, C.

(2010). Vascular endothelial growth factor receptors VEGFR-2 and VEGFR-3 are localized primarily to the vasculature in human primary solid cancers. *Clinical Cancer Research*, *16*(14), 3548–3561. https://doi.org/10.1158/1078-0432.CCR-09-2797

Sodir, N. M., Chen, X., Park, R., Nickel, A. E., Conti, P. S., Moats, R., … Laird, P. W. (2006). Smad3 deficiency promotes tumorigenesis in the distal colon of Apc Min/+ mice. *Cancer Research*, *66*(17), 8430–8438. https://doi.org/10.1158/0008-5472.CAN-06-1437

Sokol, R. J., Devereaux, M. W., O'Brien, K., Khandwala, R. A., & Loehr, J. P. (1993). Abnormal hepatic mitochondrial respiration and cytochrome C oxidase activity in rats with long-term copper overload. *Gastroenterology*, *105*(1), 178–187. https://doi.org/10.1016/0016-5085(93)90024-7

Son, J., Lyssiotis, C. A., Ying, H., Wang, X., Hua, S., Ligorio, M., … Kimmelman, A. C. (2013). Glutamine supports pancreatic cancer growth through a KRAS-regulated metabolic pathway. *Nature*, *496*(7443), 101–105. https://doi.org/10.1038/nature12040

Soncin, F., Guitton, J. D., Cartwright, T., & Badet, J. (1997). Interaction of human angiogenin with copper modulates angiogenin binding to endothelial cells. *Biochemical and Biophysical Research Communications*, *236*(3), 604–610. https://doi.org/10.1006/bbrc.1997.7018

Subramanian, A., Tamayo, P., Mootha, V. K., Mukherjee, S., & Ebert, B. L. (2005). Gene set enrichment analysis : A knowledge-based approach for interpreting genome-wide.

Sudhahar, V., Okur, M. N., Bagi, Z., O'Bryan, J. P., Hay, N., Makino, A., … Fukai, T. (2018). Akt2 (Protein Kinase B Beta) Stabilizes ATP7A, a Copper Transporter for Extracellular Superoxide Dismutase, in Vascular Smooth Muscle: Novel Mechanism to Limit Endothelial Dysfunction in Type 2 Diabetes Mellitus. *Arteriosclerosis, Thrombosis, and Vascular Biology*, *38*(3), 529–541. https://doi.org/10.1161/ATVBAHA.117.309819

Sun, C., Hobor, S., Bertotti, A., Zecchin, D., Huang, S., Galimi, F., … Bernards, R. (2014). Intrinsic resistance to MEK inhibition in KRAS mutant lung and colon cancer through transcriptional induction of ERBB3. *Cell Reports*, *7*(1), 86–93. https://doi.org/10.1016/j.celrep.2014.02.045

Tabernero, J., Yoshino, T., Cohn, A. L., Obermannova, R., Bodoky, G., Garcia-Carbonero, R., … Nasroulah, F. (2015). Ramucirumab versus placebo in combination with second-line FOLFIRI in patients with metastatic colorectal carcinoma that progressed during or after first-line therapy with bevacizumab, oxaliplatin, and a fluoropyrimidine (RAISE): A randomised, double-blin. *The Lancet Oncology*, *16*(5), 499–508. https://doi.org/10.1016/S1470-2045(15)70127-0

Tajiri, H., Uruno, T., Shirai, T., Takaya, D., Matsunaga, S., Setoyama, D., … Fukui, Y. (2017). Targeting Ras-Driven Cancer Cell Survival and Invasion through Selective Inhibition of DOCK1. *Cell Reports*, *19*(5), 969–980. https://doi.org/10.1016/j.celrep.2017.04.016

Takaku, K., Oshima, M., Miyoshi, H., Matsui, M., Seldin, M. F., & Taketo, M. M. (1998). Intestinal tumorigenesis in compound mutant mice of both Dpc4 (Smad4) and Apc genes. *Cell*, *92*(5), 645–656. https://doi.org/10.1016/S0092-8674(00)81132-0

Tassabehji, N. M., VanLandingham, J. W., & Levenson, C. W. (2005). Copper alters the conformation and transcriptional activity of the tumor suppressor protein p53 in human Hep G2 cells. *Experimental Biology and Medicine (Maywood, N.J.)*, *230*(10), 699–708. https://doi.org/10.1177/153537020523001002

Taylor, D. P., Burt, R. W., Williams, M. S., Haug, P. J., & Cannon–Albright, L. A. (2010). Population-Based Family History–Specific Risks for Colorectal Cancer: A Constellation

Approach. *Gastroenterology*, *138*(3), 877–885. https://doi.org/10.1053/j.gastro.2009.11.044
Tefft, D., Lee, M., Smith, S., Crowe, D. L., Bellusci, S., & Warburton, D. (2002). mSprouty2 inhibits FGF10-activated MAP kinase by differentially binding to upstream target proteins. *American Journal of Physiology. Lung Cellular and Molecular Physiology*, *283*(4), L700-6. https://doi.org/10.1152/ajplung.00372.2001
Temraz, S., Mukherji, D., & Shamseddine, A. (2015). Dual inhibition of MEK and PI3K pathway in KRAS and BRAF mutated colorectal cancers. *International Journal of Molecular Sciences*, *16*(9), 22976–22988. https://doi.org/10.3390/ijms160922976
Terada, K., Aiba, N., Yang, X. L., Iida, M., Nakai, M., Miura, N., & Sugiyama, T. (1999). Biliary excretion of copper in LEC rat after introduction of copper transporting P-type ATPase, ATP7B. *FEBS Letters*, *448*(1), 53–56. https://doi.org/10.1016/s0014-5793(99)00319-1
Terada, K., Nakako, T., Yang, X. L., Iida, M., Aiba, N., Minamiya, Y., … Sugiyama, T. (1998). Restoration of holoceruloplasmin synthesis in LEC rat after infusion of recombinant adenovirus bearing WND cDNA. *The Journal of Biological Chemistry*, *273*(3), 1815–1820. https://doi.org/10.1074/jbc.273.3.1815
TeSlaa, T., & Teitell, M. A. (2014). Techniques to monitor glycolysis. *Methods in Enzymology*, *542*, 91–114. https://doi.org/10.1016/B978-0-12-416618-9.00005-4
Thorn, C. F., Marsh, S., Carrillo, M. W., McLeod, H. L., Klein, T. E., & Altman, R. B. (2011). Pharm GKB summary: Fluoropyrimidine pathways. *Pharmacogenetics and Genomics*, *21*(4), 237–242. https://doi.org/10.1097/FPC.0b013e32833c6107
Tischfield, J. A. (1997). Loss of heterozygosity or: how I learned to stop worrying and love mitotic recombination. *American Journal of Human Genetics*, *61*(5), 995–999. https://doi.org/10.1086/301617
Toda, K., Kawada, K., Iwamoto, M., Inamoto, S., Sasazuki, T., Shirasawa, S., … Sakai, Y. (2016). Metabolic Alterations Caused by KRAS Mutations in Colorectal Cancer Contribute to Cell Adaptation to Glutamine Depletion by Upregulation of Asparagine Synthetase. *Neoplasia (New York, N.Y.)*, *18*(11), 654–665. https://doi.org/10.1016/j.neo.2016.09.004
Toda, K., Nishikawa, G., Iwamoto, M., Itatani, Y., Takahashi, R., Sakai, Y., & Kawada, K. (2017). Clinical Role of ASCT2 (SLC1A5) in KRAS-Mutated Colorectal Cancer. *International Journal of Molecular Sciences*, *18*(8). https://doi.org/10.3390/ijms18081632
Tokunaga, T., Nakamura, M., Oshika, Y., Abe, Y., Ozeki, Y., Fukushima, Y., … Ueyama, Y. (1999). Thrombospondin 2 expression is correlated with inhibition of angiogenesis and metastasis of colon cancer. *British Journal of Cancer*, *79*(2), 354–359. https://doi.org/10.1038/sj.bjc.6690056
Tomino, T., Tajiri, H., Tatsuguchi, T., Shirai, T., Oisaki, K., Matsunaga, S., … Uruno, T. (2018). DOCK1 inhibition suppresses cancer cell invasion and macropinocytosis induced by self-activating Rac1P29S mutation. *Biochemical and Biophysical Research Communications*, *497*(1), 298–304. https://doi.org/10.1016/j.bbrc.2018.02.073
Topalian, S. L., Drake, C. G., & Pardoll, D. M. (2015). Immune Checkpoint Blockade: A Common Denominator Approach to Cancer Therapy. *Cancer Cell*, *27*(4), 450–461. https://doi.org/10.1016/j.ccell.2015.03.001
Toyama, E. Q., Herzig, S., Courchet, J., Lewis, T. L., Losón, O. C., Hellberg, K., … Shaw, R. J. (2016). Metabolism. AMP-activated protein kinase mediates mitochondrial fission in response to energy stress. *Science (New York, N.Y.)*, *351*(6270), 275–281. https://doi.org/10.1126/science.aab4138

Trejo-Solís, C., Jimenez-Farfan, D., Rodriguez-Enriquez, S., Fernandez-Valverde, F., Cruz-Salgado, A., Ruiz-Azuara, L., & Sotelo, J. (2012). Copper compound induces autophagy and apoptosis of glioma cells by reactive oxygen species and JNK activation. *BMC Cancer*, *12*, 156. https://doi.org/10.1186/1471-2407-12-156

Trobridge, P., Knoblaugh, S., Washington, M. K., Munoz, N. M., Tsuchiya, K. D., Rojas, A., … Grady, W. M. (2009). TGF-beta receptor inactivation and mutant Kras induce intestinal neoplasms in mice via a beta-catenin-independent pathway. *Gastroenterology*, *136*(5), 1680-8.e7. https://doi.org/10.1053/j.gastro.2009.01.066

Tsang, T., Posimo, J. M., Gudiel, A. A., Cicchini, M., Feldser, D. M., & Brady, D. C. (2020). Copper is an essential regulator of the autophagic kinases ULK1/2 to drive lung adenocarcinoma. *Nature Cell Biology*, *22*(4), 412–424. https://doi.org/10.1038/s41556-020-0481-4

Tse, J. W. T., Jenkins, L. J., Chionh, F., & Mariadason, J. M. (2017). Aberrant DNA Methylation in Colorectal Cancer: What Should We Target? *Trends in Cancer*, *3*(10), 698–712. https://doi.org/10.1016/j.trecan.2017.08.003

Turecký, L., Kalina, P., Uhlíková, E., Námerová, S., & Krizko, J. (1984). Serum ceruloplasmin and copper levels in patients with primary brain tumors. *Klinische Wochenschrift*, *62*(4), 187–189. https://doi.org/10.1007/BF01731643

Turski, M. L., Brady, D. C., Kim, H. J., Kim, B.-E., Nose, Y., Counter, C. M., … Thiele, D. J. (2012). A novel role for copper in Ras/mitogen-activated protein kinase signaling. *Molecular and Cellular Biology*, *32*(7), 1284–1295. https://doi.org/10.1128/MCB.05722-11

Tuveson, D. A., Shaw, A. T., Willis, N. A., Silver, D. P., Jackson, E. L., Chang, S., … Jacks, T. (2004). Endogenous oncogenic K-rasG12D stimulates proliferation and widespread neoplastic and developmental defects. *Cancer Cell*, *5*(4), 375–387. https://doi.org/10.1016/S1535-6108(04)00085-6

Twyman-Saint Victor, C., Rech, A. J., Maity, A., Rengan, R., Pauken, K. E., Stelekati, E., … Minn, A. J. (2015). Radiation and dual checkpoint blockade activate non-redundant immune mechanisms in cancer. *Nature*, *520*(7547), 373–377. https://doi.org/10.1038/nature14292

Ünal, E. B., Uhlitz, F., & Blüthgen, N. (2017). A compendium of ERK targets. *FEBS Letters*, *591*(17), 2607–2615. https://doi.org/10.1002/1873-3468.12740

Unni, A. M., Harbourne, B., Oh, M. H., Wild, S., Ferrarone, J. R., Lockwood, W. W., & Varmus, H. (2018). Hyperactivation of ERK by multiple mechanisms is toxic to RTK-RAS mutation-driven lung adenocarcinoma cells. *ELife*, *7*. https://doi.org/10.7554/eLife.33718

Valverde, R. H. F., Morin, I., Lowe, J., Mintz, E., Cuillel, M., & Vieyra, A. (2008). Cyclic AMP-dependent protein kinase controls energy interconversion during the catalytic cycle of the yeast copper-ATPase. *FEBS Letters*, *582*(6), 891–895. https://doi.org/10.1016/j.febslet.2008.02.022

Van Cutsem, E., Köhne, C. H., Hitre, E., Zaluski, J., Chien, C. R. C., Makhson, A., … Rougier, P. (2009). Cetuximab and chemotherapy as initial treatment for metastatic colorectal cancer. *New England Journal of Medicine*, *360*(14), 1408–1417. https://doi.org/10.1056/NEJMoa0805019

Van Cutsem, E., Tabernero, J., Lakomy, R., Prenen, H., Prausová, J., Macarulla, T., … Allegra, C. (2012). Addition of aflibercept to fluorouracil, leucovorin, and irinotecan improves survival in a phase III randomized trial in patients with metastatic colorectal cancer previously treated with an oxaliplatin-based regimen. *Journal of Clinical Oncology*, *30*(28), 3499–3506. https://doi.org/10.1200/JCO.2012.42.8201

van den Berghe, P. V. E., & Klomp, L. W. J. (2009). New developments in the regulation of intestinal copper absorption. *Nutrition Reviews*, *67*(11), 658–672. https://doi.org/10.1111/j.1753-4887.2009.00250.x

van Houdt, W. J., Hoogwater, F. J. H., de Bruijn, M. T., Emmink, B. L., Nijkamp, M. W., Raats, D. A. E., … Kranenburg, O. (2010). Oncogenic KRAS desensitizes colorectal tumor cells to epidermal growth factor receptor inhibition and activation. *Neoplasia (New York, N.Y.)*, *12*(6), 443–452. https://doi.org/10.1593/neo.92088

Varmus, H., Unni, A. M., & Lockwood, W. W. (2016). How Cancer Genomics Drives Cancer Biology: Does Synthetic Lethality Explain Mutually Exclusive Oncogenic Mutations? *Cold Spring Harbor Symposia on Quantitative Biology*, *81*, 247–255. https://doi.org/10.1101/sqb.2016.81.030866

Veldhuis, N. A., Valova, V. A., Gaeth, A. P., Palstra, N., Hannan, K. M., Michell, B. J., … Camakaris, J. (2009). Phosphorylation regulates copper-responsive trafficking of the Menkes copper transporting P-type ATPase. *The International Journal of Biochemistry & Cell Biology*, *41*(12), 2403–2412. https://doi.org/10.1016/j.biocel.2009.06.008

Verissimo, C. S., Overmeer, R. M., Ponsioen, B., Drost, J., Mertens, S., Verlaan-Klink, I., … Snippert, H. J. (2016). Targeting mutant RAS in patient-derived colorectal cancer organoids by combinatorial drug screening. *ELife*, *5*. https://doi.org/10.7554/eLife.18489

Vigneri, P. G., Tirrò, E., Pennisi, M. S., Massimino, M., Stella, S., Romano, C., & Manzella, L. (2017). The insulin/IGF system in colorectal cancer development and resistance to therapy. *Frontiers in Oncology*, *5*(OCT), 1–7. https://doi.org/10.3389/fonc.2015.00230

Voisin, L., Julien, C., Duhamel, S., Gopalbhai, K., Claveau, I., Saba-El-Leil, M. K., … Meloche, S. (2008). Activation of MEK1 or MEK2 isoform is sufficient to fully transform intestinal epithelial cells and induce the formation of metastatic tumors. *BMC Cancer*, *8*, 337. https://doi.org/10.1186/1471-2407-8-337

Vonk, W. I. M., de Bie, P., Wichers, C. G. K., van den Berghe, P. V. E., van der Plaats, R., Berger, R., … van de Sluis, B. (2012). The copper-transporting capacity of ATP7A mutants associated with Menkes disease is ameliorated by COMMD1 as a result of improved protein expression. *Cellular and Molecular Life Sciences : CMLS*, *69*(1), 149–163. https://doi.org/10.1007/s00018-011-0743-1

Waghmare, I., & Kango-Singh, M. (2016). Loss of cell adhesion increases tumorigenic potential of polarity deficient scribble mutant cells. *PLoS ONE*, *11*(6), 1–18. https://doi.org/10.1371/journal.pone.0158081

Wan, P. T. C., Garnett, M. J., Roe, S. M., Lee, S., Niculescu-Duvaz, D., Good, V. M., … Marais, R. (2004). Mechanism of activation of the RAF-ERK signaling pathway by oncogenic mutations of B-RAF. *Cell*, *116*(6), 855–867. https://doi.org/10.1016/S0092-8674(04)00215-6

Wang, C., Wang, G., Feng, X., Shepherd, P., Zhang, J., Tang, M., … Chen, J. (2019). Genome-wide CRISPR screens reveal synthetic lethality of RNASEH2 deficiency and ATR inhibition. *Oncogene*, *38*(14), 2451–2463. https://doi.org/10.1038/s41388-018-0606-4

Wang, F., Jiao, P., Qi, M., Frezza, M., Dou, Q. P., & Yan, B. (2010). Turning tumor-promoting copper into an anti-cancer weapon via high-throughput chemistry. *Current Medicinal Chemistry*, *17*(25), 2685–2698. https://doi.org/10.2174/092986710791859315

Wang, J., Binks, T., Warr, C. G., & Burke, R. (2014). Vacuolar-type H(+)-ATPase subunits and the neurogenic protein big brain are required for optimal copper and zinc uptake. *Metallomics : Integrated Biometal Science*, *6*(11), 2100–2108.

https://doi.org/10.1039/c4mt00196f
Wang, Tao, Xiang, P., Ha, J.-H., Wang, X., Doguer, C., Flores, S. R. L., … Collins, J. F. (2018). Copper supplementation reverses dietary iron overload-induced pathologies in mice. *The Journal of Nutritional Biochemistry*, *59*, 56–63. https://doi.org/10.1016/j.jnutbio.2018.05.006
Wang, Tim, Yu, H., Hughes, N. W., Liu, B., Kendirli, A., Klein, K., … Sabatini, D. M. (2017). Gene Essentiality Profiling Reveals Gene Networks and Synthetic Lethal Interactions with Oncogenic Ras. *Cell*, *168*(5), 890-903.e15. https://doi.org/10.1016/j.cell.2017.01.013
Wang, Tuo, & Guo, Z. (2006). Copper in Medicine: Homeostasis, Chelation Therapy and Antitumor Drug Design. *Current Medicinal Chemistry*, *13*(5), 525–537. https://doi.org/10.2174/092986706776055742
Wang, Y., Zhu, S., Weisman, G. A., Gitlin, J. D., & Petris, M. J. (2012). Conditional knockout of the Menkes disease copper transporter demonstrates its critical role in embryogenesis. *PloS One*, *7*(8), e43039. https://doi.org/10.1371/journal.pone.0043039
Weekes, M. P., Antrobus, R., Lill, J. R., Duncan, L. M., Hör, S., & Lehner, P. J. (2010). Comparative analysis of techniques to purify plasma membrane proteins. *Journal of Biomolecular Techniques : JBT*, *21*(3), 108–115. Retrieved from http://www.pubmedcentral.nih.gov/articlerender.fcgi?artid=2922835&tool=pmcentrez&rendertype=abstract
Weinberg, F., Hamanaka, R., Wheaton, W. W., Weinberg, S., Joseph, J., Lopez, M., … Chandel, N. S. (2010). Mitochondrial metabolism and ROS generation are essential for Kras-mediated tumorigenicity. *Proceedings of the National Academy of Sciences of the United States of America*, *107*(19), 8788–8793. https://doi.org/10.1073/pnas.1003428107
Weitz, J., Koch, M., Debus, J., Höhler, T., Galle, P. R., & Büchler, M. W. (2005). Colorectal cancer. *The Lancet*, *365*(9454), 153–165. https://doi.org/10.1016/S0140-6736(05)17706-X
Wernimont, A. K., Huffman, D. L., Lamb, A. L., O'Halloran, T. V, & Rosenzweig, A. C. (2000). Structural basis for copper transfer by the metallochaperone for the Menkes/Wilson disease proteins. *Nature Structural Biology*, *7*(9), 766–771. https://doi.org/10.1038/78999
White, C., Kambe, T., Fulcher, Y. G., Sachdev, S. W., Bush, A. I., Fritsche, K., … Petris, M. J. (2009). Copper transport into the secretory pathway is regulated by oxygen in macrophages. *Journal of Cell Science*, *122*(Pt 9), 1315–1321. https://doi.org/10.1242/jcs.043216
Willumsen, B. M., Norris, K., Papageorge, A. G., Hubbert, N. L., & Lowy, D. R. (1984). Harvey murine sarcoma virus p21 ras protein: biological and biochemical significance of the cysteine nearest the carboxy terminus. *The EMBO Journal*, *3*(11), 2581–2585. https://doi.org/10.1002/j.1460-2075.1984.tb02177.x
Willumsen, Berthe M., Christensen, A., Hubbert, N. L., Papageorge, A. G., & Lowy, D. R. (1984). The p21 ras C-terminus is required for transformation and membrane association. *Nature*, *310*(5978), 583–586. https://doi.org/10.1038/310583a0
Wiśniewski, J. R., Duś-Szachniewicz, K., Ostasiewicz, P., Ziółkowski, P., Rakus, D., & Mann, M. (2015). Absolute Proteome Analysis of Colorectal Mucosa, Adenoma, and Cancer Reveals Drastic Changes in Fatty Acid Metabolism and Plasma Membrane Transporters. *Journal of Proteome Research*, *14*(9), 4005–4018. https://doi.org/10.1021/acs.jproteome.5b00523
World Health, O. (2020). *WHO report on cancer: Setting priorities investing wisely and providing care for all. Investing Wisely and Providing Care for All*.
Wu, C. Y. C., Carpenter, E. S., Takeuchi, K. K., Halbrook, C. J., Peverley, L. V., Bien, H., …

Crawford, H. C. (2014). PI3K regulation of RAC1 is required for KRAS-induced pancreatic tumorigenesis in mice. *Gastroenterology*, *147*(6), 1405-1416.e7. https://doi.org/10.1053/j.gastro.2014.08.032

Wulaningsih, W., Wardhana, A., Watkins, J., Yoshuantari, N., Repana, D., & Van Hemelrijck, M. (2016). Irinotecan chemotherapy combined with fluoropyrimidines versus irinotecan alone for overall survival and progression-free survival in patients with advanced and/or metastatic colorectal cancer. *Cochrane Database of Systematic Reviews*, (October 2013), 1–224. https://doi.org/10.1002/14651858.CD008593.pub3

Xie, L., & Collins, J. F. (2011). Transcriptional regulation of the Menkes copper ATPase (Atp7a) gene by hypoxia-inducible factor (HIF2{alpha}) in intestinal epithelial cells. *American Journal of Physiology. Cell Physiology*, *300*(6), C1298-305. https://doi.org/10.1152/ajpcell.00023.2011

Xie, L., & Collins, J. F. (2013). Copper stabilizes the Menkes copper-transporting ATPase (Atp7a) protein expressed in rat intestinal epithelial cells. *American Journal of Physiology. Cell Physiology*, *304*(3), C257-62. https://doi.org/10.1152/ajpcell.00336.2012

Xie, Y. H., Chen, Y. X., & Fang, J. Y. (2020). Comprehensive review of targeted therapy for colorectal cancer. *Signal Transduction and Targeted Therapy*, *5*(1). https://doi.org/10.1038/s41392-020-0116-z

Xu, M., Casio, M., Range, D. E., Sosa, J. A., & Counter, C. M. (2018). Copper Chelation as Targeted Therapy in a Mouse Model of Oncogenic BRAF-Driven Papillary Thyroid Cancer. *Clinical Cancer Research : An Official Journal of the American Association for Cancer Research*, *24*(17), 4271–4281. https://doi.org/10.1158/1078-0432.CCR-17-3705

Xu, Y., & Pasche, B. (2007). TGF-beta signaling alterations and susceptibility to colorectal cancer. *Human Molecular Genetics*, *16 Spec No*, R14-20. https://doi.org/10.1093/hmg/ddl486

Xue, J. Y., Zhao, Y., Aronowitz, J., Mai, T. T., Vides, A., Qeriqi, B., … Lito, P. (2020). Rapid non-uniform adaptation to conformation-specific KRAS(G12C) inhibition. *Nature*, *577*(7790), 421–425. https://doi.org/10.1038/s41586-019-1884-x

Yaeger, R., Chatila, W. K., Lipsyc, M. D., Hechtman, J. F., Cercek, A., Sanchez-Vega, F., … Schultz, N. (2018). Clinical Sequencing Defines the Genomic Landscape of Metastatic Colorectal Cancer. *Cancer Cell*, *33*(1), 125-136.e3. https://doi.org/10.1016/j.ccell.2017.12.004

Yamaguchi, Y., Heiny, M. E., Suzuki, M., & Gitlin, J. D. (1996). Biochemical characterization and intracellular localization of the Menkes disease protein. *Proceedings of the National Academy of Sciences of the United States of America*, *93*(24), 14030–14035. https://doi.org/10.1073/pnas.93.24.14030

Yang, H., Ralle, M., Wolfgang, M. J., Dhawan, N., Burkhead, J. L., Rodriguez, S., … Lutsenko, S. (2018). Copper-dependent amino oxidase 3 governs selection of metabolic fuels in adipocytes. *PLoS Biology*, *16*(9), e2006519. https://doi.org/10.1371/journal.pbio.2006519

Yang, J.-Y., Zong, C. S., Xia, W., Yamaguchi, H., Ding, Q., Xie, X., … Hung, M.-C. (2008). ERK promotes tumorigenesis by inhibiting FOXO3a via MDM2-mediated degradation. *Nature Cell Biology*, *10*(2), 138–148. https://doi.org/10.1038/ncb1676

Yasuno, M., Uetake, H., Ishiguro, M., Mizunuma, N., Komori, T., Miyata, G., … Sugihara, K. (2019). mFOLFOX6 plus bevacizumab to treat liver-only metastases of colorectal cancer that are unsuitable for upfront resection (TRICC0808): a multicenter phase II trial comprising the final analysis for survival. *International Journal of Clinical Oncology*,

24(5), 516–525. https://doi.org/10.1007/s10147-018-01393-8
Yau, E. H., Kummetha, I. R., Lichinchi, G., Tang, R., Zhang, Y., & Rana, T. M. (2017). Genome-Wide CRISPR Screen for Essential Cell Growth Mediators in Mutant KRAS Colorectal Cancers. *Cancer Research*, *77*(22), 6330–6339. https://doi.org/10.1158/0008-5472.CAN-17-2043
Ye, X., Chan, K. C., Waters, A. M., Bess, M., Harned, A., Wei, B.-R., … Blonder, J. (2016). Comparative proteomics of a model MCF10A-KRasG12V cell line reveals a distinct molecular signature of the KRasG12V cell surface. *Oncotarget*, *7*(52), 86948–86971. https://doi.org/10.18632/oncotarget.13566
Yeh, J. J., Routh, E. D., Rubinas, T., Peacock, J., Martin, T. D., Shen, X. J., … Der, C. J. (2009). KRAS/BRAF mutation status and ERK1/2 activation as biomarkers for MEK1/2 inhibitor therapy in colorectal cancer. *Molecular Cancer Therapeutics*, *8*(4), 834–843. https://doi.org/10.1158/1535-7163.MCT-08-0972
Yi, L., & Kaler, S. (2014). ATP7A trafficking and mechanisms underlying the distal motor neuropathy induced by mutations in ATP7A. *Annals of the New York Academy of Sciences*, *1314*, 49–54. https://doi.org/10.1111/nyas.12427
Yoon, S., & Seger, R. (2006). The extracellular signal-regulated kinase: Multiple substrates regulate diverse cellular functions. *Growth Factors*, *24*(1), 21–44. https://doi.org/10.1080/02699050500284218
Yordy, J. S., & Muise-Helmericks, R. C. (2000). Signal transduction and the Ets family of transcription factors. *Oncogene*, *19*(55), 6503–6513. https://doi.org/10.1038/sj.onc.1204036
Yoshida, T., Yamasaki, S., Kaneko, O., Taoka, N., Tomimoto, Y., Namatame, I., … Lyssiotis, C. A. (2020). A covalent small molecule inhibitor of glutamate-oxaloacetate transaminase 1 impairs pancreatic cancer growth. *Biochemical and Biophysical Research Communications*, *522*(3), 633–638. https://doi.org/10.1016/j.bbrc.2019.11.130
Yoshii, J., Yoshiji, H., Kuriyama, S., Ikenaka, Y., Noguchi, R., Okuda, H., … Fukui, H. (2001). The copper-chelating agent, trientine, suppresses tumor development and angiogenesis in the murine hepatocellular carcinoma cells. *International Journal of Cancer*, *94*(6), 768–773. https://doi.org/10.1002/ijc.1537
Yoshii, Y., Yoshimoto, M., Matsumoto, H., Furukawa, T., Zhang, M.-R., Inubushi, M., … Saga, T. (2017). 64Cu-ATSM internal radiotherapy to treat tumors with bevacizumab-induced vascular decrease and hypoxia in human colon carcinoma xenografts. *Oncotarget*, *8*(51), 88815–88826. https://doi.org/10.18632/oncotarget.21323
Yu, X., Huang, X., Chen, X., Liu, J., Wu, C., Pu, Q., … Zhou, L. (2019). Characterization of a novel anti-human lymphocyte activation gene 3 (LAG-3) antibody for cancer immunotherapy. *MAbs*, *11*(6), 1139–1148. https://doi.org/10.1080/19420862.2019.1629239
Yu, Y., Yoon, S.-O., Poulogiannis, G., Yang, Q., Ma, X. M., Villén, J., … Blenis, J. (2011). Phosphoproteomic analysis identifies Grb10 as an mTORC1 substrate that negatively regulates insulin signaling. *Science (New York, N.Y.)*, *332*(6035), 1322–1326. https://doi.org/10.1126/science.1199484
Yu, Z., Zhou, R., Zhao, Y., Pan, Y., Liang, H., Zhang, J.-S., … Teng, C.-B. (2019). Blockage of SLC31A1-dependent copper absorption increases pancreatic cancer cell autophagy to resist cell death. *Cell Proliferation*, *52*(2), e12568. https://doi.org/10.1111/cpr.12568
Yun, J., Mullarky, E., Lu, C., Bosch, K. N., Kavalier, A., Rivera, K., … Cantley, L. C. (2015). Vitamin C selectively kills KRAS and BRAF mutant colorectal cancer cells by targeting GAPDH. *Science (New York, N.Y.)*, *350*(6266), 1391–1396.

https://doi.org/10.1126/science.aaa5004
Yun, J., Rago, C., Cheong, I., Pagliarini, R., Angenendt, P., Rajagopalan, H., … Papadopoulos, N. (2009). Glucose deprivation contributes to the development of KRAS pathway mutations in tumor cells. *Science (New York, N.Y.)*, *325*(5947), 1555–1559. https://doi.org/10.1126/science.1174229
Zadra, G., Batista, J. L., & Loda, M. (2015). Dissecting the Dual Role of AMPK in Cancer: From Experimental to Human Studies. *Molecular Cancer Research : MCR*, *13*(7), 1059–1072. https://doi.org/10.1158/1541-7786.MCR-15-0068
Zeng, H., Saari, J. T., & Johnson, W. T. (2007). Copper deficiency decreases complex IV but not complex I, II, III, or V in the mitochondrial respiratory chain in rat heart. *The Journal of Nutrition*, *137*(1), 14–18. https://doi.org/10.1093/jn/137.1.14
Zeng, L., Ai, C.-X., Zhang, J.-S., & Li, W.-C. (2020). Pre-hypoxia exposure inhibited copper toxicity by improving energy metabolism, antioxidant defence and mitophagy in the liver of the large yellow croaker Larimichthys crocea. *The Science of the Total Environment*, *708*, 134961. https://doi.org/10.1016/j.scitotenv.2019.134961
Zeng, M., Kikuchi, H., Pino, M. S., & Chung, D. C. (2010). Hypoxia activates the K-ras proto-oncogene to stimulate angiogenesis and inhibit apoptosis in colon cancer cells. *PloS One*, *5*(6), e10966. https://doi.org/10.1371/journal.pone.0010966
Zeng, Y., Ramya, T. N. C., Dirksen, A., Dawson, P. E., & Paulson, J. C. (2009). High-efficiency labeling of sialylated glycoproteins on living cells. *Nature Methods*, *6*(3), 207–209. https://doi.org/10.1038/nmeth.1305
Zhang, D., Xiong, W., Albensi, B. C., & Parkinson, F. E. (2011). Expression of human equilibrative nucleoside transporter 1 in mouse neurons regulates adenosine levels in physiological and hypoxic-ischemic conditions. *Journal of Neurochemistry*, *118*(1), 4–11. https://doi.org/10.1111/j.1471-4159.2011.07242.x
Zhang, H., Chen, D., Ringler, J., Chen, W., Cui, Q. C., Ethier, S. P., … Wu, G. (2010). Disulfiram treatment facilitates phosphoinositide 3-kinase inhibition in human breast cancer cells in vitro and in vivo. *Cancer Research*, *70*(10), 3996–4004. https://doi.org/10.1158/0008-5472.CAN-09-3752
Zhang, X.-P., Liu, F., & Wang, W. (2011). Two-phase dynamics of p53 in the DNA damage response. *Proceedings of the National Academy of Sciences of the United States of America*, *108*(22), 8990–8995. https://doi.org/10.1073/pnas.1100600108
Zhang, X., Kelaria, S., Kerstetter, J., & Wang, J. (2015). The functional and prognostic implications of regulatory T cells in colorectal carcinoma. *Journal of Gastrointestinal Oncology*, *6*(3), 307–313. https://doi.org/10.3978/j.issn.2078-6891.2015.017
Zhang, Y.-W., & Vande Woude, G. F. (2013). MIG-6 and SPRY2 in the Regulation of Receptor Tyrosine Kinase Signaling: Balancing Act via Negative Feedback Loops. In *Future Aspects of Tumor Suppressor Gene*. InTech. https://doi.org/10.5772/54393
Zhang, Y. J., Dai, Q., Sun, D. F., Xiong, H., Tian, X. Q., Gao, F. H., … Fang, J. Y. (2009). mTOR signaling pathway is a target for the treatment of colorectal cancer. *Annals of Surgical Oncology*, *16*(9), 2617–2628. https://doi.org/10.1245/s10434-009-0555-9
Zhang, Z., Kobayashi, S., Borczuk, A. C., Leidner, R. S., Laframboise, T., Levine, A. D., & Halmos, B. (2010). Dual specificity phosphatase 6 (DUSP6) is an ETS-regulated negative feedback mediator of oncogenic ERK signaling in lung cancer cells. *Carcinogenesis*, *31*(4), 577–586. https://doi.org/10.1093/carcin/bgq020
Zhao, Z., Chen, C.-C., Rillahan, C. D., Shen, R., Kitzing, T., McNerney, M. E., … Lowe, S. W.

(2015). Cooperative loss of RAS feedback regulation drives myeloid leukemogenesis. *Nature Genetics*, *47*(5), 539–543. https://doi.org/10.1038/ng.3251

Zhou, E., Huang, Q., Wang, J., Fang, C., Yang, L., Zhu, M., … Dong, M. (2015). Up-regulation of Tim-3 is associated with poor prognosis of patients with colon cancer. *International Journal of Clinical and Experimental Pathology*, *8*(7), 8018–8027.

Zhu, S., Shanbhag, V., Wang, Y., Lee, J., & Petris, M. (2017). A role for the ATP7A copper transporter in tumorigenesis and cisplatin resistance. *Journal of Cancer*, *8*(11), 1952–1958. https://doi.org/10.7150/jca.19029

Zhu, Z., Aref, A. R., Cohoon, T. J., Barbie, T. U., Imamura, Y., Yang, S., … Barbie, D. A. (2014). Inhibition of KRAS-driven tumorigenicity by interruption of an autocrine cytokine circuit. *Cancer Discovery*, *4*(4), 452–465. https://doi.org/10.1158/2159-8290.CD-13-0646

Ziche, M., Jones, J., & Gullino, P. M. (1982). Role of prostaglandin E1 and copper in angiogenesis. *Journal of the National Cancer Institute*, *69*(2), 475–482. Retrieved from http://www.ncbi.nlm.nih.gov/pubmed/6180207

Zimmermann, G., Papke, B., Ismail, S., Vartak, N., Chandra, A., Hoffmann, M., … Waldmann, H. (2013). Small molecule inhibition of the KRAS-PDEδ interaction impairs oncogenic KRAS signalling. *Nature*, *497*(7451), 638–642. https://doi.org/10.1038/nature12205

Zimmermann, M., Murina, O., Reijns, M. A. M., Agathanggelou, A., Challis, R., Tarnauskaitė, Ž., … Durocher, D. (2018). CRISPR screens identify genomic ribonucleotides as a source of PARP-trapping lesions. *Nature*, *559*(7713), 285–289. https://doi.org/10.1038/s41586-018-0291-z

Zimnicka, A. M., Tang, H., Guo, Q., Kuhr, F. K., Oh, M.-J., Wan, J., … Yuan, J. X.-J. (2014). Upregulated copper transporters in hypoxia-induced pulmonary hypertension. *PloS One*, *9*(3), e90544. https://doi.org/10.1371/journal.pone.0090544